Processing of recombinant human IgGs in agroinfiltrated leaves of *Nicotiana benthamiana*

Konstantina Beritza

University of Oxford
Department of Biology
Keble College

Thesis submitted for the degree of
Doctor of Philosophy

Trinity Term 2024

Abstract

Plants offer a powerful platform for recombinant protein expression, and have been used for successful production of human immunoglobulins G (IgGs). This offers an enticing alternative to current strategies for production of pharmaceutical antibodies. However, degradation of recombinant proteins by endogenous proteases causes severe yield losses and this minimises plants' potential as viable production platforms. To tackle this issue, we investigated the *in vitro* and *in vivo* processing of four human anti-viral IgGs by plant proteases of *Nicotiana benthamiana*. Specifically, we tested anti-HIV 2F5, anti-SARS-CoV2 COVA2-15, anti-EBOV 2G4 and anti-HIV VRC01. *In vitro* incubation of IgGs with apoplastic fluids demonstrated that subtilase SBT5.2 is the sole protease responsible for 2F5 cleavage. Moreover, we found that different antibodies exhibit varying levels of susceptibility to cleavage by subtilases. However, we also desired to ascertain if other proteases impact IgG processing intracellularly, along the secretory pathway. We also carried out *in vivo* experiments, examining the subtilases previously tested *in vitro*, along with cysteine proteases, and identified varying impact on IgG accumulation. To get a better understanding of IgG susceptibility to protease processing, we used a site-directed mutagenesis approach on 2F5 and COVA2-15 IgGs and provide preliminary evidence that formation of disulphide bonds enclosing the cleavage site can reduce processing. Finally, we followed a combined immunoblotting and confocal approach to investigate the subcellular localisation of 2F5 light and heavy chains. Furthermore, we assessed the effect of IgG targeting to the endoplasmic reticulum or the vacuole as opposed to the apoplast. Our results demonstrate that the ER can be a promising compartment to maximise IgG accumulation. Cumulatively, our results indicate that individual protease depletion does not uniformly enhance IgG accumulation in *N. benthamiana* and must be tested on a case-by-case basis. Additionally, this work reveals the need to better understand IgG subcellular localisation and their processing profile upon expression in *N. benthamiana*, in order to make this a competitive production platform.

Table of Contents

List of Abbreviations

ABPP	Activity-based protein profiling
AF	Apoplastic fluids
ANOVA	Analysis of variance
BiP	Binding immunoglobulin protein
BSA	Bovine serum albumin
CaMV	Cauliflower Mosaic virus
cDNA	Complementary deoxyribonucleic acid
CDR	Complementarity-determining region
cGMP	Current good manufacturing practice
C_H	Constant region of heavy chain
CHO	Chinese hamster ovary
COVID	Coronavirus disease
CRISPR	Clustered Regularly Interspaced Short Palindromic Repeats
CRT	Calreticulin
Ct	C-terminal
CTT	Phosphocholine cytidyltransferase
DCL	Dicer-like protein
DMSO	Dimethyl sulfoxide
DNA	Deoxyribonucleic acid
dpi	Days post infiltration/infection
dsRNA	Double-stranded ribonucleic acid
DTT	Dithiothreitol
EDTA	Ethylenediaminetetraacetic acid
ELISA	Enzyme-linked immunosorbent assay
EPO	Erythropoietin
ER	Endoplasmic reticulum
ERQC	Endoplasmic reticulum quality control
EU	European Union
FDA	Food and Drug Administration
FGF1	Fibroblast growth factor 1
FNIII	Fibronectin type III
FP-TAMRA	Tetramethylrhodamine fluorophosphate
GFP	Green fluorescent protein
gp	Glycoprotein
H_2L_2	Heavy-light chain heterodimer
HC	Heavy chain
HIV	Human Immunodeficiency Virus
HRP	Horseradish peroxidase
HSP90	Heat-shock protein 90
HT	Hyper-translatable
IgA	Immunoglobulin A
IgG	Immunoglobulin G
IL-10	Interleukin 10
LC	Light chain
mAbs	Monoclonal antibodies
MES	2-Morpholinoethanesulphonic acid

mRNA	Messenger ribonucleic acid
MS	Mass spectrometry
PBS	Phosphate-buffered saline
PBST	Phosphate-buffered saline with Tween-20
PDB	Protein Data Bank
PDI	Protein disulfide isomerase
PI	Protease inhibitor
PLCP	Papain-like cysteine protease
PMF or PMP	Plant Molecular Farming/Pharming
PMSF	Plenyl methyl sulfonyl fluoride
PPI	Peptidyl-propyl isomerase
PSV	Protein storage vacuole
PTGS	Post-transcriptional gene silencing
PTI	Pattern-triggered immunity
PVDF	Polyvinylidene fluoride
RDR6	RNA-dependent RNA polymerase 6
RFP	Red fluorescence protein
RNA	Ribonucleic acid
RNAi	Ribonucleic acid interference
ROS	Reactive oxygen species
RP	Recombinant protein
RPKM	Reads per kilobase per million mapped reads
RT	Room temperature
RT-qPCR	Reverse transcriptase-quantitative polymerase chain reaction
SAR	Systemic acquired resistance
SBT	Subtilisin-like protease or subtilase
scFvs	Single-chain variable fragments
SDS-PAGE	Sodium dodecyl-sulfate polyacrylamide gel electrophoresis
siRNA	Small interfering RNA
SPP	Signal peptide peptidase
ss	Sequence-specific
T4SS	Type IV secretion system
TALEN	Transcription activator-like effector nuclease
T-DNA	Transfer deoxyribonucleic acid
TE	Total extracts
Ti	Tumour inducing
TRV	Tobacco rattle virus
TSP	Total soluble protein
UPR	Unfolded protein response
USDA	United States Department of Agriculture
UTR	Untranslated region
VEGFR2	Vascular endothelial growth factor receptor 2
VIGS	Virus-induced gene silencing
VLP	Virus-like particle
VPE	Vacuolar processing enzyme
VSS	Vacuolar sorting signal
YFP	Yellow fluorescent protein

List of Figures & Tables

Chapter 1

General Introduction

Recombinant proteins (RPs) are used as therapeutic or diagnostic reagents, creating an emerging demand for their production on an industrial scale. Microbial and mammalian cell lines have been traditionally preferred for commercial protein production, but disadvantages in terms of cost, scalability and safety make plants an attractive alternative (Dirisala et al., 2016). In recent years, the advancements in plant genetic engineering and the demand of industrial scalability has led to significant gains in the usage of plants for pharmaceutical production. Diverse plant-based expression systems, such as transient expression, plant cell-suspension cultures, recombinant plant viruses, plant cell packs, BY-2 cell lysates, hairy roots or the chloroplast transgenic system are being investigated (Fischer & Buyel, 2020; Ma et al., 2003; Sack et al., 2007; Waheed et al., 2015; Xu et al., 2018).

1.1 The Chronicle of Plant Molecular Pharming

Chinese hamster ovary (CHO) cell line is the most used mammalian expression system and are responsible for the production of 60-70% of all recombinant pharmaceutical proteins (Wurm, 2004). Plant Molecular Pharming is considered a cost-effective and more carbon neutral technology that has been evolving since the advancements of plant genetic engineering in the 1980s (Shanmugaraj et al., 2020; **Figure 1.1**). When it comes to heterologous hosts, plants can be a desirable chassis due to their ability to grow by simply requiring water, carbon dioxide, inorganic nutrients and light compared to expensive mammalian culture media. They do not demand special facilities such as fermenters and they can grow on a field-scale, making them an ideal candidate for developing countries (Murad et al., 2020). Moreover, plants are able to perform types of glycosylation that prokaryotic systems such as *Escherichia coli* cannot

perform. Also, glycosylation in insects and yeast is limited to high mannose forms (Chen and H. Lai 2013) may negatively affect the function of virus-like particles (VLPs) and other recombinant proteins. Plants, on the other hand, have been successfully genetically engineered to "humanise" the N-glycan modification (Strasser, 2013). However, fine-tuning of expression levels, delivery of precursors or accuracy of post-translational modifications are some of the challenges in selecting the optimal host for heterologous production (Smanski et al., 2017).

Various valuable therapeutic and diagnostic proteins have been produced in *Nicotiana* plants, including secondary metabolites (Reed & Osbourn, 2018; Wang et al., 2016), enzymes (Kytidou et al., 2017; Vardakou et al., 2012), viral antigens and antibodies (Blokhina et al., 2020; Garabagi, McLean, et al., 2012a; Pang et al., 2019). Transformation methods and propagation in *Nicotiana* species are simple and reproducible (Wuest et al., 2011). *N. tabacum* plant suspension cells are the most frequently used cell type in biotechnology, grown in stirred tanks and bioreactors. Cell suspensions can be transformed with recombinant DNA either by co-cultivation with *A. tumefaciens* or by particle bombardment (Hellwig et al., 2004). Genome editing with CRISPR/Cas9 and TALEN have been also successful (Gao et al., 2015; Zhang et al., 2013). *N. benthamiana* is often used for transient expression, while *N. tabacum* is typically used for production of stable transgenic plants, a procedure that requires a longer period of development (Garabagi, McLean, et al., 2012b).

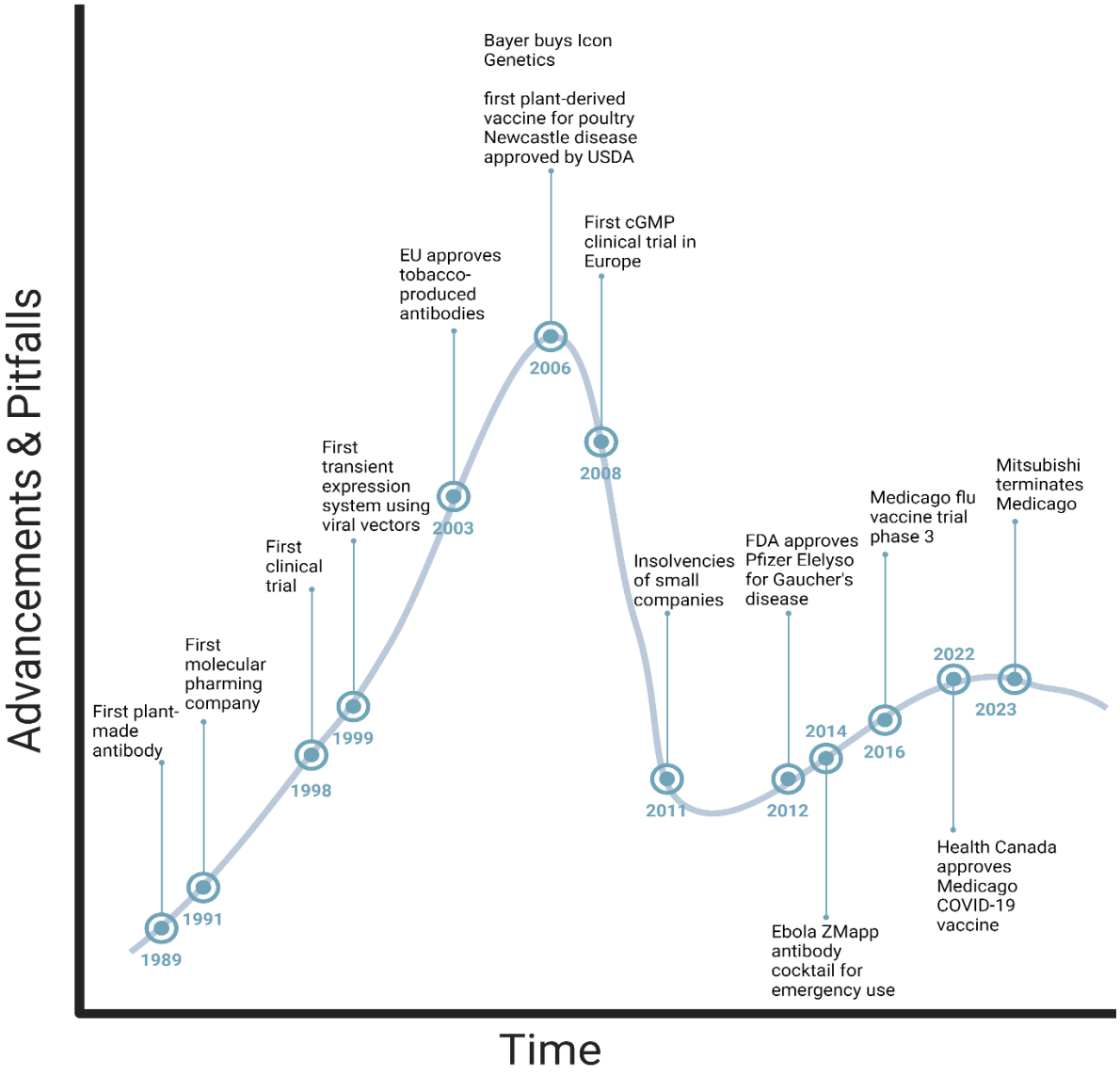

Figure 1.1 Key events of plant molecular pharming.

In 2012, the Food and Drug Administration (FDA) approved the first biopharmaceutical protein produced in plants for use in humans: taliglucerase alfa for treatment of Gaucher disease (Marc-André, 2016). This was the first success in Plant Molecular Pharming, proving that pharmaceuticals can be successfully made for human use in plants. Other pharmaceuticals are on their way to approval for human use. Recently,

Health Canada has granted approval for a *N. benthamiana*-based vaccine against coronavirus disease 2019 (COVID-19; Hager et al., 2022).

1.2 *Nicotiana* species for heterologous protein expression

Recombinant protein production has primarily been focused on using tobacco, as it comprises the most promising and well-established chassis due to its amenability to genetic engineering and its high biomass yield (Sheen, 1983). Most importantly, the tobacco expression system minimises the risk of gene leakage via pollen or seed dispersal into the environment, as it does not require flowering but simply leaves (Conley et al., 2011). Moreover, tobacco is a non-food crop, eliminating the risk of plant-made recombinant proteins entering the food chain (Twyman et al., 2003). Furthermore, while the presence of toxic alkaloids in tobacco may limit its therapeutic applications, low-alkaloid varieties of tobacco have been established to promote direct oral administration of plant tissue or crude protein extracts (Joensuu et al., 2008). Although tobacco is considered biosafe, it is not yet embraced by industry due to the low production yields obtained for recombinant proteins (Doran, 2006).

To address the aforementioned issues, several attempts were made to evaluate the ideal *Nicotiana* variety that possesses the most desirable agronomic features, such as fast growth rates, high biomass yields, high concentration of soluble recombinant protein, and low-alkaloid content. In a comparative analysis of 52 *Nicotiana* varieties*, N tabacum* (cv. I 64) generated the highest protein levels, in combination with high biomass yields and a relatively low amount of alkaloids following *Agrobacterium*-mediated transformation for transient expression of human erythropoietin (EPO) and interleukin-10 (IL-10) (Conley

et al., 2011). In addition, Sheludko et al., after comparing six *Nicotiana* species for transient expression of green fluorescent protein (GFP) under 35S Cauliflower Mosaic Virus (CaMV) promoter, observed that GFP expressed in all species, but in significantly higher levels in leaves of *N. benthamiana, N. exigua,* and *N. excelsior* (3.8, 3.7, and 2.0% TSP, respectively; Sheludko et al., 2007). However, after using a viral-based expression system they detected a substantial increase in accumulation of GFP in *N. excelsior* and *N. benthamiana* (63.5 and 16.2% TSP, respectively), concluding that *N. excelsior* would make the ideal candidate for both types of expression systems tested. A different promising *Nicotiana* species proposed by Sindarovska et al., *N. cavicola,* belongs to the same subgenus as *N. benthamiana* and their fully expanded leaves are larger than those of *N. benthamiana*, resulting in a statistically significant enhanced GFP content under the 35S system (Sindarovska et al., 2019). In another study, the maximum accumulation of the anti-VEGFR2 (VEGFR2; vascular endothelial growth factor receptor 2) nanobody was 0.45% and 0.2% of total soluble proteins (TSP) in *N. benthamiana* and *N. tabacum*, respectively (Modarresi et al., 2018). Similar levels of GFP and human papillomavirus capsid protein were reported by Chen et al. and Matić et al, respectively (Chen et al., 2007; Matić et al., 2012). Although *N. benthamiana* has very small biomass relative to the larger tobacco varieties more suitable for commercial use, it remains the model plant system for transient expression due to its rapid growth and susceptibility to agroinfiltration (Marillonnet et al., 2005; McCormick et al., 1999; Nausch et al., 2016).

1.2 Transforming *Nicotiana benthamiana*

The two different approaches used for recombinant protein production consist of stable genetic transformation and transient gene expression. Stable nuclear

transformation results in stable expression in plant tissues by ensuring the insertion of recombinant DNA into the nuclear or the plastid genome of the plant cell (Hwang et al., 2017). The transfer of recombinant DNA is carried out by using direct and indirect methods and this preference varies according to the target plant species, target genome (nuclear or plastid), and gene construct to be introduced. *Agrobacterium tumefaciens* and *A. rhizogenes* are used for indirect gene transfer and are generally preferred for nuclear transformation. Biolistic transformation by microparticle bombardment, is the most preferred direct method and is mostly used to transform plastid genomes and plant species where transformation mediated by *Agrobacteria* is not applicable (Ream, 2009). By using plant tissue culture methods, a transgenic plant or plant tissue cultures (callus, hairy roots) can be established for recombinant protein production from various plant tissues.

Although in general transgenic plants allow for large-scale protein production, plant transformation is time-consuming and needs fine-tuning due to the low protein expression compared to other plant-based expression systems (Gao & Nielsen, 2013). Another disadvantage is that transgene expression may differ due to positional effects of random gene integration. Additionally, multiple insertions can lead to gene silencing and unstable gene expression. By contrast, transient expression has many advantages when expressing recombinant proteins in plants. Transient transformation is achieved either by *Agrobacterium* infiltration or by viral vector-based transient expression. These two processes are based on the expression of transgenes delivered by bacteria or viral vectors, and stable integration of the transgene into the genome is not required. The most important advantage of these systems is the rapid recombinant protein production. Expression of extra chromosomal transgenes can be detected in 3–4 hours after DNA

transfer, while maximum protein expression levels are reached in 18–48 hours, and gene expression can be maintained for 10–14 days afterwards (Diego-Martin et al., 2020).

A. tumefaciens exists in many genetically distinct strains that differ in their ability to infect plants (Newell, 2000). *A. tumefaciens* uses plant hormone regulation to cause tumour formation on the host plant. They are able to do this due to the presence of a distinct plasmid called a 'tumour inducing' (Ti) plasmid, of which a fragment can be transferred into host plant cells. This fragment is called transfer-DNA (T-DNA).

In natural oncogenic strains of *Agrobacterium*, the T-DNA carries genes for auxin and opine production (Pitzschke & Hirt, 2010). This allows the bacteria to use hormones to promote tumour growth and produce opine as a nitrogen source. Different strains can produce enzymes for synthesis of different opines. For instance, the oncogenic C58 strain produces nopaline (Hwang et al., 2017). Three of the strains commonly used in biotechnology are AGL1, GV3101 and EHA105. These three strains share a common background, all derived from the *A. tumefaciens* C58, but they do not carry oncogenes on the T-DNA and therefore are not oncogenic. The *A. tumefaciens* strain GV3101 pMP90 has had its TiC58 plasmid replaced with another Ti plasmid called pMP90, which was made by deleting the T-region of pTiC58 containing nopaline synthesis genes. As a result, this *A. tumefaciens* strain has a C58 chromosomal background and a Ti plasmid carrying a gentamycin resistance gene. These disarmed strains lack the T-DNA of their background strain but still express the virulence (vir) proteins, which are also encoded on the Ti plasmid but not in the T-DNA region, that are vital for infection and T-DNA transfer. Acetosyringone is often added to the infiltration buffer to induce the expression of the *vir* genes, that promote the formation of the type II secretion system (T4SS) and T-DNA transfer (Stachel et al., 1986).

1.3 Monoclonal immunoglobulin G as a promising RP candidate

Monoclonal antibodies (mAbs) are a major class of pharmaceutical products with an increasing demand worldwide (Donini & Marusic, 2019). The first mAb was successfully expressed in tobacco plants in 1989 (Hiatt et al., 1989). Since then, different antibody derivatives have been expressed in plants such as secretory IgA, Fab fragments, single-chain antibody fragments (scFvs), minibodies, single variable domains, antibody fusion proteins (immunocytokines), scFv-Fc antibodies and camelid heavy-chain antibodies (Donini & Marusic, 2019).

Monoclonal IgG antibody production in plants requires the co-expression of two types of polypeptides, the light (LC) and heavy chain (HC). A signal peptide to enter the secretory pathway is essential to ensure correct folding and post-translational modifications (Strasser, 2018). These chains are then assembled into a Y-shaped heterodimeric structure containing four polypeptides (**Figure 1.2**). Light and heavy chain are translocated to endoplasmic reticulum following translation (Bergman & Kuehl, 1979). When entering the ER, signal peptide peptidase cleaves off the N-terminal signal peptide and folding begins before the polypeptide chains are completely translated. Most IgGs assemble first into HC dimers ready to be covalently bound with LC via a disulphide bond between the C_L and C_{H1} domains (Baumal et al., 1970). It has been reported that when C_{H3} domain is absent e.g. in tested HC mutants, HC dimers are not formed and HC-LC hemimers are secreted instead (Zack et al., 1981). Fc dimerisation is dependent on the interaction between the C_{H3} domains and stabilised by disulphide bonds at the hinge region. The two C_{H2} domains interact via N-linked glycans that control their orientation and spacing, and ultimately the binding of downstream effectors (Feige et al., 2009, 2010).

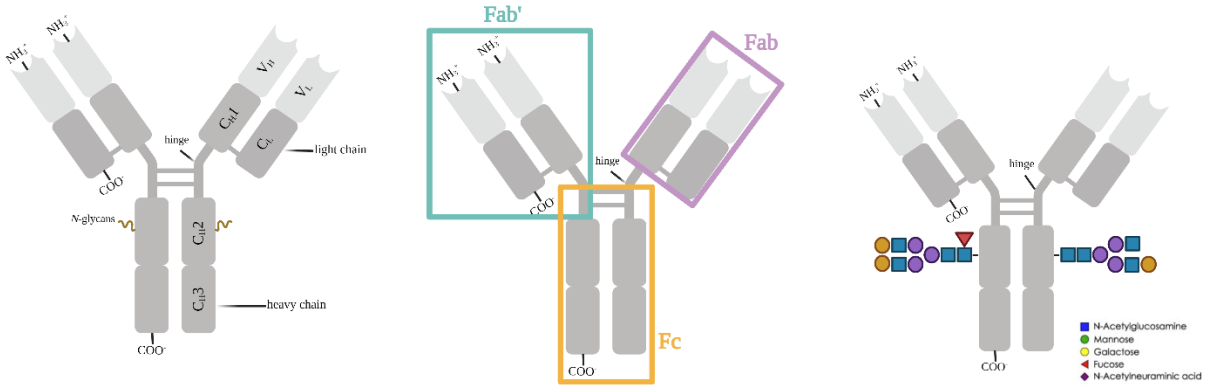

Figure 1.2 Immunoglobulin G structure.

IgG antibody has four polypeptide chains, comprising two identical light and two identical heavy chains. Each of the four chains has a variable (V) domain, which contributes to the antigen-binding domain, and a constant (C) domain, which determines the isotype G. The light chains are bound to the heavy chains by disulphide bonds. Fab', Fab, Fc domains are highlighted on the middle IgG structure, as well as N-glycosylation profile shown on right structure.

1.4 Challenges of plant production platforms

Plants have many advantages compared to traditional systems for recombinant protein production. However, immune responses due to agroinfiltration or post-translational gene silencing might impede recombinant protein accumulation (**Figure 1.3**). Moreover, protein quality and stability have significant bearing on the overall performance of a plant expression platform. Protein quality includes correct folding and accurate post-translational modifications, such as glycosylation, whereas stability refers to the proteolytic degradation of recombinant proteins by endogenous proteases.

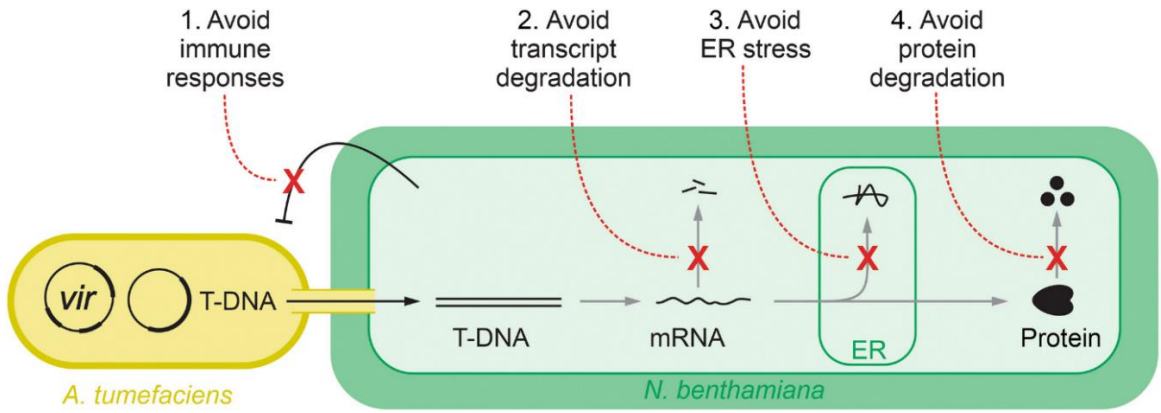

Figure 1.3 Main challenges and current research focus on optimising transient protein expression. Adapted from previous work (Beritza et al., 2024).

Transient expression by agroinfiltration of *Nicotiana benthamiana* with *Agrobacterium tumefaciens* is mediated by the transfer DNA (T-DNA) that enters the plant cells through the type-IV secretion system.

Immune Responses upon Agroinfiltration

Agroinfiltration of *N. benthamiana* leaves induces significant cellular changes, including enhanced immune responses and reduced cell homeostasis, as revealed by transcriptomic, proteomic, and metabolomic analyses (**Table 1.1**). Approximately 25% of transcripts change in abundance post-agroinfiltration, with upregulation of genes related to pathogen recognition, immune signalling, protein folding, oxidative stress response, and lignin production, and downregulation of those involved in photosynthesis, basic cellular functions, and SWEET family sugar efflux transporters (Grosse-Holz et al., 2018; Hamel et al., 2024). The extracellular protein profile shows a 70% increase in proteins, often without corresponding transcript changes, suggesting post-transcriptional control (Grosse-Holz et al., 2018). Metabolic shifts include higher levels of phytol, α-tocopherol, and chlorogenic acid derivatives (Drapal et al., 2021). These changes resemble a basic immune response, similar to PAMP-triggered immunity (PTI)

(Zhang & Zhou, 2010). Improving transformation efficiencies can be achieved by circumventing or inhibiting immune responses during agroinfiltration, such as through silencing of the *Nb*CORE receptor (Dodds et al., 2023) or expression of the bacterial effector AvrPto (Raman et al., 2022).

Table 1.1 Differential gene expression in *Nicotiana benthamiana* upon agroinfiltration. Adapted from previous work (Beritza et al., 2024).

↓, significant decrease in abundance; ↑, significant increase in abundance; –, no significant change; n/a, not assessed; UPR, unfolded protein response (Drapal et al., 2021; Grosse-Holz et al., 2018; Hamel et al., 2023, 2024).

Function	Transcriptomics	Proteomics	Metabolomics
Photosynthesis	↓	↓	↓
Cell wall remodelling (mainly lignification)	↑	↑	↑
Sugar depletion	↑	↑	–
ROS generation	↑	↑	↑
Immune perception and signalling	↑	↑	n/a
Proteases and inhibitors	↑	↑	n/a
Lipases and esterases	↑	↑	n/a
Salicylic acid signalling and SAR	↑	↑	n/a
Chaperones and UPR-related	↑	↑	n/a

Post-Transcriptional Gene Silencing

Stabilising transcripts is essential, because T-DNA-encoded transcripts often destabilise due to post-transcriptional gene silencing (PTGS), which starts approximately three days post-agroinfiltration. PTGS initiates with small antisense RNA amounts produced by random T-DNA insertion or RNA-dependent RNA polymerase, leading to double-stranded RNA (dsRNA) formation. Dicer processes this dsRNA into small interfering RNAs (siRNAs) that degrade homologous mRNAs. To counteract this, the silencing inhibitor P19 from tomato bushy stunt virus (TBSV) is co-expressed to bind siRNAs and inhibit PTGS (Lombardi et al., 2009). Additionally, knockout lines reducing PTGS machinery have been developed. Eliminating dicer-like proteins 2 and 4 (*Nb*DCL2 and *Nb*DCL4) in *N. benthamiana* enhanced transient expression in *dcl2dcl4* double-knockout plants (Matsuo, 2022; Matsuo & Matsumura, 2017). Removing RNA-dependent RNA polymerase 6 (*rdr6*) also increased transient GFP expression compared to wild-type plants (Matsuo & Atsumi, 2019). However, *dcl2dcl4* plants exhibited higher transient GFP and human fibroblast growth factor-1 (FGF1) expression than both wild-type and rdr6 plants (Matsuo, 2022). Strategies to enhance mRNA stability further boost transient expression. Plant untranslated regions (UTRs) can increase mRNA stability, even when P19 is present (Garabagi et al., 2012). Additionally, the hypertranslatable (HT) vector system uses virus-derived elements to enhance transcription and translation by increasing gene copy number and inhibiting PTGS (Peyret & Lomonossoff, 2013; Sainsbury et al., 2009).

Protein Quality Control in the Endoplasmic Reticulum

The endoplasmic reticulum quality control system (ERQC) in plants ensures proper protein folding and manages misfolded proteins (Strasser, 2018). The ER lumen contains folding factors and chaperones, such as binding protein (BiP), HSP90 family proteins, calnexin, calreticulin, protein disulfide isomerases (PDIs), and peptidyl-prolyl isomerases (PPIs), which aid in correct polypeptide folding (Gupta & Tuteja, 2011). During agroinfiltration in *N. benthamiana*, expressing large amounts of secreted or membrane proteins often leads to upregulation of chaperones, a primary ER-stress response (Hamel et al., 2023; Margolin et al., 2020; Ye et al., 2011). Proteomic studies have confirmed increased levels of PDIs, CRT, BiP, and ER-associated degradation components during transient expression of viral glycoproteins and IgG antibodies that induce ER-stress (Hamel, Comeau, et al., 2024; Hamel, Tardif, et al., 2024). Different recombinant proteins may require specific chaperones for proper folding, as evidenced by varying accumulation and ER-stress induction of IgG antibodies (Hamel et al., 2023). To mitigate ER stress during agroinfiltration, co-expressing molecular chaperones alongside the target product has been employed. Human chaperones are considered more effective at folding human proteins compared to plant chaperones due to evolutionary differences. Co-expression with human calreticulin increased the transient expression of HIV glycoprotein gp140 by 13-fold and the S protein ectodomain by 3-fold while avoiding ER stress marker gene induction (Margolin et al., 2020; Song et al., 2018). The growing consensus suggests that co-expression with specific chaperones may be necessary to alleviate ER-stress and improve protein folding and accumulation for different recombinant proteins.

Plant-specific glycosylation

Specifically, *N*-glycosylation is important for IgGs and regulates secretion into the apoplast. The *N*-glycans affect processes such as protein folding, quality control, protein trafficking, and the interaction with other proteins (Ruiz-May et al., 2012). While the first steps of *N*-glycosylation in the endoplasmic reticulum are conserved between mammals and plants, *N*-glycan-processing steps differ considerably in the Golgi apparatus. Compared to humans, the structural diversity of *N*-glycans in plants is reduced, which is related to the fact that plants have fewer glycosyltransferases that elongate complex *N*-glycans. Plant-produced recombinant glycoproteins carry α1,3-fucose and β1,2-xylose residues attached to the common core *N*-glycan, which are not found on human glycoproteins and, therefore, are potentially immunogenic. Following maturation in the ER and the Golgi, plant *N*-glycans can be further modified during the transit of glycoproteins to their final destinations, which can include the chloroplast, vacuole, and apoplast (Strasser, 2018). Although cargo sorting can occur in earlier secretory compartments and also continue beyond the *trans*-Golgi network, it may reach a particularly high level of complexity, where the sorting machinery controls multiple pathways to spatially segregated acceptor compartments (de Matteis & Luini, 2008).

Recombinant protein degradation

Proteases are abundant enzymes in all organisms that hydrolyse peptide bonds, releasing peptides or amino acids. Proteolysis may occur *in planta* or during protein extraction, requiring the addition of protease inhibitors during extraction to improve protein stability and yield (Pillay et al., 2014). In *N. benthamiana,* about 1200 putative proteases act in different subcellular compartments, including the cytosol, the vacuole,

the chloroplast, the mitochondria and the lysosome, or they are delivered extracellularly, residing in the apoplast. However, not all proteases degrade recombinant proteins, as some are organelle-specific, others are not expressed in leaves, or are inactive at molecular pharming conditions (Jutras et al., 2020). The papain-like Cys proteases (PLCPs), subtilisins (SBTs), and pepsin-like Asp proteases are abundant in the apoplast and might process recombinant proteins.

1.5 Tackling unintended proteolysis of recombinant proteins

The most straightforward approach to avoid proteolysis is to deplete or silence the endogenous proteases (Buyel et al., 2021). RNAi-mediated gene silencing for downregulation of certain proteases increases the accumulation of recombinant proteins in rice (Kim et al., 2008), tobacco BY-2 cells (Mandal et al., 2014), and tobacco leaves (Duwadi et al., 2015). Moreover, gene knockout by the CRISPR/Cas9 system can also be an effective strategy. For instance, Hoernstein et al., knocked out a specific subtilisin family protease from *Physcomitrium* by gene editing, resulting in considerable reduction of extracellular proteolytic activity and a small increase in protein production yields, with insignificant impact on growth and development (Hoernstein et al., 2018).

Furthermore, several studies demonstrated that co-expression of broad- spectrum protease inhibitors along with the desired recombinant protein can minimize proteolysis activity. Specifically, most studies focus on chymotrypsin and trypsin-like protease inhibitors (Goulet et al., 2012; Pillay et al., 2014). However, a single protease inhibitor can be effective against several, even unrelated, proteases (Grosse-Holz & van der Hoorn, 2016). Moreover, protease inhibitors can be targeted to the same subcellular

compartment as the desired recombinant protein (Pillay et al., 2014), but it is important to control their expression to avoid affecting plant development.

It is possible to simultaneously remove several genes by CRISPR/Cas9 to identify protease depletions that enhance the accumulation of pharmaceutical proteins in *N. benthamiana*. Goulet et al. showed that aspartic and serine protease inhibitors are the main modulators for protease activity in the apoplast of *N. benthamiana* leaves. Consequently, they transiently expressed two broad-spectrum inhibitors in tobacco leaves, resulting in an increase of the recombinant murine antibody by 70%–80%. Similarly, Robert et al. showed that co-expression of protease inhibitors led to a yield increase by up to 40%. In another study, the expression of the tomato cysteine protease inhibitor *Sl*CYS8 enhanced the accumulation of antibodies transiently expressed in *N. benthamiana* leaves (Jutras et al., 2016) and has also been used as a stabilizing fusion partner for other recombinant proteins (Sainsbury et al., 2013). More recently, two *N. benthamiana* protease inhibitors (*Nb*PR4, *Nb*Pot1) and one of human origin (*Hs*TIMP) increased the accumulation of transiently expressed α- galactosidase, erythropoietin, and an IgG antibody in agroinfiltrated *N. benthamiana* leaves (F. Grosse-Holz, Madeira, et al., 2018). Taken together, all these results suggest that these plant broad-spectrum PIs are effective companion proteins for the in planta protection of recombinant proteins transiently expressed in leaves (Clemente et al., 2019). Moreover, better knowledge of the linkage between senescence and protease activity can be particularly helpful as there is evidence that infiltration with *Agrobacteria* leads to leaf senescence and overexpression of senescence-related proteases, such as cysteine proteases (Pillay et al., 2012; Roberts et al., 2012).

Recombinant protein retention in the endoplasmic reticulum is another strategy to avoid degradation in the apoplast (Benchabane et al., 2008; Torrent et al., 2009; Yoshida et al., 2004), but this changes the type of *N*-glycosylation of the recombinant protein. C-terminal ER retention signal sequences like KDEL and HDEL are used to retain the proteins in the ER and minimize protein degradation. The plant ER contains very few proteases and provides a relatively protective environment (Desai et al., 2010). Also, targeting protein production either to oil bodies, roots or seeds are attractive approaches for limiting proteolysis (Buyel et al., 2021; Drake et al., 2009; Nykiforuk et al., 2011).

Several methods have paved the way for generating plant chasses with improved recombinant protein yields. Despite the potential to increase the sustainability of recombinant protein manufacturing, plant molecular pharming strategies have yet to be embraced broadly by industry.

1.6 Research aims and rationale

In the context of these aforementioned facts, there is a necessity of modulating endogenous protease activity and investigating proteases involved in recombinant protein processing. In addition, it is important to understand the timeline and localisation at which IgG antibodies accumulate upon transient expression to be able to address degradation by co-localised proteases accurately. This work investigated the *in vitro* and *in vivo* processing of various anti-viral IgGs, as well as their subcellular localisation and mistargeting in *N. benthamiana*, in pursuit of optimising IgG protein production *in planta*.

In **Chapter 2** we investigated the processing of the hinge region specifically or of fully assembled IgGs following incubation in apoplastic fluids. These apoplastic fluids derived from plants that were either depleted for various proteases or were previously expressed protease inhibitors.

In **Chapter 3** we tested several protease-depleted plants that were either proved to be involved in IgG processing or displayed high accumulation in the secretory pathway and/or apoplast.

In **Chapter 4** we investigated the stability of the complementarity-determining region H3 (CDR H3) loop of 2F5 and COVA2-15 IgG antibodies, following site-directed mutagenesis.

In **Chapter 5** we examined the secretion efficiency of IgGs. We also tested different IgG mistargeting strategies and explored an extended ER phenotype and its possible effect on IgG accumulation. The expanded ER was attempted by two approaches: a naturally expanded ER based on endogenous phosphocholine cytidylyltransferase increased levels, or a synthetically expanded ER based on the dimerisation of polyprotein complexes anchoring on the ER membrane.

The IgGs tested in this work were anti-viral IgGs such as the anti-HIV 2F5, the anti-COVID-19 COVA2-15, the anti-Ebola 2G4 and the anti-HIV VRC01 (**Figure 1.4**). The 2F5 antibody consists of an exemplary IgG antibody since it has a long history of published data both from the immunology side and from the successful plant expression side (Bryson et al., 2009; Julien et al., 2008; Niemer et al., 2014; Ofek et al., 2004; Sack et al., 2007). COVA2-15 IgG is a more recently isolated IgG that appears to be more stable among its isotypes (Göritzer et al., 2024; Brouwer et al., 2020), while 2G4 IgG is found in the ZMapp cocktail, one of the first plant-produced IgG cocktails that was approved for human use (Davidson et al., 2015). VRC01 is considered a relatively stable IgG as it does not display an extended CDR H3 loop and has been produced *in planta* (Teh et al., 2014). Lastly, a synthetic anti-GFP IgG was constructed only for the purposes of investigating the expanded ER interactions in Chapter 5.

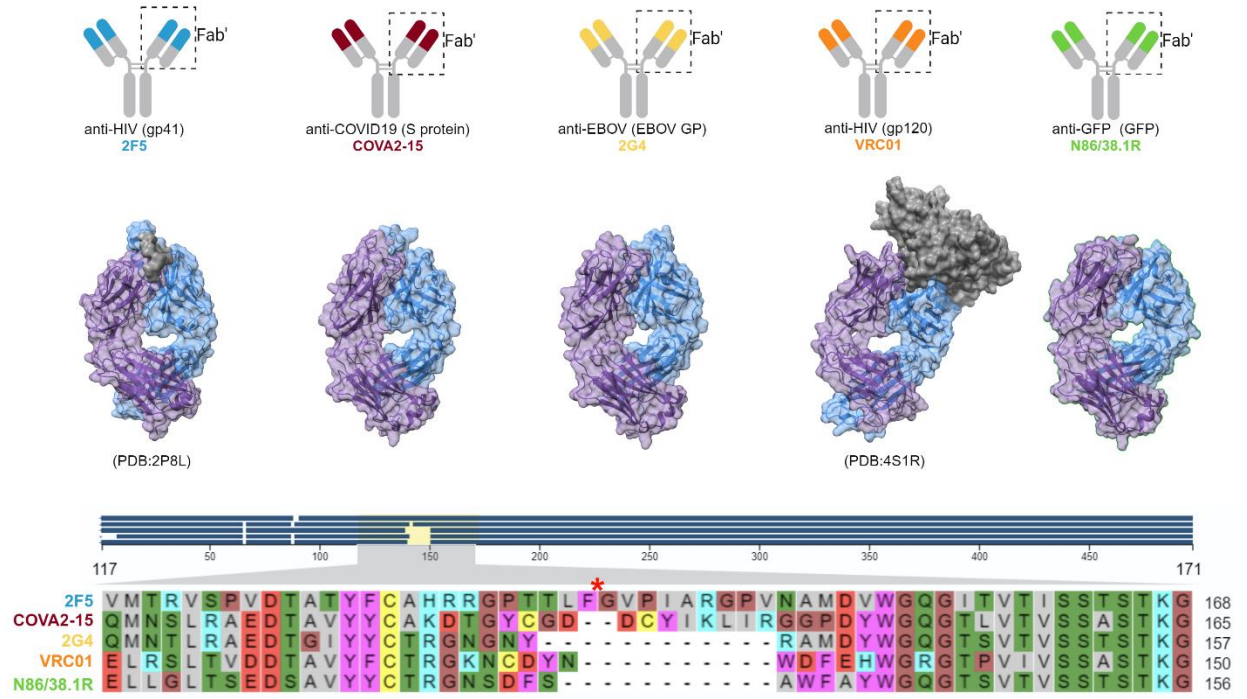

Figure 1.4 Structure of the Fab' domains of IgG antibodies used in this work.

(a) Side and top views of the antiviral IgGs (Fab' domain) of interest, obtained from Protein Data Bank (PDB) or predicted by AlphaFold. Light chain is depicted with purple colour, heavy chain with cyan and the antigen of 2F5 with grey. Multiple sequence alignment of the IgGs at the site of the variable heavy chain near the CRD H3 loop, where the 2F5 is cleaved (red asterisk).

References

Benchabane, M., Goulet, C., Rivard, D., Faye, L., Gomord, V., & Michaud, D. (2008). Preventing unintended proteolysis in plant protein biofactories. *Plant Biotechnology Journal*, *6*(7), 633–648. https://doi.org/10.1111/j.1467-7652.2008.00344.x

Bergman, L. W., & Kuehl, W. M. (1979). Formation of an intrachain disulfide bond on nascent immunoglobulin light chains. *Journal of Biological Chemistry*, *254*(18), 8869–8876. https://doi.org/10.1016/s0021-9258(19)86780-7

Beritza, K., Watts, E. C., & van der Hoorn, R. A. L. (2024). Improving transient protein expression in agroinfiltrated Nicotiana benthamiana. *New Phytologist*, *243*(3), 846–850. https://doi.org/10.1111/nph.19894

Blokhina, E. A., Mardanova, E. S., Stepanova, L. A., Tsybalova, L. M., & Ravin, N. V. (2020). Plant-produced recombinant influenza A virus candidate vaccine based on flagellin linked to conservative fragments of m2 protein and hemagglutintin. *Plants*, *9*(2). https://doi.org/10.3390/plants9020162

Bryson, S., Julien, J.-P., Hynes, R. C., & Pai, E. F. (2009). Crystallographic Definition of the Epitope Promiscuity of the Broadly Neutralizing Anti-Human Immunodeficiency Virus Type 1 Antibody 2F5: Vaccine Design Implications. *Journal of Virology*, *83*(22), 11862–11875. https://doi.org/10.1128/JVI.01604-09

Buyel, J. F., Stöger, E., & Bortesi, L. (2021). Targeted genome editing of plants and plant cells for biomanufacturing. *Transgenic Research*. https://doi.org/10.1007/s11248-021-00236-z

Chen, C.-C., Chen, T.-C., Raja, J. A. J., Chang, C.-A., Chen, L.-W., Lin, S.-S., & Yeh, S.-D. (2007). Effectiveness and stability of heterologous proteins expressed in plants by Turnip mosaic virus vector at five different insertion sites. *Virus Research*, *130*(1), 210–227. https://doi.org/https://doi.org/10.1016/j.virusres.2007.06.014

Clemente, M., Corigliano, M. G., Pariani, S. A., Sánchez-López, E. F., Sander, V. A., & Ramos-Duarte, V. A. (2019). Plant Serine Protease Inhibitors: Biotechnology Application in Agriculture and Molecular Farming. *International Journal of Molecular Sciences*, *20*(6). https://doi.org/10.3390/ijms20061345

Conley, A. J., Zhu, H., Le, L. C., Jevnikar, A. M., Lee, B. H., Brandle, J. E., & Menassa, R. (2011). Recombinant protein production in a variety of Nicotiana hosts: a comparative analysis. *Plant Biotechnology Journal*, *9*(4), 434–444. https://doi.org/https://doi.org/10.1111/j.1467-7652.2010.00563.x

Davidson, E., Bryan, C., Fong, R. H., Barnes, T., Pfaff, J. M., Mabila, M., Rucker, J. B., & Doranz, B. J. (2015). Mechanism of Binding to Ebola Virus Glycoprotein by the ZMapp, ZMAb, and MB-003 Cocktail Antibodies. *Journal of Virology*, *89*(21), 10982–10992. https://doi.org/10.1128/JVI.01490-15

de Matteis, M. A., & Luini, A. (2008). Exiting the Golgi complex. *Nature Reviews Molecular Cell Biology*, *9*(4), 273–284. https://doi.org/10.1038/nrm2378

Desai, P. N., Shrivastava, N., & Padh, H. (2010). Production of heterologous proteins in plants: Strategies for optimal expression. *Biotechnology Advances*, *28*(4), 427–435. https://doi.org/https://doi.org/10.1016/j.biotechadv.2010.01.005

Diego-Martin, B., González, B., Vazquez-Vilar, M., Selma, S., Mateos-Fernández, R., Gianoglio, S., Fernández-del-Carmen, A., & Orzáez, D. (2020). Pilot Production of SARS-CoV-2 Related Proteins in Plants: A Proof of Concept for Rapid Repurposing of Indoor Farms Into Biomanufacturing Facilities. *Frontiers in Plant Science*, *11*. https://doi.org/10.3389/fpls.2020.612781

Dirisala, V. R., Nair, R. R., Srirama, K., Reddy, P. N., Rao, K. R. S. S., Satya Sampath Kumar, N., & Parvatam, G. (2016). Recombinant pharmaceutical protein production in plants: unraveling the therapeutic potential of molecular pharming. *Acta Physiologiae Plantarum*, *39*(1), 18. https://doi.org/10.1007/s11738-016-2315-3

Dodds, I., Chen, C., Buscaill, P., & van der Hoorn, R. A. L. (2023). Depletion of the NbCORE receptor drastically improves agroinfiltration productivity in older Nicotiana benthamiana plants. *Plant Biotechnology Journal*, *21*(6), 1103–1105. https://doi.org/10.1111/pbi.14037

Donini, M., & Marusic, C. (2019). Current state-of-the-art in plant-based antibody production systems. *Biotechnology Letters*, *41*(3), 335–346. https://doi.org/10.1007/s10529-019-02651-z

Doran, P. M. (2006). Foreign protein degradation and instability in plants and plant tissue cultures. *Trends in Biotechnology*, *24*(9), 426–432. https://doi.org/https://doi.org/10.1016/j.tibtech.2006.06.012

Drake, P. M. W., Barbi, T., Sexton, A., McGowan, E., Stadlmann, J., Navarre, C., Paul, M. J., & Ma, J. K.-C. (2009). Development of rhizosecretion as a production system for recombinant proteins from hydroponic cultivated tobacco. *FASEB Journal : Official Publication of the Federation of American Societies for Experimental Biology*, *23*(10), 3581–3589. https://doi.org/10.1096/fj.09-131771

Drapal, M., Enfissi, E. M. A., & Fraser, P. D. (2021). Metabolic effects of agro-infiltration on N. benthamiana accessions. *Transgenic Research*, *30*(3), 303–315. https://doi.org/10.1007/s11248-021-00256-9

Duwadi, K., Chen, L., Menassa, R., & Dhaubhadel, S. (2015). Identification, Characterization and Down-Regulation of Cysteine Protease Genes in Tobacco for Use in Recombinant Protein Production. *PLOS ONE*, *10*(7), e0130556. https://doi.org/10.1371/journal.pone.0130556

Feige, M. J., Hendershot, L. M., & Buchner, J. (2010). How antibodies fold. In *Trends in Biochemical Sciences* (Vol. 35, Issue 4, pp. 189–198). https://doi.org/10.1016/j.tibs.2009.11.005

Feige, M. J., Nath, S., Catharino, S. R., Weinfurtner, D., Steinbacher, S., & Buchner, J. (2009). Structure of the Murine Unglycosylated IgG1 Fc Fragment. *Journal of Molecular Biology*, *391*(3), 599–608. https://doi.org/10.1016/j.jmb.2009.06.048

Fischer, R., & Buyel, J. F. (2020). Molecular farming – The slope of enlightenment. *Biotechnology Advances*, *40*, 107519. https://doi.org/https://doi.org/10.1016/j.biotechadv.2020.107519

Gao, C., & Nielsen, K. K. (2013). Comparison Between Agrobacterium-Mediated and Direct Gene Transfer Using the Gene Gun. In S. Sudowe & A. B. Reske-Kunz (Eds.), *Biolistic DNA Delivery: Methods and Protocols* (pp. 3–16). Humana Press. https://doi.org/10.1007/978-1-62703-110-3_1

Gao, J., Wang, G., Ma, S., Xie, X., Wu, X., Zhang, X., Wu, Y., Zhao, P., & Xia, Q. (2015). CRISPR/Cas9-mediated targeted mutagenesis in Nicotiana tabacum. *Plant Molecular Biology*, *87*(1), 99–110. https://doi.org/10.1007/s11103-014-0263-0

Garabagi, F., Gilbert, E., Loos, A., Mclean, M. D., & Hall, J. C. (2012). Utility of the P19 suppressor of gene-silencing protein for production of therapeutic antibodies in Nicotiana expression hosts. *Plant Biotechnology Journal*, *10*(9), 1118–1128. https://doi.org/10.1111/j.1467-7652.2012.00742.x

Garabagi, F., McLean, M. D., & Hall, J. C. (2012a). Transient and stable expression of antibodies in Nicotiana species. *Methods in Molecular Biology (Clifton, N.J.)*, *907*, 389–408. https://doi.org/10.1007/978-1-61779-974-7_23

Garabagi, F., McLean, M. D., & Hall, J. C. (2012b). Transient and stable expression of antibodies in Nicotiana species. *Methods in Molecular Biology (Clifton, N.J.)*, *907*, 389–408. https://doi.org/10.1007/978-1-61779-974-7_23

Göritzer, K., Groppelli, E., Grünwald-Gruber, C., Figl, R., Ni, F., Hu, H., Li, Y., Liu, Y., Hu, Q., Puligedda, R. D., Jung, J. W., Strasser, R., Dessain, S., & Ma, J. K. C. (2024). Recombinant neutralizing secretory IgA antibodies for preventing mucosal acquisition and transmission of SARS-CoV-2. *Molecular Therapy*, *32*(3), 689–703. https://doi.org/10.1016/j.ymthe.2024.01.025

Goulet, C., Khalf, M., Sainsbury, F., D'Aoust, M. A., & Michaud, D. (2012). A protease activity-depleted environment for heterologous proteins migrating towards the leaf cell apoplast. *Plant Biotechnology Journal*, *10*(1), 83–94. https://doi.org/10.1111/j.1467-7652.2011.00643.x

Grosse-Holz, F., Kelly, S., Blaskowski, S., Kaschani, F., Kaiser, M., & van der Hoorn, R. A. L. (2018). The transcriptome, extracellular proteome and active secretome of agroinfiltrated Nicotiana benthamiana uncover a large, diverse protease repertoire. *Plant Biotechnology Journal*, *16*(5), 1068–1084. https://doi.org/10.1111/pbi.12852

Grosse-Holz, F. M., & van der Hoorn, R. A. L. (2016). Juggling jobs: roles and mechanisms of multifunctional protease inhibitors in plants. *The New Phytologist*, *210*(3), 794–807. https://doi.org/10.1111/nph.13839

Grosse-Holz, F., Madeira, L., Zahid, M. A., Songer, M., Kourelis, J., Fesenko, M., Ninck, S., Kaschani, F., Kaiser, M., & van der Hoorn, R. A. L. (2018). Three unrelated protease inhibitors enhance accumulation of pharmaceutical recombinant proteins in Nicotiana benthamiana. *Plant Biotechnology Journal*, *16*(10), 1797–1810. https://doi.org/10.1111/pbi.12916

Gupta, D., & Tuteja, N. (2011). Chaperones and foldases in endoplasmic reticulum stress signaling in plants. In *Plant Signaling and Behavior* (Vol. 6, Issue 2, pp. 232–236). https://doi.org/10.4161/psb.6.2.15490

Hager, K. J., Pérez Marc, G., Gobeil, P., Diaz, R. S., Heizer, G., Llapur, C., Makarkov, A. I., Vasconcellos, E., Pillet, S., Riera, F., Saxena, P., Geller Wolff, P., Bhutada, K., Wallace, G., Aazami, H., Jones, C.

E., Polack, F. P., Ferrara, L., Atkins, J., … Ward, B. J. (2022). Efficacy and Safety of a Recombinant Plant-Based Adjuvanted Covid-19 Vaccine. *New England Journal of Medicine*, *386*(22), 2084–2096. https://doi.org/10.1056/NEJMoa2201300

Hamel, L. P., Comeau, M. A., Tardif, R., Poirier-Gravel, F., Paré, M. È., Lavoie, P. O., Goulet, M. C., Michaud, D., & D'Aoust, M. A. (2023). Heterologous expression of influenza haemagglutinin leads to early and transient activation of the unfolded protein response in Nicotiana benthamiana. *Plant Biotechnology Journal*. https://doi.org/10.1111/pbi.14252

Hamel, L. P., Comeau, M. A., Tardif, R., Poirier-Gravel, F., Paré, M. È., Lavoie, P. O., Goulet, M. C., Michaud, D., & D'Aoust, M. A. (2024). Heterologous expression of influenza haemagglutinin leads to early and transient activation of the unfolded protein response in Nicotiana benthamiana. *Plant Biotechnology Journal*, *22*(5), 1146–1163. https://doi.org/10.1111/pbi.14252

Hamel, L. P., Tardif, R., Poirier-Gravel, F., Rasoolizadeh, A., Brosseau, C., Giroux, G., Lucier, J. F., Goulet, M. C., Barrada, A., Paré, M. È., Roussel, É., Comeau, M. A., Lavoie, P. O., Moffett, P., Michaud, D., & D'Aoust, M. A. (2024). Molecular responses of agroinfiltrated Nicotiana benthamiana leaves expressing suppressor of silencing P19 and influenza virus-like particles. *Plant Biotechnology Journal*, *22*(5), 1078–1100. https://doi.org/10.1111/pbi.14247

Hellwig, S., Drossard, J., Twyman, R. M., & Fischer, R. (2004). Plant cell cultures for the production of recombinant proteins. *Nature Biotechnology*, *22*(11), 1415–1422. https://doi.org/10.1038/nbt1027

Hiatt, A., Caffferkey, R., & Bowdish, K. (1989). Production of antibodies in transgenic plants. *Nature*, *342*(6245), 76–78. https://doi.org/10.1038/342076a0

Hoernstein, S. N. W., Fode, B., Wiedemann, G., Lang, D., Niederkrüger, H., Berg, B., Schaaf, A., Frischmuth, T., Schlosser, A., Decker, E. L., & Reski, R. (2018). Host Cell Proteome of Physcomitrella patens Harbors Proteases and Protease Inhibitors under Bioproduction Conditions. *Journal of Proteome Research*, *17*(11), 3749–3760. https://doi.org/10.1021/acs.jproteome.8b00423

Hwang, H.-H., Yu, M., & Lai, E.-M. (2017). *Agrobacterium*-Mediated Plant Transformation: Biology and Applications. *The Arabidopsis Book*, *2017*(15). https://doi.org/10.1199/tab.0186

Joensuu, J. J., Niklander-Teeri, V., & Brandle, J. E. (2008). Transgenic plants for animal health: plant-made vaccine antigens for animal infectious disease control. *Phytochemistry Reviews*, *7*(3), 553–577. https://doi.org/10.1007/s11101-008-9088-2

Julien, J.-P., Bryson, S., Nieva, J. L., & Pai, E. F. (2008). Structural details of HIV-1 recognition by the broadly neutralizing monoclonal antibody 2F5: epitope conformation, antigen-recognition loop mobility, and anion-binding site. *Journal of Molecular Biology*, *384*(2), 377–392. https://doi.org/10.1016/j.jmb.2008.09.024

Jutras, P. V, Dodds, I., & van der Hoorn, R. A. L. (2020). Proteases of Nicotiana benthamiana: an emerging battle for molecular farming. *Current Opinion in Biotechnology*, *61*, 60–65. https://doi.org/https://doi.org/10.1016/j.copbio.2019.10.006

Jutras, P. V, Marusic, C., Lonoce, C., Deflers, C., Goulet, M.-C., Benvenuto, E., Michaud, D., & Donini, M. (2016). An Accessory Protease Inhibitor to Increase the Yield and Quality of a Tumour-Targeting mAb in Nicotiana benthamiana Leaves. *PLOS ONE*, *11*(11), e0167086. https://doi.org/10.1371/journal.pone.0167086

Kim, N. S., Kim, T. G., Kim, O. H., Ko, E. M., Jang, Y. S., Jung, E. S., Kwon, T. H., & Yang, M. S. (2008). Improvement of recombinant hGM-CSF production by suppression of cysteine proteinase gene expression using RNA interference in a transgenic rice culture. *Plant Molecular Biology*, *68*(3), 263–275. https://doi.org/10.1007/s11103-008-9367-8

Kytidou, K., Beenakker, T. J. M., Westerhof, L. B., Hokke, C. H., Moolenaar, G. F., Goosen, N., Mirzaian, M., Ferraz, M. J., de Geus, M., Kallemeijn, W. W., Overkleeft, H. S., Boot, R. G., Schots, A., Bosch, D., & Aerts, J. M. F. G. (2017). Human Alpha Galactosidases Transiently Produced in Nicotiana benthamiana Leaves: New Insights in Substrate Specificities with Relevance for Fabry Disease. *Frontiers in Plant Science*, *8*, 1026. https://doi.org/10.3389/fpls.2017.01026

Lombardi, R., Circelli, P., Villani, M. E., Buriani, G., Nardi, L., Coppola, V., Bianco, L., Benvenuto, E., Donini, M., & Marusic, C. (2009). High-level HIV-1 Nef transient expression in Nicotiana benthamiana using the P19 gene silencing suppressor protein of Artichoke Mottled Crinckle Virus. *BMC Biotechnology*, *9*. https://doi.org/10.1186/1472-6750-9-96

M Brouwer, P. J., Caniels, T. G., van der Straten, K., Snitselaar, J. L., Aldon, Y., Bangaru, S., Torres, J. L., A Okba, N. M., Claireaux, M., Kerster, G., H Bentlage, A. E., van Haaren, M. M., Guerra, D., Burger, J. A., Schermer, E. E., Verheul, K. D., van der Velde, N., van der Kooi, A., van Schooten, J., … van Gils, M. J. (2020). *Potent neutralizing antibodies from COVID-19 patients define multiple targets of vulnerability*. https://www.science.org

Ma, J. K.-C., Drake, P. M. W., & Christou, P. (2003). The production of recombinant pharmaceutical proteins in plants. *Nature Reviews Genetics*, *4*(10), 794–805. https://doi.org/10.1038/nrg1177

Mandal, M. K., Fischer, R., Schillberg, S., & Schiermeyer, A. (2014). Inhibition of protease activity by antisense RNA improves recombinant protein production in Nicotiana tabacum cv. Bright Yellow 2 (BY-2) suspension cells. *Biotechnology Journal*, *9*(8), 1065–1073. https://doi.org/10.1002/biot.201300424

Margolin, E., Oh, Y. J., Verbeek, M., Naude, J., Ponndorf, D., Meshcheriakova, Y. A., Peyret, H., van Diepen, M. T., Chapman, R., Meyers, A. E., Lomonossoff, G. P., Matoba, N., Williamson, A. L., & Rybicki, E. P. (2020). Co-expression of human calreticulin significantly improves the production of HIV gp140 and other viral glycoproteins in plants. *Plant Biotechnology Journal*, *18*(10), 2109–2117. https://doi.org/10.1111/pbi.13369

Marillonnet, S., Thoeringer, C., Kandzia, R., Klimyuk, V., & Gleba, Y. (2005). Systemic Agrobacterium tumefaciens–mediated transfection of viral replicons for efficient transient expression in plants. *Nature Biotechnology*, *23*(6), 718–723. https://doi.org/10.1038/nbt1094

Matić, S., Masenga, V., Poli, A., Rinaldi, R., Milne, R. G., Vecchiati, M., & Noris, E. (2012). Comparative analysis of recombinant Human Papillomavirus 8 L1 production in plants by a variety of expression systems and purification methods. *Plant Biotechnology Journal*, *10*(4), 410–421. https://doi.org/https://doi.org/10.1111/j.1467-7652.2011.00671.x

Matsuo, K. (2022). CRISPR/Cas9-mediated knockout of the DCL2 and DCL4 genes in Nicotiana benthamiana and its productivity of recombinant proteins. *Plant Cell Reports*, *41*(2), 307–317. https://doi.org/10.1007/s00299-021-02809-y

Matsuo, K., & Matsumura, T. (2017). Repression of the DCL2 and DCL4 genes in Nicotiana benthamiana plants for the transient expression of recombinant proteins. *Journal of Bioscience and Bioengineering*, *124*(2), 215–220. https://doi.org/10.1016/j.jbiosc.2017.02.019

McCormick, A. A., Kumagai, M. H., Hanley, K., Turpen, T. H., Hakim, I., Grill, L. K., Tusé, D., Levy, S., & Levy, R. (1999). Rapid production of specific vaccines for lymphoma by expression of the tumor-derived single-chain Fv epitopes in tobacco plants. *Proceedings of the National Academy of Sciences of the United States of America*, *96*(2), 703–708. https://doi.org/10.1073/pnas.96.2.703

Modarresi, M., Javaran, M. J., Shams-bakhsh, M., Zeinali, S., Behdani, M., & Mirzaee, M. (2018). Transient expression of anti-VEFGR2 nanobody in Nicotiana tabacum and N. benthamiana. *3 Biotech*, *8*(12), 484. https://doi.org/10.1007/s13205-018-1500-z

Murad, S., Fuller, S., Menary, J., Moore, C., Pinneh, E., Szeto, T., Hitzeroth, I., Freire, M., Taychakhoonavudh, S., Phoolcharoen, W., & Ma, J. K.-C. (2020). Molecular Pharming for low and middle income countries. *Current Opinion in Biotechnology*, *61*, 53–59. https://doi.org/https://doi.org/10.1016/j.copbio.2019.10.005

Nausch, H., Hausmann, T., Ponndorf, D., Hühns, M., Hoedtke, S., Wolf, P., Zeyner, A., & Broer, I. (2016). Tobacco as platform for a commercial production of cyanophycin. *New Biotechnology*, *33*(6), 842–851. https://doi.org/https://doi.org/10.1016/j.nbt.2016.08.001

Newell, C. A. (2000). Plant transformation technology. *Molecular Biotechnology*, *16*(1), 53–65. https://doi.org/10.1385/MB:16:1:53

Niemer, M., Mehofer, U., Torres Acosta, J. A., Verdianz, M., Henkel, T., Loos, A., Strasser, R., Maresch, D., Rademacher, T., Steinkellner, H., & Mach, L. (2014). The human anti-HIV antibodies 2F5, 2G12, and PG9 differ in their susceptibility to proteolytic degradation: Down-regulation of endogenous serine and cysteine proteinase activities could improve antibody production in plant-based expression platforms. *Biotechnology Journal*, *9*(4), 493–500. https://doi.org/10.1002/biot.201300207

Nykiforuk, C. L., Shen, Y., Murray, E. W., Boothe, J. G., Busseuil, D., Rhéaume, E., Tardif, J.-C., Reid, A., & Moloney, M. M. (2011). Expression and recovery of biologically active recombinant Apolipoprotein AIMilano from transgenic safflower (Carthamus tinctorius) seeds. *Plant Biotechnology Journal*, *9*(2), 250–263. https://doi.org/https://doi.org/10.1111/j.1467-7652.2010.00546.x

Ofek, G., Tang, M., Sambor, A., Katinger, H., Mascola, J. R., Wyatt, R., & Kwong, P. D. (2004). Structure and Mechanistic Analysis of the Anti-Human Immunodeficiency Virus Type 1 Antibody 2F5 in Complex with Its gp41 Epitope. *Journal of Virology*, *78*(19), 10724–10737. https://doi.org/10.1128/jvi.78.19.10724-10737.2004

P, L. G., & Marc-André, D. (2016). Plant-produced biopharmaceuticals: A case of technical developments driving clinical deployment. *Science*, *353*(6305), 1237–1240. https://doi.org/10.1126/science.aaf6638

Pang, E. L., Peyret, H., Ramirez, A., Loh, H.-S., Lai, K.-S., Fang, C.-M., Rosenberg, W. M., & Lomonossoff, G. P. (2019). Epitope Presentation of Dengue Viral Envelope Glycoprotein Domain III on Hepatitis B Core Protein Virus-Like Particles Produced in Nicotiana benthamiana. *Frontiers in Plant Science*, *10*, 455. https://doi.org/10.3389/fpls.2019.00455

Peyret, H., & Lomonossoff, G. P. (2013). The pEAQ vector series: The easy and quick way to produce recombinant proteins in plants. In *Plant Molecular Biology* (Vol. 83, Issues 1–2, pp. 51–58). https://doi.org/10.1007/s11103-013-0036-1

Pillay, P., Kibido, T., du Plessis, M., van der Vyver, C., Beyene, G., Vorster, B. J., Kunert, K. J., & Schlüter, U. (2012). Use of Transgenic Oryzacystatin-I-Expressing Plants Enhances Recombinant Protein Production. *Applied Biochemistry and Biotechnology*, *168*(6), 1608–1620. https://doi.org/10.1007/s12010-012-9882-6

Pillay, P., Schlüter, U., van Wyk, S., Kunert, K. J., & Vorster, B. J. (2014). Proteolysis of recombinant proteins in bioengineered plant cells. *Bioengineered*, *5*(1), 15–20. https://doi.org/10.4161/bioe.25158

Pitzschke, A., & Hirt, H. (2010). New insights into an old story: Agrobacterium-induced tumour formation in plants by plant transformation. *The EMBO Journal*, *29*(6), 1021–1032. https://doi.org/https://doi.org/10.1038/emboj.2010.8

Raman, V., Rojas, C. M., Vasudevan, B., Dunning, K., Kolape, J., Oh, S., Yun, J., Yang, L., Li, G., Pant, B. D., Jiang, Q., & Mysore, K. S. (2022). Agrobacterium expressing a type III secretion system delivers Pseudomonas effectors into plant cells to enhance transformation. *Nature Communications*, *13*(1). https://doi.org/10.1038/s41467-022-30180-3

Ream, W. (2009). Agrobacterium tumefaciens and A. rhizogenes use different proteins to transport bacterial DNA into the plant cell nucleus. In *Microbial Biotechnology* (Vol. 2, Issue 4, pp. 416–427). https://doi.org/10.1111/j.1751-7915.2009.00104.x

Reed, J., & Osbourn, A. (2018). Engineering terpenoid production through transient expression in Nicotiana benthamiana. *Plant Cell Reports*, *37*(10), 1431–1441. https://doi.org/10.1007/s00299-018-2296-3

Reuben Baumal, B., Potter, M., & Matthew Scharff, A. D. (1970). *§ Fellow of the Medical Research Council of Canada. I[Recipient of a U.S. Public Health Service Career Development Award*.

Roberts, I. N., Caputo, C., Criado, M. V., & Funk, C. (2012). Senescence-associated proteases in plants. *Physiologia Plantarum*, *145*(1), 130–139. https://doi.org/https://doi.org/10.1111/j.1399-3054.2012.01574.x

Ruiz-May, E., Kim, S. J., Brandizzi, F., & Rose, J. (2012). The Secreted Plant N-Glycoproteome and Associated Secretory Pathways. *Frontiers in Plant Science*, *3*. https://doi.org/10.3389/fpls.2012.00117

Sack, M., Paetz, A., Kunert, R., Bomble, M., Hesse, F., Stiegler, G., Fischer, R., Katinger, H., Stoeger, E., & Rademacher, T. (2007). Functional analysis of the broadly neutralizing human anti-HIV-1

antibody 2F5 produced in transgenic BY-2 suspension cultures. *The FASEB Journal*, *21*(8), 1655–1664. https://doi.org/https://doi.org/10.1096/fj.06-5863com

Sainsbury, F., Thuenemann, E. C., & Lomonossoff, G. P. (2009). PEAQ: Versatile expression vectors for easy and quick transient expression of heterologous proteins in plants. *Plant Biotechnology Journal*, *7*(7), 682–693. https://doi.org/10.1111/j.1467-7652.2009.00434.x

Sainsbury, F., Varennes-Jutras, P., Goulet, M.-C., D'Aoust, M.-A., & Michaud, D. (2013). Tomato cystatin SlCYS8 as a stabilizing fusion partner for human serpin expression in plants. *Plant Biotechnology Journal*, *11*(9), 1058–1068. https://doi.org/https://doi.org/10.1111/pbi.12098

Shanmugaraj, B., Bulaon, C. J. I., & Phoolcharoen, W. (2020). Plant molecular farming: A viable platform for recombinant biopharmaceutical production. *Plants*, *9*(7), 1–19. https://doi.org/10.3390/plants9070842

Sheen, S. J. (1983). Biomass and Chemical Composition of Tobacco Plants Under High Density Growth. *Beitrage Zur Tabakforschung International/ Contributions to Tobacco Research*, *12*(1), 35–42. https://doi.org/10.2478/cttr-2013-0523

Sheludko, Y. V, Sindarovska, Y. R., Gerasymenko, I. M., Bannikova, M. A., & Kuchuk, N. V. (2007). Comparison of several Nicotiana species as hosts for high-scale Agrobacterium-mediated transient expression. *Biotechnology and Bioengineering*, *96*(3), 608–614. https://doi.org/10.1002/bit.21075

Sindarovska, Y. R., Olevinskaya, Z. M., Demchenko, O. A., Spivak, N. Y., & Kuchuk, N. V. (2019). Nicotiana cavicola as a host for production of recombinant proteins by agrobacterium-mediated transient gene expression. *Biopolymers and Cell*, *35*(5), 340–348. https://doi.org/10.7124/bc.000A11

Smanski, Michael J.; Mead, David; Gustafsson, Claes; Thomas, M. G. (2017). Meeting Report for Synthetic Biology for Natural Products 2017: The Interface of (Meta)Genomics, Machine Learning, and Natural Product Discovery. *ACS Synthetic Biology*, *6*(5), 737–743. https://doi.org/10.1021/acssynbio.7b00132

Song, I., Kang, Y. J., Lee, Y. K., Myung, S. C., & Ko, K. (2018). Endoplasmic reticulum retention motif fused to recombinant anti-cancer monoclonal antibody (mAb) CO17-1A affects mAb expression and plant stress response. *PLoS ONE*, *13*(9). https://doi.org/10.1371/journal.pone.0198978

Stachel, S. E., Timmerman, B., & Zambryski, P. (1986). Generation of single-stranded T-DNA molecules during the initial stages of T-DNA transfer from Agrobacterium tumefaciens to plant cells. *Nature*, *322*(6081), 706–712. https://doi.org/10.1038/322706a0

Strasser, R. (2013). Engineering of human-type O-glycosylation in Nicotiana benthamiana plants. *Bioengineered*, *4*(4), 191–196. https://doi.org/10.4161/bioe.22857

Strasser, R. (2018). Protein Quality Control in the Endoplasmic Reticulum of Plants. In *Annual Review of Plant Biology* (Vol. 69, pp. 147–172). Annual Reviews Inc. https://doi.org/10.1146/annurev-arplant-042817-040331

Teh, A. Y. H., Maresch, D., Klein, K., & Ma, J. K. C. (2014). Characterization of VRC01, a potent and broadly neutralizing anti-HIV mAb, produced in transiently and stably transformed tobacco. *Plant Biotechnology Journal*, *12*(3), 300–311. https://doi.org/10.1111/pbi.12137

Torrent, M., Llompart, B., Lasserre-Ramassamy, S., Llop-Tous, I., Bastida, M., Marzabal, P., Westerholm-Parvinen, A., Saloheimo, M., Heifetz, P. B., & Ludevid, M. D. (2009). Eukaryotic protein production in designed storage organelles. *BMC Biology*, *7*(1), 5. https://doi.org/10.1186/1741-7007-7-5

Twyman, R. M., Stoger, E., Schillberg, S., Christou, P., & Fischer, R. (2003). Molecular farming in plants: host systems and expression technology. *Trends in Biotechnology*, *21*(12), 570–578. https://doi.org/https://doi.org/10.1016/j.tibtech.2003.10.002

Vardakou, M., Sainsbury, F., Rigby, N., Mulholland, F., & Lomonossoff, G. P. (2012). Expression of active recombinant human gastric lipase in Nicotiana benthamiana using the CPMV-HT transient expression system. *Protein Expression and Purification*, *81*(1), 69–74. https://doi.org/https://doi.org/10.1016/j.pep.2011.09.005

Waheed, M. T., Ismail, H., Gottschamel, J., Mirza, B., & Lössl, A. G. (2015). Plastids: The Green Frontiers for Vaccine Production. *Frontiers in Plant Science*, *6*, 1005. https://doi.org/10.3389/fpls.2015.01005

Wang, B., Kashkooli, A. B., Sallets, A., Ting, H.-M., de Ruijter, N. C. A., Olofsson, L., Brodelius, P., Pottier, M., Boutry, M., Bouwmeester, H., & van der Krol, A. R. (2016). Transient production of artemisinin in Nicotiana benthamiana is boosted by a specific lipid transfer protein from A. annua. *Metabolic Engineering*, *38*, 159–169. https://doi.org/https://doi.org/10.1016/j.ymben.2016.07.004

Wuest, D. M., Hou, S., & Lee, K. H. (2011). *3.52 - Metabolic Engineering* (M. B. T.-C. B. (Second E. Moo-Young, Ed.; pp. 617–628). Academic Press. https://doi.org/https://doi.org/10.1016/B978-0-08-088504-9.00229-4

Wurm, F. M. (2004). Production of recombinant protein therapeutics in cultivated mammalian cells. *Nature Biotechnology*, *22*(11), 1393–1398. https://doi.org/10.1038/nbt1026

Xu, J., Towler, M., & Weathers, P. J. (2018). Platforms for Plant-Based Protein Production. *Bioprocessing of Plant In Vitro Systems*, 509–548. https://doi.org/10.1007/978-3-319-54600-1_14

Ye, C., Dickman, M. B., Whitham, S. A., Payton, M., & Verchot, J. (2011). The unfolded protein response is triggered by a plant viral movement protein. *Plant Physiology*, *156*(2), 741–755. https://doi.org/10.1104/pp.111.174110

Yoshida, K., Matsui, T., & Shinmyo, A. (2004). The plant vesicular transport engineering for production of useful recombinant proteins. *Journal of Molecular Catalysis B: Enzymatic*, *28*(4), 167–171. https://doi.org/https://doi.org/10.1016/j.molcatb.2004.01.017

Zack, D. J., Morrison, S. L., Cook, W. D., Dackowski, W., Maq'q', A., & Scharff, H. D. (1981). *Somatically generated mouse myeloma variants synthesizing IgA half-molecules*.

Zhang, J., & Zhou, J. M. (2010). Plant immunity triggered by microbial molecular signatures. In *Molecular Plant* (Vol. 3, Issue 5, pp. 783–793). Oxford University Press. https://doi.org/10.1093/mp/ssq035

Zhang, Y., Zhang, F., Li, X., Baller, J. A., Qi, Y., Starker, C. G., Bogdanove, A. J., & Voytas, D. F. (2013). Transcription activator-like effector nucleases enable efficient plant genome engineering. *Plant Physiology*, *161*(1), 20–27. https://doi.org/10.1104/pp.112.205179

Chapter 2

In vitro processing of IgGs: Towards identifying proteases responsible for IgG degradation

Part of this Chapter is published as: Beritza, K., et al., (2024), SBT5.2s are the major active extracellular subtilases processing IgG antibody 2F5 in the Nicotiana benthamiana apoplast. Plant Biotechnol. J., Vol22, p.2808.

2.1 Introduction

The core protease repertoire of *N. benthamiana* includes 1,243 potential proteases (*Nb*D), with another 512 found in an additional dataset (*Nb*E; Jutras et al., 2020). Thus, recombinant proteins such as antibodies are exposed to multiple different proteases, ultimately leading to lower yields upon their overexpression in *N. benthamiana*. However, not all of these proteases contribute to recombinant protein degradation, especially those confined to organelles, while papain-like cysteine proteases (PLCPs), subtilases (SBTs), and pepsin-like aspartic proteases are most likely to affect degradation as they are prevalent in leaves and often target glycosylated proteins (Jutras et al., 2020). To date, various molecular tools have been created to assess protease activity *in vitro*, such as activity-based probes, synthetic peptide substrates, or *in vivo* within the protease microenvironment (Soleimany et al., 2022). *In vitro* assays have been used extensively to identify the substrate and/or the cleavage fragments upon proteolysis by a plant protease (Escandón et al., 2022; Niemer et al., 2014; Paulus et al., 2020).

Many studies have reported IgG processing upon expression *in planta*, often leading to the processing of the heavy chain (HC) (De Muynck et al., 2009; Hehle et al., 2015; Lombardi et al., 2009; Niemer et al., 2014; Sharp & Doran, 2001; Stevens et al., 1994). A common cleavage site is located close to the hinge region in the HC, as observed for the 2G12 and H10 IgG antibodies (Donini et al., 2015; Hehle et al., 2015). PLCPs and other proteases can cleave IgGs at this hinge region, resulting in Fab and Fc fragments (Gorevic et al., 1985; Porter, 1959). In addition, the HC of antiviral IgGs are often cleaved within the variable region (Puchol Tarazona et al., 2021), likely because these IgGs contain extended H3 loops that are sensitive to proteases. HIV-neutralising 2F5, for instance, is

cleaved in the H3 loop when incubated with apoplastic fluids isolated from *Nicotiana benthamiana* leaves by PMSF-sensitive proteases (Puchol Tarazona et al., 2021).

To investigate the responsible proteases for the processing of antiviral IgGs, we initially set up in vitro assays using apoplastic fluids to simulate the apoplast (Sueldo et al., 2023; Wang et al., 2021). According to literature, secreted proteins are expected to reside in the apoplast and since all the antibodies we expressed in *N. benthamiana* leaves carry the N-terminal PR1a signal peptide, we expect that the IgGs will be secreted (Diego-Martin et al., 2020; Goulet et al., 2012a; Ocampo et al., 2016; Robert et al., 2013a; Schillberg et al., 1999). This Chapter investigates the processing of different antiviral IgGs such as the anti-HIV 2F5, the anti-COVID-19 COVA2-15, and the anti-Ebola 2G4 (**Figure 2.1**). The 2F5 antibody consists of an exemplary IgG antibody since it has a long history of published data both from the immunology side and from the successful plant expression side (Bryson et al., 2009; Julien et al., 2008; Niemer et al., 2014; Ofek et al., 2004; Sack et al., 2007). COVA2-15 IgG is a more recently isolated IgG that appears to be more stable among its isotypes (Göritzer et al., 2024; Brouwer et al., 2020), while 2G4 IgG is found in the ZMapp cocktail, one of the first plant-produced IgG cocktails that was approved for human use (Davidson et al., 2015).

To date, several strategies have been implemented to prevent recombinant protein degradation *in planta*, with protease inhibitor co-expression being amongst the most promising (**Table 2.1**). Before testing the *in planta* effect of inhibitors, *in vitro* incubation of the protein of interest with and without inhibitor candidates can help identify target proteases, *e.g.*, serine proteases, and have been used extensively in the past (Hehle et al., 2011; Jutras et al., 2019; Niemer et al., 2014; Puchol Tarazona et al., 2021; Robert et al., 2015).

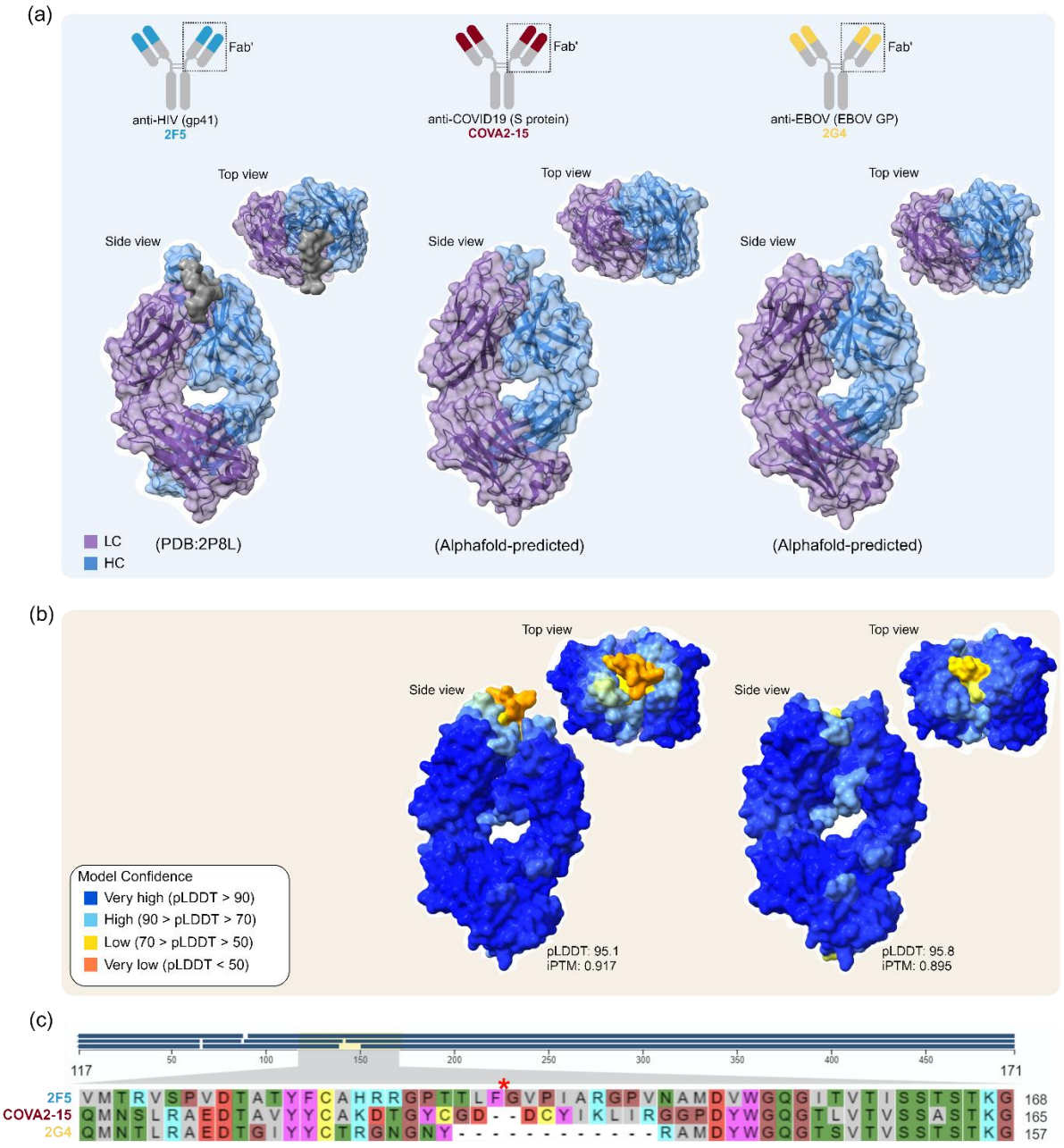

Figure 2.1 Structure of the Fab' domains of 2F5, COVA2-15 and 2G4 IgG antibodies.

(a) Side and top views of the antiviral IgGs (Fab' domain) of interest, obtained from Protein Data Bank (PDB) or predicted by AlphaFold. Light chain is depicted with purple colour, heavy chain with cyan and the antigen of 2F5 with grey. **(b)** Predicted Fab' structures of COVA2-15 and 2G4, coloured by model confidence according to AlphaFold predictions. **(c)** Multiple sequence alignment of the three IgGs at the site of the variable heavy chain, where the 2F5 is cleaved (red asterisk).

Table 2.1 Co-expression with protease inhibitors can lead to increased recombinant protein levels. Ser: serine, Asp: aspartic, Cys: cysteine, LC: light chain, HC: heavy chain.

Protease Inhibitor	Target Proteases	IgG Accumulation	Reference
*Sl*CDI; *Sl*CYS9	Ser/Asp; Cys	C5-1 IgG antibody (LC; 70-80%)	*Goulet et al., 2012*
*Sl*CDI	Ser/Asp	C5-1 IgG antibody (HC; 85%)	*Goulet et al., 2012*
*Sl*CYS8	Cys	C5-1 IgG antibody (40%)	*Robert et al., 2013*
*Sl*CYS8	Cys	H10 IgG antibody (HC; 7.5-fold)	*Jutras et al., 2016*
*Nb*PR4, *Nb*Pot1 & *Hs*TIMP	Cys/Ser/Metallo	VRC01 IgG antibody (2-10-fold)	*Grosse-Holz et al., 2018*

Results

2.2 The hinge region of IgGs is susceptible to proteolysis from apoplastic proteases

Besides the complementarity-determining region (CDR) H3 loop, IgGs are also often cleaved upstream the hinge region (Deveuve et al., 2020; Robotham & Kelly, 2020; Suzuki et al., 2018). To study the processing of the hinge region, quenched peptide was commercially synthesised by GenScript (cleavage site peptide: $KVD^{246}\downarrow K^{247}KVEP$). When the peptide remains intact, the quencher is near the fluorophore, effectively suppressing fluorescence emission, whereas if protease(s) cleave the peptide, the fluorophore and quencher are separated, allowing fluorescence to be emitted and detected (Neefjes & Dantuma, 2004). To confirm that cleavage of the hinge peptide can be blocked by chemical protease inhibitors, we pre-incubated apoplastic fluids with either Cys protease inhibitor E-64 or Ser protease inhibitor phenylmethylsulfonyl fluoride (PMSF) and then added the quenched peptide. Plate reader analysis revealed that processing of this peptide resulted in emission of fluorescence, as seen when incubated with wild-type apoplastic fluids (**Figure 2.2a,b**; grey). Addition of protease inhibitor PSMF blocked cleavage of the quenched peptide, whereas E-64 cysteine protease inhibitor did not affect cleavage (**Figure 2.2a,b**). To test if subtilases are responsible for cleaving the hinge region of IgGs, we incubated the quenched peptide with apoplastic fluids from Epi1 expressing leaves and the empty vector control (**Figure 2.2c**), as Epi1 is a subtilase protease inhibitor. Processing of the quenched peptide was reduced by Epi1 compared to the empty vector control, suggesting a role of subtilases in processing the hinge region.

Additionally, we incubated the peptide with apoplastic fluids from leaves expressing a variety of protease inhibitors protease inhibitors, namely *Hs*TIMP, *Sl*CYS8, *Sl*CDI, *Nb*Pot1, *Nb*PR4, Epi12, and two mutant inhibitor controls Ala*Hs*TIMP and *Sl*CYS8-Q47P (Grosse-Holz et al., 2018; **Figure 2.3a,b**; **Table 2.2**), including PMSF and Epi1 that were previously tested as a comparison with the diverse inhibitors. All inhibitors apart from PMSF were transiently expressed in *N. benthamiana*, and apoplastic fluids from these plants were used in the assays. PMSF was added in wild-type apoplastic fluids as previously. None of the rest of the inhibitors tested was able to impede peptide processing in a significant manner.

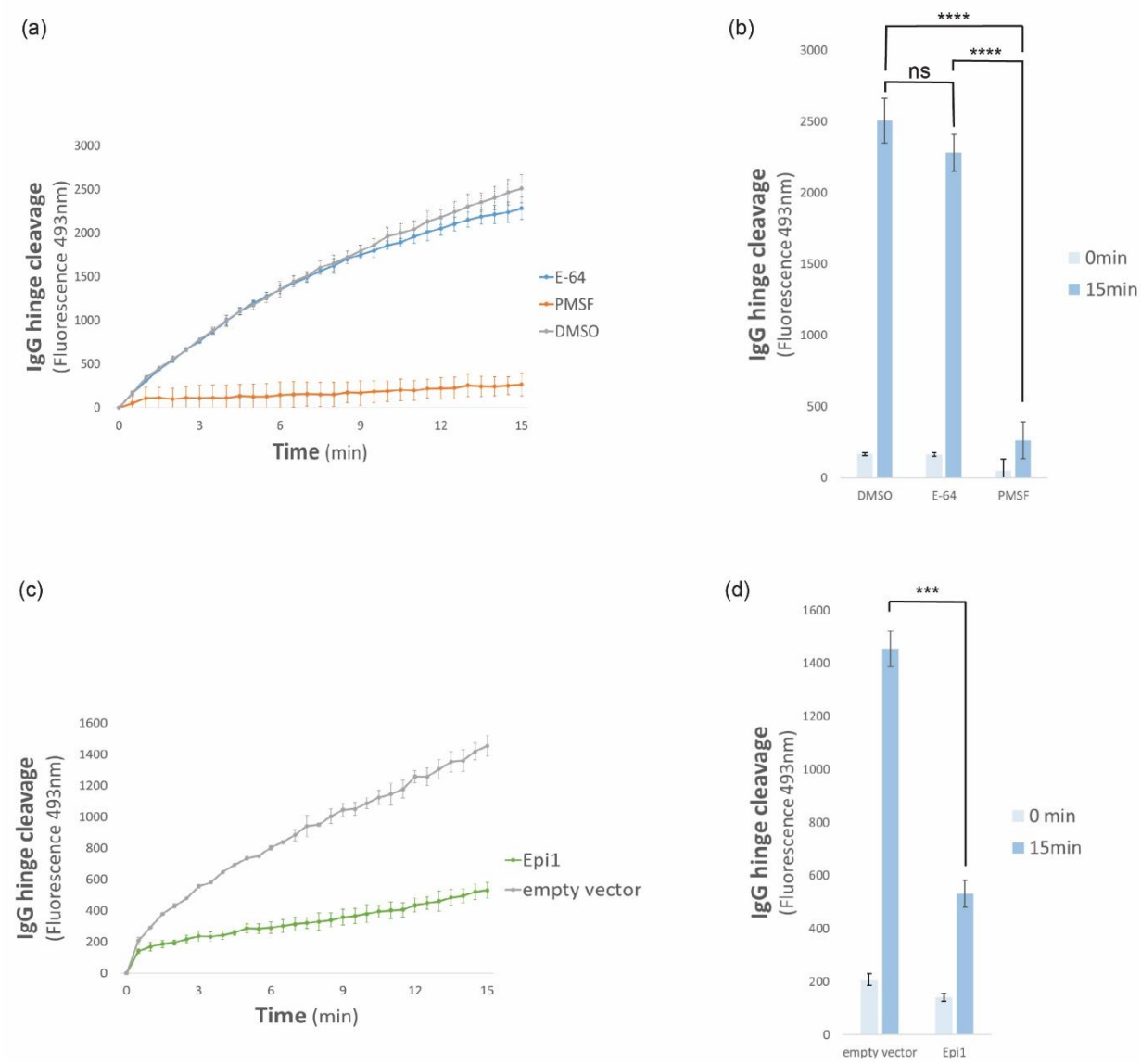

Figure 2.2 Quenched-IgG peptide cleavage is hindered by PMSF and Epi1 protease inhibitors.

The quenched peptide was incubated with apoplastic fluids isolated from **(a, b)** wild-type *N. benthamiana* leaves, previously incubated with chemical inhibitors PMSF or E-64 or **(c, d)** with apoplastic fluids isolated from plants expressing the Epi1 protease inhibitor. A DMSO or empty vector control was used in each experiment. Graphs (a, c) were normalised for the first measurement (t=0), while graphs (b, d) depict the raw intensity values at zero and fifteen minutes. Data were tested for normal distribution, while significance was determined with one-way ANOVA (b) or t-test (d), following multiple comparisons and Tukey's post-hoc test where applicable. Error intervals: mean ±SE of n=3 technical replicates.

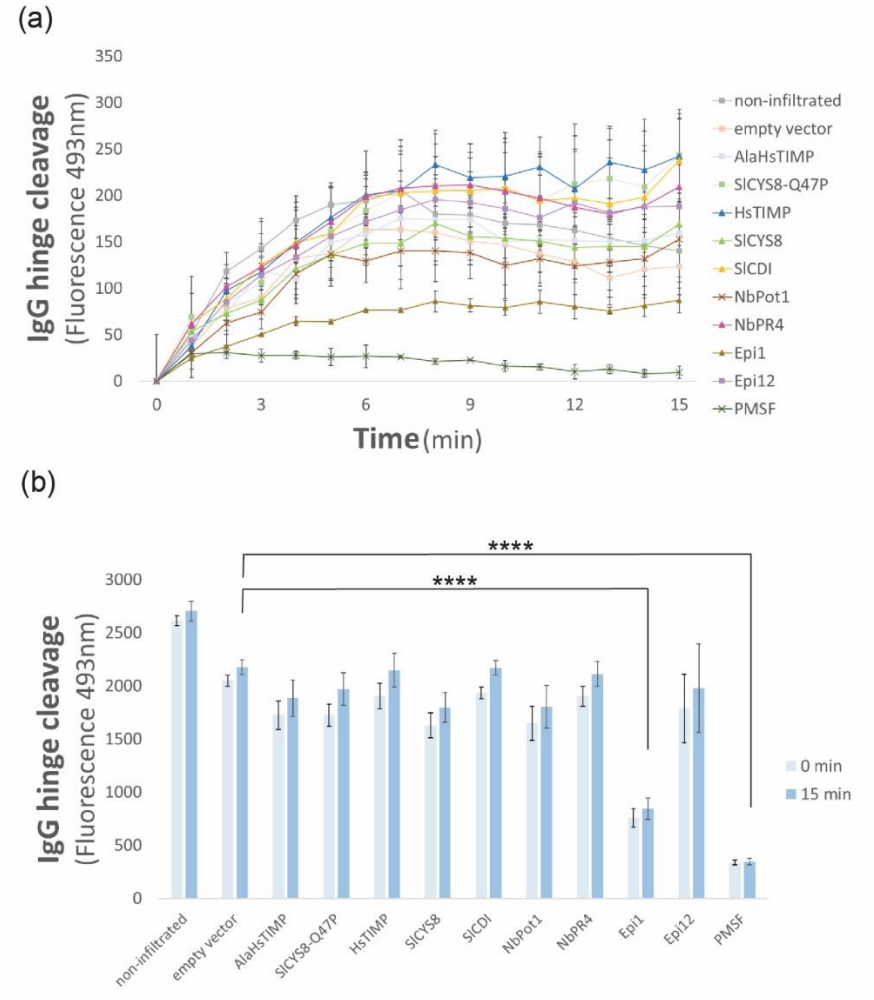

Figure 2.3 Quenched-IgG peptide cleavage is hindered by PMSF and Epi1 protease inhibitors.

The quenched peptide was incubated with apoplastic fluids isolated from wild-type *N. benthamiana* leaves, overexpressing a different protease inhibitor. PMSF pre-incubation with apoplastic fluids from non-infiltrated leaves was used as a positive control, whereas empty vector was used as a negative control. The top graphs were normalised for the first measurement (t=0) while the bottom graph depicts the raw intensity values at zero and fifteen minutes. Data were tested for normal distribution, while significance was determined with one-way ANOVA, following multiple comparisons and Tukey's post-hoc test. Error intervals: mean ±SE of n=3 technical replicates.

Table 2.2 Secreted protease inhibitors used for *in vitro* assays, transiently expressed in *N. benthamiana* and previously validated in Grosse-Holz et al., 2018.

Protease Inhibitor	Target Proteases	Family (MEROPS)	Origin
*Hs*TIMP	Metallo	I35	*Homo sapiens*
*Sl*CYS8	Cys	I25 (Cystatin)	*Solanum lycopersicum*
*Sl*CDI	Ser/Asp	I3 (Kunitz)	*Solanum lycopersicum*
*Nb*Pot1	Ser	I13	*Nicotiana benthamiana*
*Nb*PR4	Cys	I43	*Nicotiana benthamiana*
Epi12	Ser/Cys	I1	*Phytophthora infestans*
Epi1	Ser/Cys	I1	*Phytophthora infestans*

Since PMSF and Epi1 prevented cleavage, a subtilase protease is most likely responsible for this processing. Among serine proteases, subtilases are abundant in the apoplast with SBT5.2 being the most abundant (Grosse-Holz, Kelly, et al., 2018; Jutras et al., 2019). Hence, our next assay contained incubation of the hinge peptide with apoplastic fluids from protease-depleted plants. Our first approach was to obtain CRISPR-Cas9 knockouts of different subtilases, where apoplastic fluids were used to determine hinge peptide cleavage. Two different subtilase knockout lines, *sbt*1.4 and *sbt*5.2 were used for this assay (**Figure 2.4a,b**). Incubation with apoplastic fluids from both knockout lines resulted in significant interruption of the hinge peptide processing. Further information on these knockout lines can be found on **Figures 2.8**, **2.10**, and **Table 3.2**.

The other approach was to deplete proteases by virus-induced gene silencing (VIGS; Liu et al., 2002). Using VIGS, the following subtilase family proteases, SBT1.7a,

SBT1.7c, and SBT1.9a were depleted. When apoplastic fluids from these subtilase-depleted plants were used, all three resulted in reduced hinge peptide cleavage, with SBT1.9a displaying the most effective cleavage prevention (**Figure 2.4c,d**). These proteases were depleted according to the phylogenetic tree on **Figure 2.8** and **Table 3.2**. It is noteworthy that SBT5.2, SBT1.7a, SBT1.7c, and SBT1.9 are the four most abundant subtilases in the apoplast (Jutras et al., 2019; Puchol Tarazona et al., 2021; Sueldo et al., 2023).

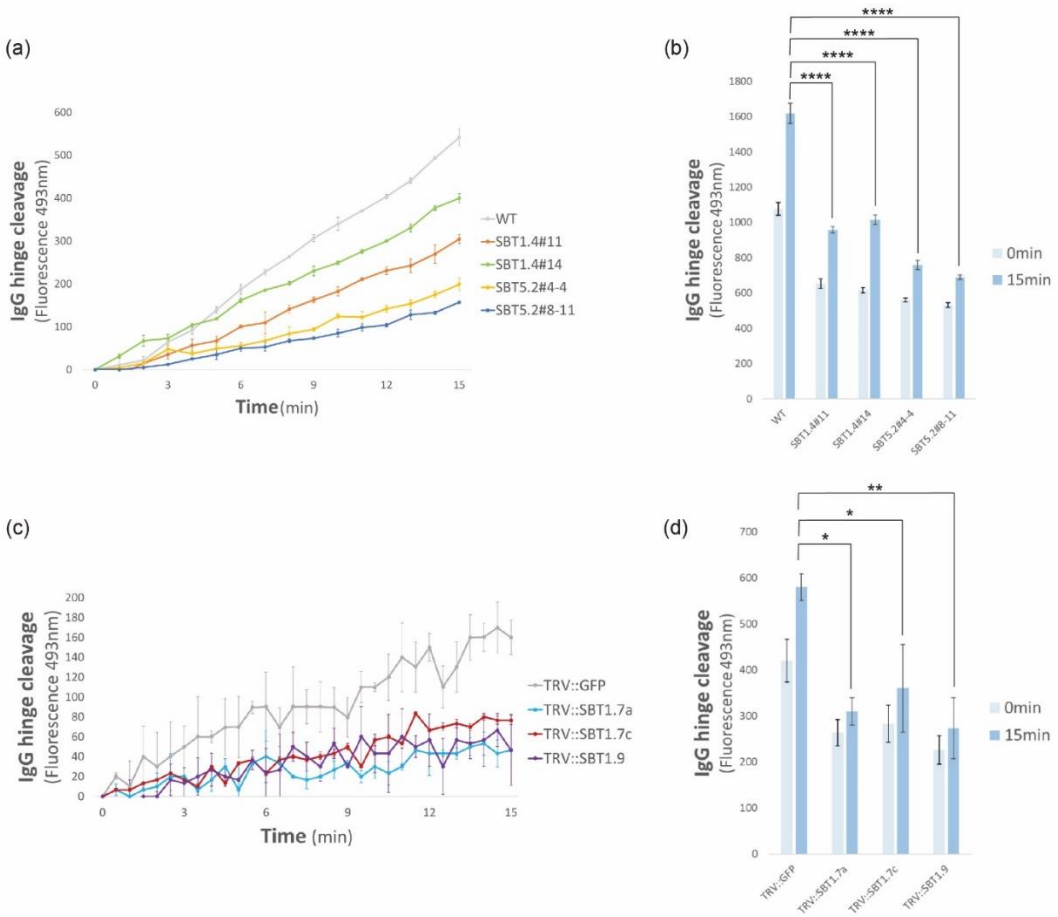

Figure 2.4 Quenched-IgG peptide cleavage is hindered in apoplastic fluids from SBT-silenced plants.

The quenched peptide was incubated with apoplastic fluids isolated from SBT-depleted *N. benthamiana* leaves, following knockout **(a, b)** or knockdown **(c, d)** approach. Wild-type plants or plants infiltrated with

TRV::GFP were used as negative controls, respectively. Graphs (a, c) were normalised for the first measurement (t=0), while graphs (b, d) depict the raw intensity values at zero and fifteen minutes. Error intervals: mean ±SE of n=3 technical replicates. Data were tested for normal distribution, while significance was determined with one-way ANOVA, following multiple comparisons and Tukey's post-hoc test. Error intervals: mean ±SE of n=3 technical replicates.

2.3 Fluorescent 2F5 is also cleaved in apoplastic fluid

To increase speed and accuracy of detecting *in vitro* processing of IgGs, we have established another method for rapid visualisation of IgGs in protein gels. The amine-reactive dye from the DyLight® series (Thermo Fisher Scientific), reacts with the antibody's lysine residues, leading to a fluorescent IgG, which can be detected by a fluorescence image scanner. Incubation of the dye with the pure IgG antibody for an hour is enough for *in vitro* assays. Fluorescent labelling does not prevent processing by proteases, enabling an efficient and fast way to screen for IgG processing patterns (**Figure 2.5c**). The cleavage site TTLF^{107}↓G^{108}VP is located at the variable heavy chain of 2F5 and can be recognised as an exposed loop as it is part of the extended H3 loop of the CDR (**Figure 2.5a**). We found that when 2F5 was incubated with apoplastic fluid from wild-type plants, an additional band at approximately 40 kDa was apparent, consistent with the published study (**Figure 2.5b,c**), which is the expected molecular weight of a heavy chain fragment after cleavage by the most abundant serine protease in the apoplast, *Nb*SBT1 (Puchol Tarazona et al., 2021).

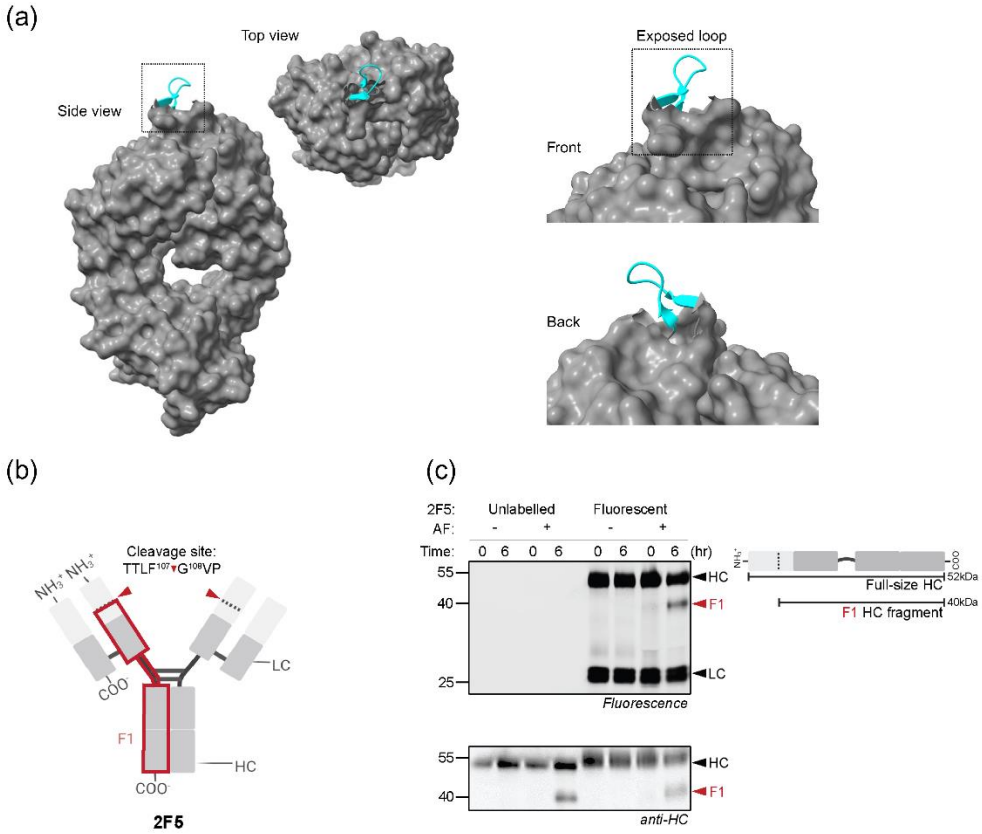

Figure 2.5 Amine-reactive dye labelling does not affect 2F5 cleavage in vitro.

(a) Side and top views of the 2F5 IgG (Fab' domain), obtained from PDB (left-hand side). The cleavage site is located at the exposed loop which is part of the extended H3 loop (cyan; front/back views at right-hand side). **(b)** Schematic representation of IgG antibody 2F5 with two LC and two HC, with the red arrow indicating the previously described cleavage site TTLF^{107}↓G^{108}VP (Puchol-Tarazona et al., 2021), caused by cleavage of 2F5 in the variable region of the HC, resulting in 12 and 40 kDa fragments. The detected 40 kDa F1 fragment is highlighted with a red box. **(c)** Processing of labelled and unlabelled 2F5 in apoplastic fluids. 2F5 was incubated with and without apoplastic fluids for 0 or 6 hours, separated on reducing protein gels and analysed by fluorescence scanning and western blotting using anti-HC antibodies.

2.4 2F5 processing is blocked by serine protease inhibitor PMSF

To confirm that cleavage of fluorescent 2F5 can be blocked by chemical protease inhibitors, we pre-incubated apoplastic fluids with either Cys protease inhibitor E-64 or

Ser protease inhibitor phenylmethylsulfonyl fluoride (PMSF) and then added fluorescent 2F5. Gel-based analysis revealed that PMSF but not E-64 can completely block processing of fluorescent 2F5 (**Figure 2.6a,b**), consistent with previous reports (Niemer et al., 2014). This indicates that a Ser protease is required for cleaving 2F5.

2.5 2F5 processing is blocked by subtilase inhibitor EPI1

To further test the effect of candidate protease inhibitors on IgG proteolysis, we tested the Kazal-like subtilase protease inhibitor Epi1, derived from *Phytophthora infestans* (Tian et al., 2005). Apoplastic fluid from Epi1 expressing plants was incubated for zero and six hours with the 2F5 antibody. Epi1 blocks 2F5 degradation, suggesting that subtilases cleave 2F5 in apoplastic fluid.

To test the effect of candidate protease inhibitors on IgG proteolysis, we isolated apoplastic fluids from leaves transiently expressing protease inhibitors *Hs*TIMP, *Sl*CYS8, *Sl*CDI, *Nb*Pot1, *Nb*PR4, Epi12 and Epi1, and two mutant inhibitor controls Ala*Hs*TIMP and *Sl*CYS8-Q47P (Grosse-Holz et al., 2018; **Figure 2.6c**; **Table 2.2**). Apart from Epi1, no other protease inhibitor was able to completely inhibit processing of 2F5 *in vitro*, but rather some delay it compared to EV control.

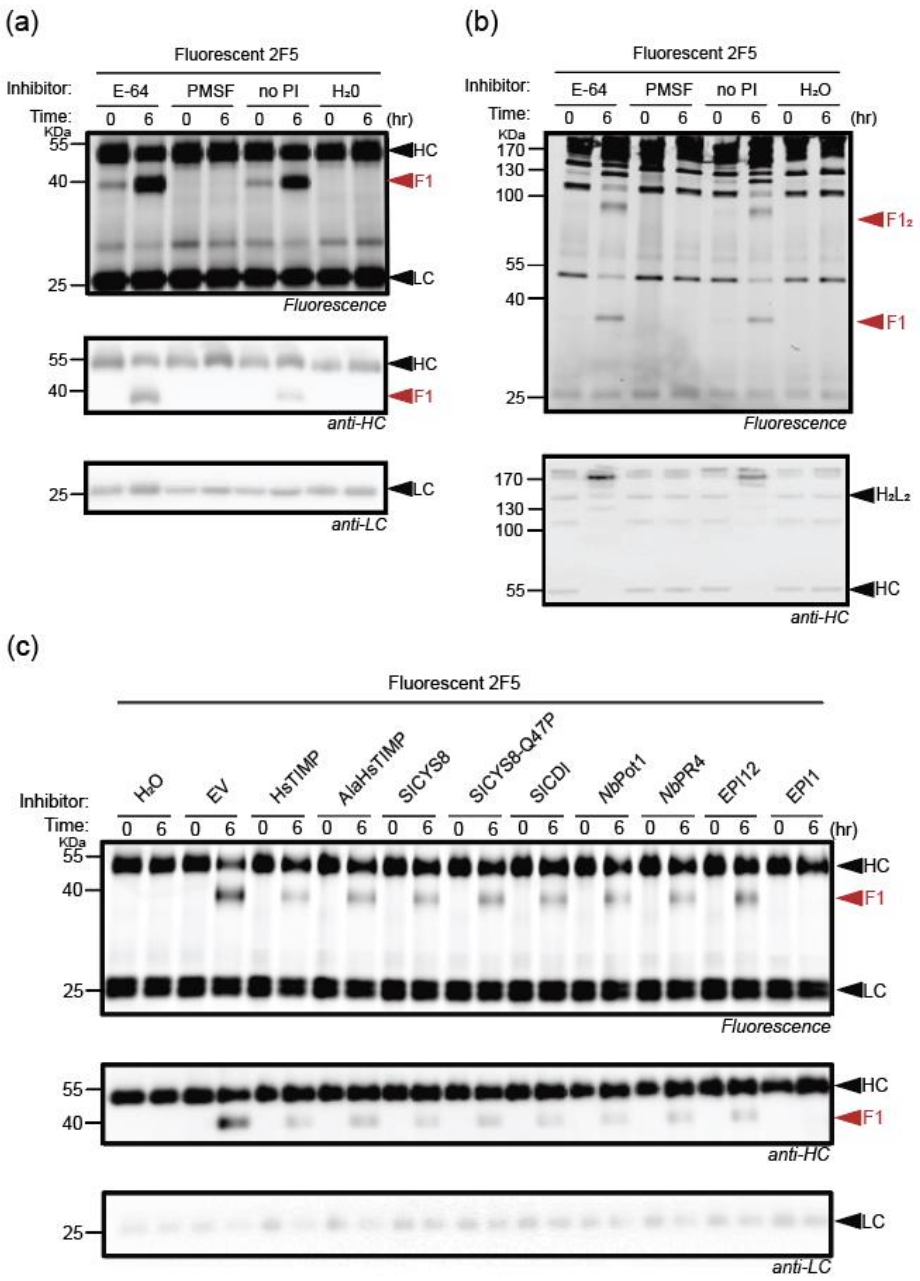

Figure 2.6 PMSF and Epi1 block 2F5 processing in apoplastic fluids.

(a) PMSF blocks 2F5 processing. Apoplastic fluids were incubated with Cys protease inhibitor E-64, Ser protease PMSF, AF+DMSO or water from left to right (negative controls) and 2F5 was added for 0 or 6 hours, separated on reducing protein gels and analysed by fluorescence scanning and western blotting using anti-HC and anti-LC antibodies. **(b)** Same as (a), run under non-reducing conditions. **(c)** Apoplastic fluids from plants transiently expressing various inhibitors were incubated with fluorescent 2F5 for 0 or 6 hours, separated on reducing or non-reducing protein gels and analysed by fluorescence scanning and western

blotting using anti-HC and anti-LC antibodies. Water and apoplastic fluids from empty vector (EV) agroinfiltrated plants were used as positive and negative controls from left to right. PI: protease inhibitor.

2.6 2F5 processing is hampered in SBT5.2-silenced plants

2.6.1 VIGS-mediated protease depletion

To examine which subtilase is responsible for 2F5 processing, plants were depleted of different subtilases using VIGS. We selected four subtilases that were consistently detected as active proteases in the apoplast of *Nicotiana benthamiana* by activity-based proteomics (Jutras et al., 2019; Puchol Tarazona et al., 2021; Sueldo et al., 2023). Plants were inoculated with tobacco rattle virus (TRV) carrying 300 bp fragments targeting these subtilases and a fragment of GFP as a negative control. Apoplastic fluids were isolated three weeks post TRV infection and incubated with fluorescent 2F5 antibody. Cleavage of the IgG is absent in apoplastic fluids isolated from *TRV::SBT5.2* plants and not from *TRV::GFP, TRV::SBT1.7a; TRV::SBT1.7c* or *TRV::SBT1.9a* plants (**Figure 2.7**), indicating that SBT5.2 is required for 2F5 processing in the apoplast.

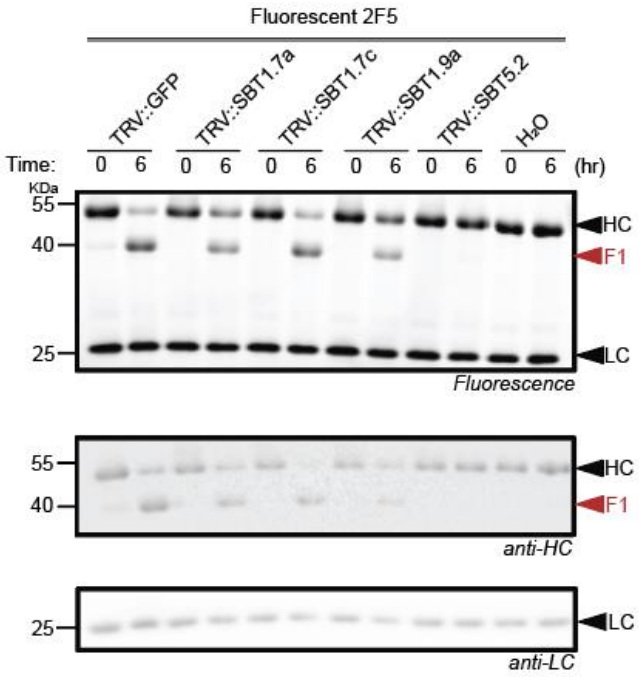

Figure 2.7. SBT5.2 silencing prevents 2F5 processing in apoplastic fluids.

Apoplastic fluids from plants silenced for different subtilases were incubated with fluorescent 2F5 for 0 or 6 hours, separated on reducing protein gels and analysed by fluorescence scanning and western blotting using anti-HC and anti-LC antibodies. Water incubated with the antibody was used as a negative control.

2.6.2 CRISPR-Cas protease depletion

SBT5.2 is the most abundant active protease in the apoplast of *N. benthamiana*, and was therefore also called SBT1 (Puchol Tarazona et al., 2021). Phylogenetic analysis of *N. benthamiana* subtilases, however, classifies this subtilase robustly in the SBT5.2 subfamily (Grosse-Holz et al., 2018; Paulus et al., 2020; **Figure 2.8a**). Analysis of our transcriptomic data (Grosse-Holz et al., 2018) revealed that there are three genes encoding SBT5.2, which are all expressed in agroinfiltrated leaves (**Figure 2.8b**). The 300 bp fragment designed by lab member Dr Pierre Buscaill and used for *SBT5.2* silencing, has sufficient homology to silence all three SBT5.2-encoding genes (**Figure 2.9**).

To generate knock-out *Nicotiana benthamiana* plants lacking all three SBT5.2 subtilases, we used CRISPR-Cas9 genome editing using six guide RNAs targeting all three genes. The homogeneity of mutants was confirmed by lab member Dr Shi-Jian Song. We were able to select two different triple knockout lines that have identical mutations in *SBT5.2a* and *SBT5.2b* but carry different mutations in *SBT5.2c* (**Figure 2.10**). The mutant lines grew indistinguishable from wild-type plants (**Figure 2.10b**). However, activity-based labelling of Ser hydrolases with FP-TAMRA (Liu et al., 1999) on apoplastic fluids isolated from these plants revealed that the major subtilase signal at 68 kDa is absent from these lines, with weak signals remaining at 70-74 kDa, presumably caused by other subtilases (**Figure 2.10c**). These data confirm that SBT5.2 proteases are the most abundant active subtilases in the apoplast of *N. benthamiana* leaves. Importantly, incubation of fluorescent 2F5 with these apoplastic fluids revealed that 2F5 processing is absent in apoplastic fluids from *sbt5.2* mutant plants (**Figure 2.10d**). These data are consistent with the *TRV::SBT5.2* experiments and further demonstrate that SBT5.2 is required for 2F5 processing in the apoplast.

(a)

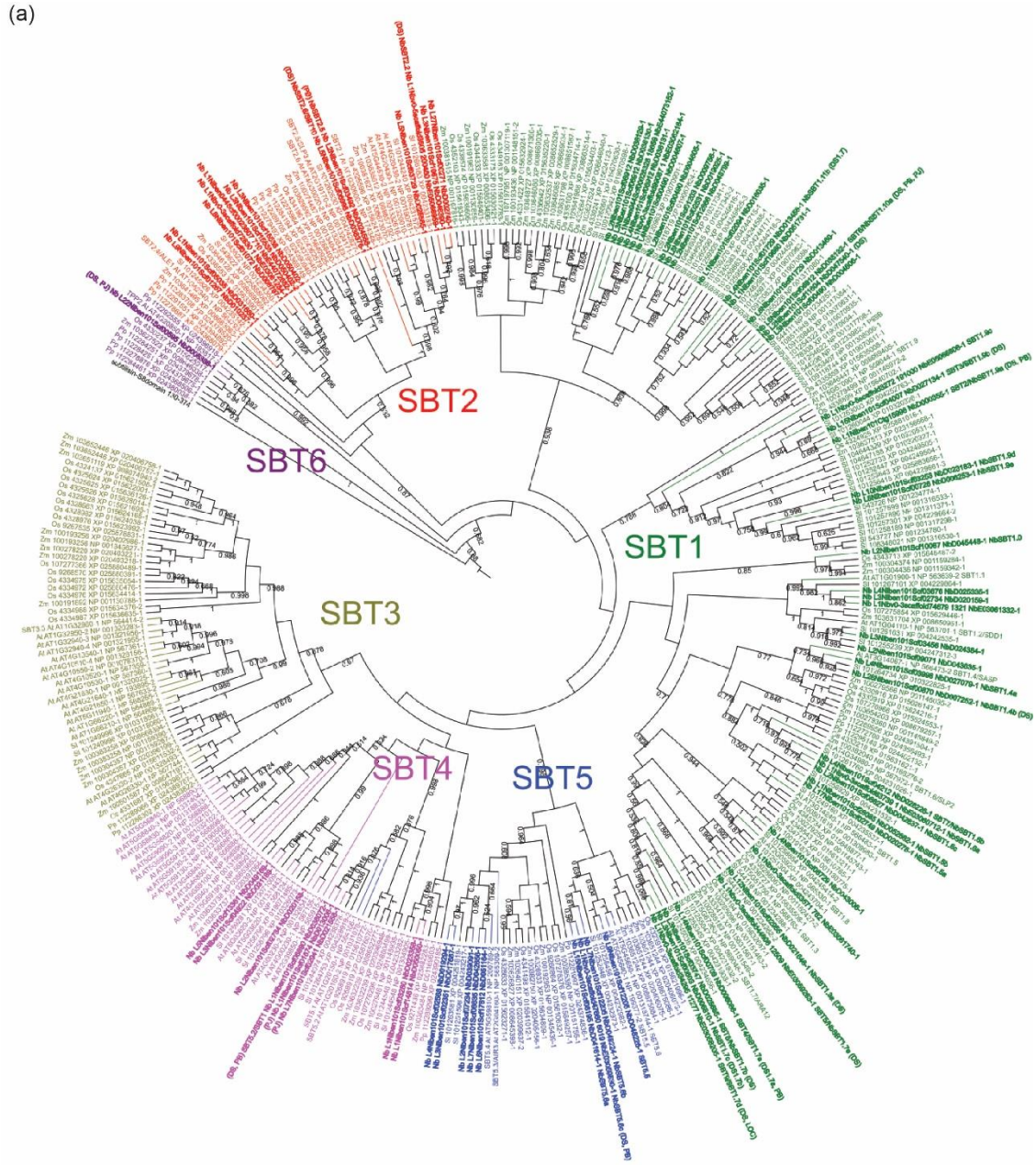

(b)

LAB360	Mock (mean)	Mock (SD)	Agroinfiltrated (mean)	Agroinfiltrated (SD)	Final name
NbL03g17160.1	0	0	0.093467031	0.042122779	*Nb* SBT5.2a
NbL16g29730.1	9.744890966	2.14370341	4.553243162	0.921318851	*Nb* SBT5.2b
NbL16g29740.1	0.618187564	0.27390427	0.523724281	0.303865567	*Nb* SBT5.2c

Figure 2.8 Phylogenetic analysis of subtilases and RPKM values for three *NbSBT5.2* genes.

(a) Phylogenetic analysis of subtilase-specific S8 domain protein sequences from *N. benthamiana* (**bold, *Nb***), *Arabidopsis thaliana* (*At*), *Oryza sativa* (*Os*), *Physcomitrium patens* (*Pp*), *Solanum lycopersicum* (*Sl*), and *Zea mays* (*Zm*). Subtilases form six subfamilies, SBT1-6**.** Phylogenetic tree was provided by Dr Pierre Buscaill. **(b)** Reads Per Kilobase of transcript per Million mapped reads (RPKM) values of *Nb*SBT5.2a, *Nb*SBT5.2b, and *Nb*SBT5.2c in mock-treated or agroinfiltrated plants (Grosse-Holz et al., 2018)**.**

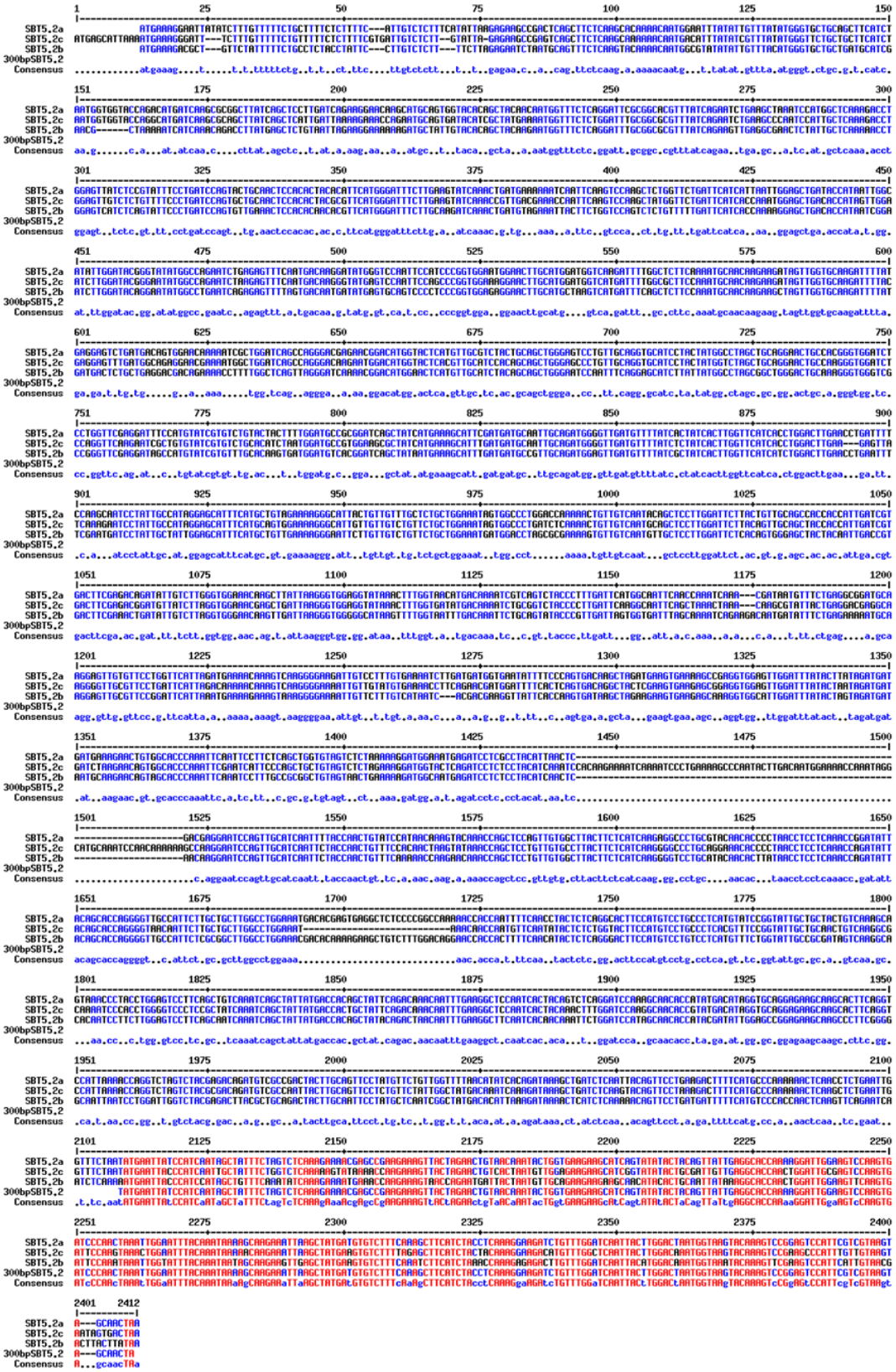

Figure 2.9 Alignment of VIGS fragments with three *SBT5.2* genes.

The 300bp fragment used for *SBT5.2* silencing has sufficient homology to silence all three SBT5.2-encoding genes.

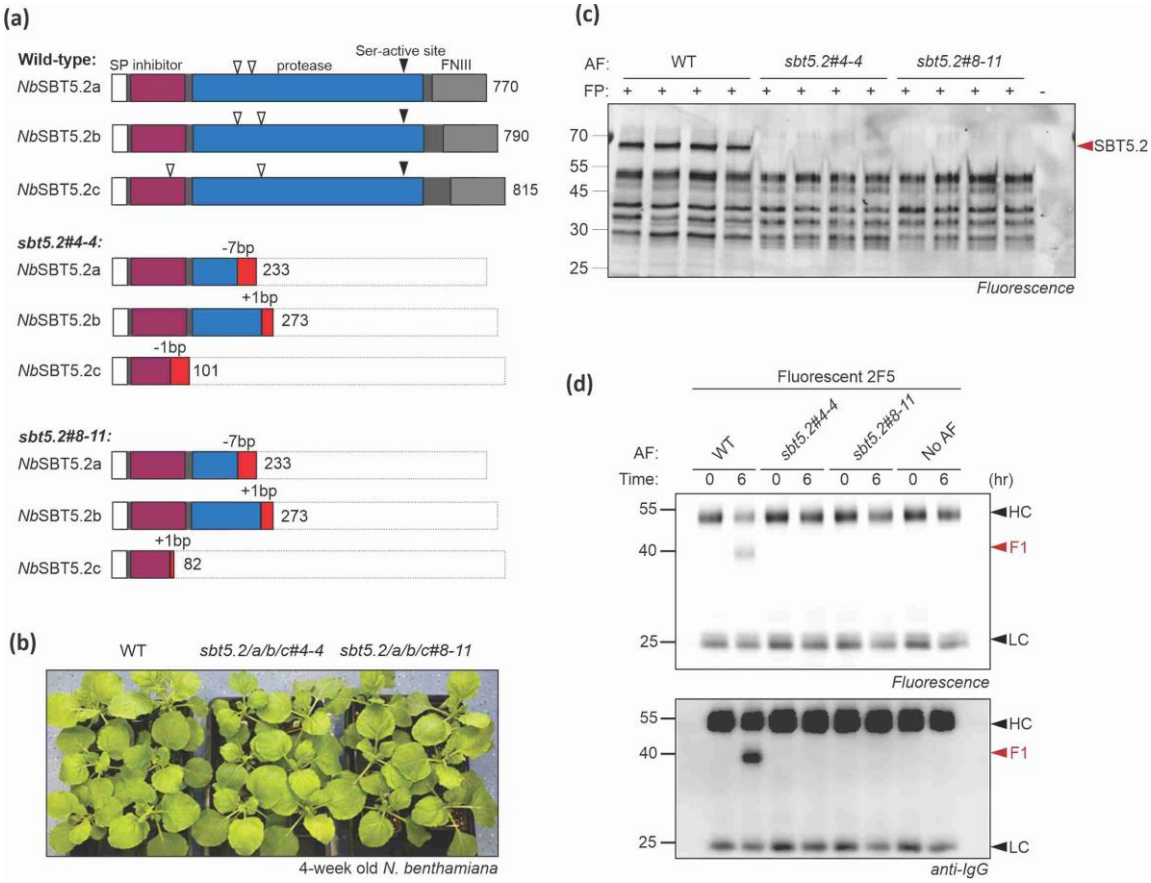

Figure 2.10 Triple *sbt5.2* knockouts lack the major active subtilase and cannot process 2F5 in apoplastic fluids.

(a) Schematic representation of the three SBT5.2 isoforms encoded in wild-type plants and the triple *sbt5.2* knockout lines. The protease comprises of a signal peptide (white), inhibitor domain (magenta), protease domain (blue), fibronectin type-III domain (FNIII; grey), the out-of-frame translation caused by frameshift mutations (red), and the non-translated ORF (dashed line). The positions of the sgRNAs used for gene editing are indicated in white arrows and the active site Ser with black arrows. **(b)** Both triple *sbt5.2* knockout lines grown indistinguishably from wild-type plants at 4-week growth. **(c)** The *sbt5.2* triple knockout lines lack the major active subtilase in the apoplast. Apoplastic fluids from four independent plants of wild-type or knockout lines were labelled with FP-TAMRA and separated on a 12% reducing SDS-PAGE gel and scanned for fluorescence. **(d)** 2F5 is not cleaved in apoplastic fluids of 2F5 knockout lines. Apoplastic fluids from wild-type and *sbt5.2* triple knockout plants were incubated with fluorescent 2F5 for 0 or 6 hours, separated on reducing protein gels and analysed by fluorescence scanning and western blotting using anti-HC and anti-LC antibodies. Water incubated with the antibody was used as a control.

2.7 COVA2-15 is more stable than the 2F5 antibody, while both E-64 and PMSF inhibitors can delay its processing

Compared to 2F5, degradation of which occurs within a few minutes, COVA2-15 appears to be stable when incubated in apoplastic fluids for at least 24 hours (**Figure 2.11b**), with processing being visible after 32 hours of *in vitro* incubation with apoplastic fluids (**Figure 2.11c**). COVA2-15 is partially degraded after 32 hours and this was also reduced by both Cys inhibitor E-64 and Ser inhibitor PMSF (**Figure 2.11d**), but not completely hindered. Regarding Epi1-expressing leaves, apoplastic fluids added in with COVA2-15 did not lead to blocking proteolysis after 48 hours as the IgG appears to get completely degraded at the 48-hour timepoint, leaving no traces of cleavage products (**Figure 2.11e**).

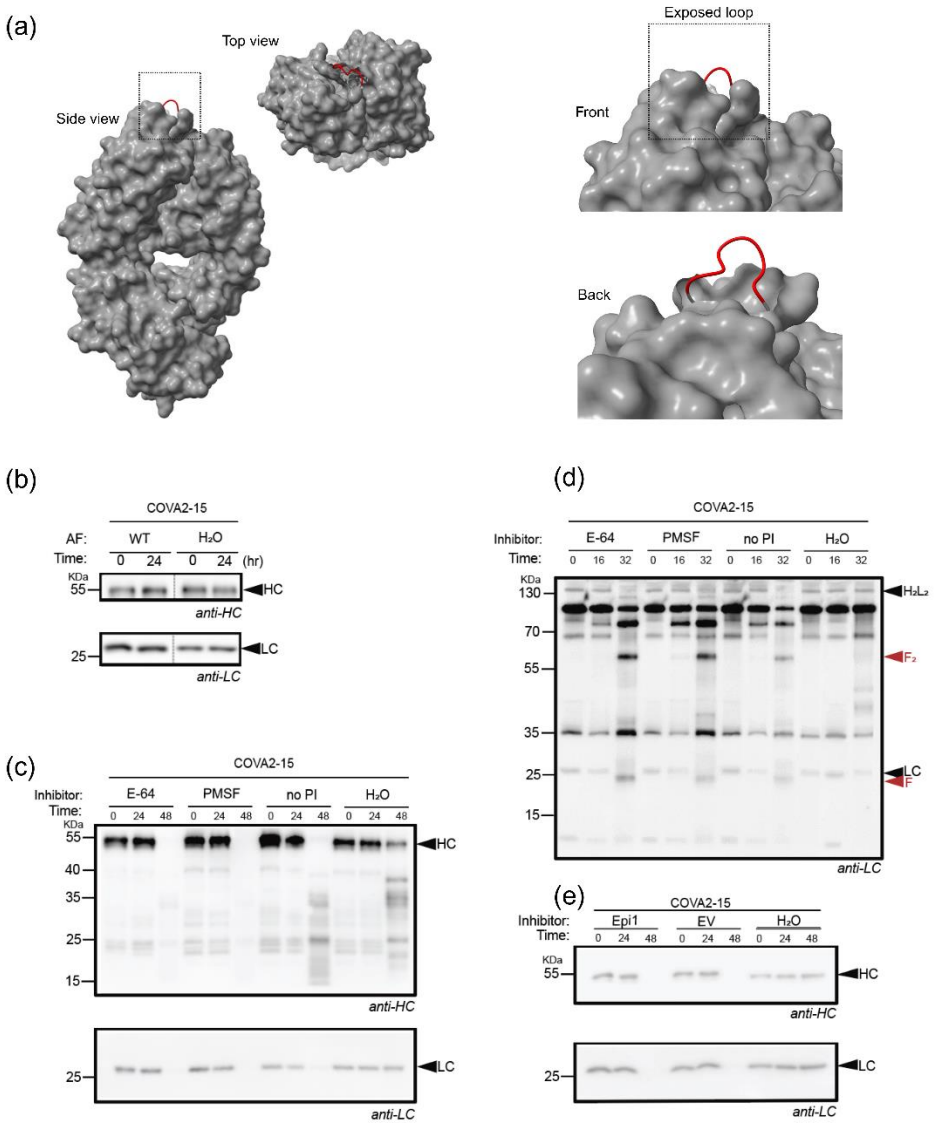

Figure 2.11 E-64 and PMSF can delay COVA2-15 processing in apoplastic fluids.

(a) Side and top views of the COVA2-15 IgG (Fab' domain), from AlphaFold prediction (left-hand side). The coloured loop is the aligned sequence with 2F5 IgG at the exposed loop where 2F5 cleavage site is located (red; front/back views at right-hand side). **(b)** Apoplastic fluids were incubated with COVA2-15 without protease inhibitors for 0 or 24 hours, separated on reducing protein gels and analysed by western blotting using anti-HC and anti-LC antibodies. **(c)** Apoplastic fluids were incubated with Cys protease inhibitor E-64, Ser protease PMSF, AF+DMSO or water from left to right (negative controls) and COVA2-15 was added for 0, 24 or 48 hours, separated on reducing protein gels and analysed by western blotting using anti-HC and anti-LC antibodies. **(d)** Apoplastic fluids were incubated with Cys protease inhibitor E-64, Ser protease PMSF, AF+DMSO or water from left to right (negative controls) and COVA2-15 was added for 0, 24 or 32

hours, separated on non-reducing protein gels and analysed by western blotting using anti-HC and anti-LC antibodies. **(e)** Apoplastic fluids from plants transiently expressing Epi1 was incubated with COVA2-15 for 0, 24 or 48 hours, separated on reducing protein gels and analysed by western blotting using anti-HC and anti-LC antibodies. Apoplastic fluids from empty vector (EV) agroinfiltrated plants or water were used as negative controls. PI: protease inhibitor.

2.8 2G4 processing is likely not mediated by SBT5.2

Compared to 2F5, 2G4 also appears to be stable when incubated in apoplastic fluids for at least 6 hours (**Figure 2.12b,c**). Regarding the chemical inhibitors E-64 and PMSF, or in Epi1-expressing apoplastic fluids, no difference can be observed, because 2G4 is stable for the duration of the *in vitro* assay (**Figure 2.12b,c**).

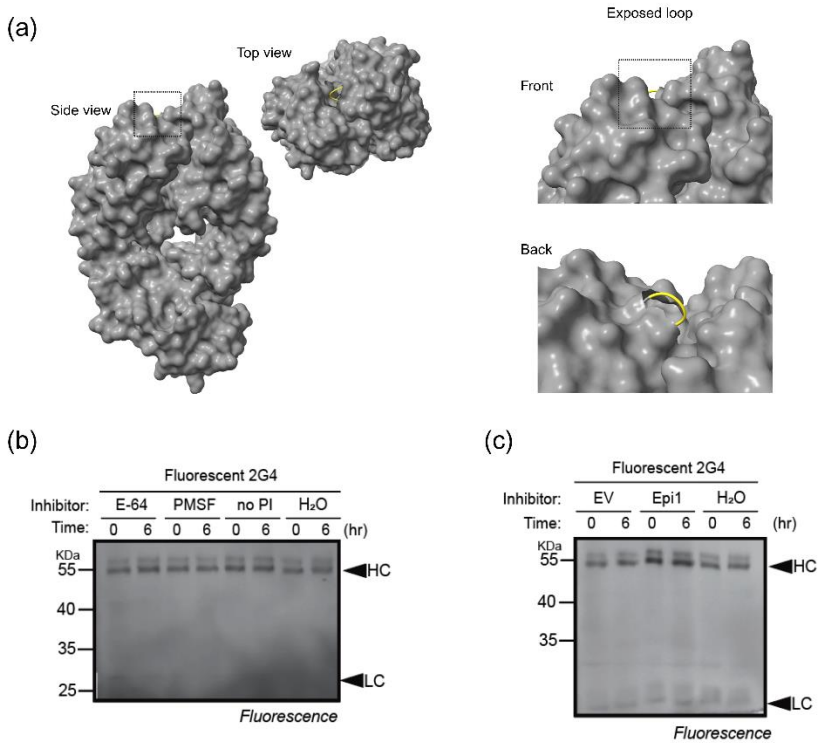

Figure 2.12 E-64 and PMSF can delay 2G4 processing in apoplastic fluids.

(a) Side and top views of the 2G4 IgG (Fab' domain), from AlphaFold prediction (left-hand side). The coloured loop is the aligned sequence with 2F5 IgG at the exposed loop where 2F5 cleavage site is located

(yellow; front/back views at right-hand side). **(b)** Apoplastic fluids were incubated with Cys protease inhibitor E-64, Ser protease PMSF, AF+DMSO or water from left to right (negative controls) and 2G4 was added for 0 or 6 hours, separated on reducing protein gels and analysed by fluorescence scanning. **(c)** Apoplastic fluids from plants transiently expressing Epi1 was incubated with 2G4 for 0 or 6 hours, separated on reducing protein gels and analysed by fluorescence scanning. Apoplastic fluids from empty vector (EV) agroinfiltrated plants or water were used as negative controls. PI: protease inhibitor.

Conclusions and Discussion

In this Chapter, we first examined the effect of inhibitors or protease silencing on the processing of the site upstream the hinge, a domain which is common across different IgGs and is located between the CH1 and CH2 domains of the constant heavy chain (Vidarsson et al., 2014). Protease inhibitors PMSF and Epi1 could inhibit hinge cleavage, confirming that in apoplastic fluids subtilases are responsible for this processing (**Figure 2.2, 2.3**). After testing several SBT-depleted plants, they all exhibited inhibition of the peptide processing, with *sbt*1.4 and *sbt*5.2 mutants leading to the strongest inhibition compared to the control (**Figure 2.4**). This same cleavage site was also confirmed by the literature in different antibodies such as a truncated form of the 2F5 heavy chain, leaving a 30 kDa degradation fragment (Niemer et al., 2014), the IgG antibodies 2G12 and H10 (Hehle et al., 2015). However, as our assay only contains the peptide in question, the way that each whole IgG antibody is folded, could affect the accessibility of the CH1-hinge domain to proteases *in vivo*, ultimately leading to different degradation patterns.

In these experiments the plant protease-mediated degradation pattern of different IgGs, 2F5, COVA2-15 and 2G4, was investigated using gel-based approaches to identify their fragmentation. The *in vitro assays* consisted of incubation of pure antibodies with apoplastic fluid (AF) from e wild-type plants, plants expressing the protease inhibitors, or plants depleted of proteases. When incubating pure 2F5 with AF from wild-type plants, the effect of the chemical protease inhibitors PMSF and E-64 was assessed. Detecting antibody degradation was accomplished by western blotting, Coomassie staining, or by detecting fluorescence from an appropriately labelled, pure 2F5 antibody. When the 2F5 antibody was incubated in vitro with AF from WT plants in the absence of chemical

inhibitors, or from plants expressing an empty vector, an additional band at approximately 40 kDa was apparent, consistent with the recent study where it is demonstrated that subtilisin-like protease *Nb*SBT1, which is homologous to Arabidopsis thaliana SBT5.2, can cleave 2F5 at one position, resulting in an intact light chain and two heavy chain fragments arising from cleavage at TTLF^{107}↓G^{108}VP that were detected by mass spectrometry (Puchol Tarazona et al., 2021). This cleavage site is located at the CDR H3 extended loop. Importantly, addition of PMSF or apoplastic fluid containing the Epi1 protease inhibitor suppresses cleavage. Cleavage is also prevented in apoplastic fluids of SBT5.2-depleted plants, confirming this hypothesis. Taken together, these experiments demonstrate that SBT5.2 is responsible for processing the H3 loop of fully assembled 2F5 in apoplastic fluids.

Surprisingly the COVA2-15 antibody is more stable than 2F5 for at least 24 hours in apoplastic fluids, with degradation fragments possibly resulting from processing of the light chain instead. For the heavy chain, although this is degraded at later timepoints, there is no readily discernible fragment compared to the water control that could indicate protease processing. The fragments observed might be due to long incubation at room temperature due to the assays' setup (**Figure 2.11c**). On the contrary, the light chain resulted in an additional fragment (F fragment) at around 20 kDa with is smaller than an intact light chain of 25-28 kDa (**Figure 2.11d**). However, the addition of chemical protease inhibitors did not alter the fragmentation pattern, but rather delayed its processing which might indicate processing by different types of proteases or sequential processing. Mass spectrometry analysis for fragments released after degradation is needed to confirm the protease cleavage sites. The 2G4 antibody appeared to be more stable than 2F5 and less stable than COVA2-15, as degradation was observed after 24

hours of its incubation with apoplastic fluids (**Figure 2.12**). However, in this case no specific proteolytic patterns were detected that were different to the water control, making it difficult to draw a conclusion about candidate proteases or cleavage products.

IgG degradation is generally examined using *in vitro* assays and western blot analysis for the light and heavy chains. However, this method does not exclude antibodies with incomplete epitopes, which can result in underestimation of the extent of IgG proteolysis (Hehle et al., 2015). Moreover, some IgG fragments being observed can represent assembly intermediates of IgGs, such as free heavy or light chains, Fab, Fab', H/L heterodimers or H/H homodimers making the determination of cleavage fragments more complex. Antibody sequencing has been used to provide a more detailed profile of antibody fragments, with strategies such as Edman degradation for N-terminal peptide sequencing or mass spectrometry (MS)-based methods (Mao et al., 2019; Peng et al., 2021; Vlasak & Ionescu, 2011). MS-based methods for antibody sequencing consists of a bottom-up liquid chromatography tandem mass spectrometry (LC-MS/MS) workflow, where antibodies are cleaved in even smaller fragments with specific protease cocktails for subsequent analyses (Peng et al., 2021). Another caveat would be determining the existence of a proteolytic cascade. Although in plants sequential processing research is fragmentary, there are examples in eukaryotes that validate this theory. For example, furin, which is a subtilisin-like S8 protease residing in the Golgi can further activate MMP11 (stromelysin-3) and MMP14 (MT1-MMP) (Pei & Weiss, 1995). Another example comes in response to injury, where tissue factor is released and forms a complex with the serine protease FVII, activating it and triggering the activation of protease FX, which then activates thrombin to cleave fibrinogen into fibrin, forming a blood clot (Amara et al., 2008). Subtilisin and pepsin protease families are extended protease families that may

have been evolved to participate in proteolytic cascades (Paulus & Van Der Hoorn, 2019). Moreover, there are additional caveats to take into account when it comes to using apoplastic fluids from plants expressing different protease inhibitors, as shown on **Figures 2.2**, **2.3**, and **2.6**. The lack of information on the expression levels of co-expressed protease inhibitors introduces several limitations in interpreting the impact on IgG degradation. Without quantifying these inhibitors, it is unclear whether they are present in sufficient amounts to effectively prevent recombinant protein degradation, leading to uncertainty about their actual protective role. Variability in transient expression can result in fluctuating levels of the inhibitor, making it difficult to ensure consistency across experiments. Additionally, some protease inhibitors may have off-target effects on plant metabolism, potentially influencing protein production or plant fitness in unintended ways.

References

Amara, U., Rittirsch, D., Flierl, M., Bruckner, U., Klos, A., Gebhard, F., Lambris, J. D., Huber-Lang, M., & Lambris, J. D. (2008). *Interaction Between the Coagulation and Complement System*.

Bryson, S., Julien, J.-P., Hynes, R. C., & Pai, E. F. (2009). Crystallographic Definition of the Epitope Promiscuity of the Broadly Neutralizing Anti-Human Immunodeficiency Virus Type 1 Antibody 2F5: Vaccine Design Implications. *Journal of Virology*, *83*(22), 11862–11875. https://doi.org/10.1128/JVI.01604-09

Davidson, E., Bryan, C., Fong, R. H., Barnes, T., Pfaff, J. M., Mabila, M., Rucker, J. B., & Doranz, B. J. (2015). Mechanism of Binding to Ebola Virus Glycoprotein by the ZMapp, ZMAb, and MB-003 Cocktail Antibodies. *Journal of Virology*, *89*(21), 10982–10992. https://doi.org/10.1128/JVI.01490-15

De Muynck, B., Navarre, C., Nizet, Y., Stadlmann, J., & Boutry, M. (2009). Different subcellular localization and glycosylation for a functional antibody expressed in Nicotiana tabacum plants and suspension cells. *Transgenic Research*, *18*(3), 467–482. https://doi.org/10.1007/s11248-008-9240-1

Deveuve, Q., Lajoie, L., Barrault, B., & Thibault, G. (2020). The Proteolytic Cleavage of Therapeutic Monoclonal Antibody Hinge Region: More Than a Matter of Subclass. *Frontiers in Immunology*, *11*. https://doi.org/10.3389/fimmu.2020.00168

Diego-Martin, B., González, B., Vazquez-Vilar, M., Selma, S., Mateos-Fernández, R., Gianoglio, S., Fernández-del-Carmen, A., & Orzáez, D. (2020). Pilot Production of SARS-CoV-2 Related Proteins in Plants: A Proof of Concept for Rapid Repurposing of Indoor Farms Into Biomanufacturing Facilities. *Frontiers in Plant Science*, *11*. https://doi.org/10.3389/fpls.2020.612781

Donini, M., Lombardi, R., Lonoce, C., Di Carli, M., Marusic, C., Morea, V., & Di Micco, P. (2015). Antibody proteolysis: a common picture emerging from plants. *Bioengineered*, *6*(5), 299–302. https://doi.org/10.1080/21655979.2015.1067740

Escandón, M., Bigatton, E. D., Guerrero-Sánchez, V. M., Hernández-Lao, T., Rey, M. D., Jorrín-Novo, J. V., & Castillejo, M. A. (2022). Identification of Proteases and Protease Inhibitors in Seeds of the Recalcitrant Forest Tree Species Quercus ilex. *Frontiers in Plant Science*, *13*. https://doi.org/10.3389/fpls.2022.907042

Gorevic, P. D., Prelli, F. C., & Frangione, B. (1985). [1] Immunoglobulin G (IgG). *Methods in Enzymology*, *116*, 3–25. https://doi.org/10.1016/S0076-6879(85)16003-9

Göritzer, K., Groppelli, E., Grünwald-Gruber, C., Figl, R., Ni, F., Hu, H., Li, Y., Liu, Y., Hu, Q., Puligedda, R. D., Jung, J. W., Strasser, R., Dessain, S., & Ma, J. K. C. (2024). Recombinant neutralizing secretory IgA antibodies for preventing mucosal acquisition and transmission of SARS-CoV-2. *Molecular Therapy*, *32*(3), 689–703. https://doi.org/10.1016/j.ymthe.2024.01.025

Goulet, C., Khalf, M., Sainsbury, F., D'Aoust, M. A., & Michaud, D. (2012a). A protease activity-depleted environment for heterologous proteins migrating towards the leaf cell apoplast.

Plant Biotechnology Journal, *10*(1), 83–94. https://doi.org/10.1111/j.1467-7652.2011.00643.x

Goulet, C., Khalf, M., Sainsbury, F., D'Aoust, M.-A., & Michaud, D. (2012b). A protease activity–depleted environment for heterologous proteins migrating towards the leaf cell apoplast. *Plant Biotechnology Journal*, *10*(1), 83–94. https://doi.org/https://doi.org/10.1111/j.1467-7652.2011.00643.x

Grosse-Holz, F., Kelly, S., Blaskowski, S., Kaschani, F., Kaiser, M., & van der Hoorn, R. A. L. (2018). The transcriptome, extracellular proteome and active secretome of agroinfiltrated Nicotiana benthamiana uncover a large, diverse protease repertoire. *Plant Biotechnology Journal*, *16*(5), 1068–1084. https://doi.org/10.1111/pbi.12852

Grosse-Holz, F., Madeira, L., Zahid, M. A., Songer, M., Kourelis, J., Fesenko, M., Ninck, S., Kaschani, F., Kaiser, M., & van der Hoorn, R. A. L. (2018). Three unrelated protease inhibitors enhance accumulation of pharmaceutical recombinant proteins in Nicotiana benthamiana. *Plant Biotechnology Journal*, *16*(10), 1797–1810. https://doi.org/10.1111/pbi.12916

Hehle, V. K., Lombardi, R., van Dolleweerd, C. J., Paul, M. J., Di Micco, P., Morea, V., Benvenuto, E., Donini, M., & Ma, J. K. C. (2015). Site-specific proteolytic degradation of IgG monoclonal antibodies expressed in tobacco plants. *Plant Biotechnology Journal*, *13*(2), 235–245. https://doi.org/10.1111/pbi.12266

Hehle, V. K., Paul, M. J., Drake, P. M., Ma, J. K. C., & van Dolleweerd, C. J. (2011). Antibody degradation in tobacco plants: A predominantly apoplastic process. *BMC Biotechnology*, *11*. https://doi.org/10.1186/1472-6750-11-128

Julien, J.-P., Bryson, S., Nieva, J. L., & Pai, E. F. (2008). Structural details of HIV-1 recognition by the broadly neutralizing monoclonal antibody 2F5: epitope conformation, antigen-recognition loop mobility, and anion-binding site. *Journal of Molecular Biology*, *384*(2), 377–392. https://doi.org/10.1016/j.jmb.2008.09.024

Jutras, P. V, Dodds, I., & van der Hoorn, R. A. L. (2020). Proteases of Nicotiana benthamiana: an emerging battle for molecular farming. *Current Opinion in Biotechnology*, *61*, 60–65. https://doi.org/https://doi.org/10.1016/j.copbio.2019.10.006

Jutras, P. V., Grosse-Holz, F., Kaschani, F., Kaiser, M., Michaud, D., & van der Hoorn, R. A. L. (2019). Activity-based proteomics reveals nine target proteases for the recombinant protein-stabilizing inhibitor SlCYS8 in Nicotiana benthamiana. *Plant Biotechnology Journal*, *17*(8), 1670–1678. https://doi.org/10.1111/pbi.13092

Jutras, P. V, Marusic, C., Lonoce, C., Deflers, C., Goulet, M.-C., Benvenuto, E., Michaud, D., & Donini, M. (2016). An Accessory Protease Inhibitor to Increase the Yield and Quality of a Tumour-Targeting mAb in Nicotiana benthamiana Leaves. *PLOS ONE*, *11*(11), e0167086. https://doi.org/10.1371/journal.pone.0167086

Liu, Y., Schiff, M., & Dinesh-Kumar, S. P. (2002). Virus-induced gene silencing in tomato. *Plant Journal*, *31*(6), 777–786. https://doi.org/10.1046/j.1365-313X.2002.01394.x

Lombardi, R., Circelli, P., Villani, M. E., Buriani, G., Nardi, L., Coppola, V., Bianco, L., Benvenuto, E., Donini, M., & Marusic, C. (2009). High-level HIV-1 Nef transient expression in Nicotiana

benthamiana using the P19 gene silencing suppressor protein of Artichoke Mottled Crinckle Virus. *BMC Biotechnology*, *9*. https://doi.org/10.1186/1472-6750-9-96

M Brouwer, P. J., Caniels, T. G., van der Straten, K., Snitselaar, J. L., Aldon, Y., Bangaru, S., Torres, J. L., A Okba, N. M., Claireaux, M., Kerster, G., H Bentlage, A. E., van Haaren, M. M., Guerra, D., Burger, J. A., Schermer, E. E., Verheul, K. D., van der Velde, N., van der Kooi, A., van Schooten, J., … van Gils, M. J. (2020). *Potent neutralizing antibodies from COVID-19 patients define multiple targets of vulnerability*. https://www.science.org

Mao, Y., Zhang, L., Kleinberg, A., Xia, Q., Daly, T. J., & Li, N. (2019). Fast protein sequencing of monoclonal antibody by real-time digestion on emitter during nanoelectrospray. *MAbs*, *11*(4), 767–778. https://doi.org/10.1080/19420862.2019.1599633

Neefjes, J., & Dantuma, N. P. (2004). Fluorescent probes for proteolysis: Tools for drug discovery. In *Nature Reviews Drug Discovery* (Vol. 3, Issue 1, pp. 58–69). Nature Publishing Group. https://doi.org/10.1038/nrd1282

Niemer, M., Mehofer, U., Torres Acosta, J. A., Verdianz, M., Henkel, T., Loos, A., Strasser, R., Maresch, D., Rademacher, T., Steinkellner, H., & Mach, L. (2014). The human anti-HIV antibodies 2F5, 2G12, and PG9 differ in their susceptibility to proteolytic degradation: Down-regulation of endogenous serine and cysteine proteinase activities could improve antibody production in plant-based expression platforms. *Biotechnology Journal*, *9*(4), 493–500. https://doi.org/10.1002/biot.201300207

Ocampo, C. G., Lareu, J. F., Marin Viegas, V. S., Mangano, S., Loos, A., Steinkellner, H., & Petruccelli, S. (2016). Vacuolar targeting of recombinant antibodies in Nicotiana benthamiana. *Plant Biotechnology Journal*, *14*(12), 2265–2275. https://doi.org/10.1111/pbi.12580

Ofek, G., Tang, M., Sambor, A., Katinger, H., Mascola, J. R., Wyatt, R., & Kwong, P. D. (2004). Structure and Mechanistic Analysis of the Anti-Human Immunodeficiency Virus Type 1 Antibody 2F5 in Complex with Its gp41 Epitope. *Journal of Virology*, *78*(19), 10724–10737. https://doi.org/10.1128/jvi.78.19.10724-10737.2004

Paulus, J. K., Kourelis, J., Ramasubramanian, S., Homma, F., Godson, A., Hörger, A. C., Hong, N., Krahn, D., Carballo, L. O., Wang, S., Win, J., Smoker, M., Kamoun, S., Dong, S., & Van Der Hoorn, R. A. L. (2020). *Extracellular proteolytic cascade in tomato activates immune protease Rcr3*. https://doi.org/10.1073/pnas.1921101117/-/DCSupplemental

Paulus, J. K., & Van Der Hoorn, R. A. L. (2019). Do proteolytic cascades exist in plants? *Journal of Experimental Botany*, *70*(7), 1997–2002. https://doi.org/10.1093/jxb/erz016

Pei, D., & Weiss, SJ. (1995). Furin-dependent Intracellular Activation Of The Human Stromelysin-3 Zymogen. *Nature*, *375*(6528), 244–247.

Peng, W., Pronker, M. F., & Snijder, J. (2021). Mass Spectrometry-BasedDe NovoSequencing of Monoclonal Antibodies Using Multiple Proteases and a Dual Fragmentation Scheme. *Journal of Proteome Research*, *20*(7), 3559–3566. https://doi.org/10.1021/acs.jproteome.1c00169

Porter, R. R. (1959). The hydrolysis of rabbit γ-globulin and antibodies with crystalline papain. *Biochem J.*, *73 (1)*, 119–127.

Puchol Tarazona, A. A., Maresch, D., Grill, A., Bakalarz, J., Torres Acosta, J. A., Castilho, A., Steinkellner, H., & Mach, L. (2021). Identification of two subtilisin-like serine proteases engaged in the degradation of recombinant proteins in Nicotiana benthamiana. *FEBS Letters*, *595*(3), 379–388. https://doi.org/https://doi.org/10.1002/1873-3468.14014

Robert, S., Goulet, M.-C., D'Aoust, M.-A., Sainsbury, F., & Michaud, D. (2015). Leaf proteome rebalancing in Nicotiana benthamiana for upstream enrichment of a transiently expressed recombinant protein. *Plant Biotechnology Journal*, *13*(8), 1169–1179. https://doi.org/https://doi.org/10.1111/pbi.12452

Robert, S., Khalf, M., Goulet, M. C., D'Aoust, M. A., Sainsbury, F., & Michaud, D. (2013a). Protection of Recombinant Mammalian Antibodies from Development-Dependent Proteolysis in Leaves of Nicotiana benthamiana. *PLoS ONE*, *8*(7). https://doi.org/10.1371/journal.pone.0070203

Robert, S., Khalf, M., Goulet, M.-C., D'Aoust, M.-A., Sainsbury, F., & Michaud, D. (2013b). Protection of Recombinant Mammalian Antibodies from Development-Dependent Proteolysis in Leaves of Nicotiana benthamiana. *PLOS ONE*, *8*(7), e70203-. https://doi.org/10.1371/journal.pone.0070203

Robotham, A. C., & Kelly, J. F. (2020). Chapter 1 - LC-MS characterization of antibody-based therapeutics: recent highlights and future prospects. In A. Matte (Ed.), *Approaches to the Purification, Analysis and Characterization of Antibody-Based Therapeutics* (pp. 1–33). Elsevier. https://doi.org/https://doi.org/10.1016/B978-0-08-103019-6.00001-1

Sack, M., Paetz, A., Kunert, R., Bomble, M., Hesse, F., Stiegler, G., Fischer, R., Katinger, H., Stoeger, E., & Rademacher, T. (2007). Functional analysis of the broadly neutralizing human anti-HIV-1 antibody 2F5 produced in transgenic BY-2 suspension cultures. *The FASEB Journal*, *21*(8), 1655–1664. https://doi.org/https://doi.org/10.1096/fj.06-5863com

Schillberg, S., Zimmermann, S., Voss, A., & Fischer, R. (1999). Apoplastic and cytosolic expression of full-size antibodies and antibody fragments in Nicotiana tabacum. In *Transgenic Research* (Vol. 8).

Sharp, J. M., & Doran, P. M. (2001). Characterization of monoclonal antibody fragments produced by plant cells. *Biotechnology and Bioengineering*, *73*(5), 338–346. https://doi.org/10.1002/bit.1067

Soleimany, A. P., Martin-Alonso, C., Anahtar, M., Wang, C. S., & Bhatia, S. N. (2022). Protease Activity Analysis: A Toolkit for Analyzing Enzyme Activity Data. *ACS Omega*, *7*(28), 24292–24301. https://doi.org/10.1021/acsomega.2c01559

Stevens, L. H., Stoopen, G. M., Elbers, I. J. W., Molthoff, J. W., Bakker, H. A. C., Lommen, A., Bosch, D., & Jordi, W. (1994). *Effect of Climate Conditions and Plant Developmental Stage on the Stability of Antibodies Expressed in Transgenic Tobacco*. Whitelam and Cockburn. https://academic.oup.com/plphys/article/124/1/173/6098837

Sueldo, D. J., Godson, A., Kaschani, F., Krahn, D., Kessenbrock, T., Buscaill, P., Schofield, C. J., Kaiser, M., & van der Hoorn, R. A. L. (2023). Activity-based proteomics uncovers suppressed hydrolases and a neo-functionalised antibacterial enzyme at the plant–pathogen interface. *New Phytologist*. https://doi.org/10.1111/nph.18857

Suzuki, S., Annaka, H., Konno, S., Kumagai, I., & Asano, R. (2018). Engineering the hinge region of human IgG1 Fc-fused bispecific antibodies to improve fragmentation resistance. *Scientific Reports*, *8*(1), 17253. https://doi.org/10.1038/s41598-018-35489-y

Tian, M., Benedetti, B., & Kamoun, S. (2005). A second Kazal-like protease inhibitor from Phytophthora infestans inhibits and interacts with the apoplastic pathogenesis-related protease P69B of tomato. *Plant Physiology*, *138*(3), 1785–1793. https://doi.org/10.1104/pp.105.061226

Vidarsson, G., Dekkers, G., & Rispens, T. (2014). IgG subclasses and allotypes: From structure to effector functions. *Frontiers in Immunology*, *5*(OCT). https://doi.org/10.3389/fimmu.2014.00520

Vlasak, J., & Ionescu, R. (2011). Fragmentation of monoclonal antibodies. In *mAbs* (Vol. 3, Issue 3, pp. 253–263). https://doi.org/10.4161/mabs.3.3.15608

Wang, S., Xing, R., Wang, Y., Shu, H., Fu, S., Huang, J., Paulus, J. K., Schuster, M., Saunders, D. G. O., Win, J., Vleeshouwers, V., Wang, Y., Zheng, X., van der Hoorn, R. A. L., & Dong, S. (2021). Cleavage of a pathogen apoplastic protein by plant subtilases activates host immunity. *New Phytologist*, *229*(6), 3424–3439. https://doi.org/10.1111/nph.17120

Chapter 3

In vivo processing of IgGs: Towards identifying proteases responsible for IgG degradation

Part of this Chapter is published as: Beritza, K., et al., (2024), SBT5.2s are the major active extracellular subtilases processing IgG antibody 2F5 in the Nicotiana benthamiana apoplast. Plant Biotechnol. J., Vol22, p.2808.

3.1 Introduction

Proteases are abundant enzymes found in all organisms that degrade proteins irreversibly, thus terminating their function and removing it from the cell (Thomas & van der Hoorn, 2018). In *N. benthamiana*, about 1,243 putative proteases act in different subcellular compartments, including the cytosol, the vacuole, the chloroplast, the mitochondria, and the lysosome, or they are delivered extracellularly, residing in the apoplast (Jutras, Dodds, et al., 2020). However, not all proteases are thought to degrade recombinant proteins. For instance, as organelle-specific proteases that are not present along the secretory pathway the recombinant proteins usually travel to ultimately reach the extracellular space. Moreover, some proteases are not expressed in leaves where overexpression occurs in transient expression techniques. Several studies have reported recombinant protein processing along the secretory pathway by proteases residing in the endoplasmic reticulum, the Golgi, the vacuole and ultimately the apoplast (Badri et al., 2009; Benchabane et al., 2008; De Muynck et al., 2009; Jutras, Sainsbury, et al., 2020; Schiermeyer et al., 2005). Subtilase-like proteases, papain-like Cys proteases (PLCPs), and pepsin-like Asp proteases are the key proteases that seem to be involved in recombinant protein processing, with the majority of these protease families being associated with plant senescence (Roberts et al., 2012). There is also evidence that *ex vivo* processing might occur during extraction and purification due to tissue disruption releasing proteases that recombinant proteins would not normally be exposed to during *in vivo* expression (Drake et al., 2009; Hehle et al., 2011; T. G. Kim et al., 2008; Nykiforuk et al., 2011). To tackle unwanted proteolysis, several strategies to prevent recombinant protein degradation have been implemented, such as co-expression with protease inhibitors, fusion proteins, stabilising agents, protease gene knockdown/out and subcellular

targeting (Duwadi et al., 2015; Goulet et al., 2012; F. Grosse-Holz, Madeira, et al., 2018; N. S. Kim et al., 2008; Pillay et al., 2014).

Protease inhibitor (PI) co-expression is a promising approach to reduce protease activity for various reasons. Some PIs can target multiple protease families, overcoming redundancy (Grosse-Holz et al., 2018; Grosse-Holz & van der Hoorn, 2016). PIs can also be targeted to the apoplast accompanying recombinant proteins through the secretory pathway(Goulet et al., 2010; Jutras et al., 2016). During agroinfiltration conditions, PIs are only overexpressed temporarily and in localised leaf areas without affecting other tissues and potentially causing undesirable effects on plant health. Another promising strategy is protease depletion of proteases involved in the processing of recombinant proteins. Together, these two approaches have been explored previously in pursuit of increasing IgG accumulation (**Table 3.1**).

Table 3.1 Co-expression with protease inhibitors or protease depletion can lead to increased recombinant protein levels. Ser: serine, Asp: aspartic, Cys: cysteine, LC: light chain, HC: heavy chain. Approximate accumulation according to authors' statements, – indicates no significant change, n/s indicates not specified.

Approach	Description	IgG Accumulation*	Component	Reference
Protease knockdown/out	RNAi and gene editing	CAP256 IgG antibody (-)	*Nb*VPE-1a, *Nb*VPE-1b, and *Nb*CysP6	*Singh et al., 2022*
		2F5 IgG antibody (3-fold)	*Nb*SBT5.2	*Beritza et al., 2024*
Protease inhibitor	Co-expression with protease inhibitors	C5-1 IgG antibody (LC; 70-80%)	*Sl*CDI; *Sl*CYS9	*Goulet et al., 2012*
		C5-1 IgG antibody (HC; 85%)	*Sl*CDI	*Goulet et al., 2012*
		C5-1 IgG antibody (40%)	*Sl*CYS8	*Robert et al., 2013*
		H10 IgG antibody (HC; 7.5-fold)	*Sl*CYS8	*Jutras et al., 2016*
		VRC01 IgG antibody (2-10-fold)	*Nb*PR4, *Nb*Pot1 & *Hs*TIMP	*Grosse-Holz et al., 2018*

In this **Chapter**, by using the information of *in vitro* studies (**Chapter 2**) and of existing literature, we investigated the impact of PI co-expression or protease depletion on IgG accumulation and/or processing. We first screened several PIs targeting different protease families. Since the *in vitro* studies strongly suggested the involvement of SBT5.2 subtilase in 2F5 IgG processing, the next step was to examine SBT5.2 depletion along with other subtilases to determine if a sole protease is responsible for 2F5 and/or other IgG processing. Plants were initially depleted for different subtilases using virus-induced gene silencing (VIGS). Following VIGS, we tested CRISPR-Cas9 knockout lines of proteases we previously screened with VIGS and some additional proteases as these lines were becoming available. We selected four subtilases (Ser proteases) and two Cys proteases (**Table 3.2**) that were either consistently detected as active proteases in the apoplast of *Nicotiana benthamiana* by activity-based proteomics or confirmed to be involved in protein processing in the literature (Jutras et al., 2019; Puchol Tarazona et al., 2021; Singh et al., 2022; Sueldo et al., 2023).

Table 3.2 Protease knockouts tested in this Chapter for effect on IgG processing and IgG overall accumulation. Exemplary protease domains and structures from InterPro and AlphaFold, respectively. Ser: serine, Cys: cysteine, FNIII: fibronectin type-III, PSV: protein storage vacuole.

Name & Protease Family	Localisation *GO Annotation*	Protein Domains *InterPro*	Structure *AlphaFold*
sbt1.4 subtilisin-like 1.4 (Ser) *1 gene*	apoplast cytoplasm vacuole secretory vesicles	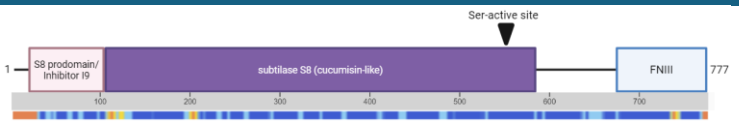	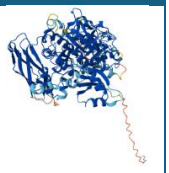
sbt1.7 subtilisin-like 1.7 (Ser) *4 genes*	apoplast secretory vesicles		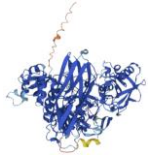
sbt1.9 subtilisin-like 1.9 (Ser) *2 genes*	apoplast	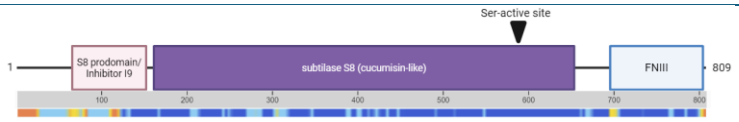	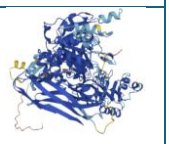
sbt5.2 subtilisin-like 5.2 (Ser) *3 genes*	apoplast	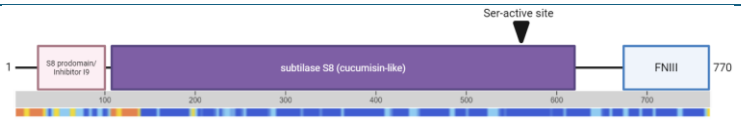	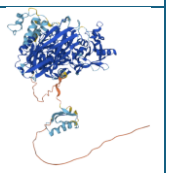
rd21 responsive to desiccation 21 (Cys) *3 genes*	vacuole Golgi apparatus apoplast cytoplasm plasma membrane plasmodesma nucleus secretory vesicles	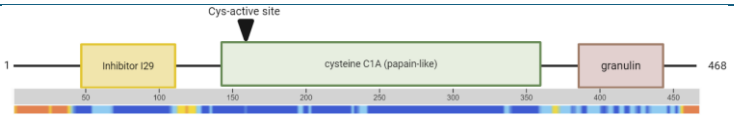	
vpeabc vacuolar processing enzyme (Cys) *3 genes* ***vpe1d*** vacuolar processing enzyme (Cys) *1 gene*	vacuole PSV	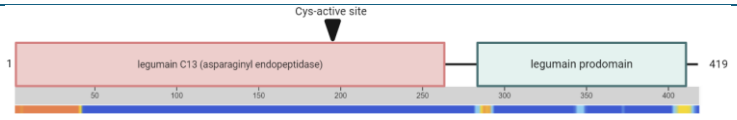	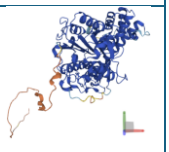

Results

3.2 Different antiviral IgGs exhibit distinct overexpression profile during transient expression

To investigate the expression of different antiviral IgGs in the days following infiltration, the light and heavy chains of 2F5, COVA2-15 or 2G4 were co-expressed in the same batch of wild-type plants. Samples were harvested at three, five and seven days following infiltration (**Figure 3.1**). Each sample corresponds to six leaf discs (6 x 1 cm^2 diameter) pooled from six different plants, with each leaf representing the same developmental stage. 2F5 antibody was successfully expressed as free light (LC) and heavy (HC) chains on day 3, however the fully assembled form was more abundant on days 5 and 7. F1 fragment that was previously detected and is due to processing by endogenous proteases is also visible in all three timepoints. On days 5 and 7 IgG intermediates are more visible, with day 7 exhibiting the highest relative concentration of both the fully-assembled 2F5 but also of its intermediates. While free LC is observed in all three timepoints, free heavy chain on days 5 and 7 is less abundant. Regarding the COVA2-15 antibody, the fully-assembled IgG and its intermediates are formed and are abundant in all three timepoints. Similarly, free HC seems stable and in similar abundance in all three timepoints, while free LC accumulates more as days progress. 2G4 antibody full complex is more abundant on day 5, as are the intermediate complexes. 2G4 free HC accumulates more as days progress, while free LC has a peak increase on day 5 but decreases on day 7.

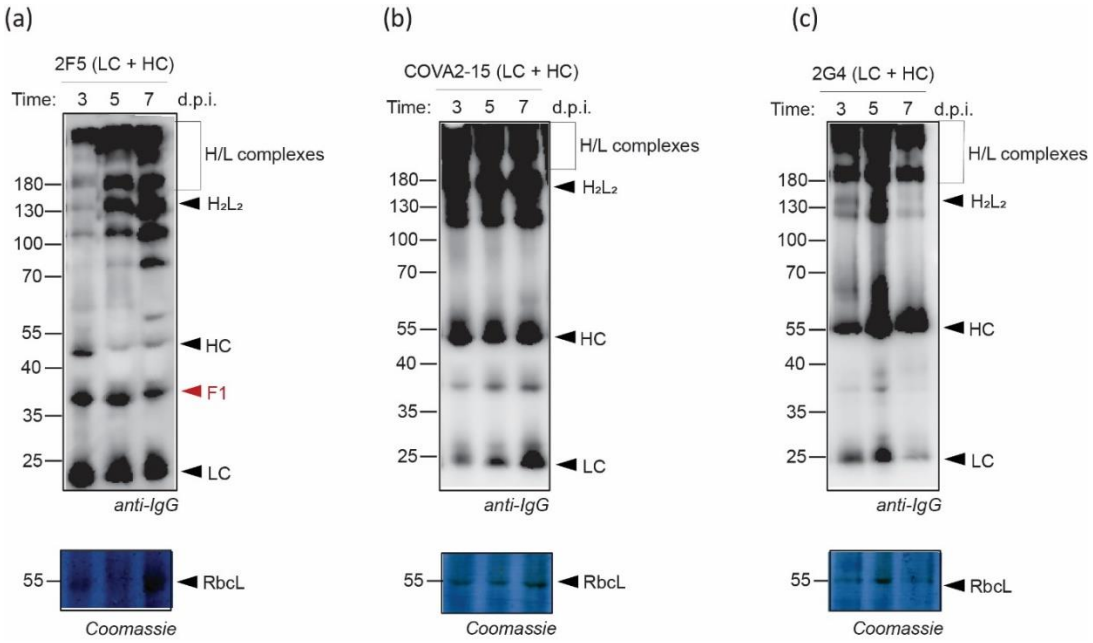

Figure 3.1 Overexpression profile of antiviral IgGs upon transient expression.

LC and HC of **(a)** 2F5, **(b)** COVA2-15, or **(c)** 2G4 IgG antibody were transiently co-expressed in *N. benthamiana* for 3, 5, and 7 days post infiltration (d.p.i.). Total extracts were generated and separated by reducing 12% SDS-PAGE and analysed by western blot using whole anti-IgG antibody. Coomassie staining of the large subunit of Rubisco (RbcL) was used to show loading. H/L complexes are non-reduced immunoglobulin aggregates or covalently linked heavy chain and light chain, potentially due to incomplete reduction, interchain disulfide bonding, or protein-protein interactions.

3.3 Co-expression with *Nb*Pot1 or *Sl*CDI protease inhibitors might lead to reduced 2F5 IgG levels

To test whether protease inhibitors against different proteases have an impact on 2F5 accumulation, 2F5 LC and HC were co-expressed with various inhibitors, previously listed on **Table 2.3**. None of the tested protease inhibitors led to significantly higher yields of 2F5 antibody, while some demonstrated lower yields of 2F5 when compared to the empty vector control (**Figure 3.2**). Specifically, the Cys/Asp inhibitor *Sl*CDI (Family I3) and the

Ser inhibitor *Nb*Pot1 led to less accumulation of 2F5 antibody. The F1 fragment signal at 40 kDa is relatively weak, while we also detect a second fragment of the HC, F2, which was previously described as a truncated form of the HC (Niemer et al., 2014).

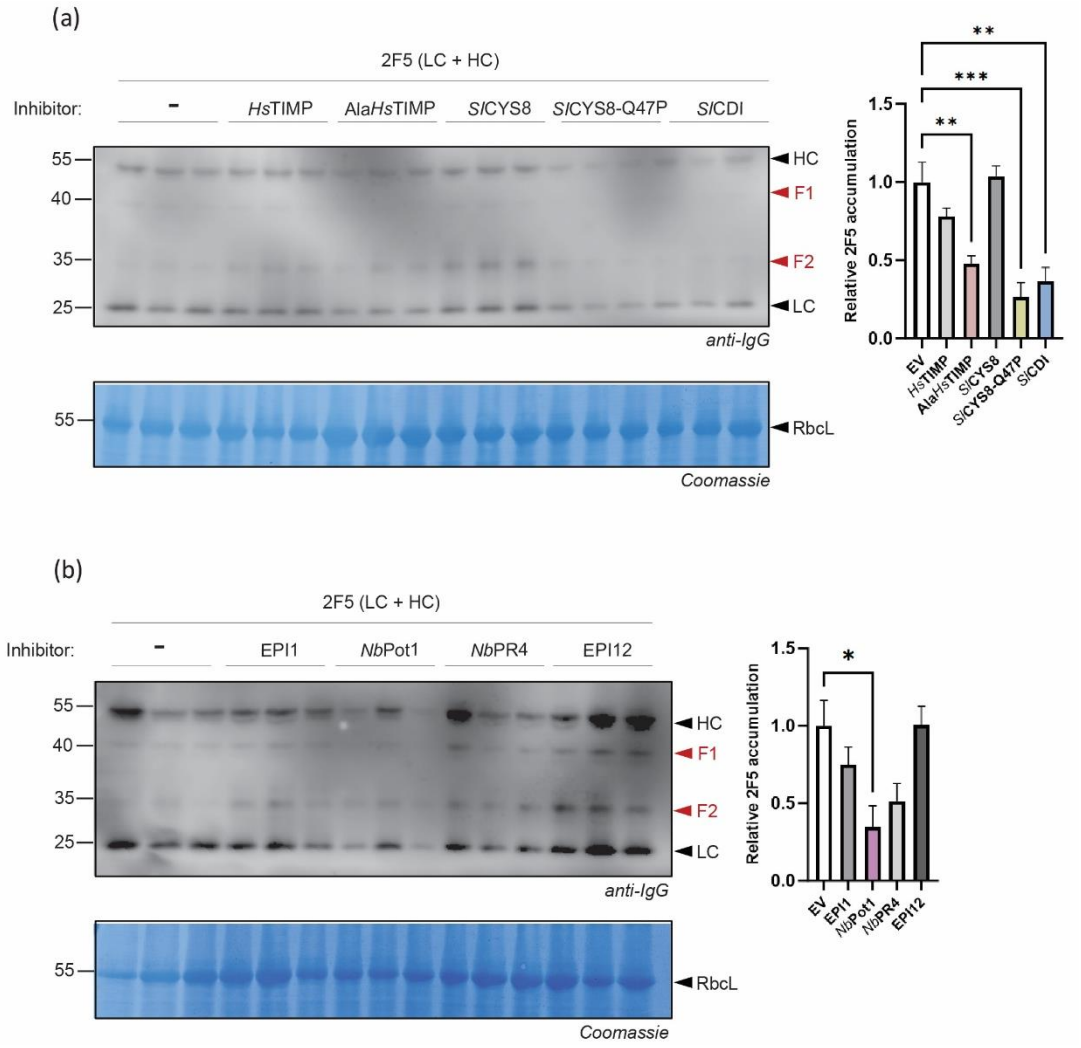

Figure 3.2 Co-expression of 2F5 with protease inhibitors *in vivo*.

The LC and HC of 2F5 were transiently co-expressed by agroinfiltration for 5 days in triplicate with inhibitors **(a)** *Hs*TIMP, *Sl*CYS8, *Sl*CDI, **(b)** Epi1, *Nb*Pot1, *Nb*PR4 and Epi12, as detailed in **Table 2.2**. Empty vector (EV) was used as the positive control, while Ala*Hs*TIMP, and *Sl*CYS8-Q47P were used as negative controls of *Hs*TIMP and *Sl*CYS8, respectively. Total extracts were generated and separated by reducing 12% SDS-PAGE and analysed by western blot using whole anti-IgG antibody. F1 and F2 indicate two different fragments of the 2F5 HC. Coomassie staining of the large subunit of Rubisco (RbcL) was used to show

loading. Band intensity quantification of 2F5 accumulation (LC+HC) is depicted in graphs next to the respective blot. Data were tested for normal distribution, while significance was determined with one-way ANOVA, following multiple comparisons and Tukey's post-hoc test. Error bars represent SE of n=3 experimental replicates. *p<0.05 ,**p<0.01, ***p<0.001.

3.4 2F5 processing in SBT-depleted plants by VIGS (knockdown)

To examine which subtilase is responsible for 2F5 processing, plants were depleted for different subtilases using virus-induced gene silencing (VIGS). We selected four subtilases that were consistently detected as active proteases in the apoplast of *Nicotiana benthamiana* by activity-based proteomics (Jutras et al., 2019; Puchol Tarazona et al., 2021; Sueldo et al., 2023). Plants were inoculated with tobacco rattle virus (TRV) carrying 300 bp fragments targeting these subtilases or a fragment of GFP as a negative control. Three weeks following inoculation with TRV, plants were agroinfiltrated with the LC and HC of 2F5. SBT1.9a-depleted plants demonstrated a dwarf phenotype, while the rest of the SBT-depleted plants grew indistinguishably from *TRV::GFP* control plants. Sampling targeted non-senescent leaves of the same developmental stage, while leaf discs from multiple plants per were collected and pooled to account for localised differences following VIGS silencing. Cleavage of the IgG is absent in apoplastic fluids isolated from *TRV::SBT5.2* plants and not from *TRV::GFP, TRV::SBT1.7a; TRV::SBT1.7c* or *TRV::SBT1.9a* plants (**Figure 3.3b**), indicating that SBT5.2 is required for 2F5 processing in the apoplast. Surprisingly, western blot analysis of total extracts from agroinfiltrated plants revealed no difference in the pattern of 2F5 processing upon SBT5.2 depletion when compared to the controls in independent experiments (**Figure 3.3b,c**). Besides a relatively weak F1 signal at 40 kDa, we detect a second fragment of the HC, called F2, and relatively strong signals for the HC and LC.

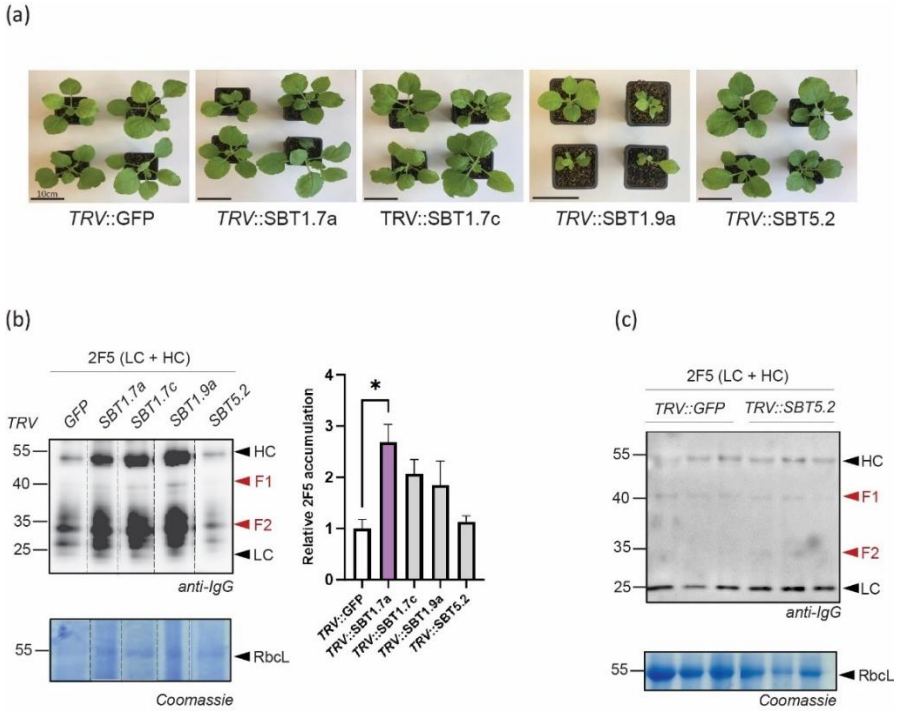

Figure 3.3 Co-expression of 2F5 in SBT-silenced plants.

(a) *TRV::SBT1.7a*, *TRV::SBT1.7c*, and *TRV::SBT5.2* grew indistinguishably from *TRV::GFP* plants. *TRV::SBT1.9a* plants showed a dwarf phenotype compared to *TRV::GFP.* Shown are four 7-week-old *N. benthamiana* plants, following three weeks from *TRV* infection and on the day of agroinfiltration with bacteria harbouring the LC and HC of 2F5. **(b)** LC and HC of 2F5 were transiently co-expressed for 5 days using agroinfiltration in *TRV::GFP*, *TRV::SBT1.7a*, *TRV::SBT1.7c*, *TRV::SBT1.9a*, and *TRV::SBT5.2* plants. One representative replicate of the triplicate is shown. Quantification of 2F5 accumulation (LC+HC) is depicted in graph. Total extracts were generated and separated by reducing 12% SDS-PAGE and analysed by western blot using whole anti-IgG antibody. F1 and F2 indicate two different fragments of the 2F5 HC. Coomassie staining of the large subunit of Rubisco (RbcL) was used to show loading. Data were tested for normal distribution, while significance was determined with one-way ANOVA, following multiple comparisons and Tukey's post-hoc test. Error bars represent SE of n=3 experimental replicates. **(c)** All three triplicates shown of LC and HC transient expression in *TRV::GFP*, *TRV::SBT5.2* plants. Total extracts were generated and separated by reducing 12% SDS-PAGE and analysed by western blot using whole anti-IgG antibody. F1 and F2 indicate two different fragments of the 2F5 HC. Coomassie staining of the large subunit of Rubisco (RbcL) was used to show loading.

3.5 Cytoplasmic GFP accumulation is not altered in protease mutants (knockouts)

To determine whether various protease-depleted plants would result in cytoplasmic GFP increase, 4-week-old wild type or protease-depleted plants were co-infiltrated with cytosolic GFP and 2F5 IgG, and leaves were scanned for fluorescence at five days post infiltration, because this timepoint was used for subsequent transient expression experiments for IgGs. The protease-depleted lines used were *sbt5.2#4*, *sbt5.2#8*, *rd21*, *vpeabc* and *vpe1d* as described in **Table 3.2**. Although the *vpe*-mutants exhibited a tendency of increased accumulation, there was no significant increase in accumulation in any of the mutants compared to wild-type plants (**Figure 3.4**). Finally, it is noteworthy that a trend of decreased GFP accumulation was observed in *rd21* mutant plants.

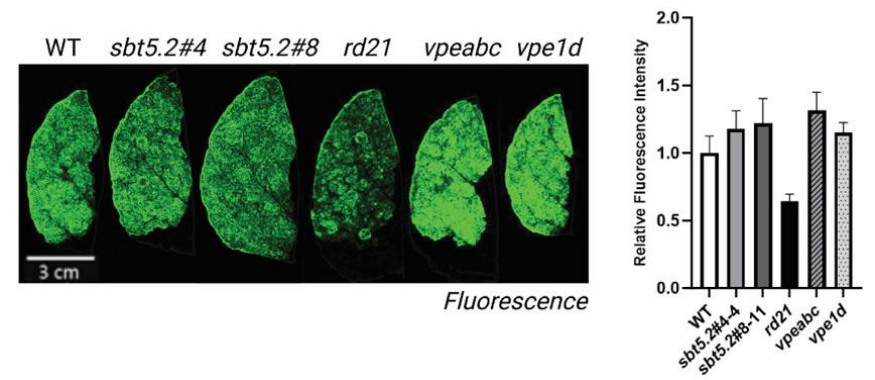

Figure 3.4 Co-expressed 2F5 IgG with cytoplasmic GFP, shows that the latter is not different between WT and different protease mutants.

GFP fluorescence (488 nm) was measured from six different half-leaves in three experimental replicates in WT, *sbt5.2#4*, *sbt5.2#8*, *rd21*, *vpeabc*, and *vpe1d* knockout plants. One representative replicate of the triplicate is shown. Quantification of cytoplasmic GFP is depicted in the graph. Data were tested for normal distribution, while significance was determined with one-way ANOVA, following multiple comparisons and Tukey's post-hoc test. Error bars represent SE of n=3 experimental replicates.

3.6 2F5 is significantly increased in SBT1.4 and SBT5.2-depleted lines (knockouts)

To study 2F5 accumulation upon protease depletion, the LC and HC of 2F5 were co-expressed in various protease mutants, such as *sbt1.4, sbt1.7, sbt5.2, rd21* and the vacuolar protease mutants *vpeabc* and *vpe1d*. Western blot analysis of total extracts from agroinfiltrated plants revealed no difference in the pattern of 2F5 processing upon SBT1.4, SBT1.7, SBT5.2, RD21, or VPE depletion when compared to the controls (**Figure 3.5**). Besides a relatively weak F1 signal at 40 kDa, we detect a second fragment of the HC, called F2, and relatively strong signals for the HC and LC. Interestingly, however, the accumulation of 2F5 in *sbt1.4* is consistently 4-fold higher, and in both *sbt5.2* mutants is consistently 3-fold higher. Regarding the *vpe* mutants, neither of the two lines seemed to have increased 2F5 accumulation or have an impact on the processing pattern.

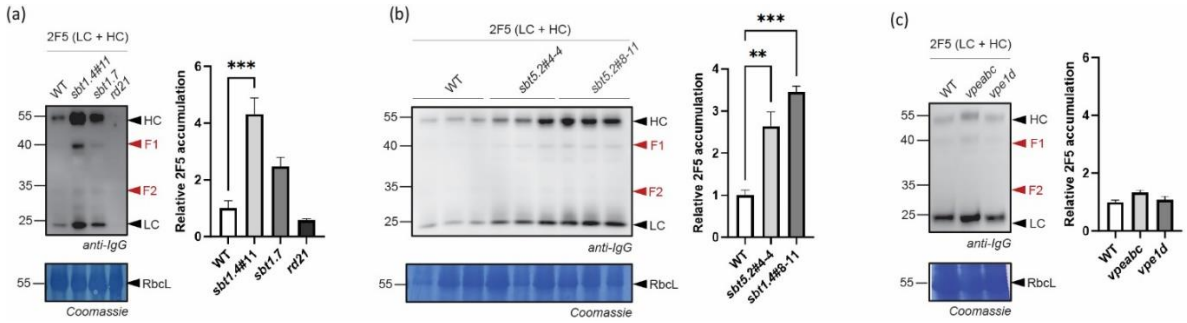

Figure 3.5 SBT1.4 and SBT5.2 depletion increases overall accumulation of 2F5 *in vivo*.

(a) LC and HC of 2F5 were transiently co-expressed for 5 days by agroinfiltration in WT, *sbt1.4#11, sbt1.7 and rd21* knockout plants. One representative replicate of the triplicate is shown. **(b)** All three triplicates shown of LC and HC transient expression in WT, *sbt5.2#4-4* and *sbt5.2#8-11* plants. **(c)** LC and HC of 2F5 were transiently co-expressed for 5 days by agroinfiltration in WT, *vpeabc and vpe1d* knockout plants One representative replicate of the triplicate is shown. Total extracts were generated and separated by reducing 12% SDS-PAGE and analysed by western blot using whole anti-IgG antibody. F1 and F2 indicate two

different fragments of the 2F5 HC. Coomassie staining of the large subunit of Rubisco was used to show loading. Band intensity quantification of 2F5 accumulation (LC+HC) is depicted in respective graphs. Data were tested for normal distribution, while significance was determined with one-way ANOVA, following multiple comparisons and Tukey's post-hoc test. Error bars represent SE of n=3 experimental replicates.

3.7 Accumulation of other anti-viral IgGs in protease depleted plants by CRISPR-Cas9 (knockout)

To study the accumulation of other IgGs upon protease depletion, the LC and HC of COVA2-15 (anti-CoV-SARS-2), VRC01 (anti-HIV), or 2G4 (anti-Ebola) were co-expressed in various protease mutants, such as *sbt1.4, sbt1.7, sbt1.9, sbt5.2, rd21* and the vacuolar protease mutants *vpeabc* and *vpe1d,* where available (**Figure 3.6**). SBT1.4 depletion contributes to substantial 2G4 accumulation, while it seems to have no effect on COVA2-15 yields. Interestingly, SBT1.4-depleted plants result in less accumulation of VRC01 IgG compared to wild-type. SBT1.7 depletion seem to have a negative impact on accumulation of all three IgGs, while SBT5.2 depletion has a trend of increasing COVA2-15 IgGs and significantly increasing 2G4 IgG by a maximum of 3-fold. SBT5.2-depleted plants accumulate similar levels of VRC01compared to wild-type plants. The RD21-depleted plants had no effect on COVA2-15 accumulation. However, VRC01 overexpression resulted in approximately 2-fold increase in these same mutants. VPE-depleted plants resulted in increased accumulation of both COVA2-15 and 2G4, and more specifically more than 2-fold increase of COVA2-15 in *vpeabc* mutants, and approximately 3- or 2-fold increase of VRC01 in *vpeabc* and *vpe1d* mutants, respectively. It is worth noting that additional fragmentation (F fragments) that might be due to processing was observed in COVA2-15 overexpression in *vpeabc* mutants, in VRC01 overexpression in both vpeabc and vpe1d

mutants that are approximately 35-40 kDa. Similarly, 2G4 overexpression in all mutants and wild-type tested generated 30-40 kDa fragments.

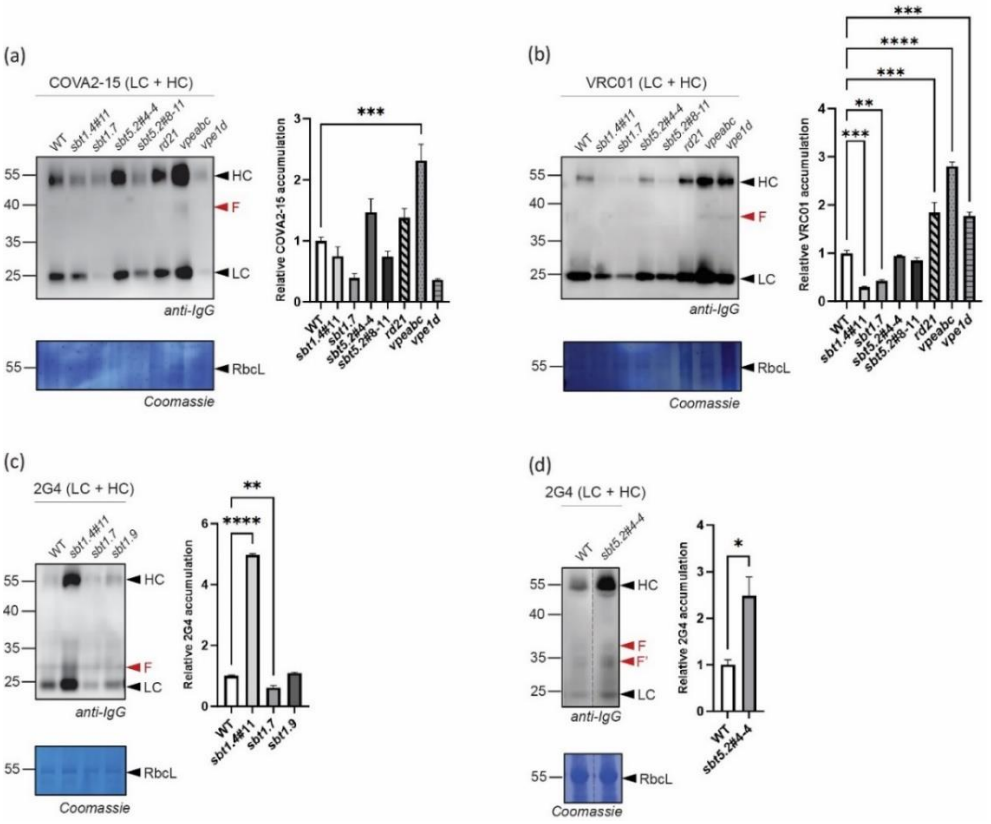

Figure 3.6 Overexpression of other IgGs in subtilase (Ser) or Cys mutants.

(a) LC and HC of COVA2_15 were transiently co-expressed for 5 days by agroinfiltration in WT, *sbt1.4#11*, *sbt1.7*, *sbt5.2#4-4*, *sbt5.2#8-11*, *rd21*, *vpeabc* and *vpe1d* knockout plants. **(b)** LC and HC of VRC01 were transiently co-expressed for 5 days by agroinfiltration in WT, *sbt1.4#11*, *sbt1.7*, *sbt5.2#4-4*, *sbt5.2#8-11*, *rd21*, *vpeabc* and *vpe1d* knockout plants. (c) LC and HC of 2G4 were transiently co-expressed for 5 days by agroinfiltration in WT, *sbt1.4#11*, *sbt1.7*, *sbt1.9*, and *(d) sbt5.2#4-4*, knockout plants. Total extracts were generated and separated by reducing 12% SDS-PAGE and analysed by western blot using whole anti-IgG antibody. F (or F') fragments indicate processing products. Coomassie staining of the large subunit of Rubisco was used to show loading. One representative replicate is shown. Quantification of IgG accumulation (LC+HC) is depicted in respective graphs. Data were tested for normal distribution, while significance was determined with one-way ANOVA, following multiple comparisons and Tukey's post-hoc test. Error bars represent SE of n=3 experimental replicates.

Conclusions and Discussion

This Chapter explored the accumulation and processing patterns of different anti-viral IgGs in various proteas-depleted mutants. The focus was primarily on subtilases, which are Ser proteases with high activity in the apoplast, and Cys proteases RD21 and VPE all which had been previously identified in the literature as prime candidates involved in protein processing (Jutras et al., 2019; Niemer et al., 2014; Paireder et al., 2017; Puchol Tarazona et al., 2021; Singh et al., 2022; Sueldo et al., 2023; Zheng et al., 2024). Before investigating the impact of protease depletion on IgG yields, we examined the timeline of transient expression of three IgGs that were also used in the protease-depletion screen to determine general recombinant IgG fragmentation and accumulation upon agroinfiltration. Hence, we used wild-type plants to transiently express 2F5, COVA2-15, and 2G4 over three, five, and seven days, with varying patterns of assembly and proteolytic processing being observed. The 2F5 antibody was expressed as free light chain (LC) and heavy chain (HC) by day 3, with more fully assembled IgG and intermediates appearing by days 5 and 7. COVA2-15 showed stable assembly across all timepoints, with the fully assembled IgG and intermediates present throughout. Free LC increased over time, while free HC remained consistent. For 2G4, the fully assembled form peaked on day 5, with free HC increasing steadily and free LC peaking at day 5 before decreasing by day 7. This pattern suggests that the faster transcription and/or translation rate of the smaller LC**,** or its lower susceptibility to proteases, may account for the differences in accumulation between LC and HC over time. Our observation that the fully assembled 2G4 peaked on day 5 correlates with the notion that younger tissues, which are typically more metabolically active, offer higher yields of recombinant proteins (Bashandy et al., 2015). Similarly, the increase in fully assembled 2F5 by days 5 and 7

correlates with other studies showing that harvesting around 5–7 days post-infiltration often yields the best expression results due to optimal conditions for protein accumulation and minimal leaf damage (Halfhill et al., 2003; Munné-Bosch & Alegre, 2002). Kim et al., reported that antibody fragment Fc expression levels increased in the top and middle leaves until around 5 dpi, after which they began to decline (K. Kim et al., 2021). This decline was attributed to transient stress in the plant cells, such as endoplasmic reticulum stress or activation of proteases, which likely interferes with continued high-level protein expression (Howell, 2013). High levels of recently identified SARS-CoV-2 IgGs can also be achieved at 7 or even 14 days post infiltration (Diego-Martin et al., 2020). However, when it comes to recombinant protein yields, it has also been reported that later timepoints exhibit higher variability across plants (Arzola et al., 2011).

Our next step was to examine the impact of protease inhibitors co-expression on IgG processing. The use of protease inhibitors in plants can help protect recombinant proteins from degradation (Goulet et al., 2012; Grosse-Holz et al., 2018; Jutras et al., 2016; Robert et al., 2013). However, inhibiting proteases may disrupt normal protein biosynthesis or turnover, which can either positively or negatively affect the overall yield of proteins (Mangena, 2022). In our case, none of the protease inhibitors resulted in higher accumulation of 2F5 compared to the empty vector control plants. In response to protease inhibition, plants may increase the transcription of protease-encoding genes to maintain homeostasis and hence, counteract the effect of a promising protease inhibitor. For example, when the proteasome is inhibited by syringolin A, the expression of proteasome-related genes is upregulated (Michel et al., 2006). This suggests that protease inhibition might not only protect recombinant proteins but could also induce an immune response. Another caveat is that protease inhibitors might not be accumulating in the

same compartments as the other recombinant protein, or might even be inactive in certain pH levels.

When it comes to transient expression in *N. benthamiana,* several studies confirmed high protease activity (Jutras et al., 2019; Puchol Tarazona et al., 2021; Roberts et al., 2012) and fluctuations of protease RPKM (reads per kilobase of transcript per million mapped reads) values upon agroinfiltration (Grosse-Holz et al., 2018). The protease-depleted lines we examined were either consistently detected as active proteases in the apoplast of *N. benthamiana* or were involved in protein processing according to literature (Jutras et al., 2019; Puchol Tarazona et al., 2021; Singh et al., 2022; Sueldo et al., 2023).

Regarding the protease-depleted plants, each IgG was transiently co-expressed with GFP, as GFP can act as a control recombinant protein. GFP fluorescence of agroinfiltrated leaves was not significantly different in the any of the tested mutants, indicating that increased or decreased levels of IgG expression is not caused by increased transformation or transgene expression efficiency. It is essential to highlight that when using multiple T-DNAs derived from multiple agrobacterium cultures, the frequency at which all T-DNAs are simultaneously transferred into the cell is high (Carlson et al., 2023). However there is still a possibility that fluctuating T-DNA transfer or insertion levels can lead to chimeric expression across epidermal leaves (Pereman et al., 2019; Verhage, 2021). Additionally, immune reactions in *N. benthamiana*, triggered by *Agrobacterium* cold shock proteins, can limit T-DNA delivery during transformation (Saur et al., 2016).

Our data from *in vitro* studies in Chapter 2 confirmed that the protease SBT5.2 is responsible for cleaving the H3 loop of the 2F5 antibody in isolated apoplastic fluids. This

finding is supported by prior work showing that the Ser protease inhibitor PMSF blocks 2F5 processing and that purified SBT5.2 is PMSF-sensitive (Puchol Tarazona et al., 2021). However, when 2F5 is expressed *in vivo*, only a small portion of the heavy chain (HC) is cleaved into two fragments (F1 and F2), even in the absence of SBT5.2, indicating that other proteases may be responsible for this cleavage.

Most of the transiently expressed 2F5 does not undergo processing in wild-type plants, which suggests either that 2F5 is not exposed to SBT5.2, or that plant-specific 2F5 N-glycans could confer protection from cleavage. Interestingly, however, the accumulation of 2F5 in both *sbt5.2* mutants is consistently 3-fold higher. Similarly, 2G4 was also increased in SBT5.2-depleted plants upon transient expression. Although 2F5 and 2G4 were not tested in *in vitro* incubation with apoplastic fluids from SBT1.4-depleted plants, their *in vivo* overexpression in these mutants resulted in significantly higher levels. In contrast, COVA2-15 and VRC01 IgGs displayed significantly higher levels in *vpe* mutants, but no significant increase was observed in the various SBT-depleted mutant plants. These data suggest that mapping the processing profile across different IgGs, across different protease mutants can enlighten the complex network of unintended proteolysis from proteases.

More research on where different IgGs accumulate upon transient expression, and establishing their proteolytic processing patterns can provide a wider picture of how to tackle unwanted proteolysis more accurately. In some cases, protease mutants resulted in significantly lower levels of the IgGs, for example in *sbt1.4* and *sbt1.7* mutants when VRC01 was transiently expressed, or in *sbt1.7* mutants when 2G4 was transiently expressed. Proteomic data suggest that agroinfiltration alters the proteolytic environment of *N. benthamiana*, possibly inducing protease synthesis involved in

degrading recombinant proteins (Grosse-Holz et al., 2018). However, the SBTs we tested remain abundant and active in both mock and agroinfiltrated leaves, indicating that these proteases are not specifically upregulated by agroinfiltration. Other proteases, such as papain-like cysteine proteinases and legumains, are known to be upregulated during agroinfiltration and are implicated in recombinant protein degradation (Duwadi et al., 2015; Niemer et al., 2014; Paireder et al., 2017; Pillay et al., 2016). Moreover, protease depletion might alter the levels of other proteases, in an attempt of the cell to ensure homeostasis. RNA-sequencing of these protease mutants could reveal upregulated or downregulated genes of other proteases or other proteins e.g. chaperones that might be involved in the processing, correct folding and ultimately accumulation of transiently expressed IgGs. Additionally, SBT5.2 mediates the degradation of elicitors of both flagellin and cold shock proteins and that these elicitors are more stable in these *sbt5.2* mutants, causing increased disease resistance to *Pseudomonas syringae* (Buscaill et al., 2024; Chen et al., 2024). We also previously found that *SBT5.2* silencing would prevent the maturation of tomato immune protease Rcr3 from its precursor protein (Paulus et al., 2020). According to the aforementioned it might be possible for *sbt5.2* knockout to lead to enhanced immune response when infected with agrobacteria such as wound responses, hence indicating more efficient T-DNA transfer (Pitzschke & Hirt, 2010).

References

Arzola, L., Chen, J., Rattanaporn, K., Maclean, J. M., & McDonald, K. A. (2011). Transient co-expression of post-transcriptional gene silencing suppressors for increased in planta expression of a recombinant anthrax receptor fusion protein. *International Journal of Molecular Sciences*, *12*(8), 4975–4990. https://doi.org/10.3390/ijms12084975

Badri, M. A., Rivard, D., Coenen, K., & Michaud, D. (2009). Unintended molecular interactions in transgenic plants expressing clinically useful proteins: The case of bovine aprotinin traveling the potato leaf cell secretory pathway. *Proteomics*, *9*(3), 746–756. https://doi.org/10.1002/pmic.200700234

Bashandy, H., Jalkanen, S., & Teeri, T. H. (2015). Within leaf variation is the largest source of variation in agroinfiltration of Nicotiana benthamiana. *Plant Methods*, *11*(1). https://doi.org/10.1186/s13007-015-0091-5

Benchabane, M., Goulet, C., Rivard, D., Faye, L., Gomord, V., & Michaud, D. (2008). Preventing unintended proteolysis in plant protein biofactories. In *Plant Biotechnology Journal* (Vol. 6, Issue 7, pp. 633–648). https://doi.org/10.1111/j.1467-7652.2008.00344.x

Beritza, K., Buscaill, P., Song, S.-J., Jutras, P. V, Huang, J., Mach, L., Dong, S., & Van Der Hoorn, R. A. L. (2024). *SBT5.2s are the major active extracellular subtilases processing IgG antibody 2F5 in the Nicotiana benthamiana apoplast*.

Buscaill, P., Sanguankiattichai, N., Kaschani, F., Huang, J., Mooney, B. C., Li, Y., Lyu, J., Sueldo, D., Kaiser, M., & van der Hoorn, R. A. L. (2024). Subtilase SBT5.2 inactivates flagellin immunogenicity in the plant apoplast. *Nature Communications*, *15*(1), 10431. https://doi.org/10.1038/s41467-024-54790-1

Carlson, E. D., Rajniak, J., & Sattely, E. S. (2023). Multiplicity of the Agrobacterium Infection of Nicotiana benthamiana for Transient DNA Delivery. *ACS Synthetic Biology*, *12*(8), 2329–2338. https://doi.org/10.1021/acssynbio.3c00148

Chen, C., Buscaill, P., Sanguankiattichai, N., Huang, J., Kaschani, F., Kaiser, M., & van der Hoorn, R. A. L. (2024). Extracellular plant subtilases dampen cold-shock peptide elicitor levels. *Nature Plants*, *10*(11), 1749–1760. https://doi.org/10.1038/s41477-024-01815-8

De Muynck, B., Navarre, C., Nizet, Y., Stadlmann, J., & Boutry, M. (2009). Different subcellular localization and glycosylation for a functional antibody expressed in Nicotiana tabacum plants and suspension cells. *Transgenic Research*, *18*(3), 467–482. https://doi.org/10.1007/s11248-008-9240-1

Diego-Martin, B., González, B., Vazquez-Vilar, M., Selma, S., Mateos-Fernández, R., Gianoglio, S., Fernández-del-Carmen, A., & Orzáez, D. (2020). Pilot Production of SARS-CoV-2 Related Proteins in Plants: A Proof of Concept for Rapid Repurposing of Indoor Farms Into Biomanufacturing Facilities. *Frontiers in Plant Science*, *11*. https://doi.org/10.3389/fpls.2020.612781

Drake, P. M. W., Barbi, T., Sexton, A., McGowan, E., Stadlmann, J., Navarre, C., Paul, M. J., & Ma, J. K.-C. (2009). Development of rhizosecretion as a production system for recombinant proteins

from hydroponic cultivated tobacco. *The FASEB Journal*, *23*(10), 3581–3589. https://doi.org/10.1096/fj.09-131771

Duwadi, K., Chen, L., Menassa, R., & Dhaubhadel, S. (2015). Identification, Characterization and Down-Regulation of Cysteine Protease Genes in Tobacco for Use in Recombinant Protein Production. *PLOS ONE*, *10*(7), e0130556. https://doi.org/10.1371/journal.pone.0130556

Goulet, C., Benchabane, M., Anguenot, R., Brunelle, F., Khalf, M., & Michaud, D. (2010). A companion protease inhibitor for the protection of cytosol-targeted recombinant proteins in plants. *Plant Biotechnology Journal*, *8*(2), 142–154. https://doi.org/10.1111/j.1467-7652.2009.00470.x

Goulet, C., Khalf, M., Sainsbury, F., D'Aoust, M.-A., & Michaud, D. (2012). A protease activity–depleted environment for heterologous proteins migrating towards the leaf cell apoplast. *Plant Biotechnology Journal*, *10*(1), 83–94. https://doi.org/https://doi.org/10.1111/j.1467-7652.2011.00643.x

Grosse-Holz, F., Kelly, S., Blaskowski, S., Kaschani, F., Kaiser, M., & van der Hoorn, R. A. L. (2018). The transcriptome, extracellular proteome and active secretome of agroinfiltrated Nicotiana benthamiana uncover a large, diverse protease repertoire. *Plant Biotechnology Journal*, *16*(5), 1068–1084. https://doi.org/10.1111/pbi.12852

Grosse-Holz, F. M., & van der Hoorn, R. A. L. (2016). Juggling jobs: roles and mechanisms of multifunctional protease inhibitors in plants. *The New Phytologist*, *210*(3), 794–807. https://doi.org/10.1111/nph.13839

Grosse-Holz, F., Madeira, L., Zahid, M. A., Songer, M., Kourelis, J., Fesenko, M., Ninck, S., Kaschani, F., Kaiser, M., & van der Hoorn, R. A. L. (2018). Three unrelated protease inhibitors enhance accumulation of pharmaceutical recombinant proteins in Nicotiana benthamiana. *Plant Biotechnology Journal*, *16*(10), 1797–1810. https://doi.org/10.1111/pbi.12916

Halfhill, M. D., Millwood, R. J., Rufty, T. W., Weissinger, A. K., & Stewart, C. N. (2003). Spatial and temporal patterns of green fluorescent protein (GFP) fluorescence during leaf canopy development in transgenic oilseed rape, Brassica napus L. *Plant Cell Reports*, *22*(5), 338–343. https://doi.org/10.1007/s00299-003-0696-4

Hehle, V. K., Paul, M. J., Drake, P. M., Ma, J. K. C., & van Dolleweerd, C. J. (2011). Antibody degradation in tobacco plants: A predominantly apoplastic process. *BMC Biotechnology*, *11*. https://doi.org/10.1186/1472-6750-11-128

Howell, S. H. (2013). Endoplasmic reticulum stress responses in plants. In *Annual Review of Plant Biology* (Vol. 64, pp. 477–499). https://doi.org/10.1146/annurev-arplant-050312-120053

Jutras, P. V, Dodds, I., & van der Hoorn, R. A. L. (2020). Proteases of Nicotiana benthamiana: an emerging battle for molecular farming. *Current Opinion in Biotechnology*, *61*, 60–65. https://doi.org/https://doi.org/10.1016/j.copbio.2019.10.006

Jutras, P. V., Grosse-Holz, F., Kaschani, F., Kaiser, M., Michaud, D., & van der Hoorn, R. A. L. (2019). Activity-based proteomics reveals nine target proteases for the recombinant protein-stabilizing inhibitor SlCYS8 in Nicotiana benthamiana. *Plant Biotechnology Journal*, *17*(8), 1670–1678. https://doi.org/10.1111/pbi.13092

Jutras, P. V, Marusic, C., Lonoce, C., Deflers, C., Goulet, M.-C., Benvenuto, E., Michaud, D., & Donini, M. (2016). An Accessory Protease Inhibitor to Increase the Yield and Quality of a Tumour-Targeting mAb in Nicotiana benthamiana Leaves. *PLOS ONE*, *11*(11), e0167086. https://doi.org/10.1371/journal.pone.0167086

Jutras, P. V., Sainsbury, F., Goulet, M. C., Lavoie, P. O., Tardif, R., Hamel, L. P., D'Aoust, M. A., & Michaud, D. (2020). PH Gradient Mitigation in the Leaf Cell Secretory Pathway Attenuates the Defense Response of Nicotiana benthamiana to Agroinfiltration. *Journal of Proteome Research*, *19*(1), 106–118. https://doi.org/10.1021/acs.jproteome.9b00409

Kim, K., Kang, Y. J., Park, S. R., Kim, D. S., Lee, S. W., Ko, K., Ponndorf, D., & Ko, K. (2021). Effect of leaf position and days post-infiltration on transient expression of colorectal cancer vaccine candidate proteins GA733-Fc and GA733-FcK in Nicotiana benthamiana plant. *PeerJ*, *9*. https://doi.org/10.7717/peerj.10851

Kim, N. S., Kim, T. G., Kim, O. H., Ko, E. M., Jang, Y. S., Jung, E. S., Kwon, T. H., & Yang, M. S. (2008). Improvement of recombinant hGM-CSF production by suppression of cysteine proteinase gene expression using RNA interference in a transgenic rice culture. *Plant Molecular Biology*, *68*(3), 263–275. https://doi.org/10.1007/s11103-008-9367-8

Kim, T. G., Lee, H. J., Jang, Y. S., Shin, Y. J., Kwon, T. H., & Yang, M. S. (2008). Co-expression of proteinase inhibitor enhances recombinant human granulocyte-macrophage colony stimulating factor production in transgenic rice cell suspension culture. *Protein Expression and Purification*, *61*(2), 117–121. https://doi.org/10.1016/j.pep.2008.06.005

Mangena, P. (2022). Pleiotropic effects of recombinant protease inhibitors in plants. In *Frontiers in Plant Science* (Vol. 13). Frontiers Media S.A. https://doi.org/10.3389/fpls.2022.994710

Michel, K., Abderhalden, O., Bruggmann, R., & Dudler, R. (2006). Transcriptional changes in powdery mildew infected wheat and Arabidopsis leaves undergoing syringolin-triggered hypersensitive cell death at infection sites. *Plant Molecular Biology*, *62*(4–5), 561–578. https://doi.org/10.1007/s11103-006-9045-7

Munné-Bosch, S., & Alegre, L. (2002). Plant aging increases oxidative stress in chloroplasts. *Planta*, *214*(4), 608–615. https://doi.org/10.1007/s004250100646

Niemer, M., Mehofer, U., Torres Acosta, J. A., Verdianz, M., Henkel, T., Loos, A., Strasser, R., Maresch, D., Rademacher, T., Steinkellner, H., & Mach, L. (2014). The human anti-HIV antibodies 2F5, 2G12, and PG9 differ in their susceptibility to proteolytic degradation: Down-regulation of endogenous serine and cysteine proteinase activities could improve antibody production in plant-based expression platforms. *Biotechnology Journal*, *9*(4), 493–500. https://doi.org/10.1002/biot.201300207

Nykiforuk, C. L., Shen, Y., Murray, E. W., Boothe, J. G., Busseuil, D., Rhéaume, E., Tardif, J. C., Reid, A., & Moloney, M. M. (2011). Expression and recovery of biologically active recombinant Apolipoprotein AIMilano from transgenic safflower (Carthamus tinctorius) seeds. *Plant Biotechnology Journal*, *9*(2), 250–263. https://doi.org/10.1111/j.1467-7652.2010.00546.x

Paireder, M., Tholen, S., Porodko, A., Biniossek, M. L., Mayer, B., Novinec, M., Schilling, O., & Mach, L. (2017). The papain-like cysteine proteinases NbCysP6 and NbCysP7 are highly processive enzymes with substrate specificities complementary to Nicotiana benthamiana cathepsin B.

Biochimica et Biophysica Acta - Proteins and Proteomics, *1865*(4), 444–452. https://doi.org/10.1016/j.bbapap.2017.02.007

Paulus, J. K., Kourelis, J., Ramasubramanian, S., Homma, F., Godson, A., Hörger, A. C., Hong, N., Krahn, D., Carballo, L. O., Wang, S., Win, J., Smoker, M., Kamoun, S., Dong, S., & Van Der Hoorn, R. A. L. (2020). *Extracellular proteolytic cascade in tomato activates immune protease Rcr3*. https://doi.org/10.1073/pnas.1921101117/-/DCSupplemental

Pereman, I., Melamed-Bessudo, C., Dahan-Meir, T., Herz, E., Elbaum, M., & Levy, A. A. (2019). Single molecule imaging of T-DNA intermediates following Agrobacterium tumefaciens infection in Nicotiana benthamiana. *International Journal of Molecular Sciences*, *20*(24). https://doi.org/10.3390/ijms20246209

Pillay, P., Kunert, K. J., van Wyk, S., Makgopa, M. E., Cullis, C. A., & Vorster, B. J. (2016). Agroinfiltration contributes to VP1 recombinant protein degradation. *Bioengineered*, *7*(6), 459–477. https://doi.org/10.1080/21655979.2016.1208868

Pillay, P., Schlüter, U., van Wyk, S., Kunert, K. J., & Vorster, B. J. (2014). Proteolysis of recombinant proteins in bioengineered plant cells. *Bioengineered*, *5*(1), 15–20. https://doi.org/10.4161/bioe.25158

Pitzschke, A., & Hirt, H. (2010). New insights into an old story: Agrobacterium-induced tumour formation in plants by plant transformation. *The EMBO Journal*, *29*(6), 1021–1032. https://doi.org/https://doi.org/10.1038/emboj.2010.8

Puchol Tarazona, A. A., Maresch, D., Grill, A., Bakalarz, J., Torres Acosta, J. A., Castilho, A., Steinkellner, H., & Mach, L. (2021). Identification of two subtilisin-like serine proteases engaged in the degradation of recombinant proteins in Nicotiana benthamiana. *FEBS Letters*, *595*(3), 379–388. https://doi.org/https://doi.org/10.1002/1873-3468.14014

Robert, S., Khalf, M., Goulet, M.-C., D'Aoust, M.-A., Sainsbury, F., & Michaud, D. (2013). Protection of Recombinant Mammalian Antibodies from Development-Dependent Proteolysis in Leaves of Nicotiana benthamiana. *PLOS ONE*, *8*(7), e70203-. https://doi.org/10.1371/journal.pone.0070203

Roberts, I. N., Caputo, C., Criado, M. V., & Funk, C. (2012). Senescence-associated proteases in plants. In *Physiologia Plantarum* (Vol. 145, Issue 1, pp. 130–139). https://doi.org/10.1111/j.1399-3054.2012.01574.x

Saur, I. M. L., Kadota, Y., Sklenar, J., Holton, N. J., Smakowska, E., Belkhadir, Y., Zipfel, C., & Rathjen, J. P. (2016). NbCSPR underlies age-dependent immune responses to bacterial cold shock protein in Nicotiana benthamiana. *Proceedings of the National Academy of Sciences of the United States of America*, *113*(12), 3389–3394. https://doi.org/10.1073/pnas.1511847113

Schiermeyer, A., Schinkel, H., Apel, S., Fischer, R., & Schillberg, S. (2005). Production of Desmodus rotundus salivary plasminogen activator α1 (DSPAα1) in tobacco is hampered by proteolysis. *Biotechnology and Bioengineering*, *89*(7), 848–858. https://doi.org/10.1002/bit.20410

Singh, A. A., Pillay, P., Naicker, P., Alexandre, K., Malatji Kanyane, Mach, L., Steinkellner, H., Vorster, J., Chikwamba, R., & Tsekoa, T. L. (2022). *Transient proteolysis reduction of Nicotiana benthamiana-produced CAP256 broadly neutralizing antibodies using CRISPR/Cas9*. http://www.clcbio.com

Sueldo, D. J., Godson, A., Kaschani, F., Krahn, D., Kessenbrock, T., Buscaill, P., Schofield, C. J., Kaiser, M., & van der Hoorn, R. A. L. (2023). Activity-based proteomics uncovers suppressed hydrolases and a neo-functionalised antibacterial enzyme at the plant–pathogen interface. *New Phytologist*. https://doi.org/10.1111/nph.18857

Thomas, E. L., & van der Hoorn, R. A. L. (2018). Ten prominent host proteases in plant-pathogen interactions. *International Journal of Molecular Sciences*, *19*(2), 1–12. https://doi.org/10.3390/ijms19020639

Verhage, L. (2021). Twelve genes at one blow: multiplex genome editing with CRISPR/Cas. In *Plant Journal* (Vol. 106, Issue 1, pp. 6–7). Blackwell Publishing Ltd. https://doi.org/10.1111/tpj.15228

Zheng, K., Lyu, J. C., Thomas, E. L., Schuster, M., Sanguankiattichai, N., Ninck, S., Kaschani, F., Kaiser, M., & van der Hoorn, R. A. L. (2024). The proteome of Nicotiana benthamiana is shaped by extensive protein processing. *New Phytologist*, *243*(3), 1034–1049. https://doi.org/10.1111/nph.19891

Chapter 4

Steric accessibility of the IgG cleavage site: Stabilisation of IgGs via site-directed mutagenesis

4.1 Introduction

In protease-substrate interactions, amino acid positions surrounding the cleavage site are designated using the Schechter and Berger nomenclature (Schechter & Berger, 1967). The cleavage site is the bond hydrolysed by the protease, and the residues on either side of it are labelled relative to this point. Amino acids located upstream (N-terminal) of the cleavage site are referred to as P1, P2, P3, and so on, while those downstream (C-terminal) are labelled as P1', P2', P3', etc (**Figure 4.1a**). The P1 position is the residue immediately before the cleavage site, whereas P1' is the first residue after it. Proteases typically have specificity for certain residues at these positions, particularly P1, which often plays a crucial role in determining cleavage efficiency. These substrate positions interact with corresponding regions in the protease, known as S1, S2, S1', etc., which form the enzyme's substrate-binding pockets and contribute to recognition and cleavage specificity.

Endopeptidases exhibit diverse sequence specificities in their cleavage sites (Rawlings et al., 2012). While many plant subtilases have a broad substrate specificity (Hamilton et al., 2003), some only cleave after aspartic acid residues (Coffeen & Wolpert, 2004; Galiullina et al., 2015; **Figure 4.1b**). For instance, trypsin specifically cuts after Lys or Arg residues at P1 (Olsen et al., 2004). However, this action is typically inhibited if Pro is present in the P1' position, immediately following the scissile bond. On the contrary, plant proteases such as pepsin and papain display a much wider specificity in their cleavage patterns (Rawlings et al., 2012).

Antibodies can be susceptible to proteases depending on their primary sequence, structural features, or subcellular location (Hehle et al., 2016; Hehle et al., 2015; Niemer et al., 2014; Obregon et al., 2006). This vulnerability of antibodies might derive from the

fact that these heterologous proteins have not evolved within the host's protease environment. Previous studies on antibody proteolysis revealed that the cleavage sites are typically at exposed areas in the interdomain regions of each antibody chain (Hehle et al., 2015). Many broadly neutralizing antibodies have developed exceptionally elongated complementarity-determining region (CDR) H3 loops to access their peptide epitopes (Doria-Rose et al., 2014; Zemlin et al., 2003). For example, human immunodeficiency virus 1 (HIV-1) virions are enveloped by a dense glycan shield that conceals numerous antigenic sites on the envelope glycoprotein, dictating the elongated CDR H3 loop (Alam et al., 2009). As this loop is exposed in many IgG antibodies, mutating amino acids near the CDR H3 loop could reduce susceptibility to processing from plant proteases. Strategically introducing *de novo* disulphide bonds could improve accumulation by shielding the reactive hydrophobic core, which is typically vulnerable to proteolytic enzymes (Zabetakis et al., 2014).

Moreover, the unique domain-swapped architecture in 2G12 antibody might be responsible for its stability, and this has been validated by site-directed mutagenesis to display a standard Y-shaped quaternary structure instead (Hehle et al., 2016). This architecture of 2G12 refers to the structural rearrangement in which the variable domains of one Fab arm exchange positions with those of the other Fab arm, forming a rigid, interlocked dimer. This unique configuration enhances avidity by clustering antigen-binding sites, allowing 2G12 to simultaneously bind multiple high-mannose glycans on the HIV-1 envelope glycoprotein, improving its neutralisation potency. This observation highlights that the low flexibility of Fab domains could in general restrict access to the CDR H3 loops, preventing their proteolysis.

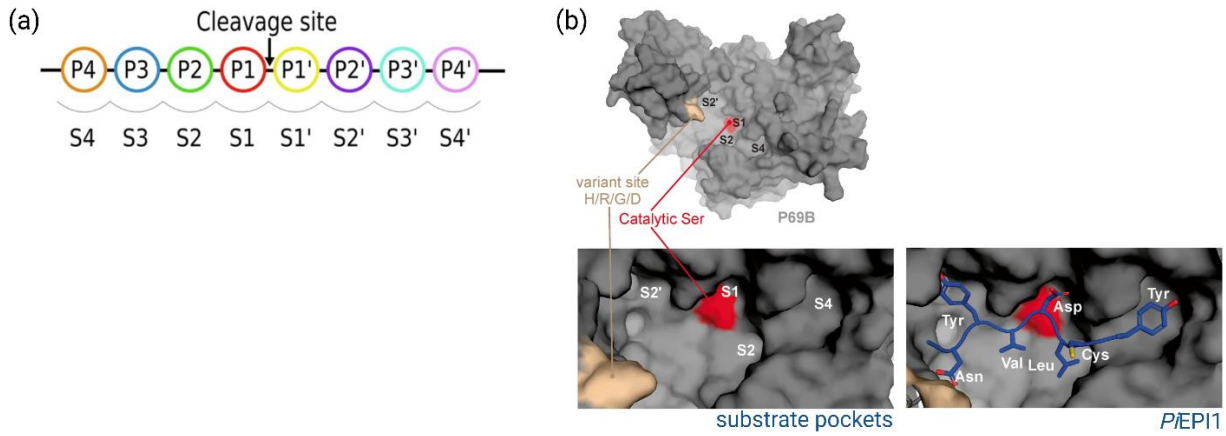

Figure 4.1 Representation of protease substrate specificity pockets.

(a) Protease-substrate interactions, amino acid positions surrounding the cleavage site are designated using the Schechter and Berger nomenclature (adapted from Ochoa et al., 2020). **(b)** AlphaFold-predicted models of P69B subtilase without inhibitor (top panel), or with *Phytophthora infestans* protease inhibitor *Pi*Epi1 (bottom panel). P69B is shown in a grey surface with the hyper-variant residue (crème) and the active site (red). Substrate binding pockets are depicted (S4-S2-S1-S2') with the respective substrate/inhibitor pockets P4, P2, P1 and P2' (adapted from Homma et al., 2023).

In this **Chapter**, we investigated the stability of the CDR H3 loop of 2F5 and COVA2-15 IgG antibodies, following site-directed mutagenesis. Mutations were carried out according to two observations. Firstly, since the 2F5 cleavage site on the CDR H3 loop is known, we tested mutations of the cleavage site at P1 position. Secondly, we detected that COVA2-15 is stable when incubated in apoplastic fluids, while 2F5 is consistently cleaved. Following multiple sequence alignment between 2F5 and COVA2-15 CDR H3 loops (MSA; Clustal Omega), we observed the formation of a disulphide bridge in the region of the COVA2-15 loop that aligns with the region where 2F5 is cleaved. Hence, we examined the substitution of residues to Cys residues near the 2F5 cleavage site that would potentially result in disulphide bridge formation, in an attempt to protect the 2F5 CDR H3 loop from processing. Additionally, we tested a variant of COVA2-15 in which the Cys residues

responsible for forming the disulphide bridge in the CDR H3 loop were modified. All mutated versions of both antibodies were tested *in vivo* and/or *in vitro* for their proteolytic processing and overall accumulation compared to the wild-type IgGs.

Results

4.2 Compared to 2F5, COVA2-15 is stable in apoplastic fluids

To examine the relative stability over time of the 2F5 and COVA2-15 IgG antibodies, the IgGs were incubated in apoplastic fluids for 0, 6, 24 and 30 hours and separated on a reducing protein gel (**Figure 4.2b**). The assay was repeated (see Chapter 2) with additional timepoints to better assess the degradation of IgGs over time, providing a more detailed understanding of their stability at different stages. Additionally, 2F5 and COVA2-15 were added together in apoplastic fluids, while 2F5 and COVA2-15 were previously labelled using Alexa Fluor 488 nm and 650 nm. Following *in vitro* incubation of 2F5 with apoplastic fluids, an additional band at approximately 40kDa is apparent, as previously stated. In contrast, COVA2-15 remains intact for at least 30 hours following incubation in apoplastic fluids. The alignment of 2F5 with COVA2-15 Fab' domains containing the CDR H3 loops was carried out on ChimeraX using the Matchmaker option (**Figure 4.2a**). 2F5 is characterized by extended CDR H3 loops consisting of 22 amino acids (Zwick et al., 2004). Similarly, the CDR H3 loop of COVA2-15 (22 residues) is also an extended CDR H3 loop considering the average length which is 12-15 amino acids (Brouwer et al., 2020). These data correlate with our *in silico* alignment, showing that both 2F5 and COVA2-15 CDR H3 loops are extended. However, when looking at the amino acid sequence and the *in silico* model, a disulphide bridge is formed within COVA2-15 loop. This disulphide bridge formation in the COVA2-15 exposed loop might be responsible for the stability of this IgG in both apoplastic fluids *in vitro* (**Figure 4.2b**) and when expressed *in vivo* (**Figure 4.4b**, lane 2). Hence, we next examined 2F5 CDR H3 mutants that could potentially form a disulphide bridge near the cleavage site or 2F5 CDR H3 mutants at the P1 cleavage site.

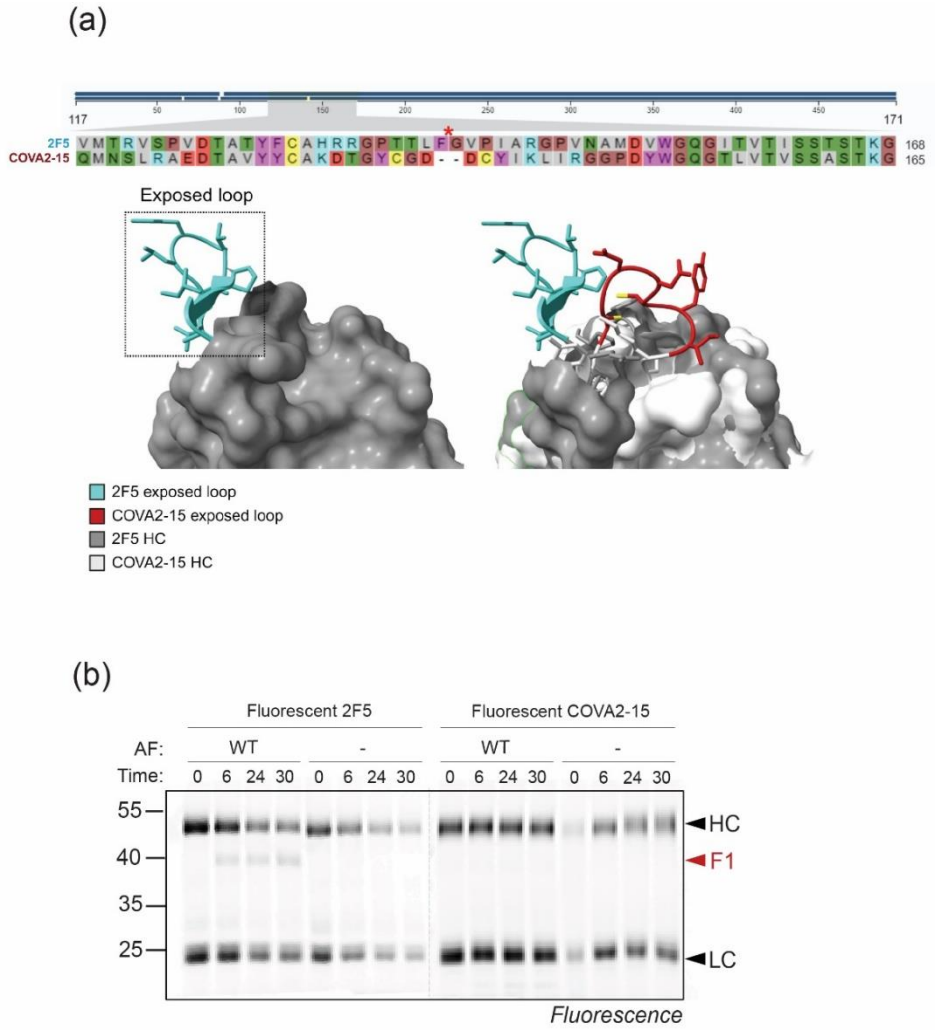

Figure 4.2 Compared to 2F5, COVA2-15 is very stable in apoplastic fluids.

(a) MSA of 2F5 and COVA2-15 including the CDR H3 loops are depicted (asterisk: known 2F5 cleavage site). Side views of the 2F5 IgG (dark grey: Fab' domain; heavy chain), obtained from PDB ID: 2P8L (left-hand side). The cleavage site is located at the exposed loop (cyan). Side views the 2F5 exposed loop in alignment with the COVA2-15 exposed loop in red (light grey: Fab' domain; heavy chain), obtained from AlphaFold prediction (right-hand side). **(b)** 2F5 or COVA2-15 IgG antibodies were incubated simultaneously in apoplastic fluids (WT) for 0, 6, 24 or 30 hours, separated on reducing protein gel and analysed by fluorescence scanning. Incubation in water was used as a control (-).

4.3 2F5 mutations of the CDR H3 loop near the cleavage site

To test whether mutations near the cleavage site of the 2F5 CDR H3 would have an impact on 2F5 processing, we produced five different mutants using site-directed mutagenesis. The promoter, terminator and backbone vectors remained the same for all constructs. Two mutants, ***m1*** **[T104C, I111C]** and ***m2*** **[L106C, V109C]** were made to examine the potential of disulphide bridge formation enclosing the cleavage site. In this case, two amino acids (double mutation) in the CDR H3 loop and near the cleavage site were mutated to Cys (C) residues. To account for disulphide bridge formation, 2F5 mutants were modelled on ChimeraX by editing the original 2F5 (PDB: 2P8L) using specific rotamers (**Figure 4.3a**). These specific rotamers were chosen based on the shortest distance between S atoms in Cys to increase the probability of forming a disulphide bridge. The cutoff S-S distance on PDB is set to 3.0 Å (Sun et al., 2017), while the distance of Cα atoms is between 3.5 Å and 7.0 Å (Gao et al., 2020). However, the shortest possible S-S distance was 3.117 Å for *m1* and 2.436 Å for *m2*. Additionally, three mutants were made by mutating one amino acid at the P1 site. In this case ***m3*** **[F107A]**, ***m4*** **[F107D]** and ***m5*** **[F107R]** mutants had a single mutation from Phe (F) to Ala (A), Asp (D) or Arg (R), respectively. In this case, the rotamers with the highest prevalence were chosen. The five 2F5 mutated HC or the wild-type HC of 2F5 were co-expressed with the 2F5 wild-type LC in *Nicotiana benthamiana* and total extracts were isolated at 5 days post infiltration. Crude extracts (CE; total extracts), flowthrough following protein A beads purification (FT) and elution (E) samples are shown in **Figure 4.3b**. From this point forward observations were mainly made by comparing FT or E samples which demonstrated a similar band profile. In **Figure 4.3b**, WT and *m3* had the lowest accumulation. F1 fragment which was previously observed in the WT HC (**Figure 4.2b**)

was also observed in all mutants *m1, m2, m3, m4* and *m5*. F2 fragment signal previously reported in *in vivo* 2F5 WT expression (**Figure 3.5**) was clearly apparent in *m1, m2, m3* and *m4* FT and E but only in *m5* CE. F3 and F4 fragments were also seen in crude extracts of *m1, m2, m4* and *m5*. Eluted WT, *m1* and *m3* are either nearly completely degraded or poorly expressed/purified. In parallel, the total or crude extracts of these samples were tested by indirect ELISA to confirm binding to HIV glycoprotein 41 (gp41). However, most data points were lower than the data points acquired from the standard curve of a commercial CHO 2F5. Hence, the raw absorbance intensities were plotted for every sample (**Figure 4.3c**). Absorbance of *m1* and *m2* was significantly higher and this observation is supported by the relative accumulation previously seen on the protein blot of the same samples (**Figure 4.3b**). However, all the above observations were made from one independent experiment. In another set of three independent experiments, 2F5 *m1* HC and 2F5 *m2* HC transient expression with the 2F5 WT LC resulted in 2.5 and 3.5-fold increase of 2F5 (LC+HC) compared to the WT HC, respectively (**Figure S4.1**). Interestingly, F1 fragment accumulation was not different across samples. F2 fragment was in similar levels to WT HC in *m1* HC mutant, while it was almost 6-fold more in the *m2* mutants. Taken all the above observations into account, *m1* and *m2* mutants are the most promising to be tested *in vitro* for their proteolytic processing in WT and protease-depleted apoplastic fluids as they consistently accumulate in higher yields.

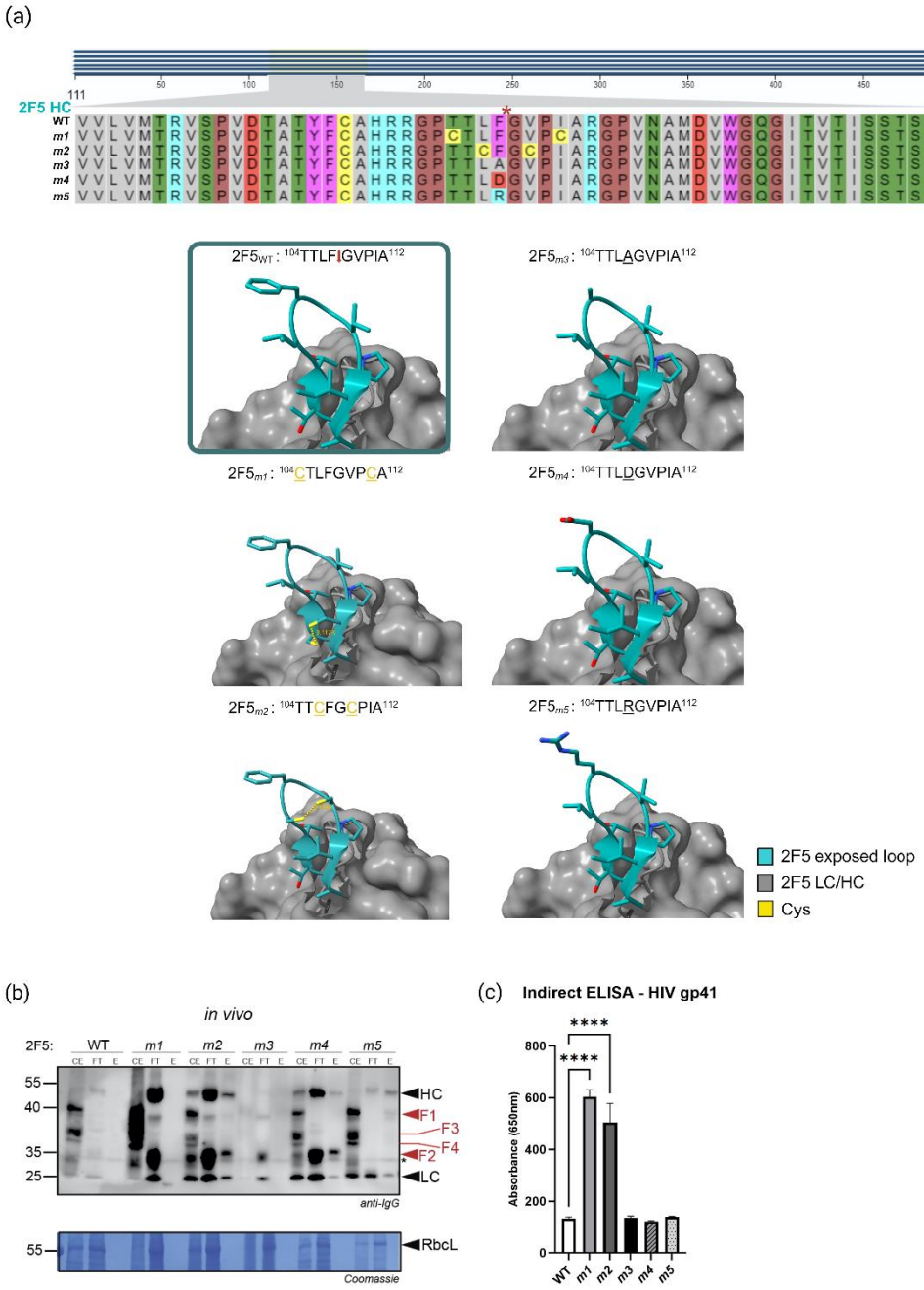

Figure 4.3 2F5 mutations of the CDR H3 loop near the cleavage site.

(a) MSA of 2F5 WT with the five mutants *m1, m2, m3, m4,* and *m5*. The sequences shown include the CDR H3 loop (asterisk: known 2F5 cleavage site). Side view of the 2F5 IgG (dark grey: Fab' domain; heavy chain), obtained from PDB ID: 2P8L (in box). Side views of 2F5 mutants, are numbered from *m1* to *m5* The cleavage site is located at the exposed loop (cyan). Mutated amino acids are either shown on MSA graph or as underlined above the respective structure. Putative S-S bond of *m1* and *m2* are highlighted between the Cys residues (yellow), with S-S distance at 3.117 Å for *m1* and 2.436 Å for *m2.* **(b)** Crude extracts (CE), flowthroughs (FT) and elution products (E), from leaves agroinfiltrated with 2F5 WT LC and 2F5 WT HC,

m1 HC, *m2* HC, *m3* HC, *m4* HC and *m5* HC. **(c)** Absorbance at 450nm from crude extracts shown in western blot (n=3 technical replicates from one independent experiment, p-value ****<0.0001). Samples CE, FT and E were generated and separated by reducing 12% SDS-PAGE and analysed by western blot using whole anti-IgG antibody. F1 fragment is a known cleavage product at approximately 40kDa. F2, F3, and F4 are additional degradation products. Coomassie staining of the large subunit of Rubisco was used to show loading. Significance was determined with one-way ANOVA, following multiple comparisons and Tukey's post-hoc test. Error bars represent SE of n=3 technical replicates from one independent experiment.

4.4 Elimination of the disulphide bridge on COVA2-15 exposed loop leads to HC processing

We previously mutated the 2F5 CDR H3 loop, where we introduced Cys residues within the loop to allow for interdomain disulphide bridge formation. Correspondingly, we mutated COVA2-15 two Cys (C) to Ala (A) at the respective CDR H3 loop, producing one mutant COVA2-15 HC ***m1*** **[C103A, C107A]**. The promoter, terminator and backbone vectors remained the same for both constructs. To visualise COVA2-15 *m1* we used ChimeraX and edited the original COVA2-15 Cys to Ala (AlphaFold-predicted), keeping the Ala rotamers with the highest prevalence (**Figure 4.4a**). The mutated HC or the wild-type HC of COVA2-15 were co-expressed with the COVA2-15 wild-type LC in *N. benthamiana* and total extracts were isolated at 5 days post infiltration. Total extracts were separated under reducing conditions. When produced in vivo, WT COVA2-15 remains stable. However, following mutations of the two Cys at the CDR H3 exposed loop, a 40 kDa fragment is evident (**Figure 4.4b**). In parallel, the same total extracts were tested by indirect ELISA to confirm binding to SARS-CoV-2 S protein. While WT and *m1* COVA2-15 appear to have comparable accumulation levels in protein blot, the concentration of the mutated COVA2-15 binding to the antigen drops dramatically compared to the WT

version. Similarly, when *m1* COVA2-15 is incubated *in vitro* with apoplastic fluids for 6 hours, it results in a fragment of the same size seen in *in vivo* processing.

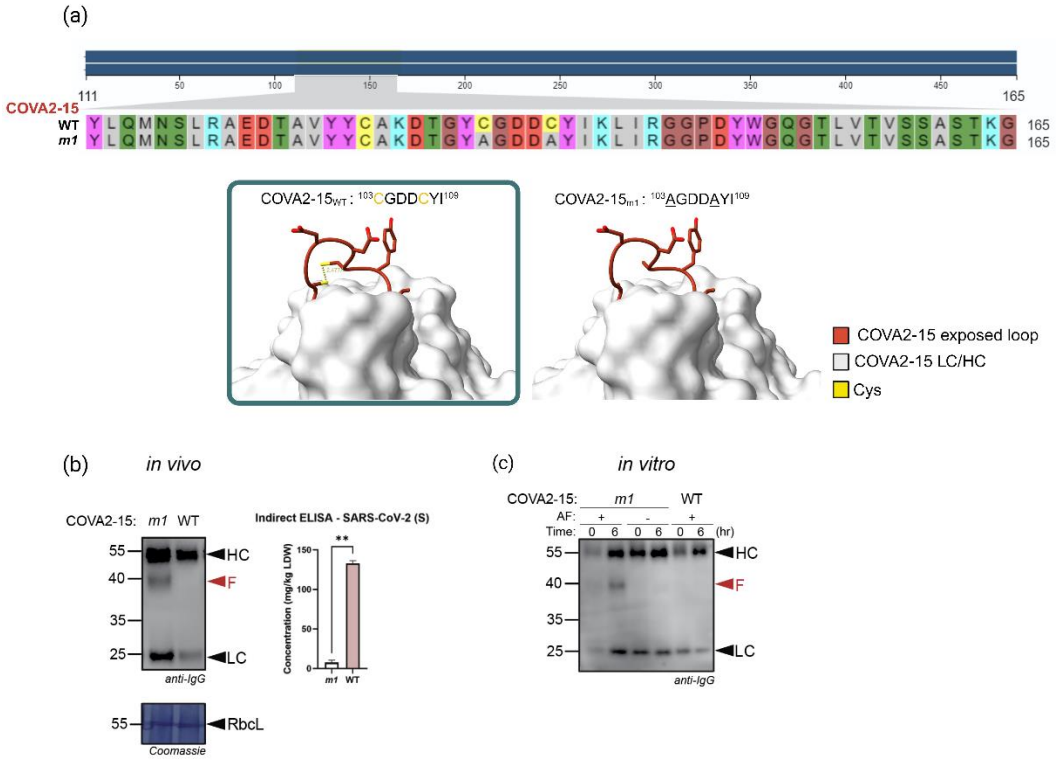

Figure 4.4 Elimination of the disulphide bridge on COVA2-15 exposed loop leads to HC processing, while also impeding antigen binding.

(a) MSA of COVA2-15 WT with the respective mutant *m1*. The sequences shown include the CDR H3 loop with Cys highlighted in yellow. Side view of the COVA2-15 IgG (light grey: Fab' domain; heavy chain), obtained from AlphaFold prediction (in box), or of the COVA2-15 *m1*, with their respective exposed loops in red. Mutated amino acids are either shown on MSA graph or as underlined above the respective structure. S-S bond of WT is highlighted between the Cys residues (yellow), with S-S distance at 2.477 Å. **(b)** Total extracts from leaves transiently expressing COVA2-15 WT HC or COVA2-15 *m1* HC. Western blot depicts one representative replicate of the triplicate. Absorbance at 450nm from crude extracts shown in western blot (n=3 independent experiments, p-value **0.0021). **(c)** COVA2-15 IgG antibody was incubated in apoplastic fluids for 0 or 30 hours, separated on reducing protein gel and analysed by western blotting. Incubation of the mutant *m1* in water was used as a control. Total extracts in (b) and (c) were generated and separated

by reducing 12% SDS-PAGE and analysed by western blot using whole anti-IgG antibody. F fragment is a cleavage product at approximately 40 kDa. Coomassie staining of the large subunit of Rubisco was used to show loading. Significance was determined with t-test. Error bars represent SE of n=3 experimental replicates.

Conclusions and Discussion

In this Chapter we investigated site-directed mutagenesis of the exposed CDR H3 loop in 2F5 antibody. We also determined the impact of intradomain disulphide bridge presence on IgG stability. Initially, we established that IgG antibodies COVA2-15 and 2F5 showed differences in stability, with COVA2-15 remaining stable for up to 30 hours in apoplastic fluids *in vitro*. This increased stability is explained by a distinct disulphide bridge in the COVA2-15 CDR H3 loop which is consistent with the literature. For example, the VRC01 CDR H3 loop is characterised for its restrained flexibility due to the presence of a disulphide bridge (Zhou et al., 2010). This could explain why the distinct 40 kDa fragment we see in 2F5 is not present in VRC01 when expressed *in planta* (Teh et al., 2014), showing that structural changes can have a major effect on antibody stability. Our mutation strategy examined the formation of disulphide bridges near the cleavage site (*m1* and *m2*), or targeting the P1 cleavage site (*m3 m4* and *m5*) directly.

Disulphide bridges have been demonstrated to stabilise proteins my maintaining overall tertiary structure through interdomain and intradomain interactions (Bechtel & Weerapana, 2017; Sevier & Kaiser, 2002). Several studies testing disulphide bridge formation on peptide or protein stability have been described (Liu et al., 2008; M. Mansfeld & Toth, 2012; Rozek et al., 2003; Sun et al., 2017). It has previously been reported that antibodies could be stabilised by mutations that lead to disulphide bond formation (Peters et al., 2012). 2F5 *m1* HC and 2F5 *m2* HC transient expression with the 2F5 WT LC resulted in 2.5 and 3.5-fold increase of 2F5 (LC+HC) compared to the WT HC, respectively (**Figure S4.1**). However, no distinct differences were observed in F1 fragment accumulation that represents the fragment following CDR H3 loop processing. Increased accumulation seen in these mutants might be explained by better overall

stability or more efficient folding and not necessarily due to protection of the cleavage site. In any case, confirming that a disulphide bond is indeed formed should be validated through more experimentation and cannot be confidently predicted solely based on *in silico* structures.

Moreover, we have established that the sole protease that cleaves 2F5 after *in vitro* incubation with apoplastic fluids is SBT5.2 (Beritza et al., 2024; Puchol Tarazona et al., 2021). Although it is known that subtilases have a very broad substrate specificity, preference for large hydrophobic residues at the primary specificity site has been reported (DeSantis et al., 1999; Peterle et al., 2020; Siezen & Leunissen, 1997). Regarding P1 mutagenesis, *m3* (F107A) mutant resulted in drastic decrease in accumulation (**Figure 4.2b**). This might be either due to overall structure instability and/or inefficient protein folding following this mutation. Hence, a mutation from a bulky hydrophobic residue (P) to a small one (A) could lead to instability. Similarly, *m5* exhibited vulnerability to processing *in vivo* as most heavy chain was cleaved resulting in F1 fragment generation (**Figure 4.2b** CE), leaving only traces of full HC in purification samples. Since this mutation was from the hydrophobic Phe to the hydrophilic Arg, this increased hydrophilic nature on the tip of the CDR H3 loop can make the cleavage site of 2F5 more accessible to proteases. In contrast, *m4* mutant demonstrated higher accumulation than *m3* and *m5*, with still however resulting in F1 fragment. This might again be the case due to changes in overall stability and folding.

Accordingly, when the Cys residues in the COVA2-15 antibody are mutated to Ala, an F1-like 40 kDa fragment arises, indicating cleavage in the CDR H3 loop. However, this mutation appeared to be detrimental for antigen binding as shown in **Figure 4.3b**. This

proves that indeed the disulphide bond is responsible for COVA2-15 stability, however this is not necessarily indicative of a one-size-fits-all solution for all IgG stability.

These results clearly indicated that site-directed mutagenesis of antibodies can be a promising strategy for enhanced stability against processing from proteases. However, this data also demonstrates that such mutations can potentially decrease antibody binding activity. Thus, careful consideration is required to ensure that the modifications do not compromise antigen-binding efficacy or virus neutralisation (Alam et al., 2009; Ofek et al., 2010; Zwick et al., 2004).

Supplementary Data

Figure S4.1 – Co-expression of 2F5 LC_{WT} with $2F5_{WT}$, $2F5_{m1}$, or $2F5_{m2}$.

Total extracts were isolated at 5d.p.i. and samples were loaded under reducing conditions. 2F5 accumulation was significantly higher in both mutated HC versions, where m1 was approximately 2.5-fold and m2 approximately 3.5-fold more compared to WT HC respectively. F1 fragment accumulation was not different across samples. F2 fragment was not significantly more in *m1* mutant, while it was almost 6-fold more in the *m2* mutants. Total extracts were generated and separated by reducing 12% SDS-PAGE and analysed by western blot using whole anti-IgG antibody. F fragment is a cleavage product at approximately 40kDa. Coomassie staining of the large subunit of Rubisco was used to show loading. Significance was determined with t-test. Error bars represent SE of n=3 experimental replicates (adjusted p-values from left to right: F2 **0.0015; **0.0019, LC+HC *0.0334; **0.002).

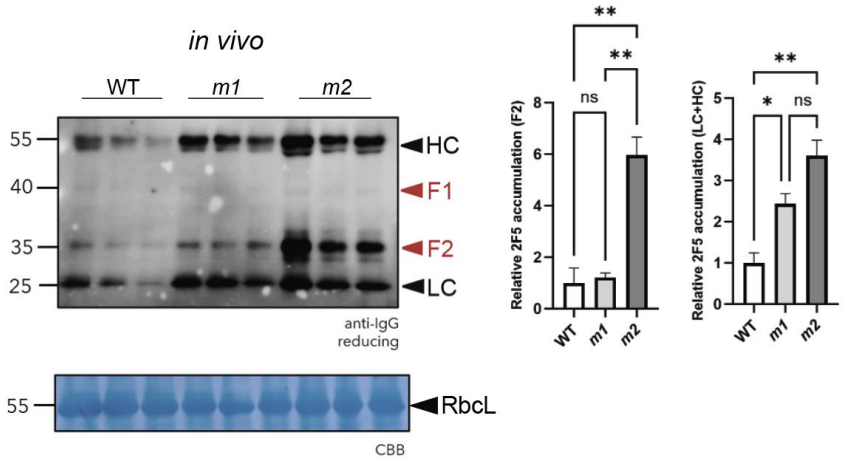

References

Alam, S. M., Morelli, M., Dennison, S. M., Liao, H.-X., Zhang, R., Xia, S.-M., Rits-Volloch, S., Sun, L., Harrison, S. C., Haynes, B. F., Chen, B., & Xiamen, E. (2009). Role of HIV membrane in neutralization by two broadly neutralizing antibodies. www.pnas.orgcgidoi10.1073pnas.0908713106

Bechtel, T. J., & Weerapana, E. (2017). From structure to redox: The diverse functional roles of disulfides and implications in disease. In Proteomics (Vol. 17, Issue 6). Wiley-VCH Verlag. https://doi.org/10.1002/pmic.201600391

Beritza, K., Buscaill, P., Song, S.-J., Jutras, P. V, Huang, J., Mach, L., Dong, S., & Van Der Hoorn, R. A. L. (2024). SBT5.2s are the major active extracellular subtilases processing IgG antibody 2F5 in the Nicotiana benthamiana apoplast.

Coffeen, W. C., & Wolpert, T. J. (2004). Purification and characterization of serine proteases that exhibit caspase-like activity and are associated with programmed cell death in Avena sativa. Plant Cell, 16(4), 857–873. https://doi.org/10.1105/tpc.017947

DeSantis, G., Shang, X., & Jones, J. B. (1999). Toward tailoring the specificity of the S1 pocket of subtilisin B. lentus: Chemical modification of mutant enzymes as a strategy for removing specificity limitations. Biochemistry, 38(40), 13391–13397. https://doi.org/10.1021/bi990861o

Doria-Rose, N. A., Schramm, C. A., Gorman, J., Moore, P. L., Bhiman, J. N., DeKosky, B. J., Ernandes, M. J., Georgiev, I. S., Kim, H. J., Pancera, M., Staupe, R. P., Altae-Tran, H. R., Bailer, R. T., Crooks, E. T., Cupo, A., Druz, A., Garrett, N. J., Hoi, K. H., Kong, R., … Mascola, J. R. (2014). Developmental pathway for potent V1V2-directed HIV-neutralizing antibodies. Nature, 508(7498), 55–62. https://doi.org/10.1038/nature13036

Galiullina, R. A., Kasperkiewicz, P., Chichkova, N. V., Szalek, A., Serebryakova, M. V., Poreba, M., Drag, M., & Vartapetian, A. B. (2015). Substrate specificity and possible heterologous targets of phytaspase, a plant cell death protease. Journal of Biological Chemistry, 290(41), 24806–24815. https://doi.org/10.1074/jbc.M115.675819

Gao, X., Dong, X., Li, X., Liu, Z., & Liu, H. (2020). Prediction of disulfide bond engineering sites using a machine learning method. Scientific Reports, 10(1). https://doi.org/10.1038/s41598-020-67230-z

Hamilton, J. M. U., Simpson, D. J., Hyman, S. C., Ndimba, B. K., & Slabas, A. R. (2003). Ara12 subtilisin-like protease from Arabidopsis thaliana: purification, substrate specificity and tissue localization. Biochemical Journal, 370(1), 57–67. https://doi.org/10.1042/bj20021125

Hehle, V. K. , Paul, M. J. , Roberts, V. A. , van Dolleweerd, C. J. , & Ma, J. K. (2016). Site-targeted mutagenesis for stabilization of recombinant monoclonal antibody expressed in tobacco (Nicotiana tabacum) plants. FASEB, 30(3), 1590–1598.

Hehle, V. K., Lombardi, R., van Dolleweerd, C. J., Paul, M. J., Di Micco, P., Morea, V., Benvenuto, E., Donini, M., & Ma, J. K. C. (2015). Site-specific proteolytic degradation of IgG monoclonal

antibodies expressed in tobacco plants. Plant Biotechnology Journal, 13(2), 235–245. https://doi.org/10.1111/pbi.12266

Homma, F., Huang, J., & van der Hoorn, R. A. L. (2023). AlphaFold-Multimer predicts cross-kingdom interactions at the plant-pathogen interface. Nature Communications, 14(1). https://doi.org/10.1038/s41467-023-41721-9

Liu, Y., Yang, Y., Qi, J., Peng, H., & Zhang, J. T. (2008). Effect of cysteine mutagenesis on the function and disulfide bond formation of human ABCG2. Journal of Pharmacology and Experimental Therapeutics, 326(1), 33–40. https://doi.org/10.1124/jpet.108.138115

M Brouwer, P. J., Caniels, T. G., van der Straten, K., Snitselaar, J. L., Aldon, Y., Bangaru, S., Torres, J. L., A Okba, N. M., Claireaux, M., Kerster, G., H Bentlage, A. E., van Haaren, M. M., Guerra, D., Burger, J. A., Schermer, E. E., Verheul, K. D., van der Velde, N., van der Kooi, A., van Schooten, J., … van Gils, M. J. (2020). Potent neutralizing antibodies from COVID-19 patients define multiple targets of vulnerability.

M. Mansfeld, F., & Toth, I. (2012). Synthesis and Plasma Stability of Disulfide-Bridged Cyclic Endomorphin-1 Derivatives. International Journal of Organic Chemistry, 02(01), 1–6. https://doi.org/10.4236/ijoc.2012.21001

Niemer, M., Mehofer, U., Torres Acosta, J. A., Verdianz, M., Henkel, T., Loos, A., Strasser, R., Maresch, D., Rademacher, T., Steinkellner, H., & Mach, L. (2014). The human anti-HIV antibodies 2F5, 2G12, and PG9 differ in their susceptibility to proteolytic degradation: Down-regulation of endogenous serine and cysteine proteinase activities could improve antibody production in plant-based expression platforms. Biotechnology Journal, 9(4), 493–500. https://doi.org/10.1002/biot.201300207

Obregon, P., Chargelegue, D., Drake, P. M. W., Prada, A., Nuttall, J., Frigerio, L., & Ma, J. K. C. (2006). HIV-1 p24-immunoglobulin fusion molecule: A new strategy for plant-based protein production. Plant Biotechnology Journal, 4(2), 195–207. https://doi.org/10.1111/j.1467-7652.2005.00171.x

Ochoa, R., Magnitov, M., Laskowski, R. A., Cossio, P., & Thornton, J. M. (2020). An automated protocol for modelling peptide substrates to proteases. BMC Bioinformatics, 21(1). https://doi.org/10.1186/s12859-020-03931-6

Ofek, G., McKee, K., Yang, Y., Yang, Z.-Y., Skinner, J., Guenaga, F. J., Wyatt, R., Zwick, M. B., Nabel, G. J., Mascola, J. R., & Kwong, P. D. (2010). Relationship between Antibody 2F5 Neutralization of HIV-1 and Hydrophobicity of Its Heavy Chain Third Complementarity-Determining Region. Journal of Virology, 84(6), 2955–2962. https://doi.org/10.1128/jvi.02257-09

Olsen, J. V., Ong, S. E., & Mann, M. (2004). Trypsin cleaves exclusively C-terminal to arginine and lysine residues. Molecular and Cellular Proteomics, 3(6), 608–614. https://doi.org/10.1074/mcp.T400003-MCP200

Peterle, D., Pontarollo, G., Spada, S., Brun, P., Palazzi, L., Sokolov, A. V., Spolaore, B., Polverino de Laureto, P., Vasilyev, V. B., Castagliuolo, I., & De Filippis, V. (2020). A serine protease secreted from Bacillus subtilis cleaves human plasma transthyretin to generate an amyloidogenic fragment. Communications Biology, 3(1). https://doi.org/10.1038/s42003-020-01493-0

Peters, S. J., Smales, C. M., Henry, A. J., Stephens, P. E., West, S., & Humphreys, D. P. (2012). Engineering an improved IgG4 molecule with reduced disulfide bond heterogeneity and increased fab domain thermal stability. Journal of Biological Chemistry, 287(29), 24525–24533. https://doi.org/10.1074/jbc.M112.369744

Puchol Tarazona, A. A., Maresch, D., Grill, A., Bakalarz, J., Torres Acosta, J. A., Castilho, A., Steinkellner, H., & Mach, L. (2021). Identification of two subtilisin-like serine proteases engaged in the degradation of recombinant proteins in Nicotiana benthamiana. FEBS Letters, 595(3), 379–388. https://doi.org/https://doi.org/10.1002/1873-3468.14014

Rawlings, N. D., Barrett, A. J., & Bateman, A. (2012). MEROPS: The database of proteolytic enzymes, their substrates and inhibitors. Nucleic Acids Research, 40(D1). https://doi.org/10.1093/nar/gkr987

Rozek, A., Powers, J. P. S., Friedrich, C. L., & Hancock, R. E. W. (2003). Structure-Based Design of an Indolicidin Peptide Analogue with Increased Protease Stability. Biochemistry, 42(48), 14130–14138. https://doi.org/10.1021/bi035643g

Schechter, I., & Berger, A. (1967). BIOCHEMICAL AND BIOPHYSICAL RESEARCH COMMUNICATIONS ON THE SIZE OF THE ACTIVE SITE IN PROTEASES. I.. PAPAIN (Vol. 27, Issue 2).

Sevier, C. S., & Kaiser, C. A. (2002). Formation and transfer of disulphide bonds in living cells. In Nature Reviews Molecular Cell Biology (Vol. 3, Issue 11, pp. 836–847). https://doi.org/10.1038/nrm954

Siezen, R. J., & Leunissen, J. A. M. (1997). Subtilases: The superfamily of subtilisin-like serine proteases. In Protein Science (Vol. 6, Issue 3, pp. 501–523). Blackwell Publishing Ltd. https://doi.org/10.1002/pro.5560060301

Sun, M. an, Wang, Y., Zhang, Q., Xia, Y., Ge, W., & Guo, D. (2017). Prediction of reversible disulfide based on features from local structural signatures. BMC Genomics, 18(1). https://doi.org/10.1186/s12864-017-3668-8

Teh, A. Y. H., Maresch, D., Klein, K., & Ma, J. K. C. (2014). Characterization of VRC01, a potent and broadly neutralizing anti-HIV mAb, produced in transiently and stably transformed tobacco. Plant Biotechnology Journal, 12(3), 300–311. https://doi.org/10.1111/pbi.12137

Zabetakis, D., Olson, M. A., Anderson, G. P., Legler, P. M., & Goldman, E. R. (2014). Evaluation of disulfide bond position to enhance the thermal stability of a highly stable single domain antibody. PLoS ONE, 9(12). https://doi.org/10.1371/journal.pone.0115405

Zemlin, M., Klinger, M., Link, J., Zemlin, C., Bauer, K., Engler, J. A., Schroeder, H. W., & Kirkham, P. M. (2003). Expressed murine and human CDR-H3 intervals of equal length exhibit distinct repertoires that differ in their amino acid composition and predicted range of structures. Journal of Molecular Biology, 334(4), 733–749. https://doi.org/10.1016/j.jmb.2003.10.007

Zhou, T., Georgiev, I., Wu, X., Yang, Z.-Y., Dai, K., Finzi, A., Kwon, Y. Do, Scheid, J. F., Shi, W., Xu, L., Yang, Y., Zhu, J., Nussenzweig, M. C., Sodroski, J., Shapiro, L., Nabel, G. J., Mascola, J. R., & Kwong, P. D. (2010). Structural Basis for Broad and Potent Neutralization of HIV-1 by Antibody VRC01. https://www.science.org

Zwick, M. B., Komori, H. K., Stanfield, R. L., Church, S., Wang, M., Parren, P. W. H. I., Kunert, R., Katinger, H., Wilson, I. A., & Burton, D. R. (2004). The Long Third Complementarity-Determining Region of the Heavy Chain Is Important in the Activity of the Broadly Neutralizing Anti-Human Immunodeficiency Virus Type 1 Antibody 2F5. Journal of Virology, 78(6), 3155–3161. https://doi.org/10.1128/jvi.78.6.3155-3161.2004

Chapter 5

IgGs localisation and mistargeting: The effect of subcellular compartmentation on IgG processing and overall accumulation

Part of this Chapter is published as: Beritza, K., et al., (2024), SBT5.2s are the major active extracellular subtilases processing IgG antibody 2F5 in the Nicotiana benthamiana apoplast. Plant Biotechnol. J., Vol22, p.2808.

5.1 Introduction

One crucial step towards understanding which proteases might cleave different IgGs or where this processing occurs upon expression is to understand where these IgGs accumulate. To visualise the intracellular movement of the HIV-neutralizing monoclonal antibody 2G12 in plant systems, a previous study fused 2G12 light and heavy chains (LC and HC) with fluorescent proteins (Irons et al., 2008). LC fusions were found in mobile pre-vacuolar compartments (PVCs) and vacuoles, with some apoplast labelling. HC fusion remained in the endoplasmic reticulum (ER), while no HC was observed in the apoplast. Co-expression of LC and HC fusions resulted in larger, distinct punctate structures associated with the ER that partially overlapped with PVC markers, without increased apoplast labelling. Similarly, 2F5 HC localises to the ER without apoplast secretion, whereas the 2F5 LC/HC complex exhibits variable cytoplasmic mobility and localisation, indicating post-Golgi and vacuolar localisation. This observation contradicts another study of electron microscopy data on untagged 2G12 in plants, in which the antibody was detected in the apoplast (Arcalis et al., 2013).

The secretory pathway includes various protease classes, with the most common being pepsin-like (A1), papain-like (C1), trypsin chymotrypsin-like (S1), subtilisin-like (S8), and serine carboxypeptidase-like (S10) (Goulet et al., 2012; Pillay et al., 2014). Targeting recombinant proteins to other compartments for molecular pharming purposes has been extensively used due to various potential benefits (Nausch et al., 2012; Niemer et al., 2014; Ocampo et al., 2016; Ponndorf et al., 2021; Thomas & Walmsley, 2014). First, directing foreign protein synthesis to the ER rather than the cytosol reduces proteolytic degradation (Doran, 2006; Jan et al., 2014). Second, the ER has a high concentration of molecular chaperones that promote protein folding (Edkins &

Blatchheditors, 2023; Gupta & Tuteja, 2011). Third, protein accumulation in the ER prevents plant-specific N-glycan modifications in the Golgi apparatus, which yields N-glycosylated proteins with consistent high-mannose glycan structures (Bosch et al., 2013; Strasser, 2018). To accumulate recombinant proteins in the plant ER, an N-terminal ER targeting or secretion signal peptide can be used with a C-terminal retention sequence (Gutiérrez et al., 2013; He et al., 2012; Nausch et al., 2012; Shin et al., 2022; Soni et al., 2022). ER-targeted-2G12 antibody increased by 2.5 fold when expressed in *N. benthamiana* (Sainsbury & Lomonossoff, 2008). In addition to the conventional C-terminal HDEL/KDEL retention signal, the development of protein bodies within the endoplasmic reticulum can greatly enhance the accumulation of recombinant proteins. This process is typically initiated by specific protein tags, such as the N-terminal proline-rich domain of γ-zein (Zera). Protein bodies accumulation due to Zera leads to an approximately 5-fold increase in the recombinant *Yersinia pestis* F1-V antigen in *N. benthamiana* leaves (Alvarez et al., 2010).

The plant vacuole in fully developed tobacco leaf cells comprises 80-90% of the cellular volume (Eisenach et al., 2015), which is promising for storing recombinant proteins. Various vacuolar sorting signals (VSSs) have been identified for directing proteins to vacuoles in tobacco. These include sequence-specific (ss) signals, which are short amino acid sequences such as NPIR or NPIXL (Ocampo et al., 2016; Xiang et al., 2013), and hydrophobic C-terminal (Ct) signals that lack a specific consensus sequence but are consistently found at the protein's C-terminus (X. Zhang et al., 2021). When the heavy chain of mAb 14D9 was combined with either the Ct VSS (KISIA) or ss VSS (NIFRGF), it resulted in a 10- to 15-fold increase in vacuolar mAb accumulation compared to the secreted mAb version in *N. benthamiana* (Ocampo et al., 2016). Hence, mistargeting to these compartments might be promising for Molecular Pharming purposes.

In this **Chapter**, we initially investigated the effect of single antibody chain expression, as well as using a single multi-gene vector to express both chains from a single T-DNA . We then validated that some IgGs transiently expressed in *N. benthamiana* and carrying a secretion signal peptide are not found in the apoplast in expected levels. Next, we examined the use of alternative signal peptides in pursuit of increased secretion efficiency. Moreover, as we proved that IgGs like 2F5 are likely trapped intracellularly, we tested depleting various intracellular proteases found along the secretory pathway.

Additionally, we explored the impact of retention to the ER or mistargeting to the vacuole on the processing and overall accumulation of 2F5 and VRC01 antibodies. Finally, following optimisation of ER retention of 2F5, we also examined the concept of an extended ER phenotype and its possible effect on IgG accumulation following two approaches: a naturally expanded ER based on endogenous phosphocholine cytidylyltransferase increased levels, or a synthetically expanded ER based on the dimerisation of polyprotein complexes anchoring on the ER membrane (Sandor et al., 2024).

Results

5.2 The 2F5 F2 fragment originates from HC overexpression

To assess the assembly of the 2F5 IgG and its intermediates, the light chain alone, the heavy chain alone or both light and heavy chains of 2F5 were transiently expressed by agroinfiltration in *N. benthamiana* and total extracts analysed five days post infiltration (d.p.i.; **Figure 5.1a**). Total extracts were also used for enzyme-linked immunosorbent assay (ELISA) to determine antigenicity of the plant-produced 2F5. When light chain was expressed no degradation products are visible. On the contrary, in HC overexpression an F2 fragment at around 32 kDa was the dominant band while full HC expected at 55 kDa was not present. Also, a less accumulated product of approximately 60 kDa was observed, possibly a hyperglycosylated free HC (grey arrow). When both chains were expressed, both light and heavy chains accumulate more compared to when they were expressed on their own. F2 fragment was also less abundant than in lone HC overexpression, while the F1 fragment derived from H3 loop cleavage was also evident. The samples from leaves expressing both chains were also run on a non-reducing gel to ensure the fully assembled 2F5 (H_2L_2) formed, this was observed at approximately 150 kDa (**Figure 5.1b**).

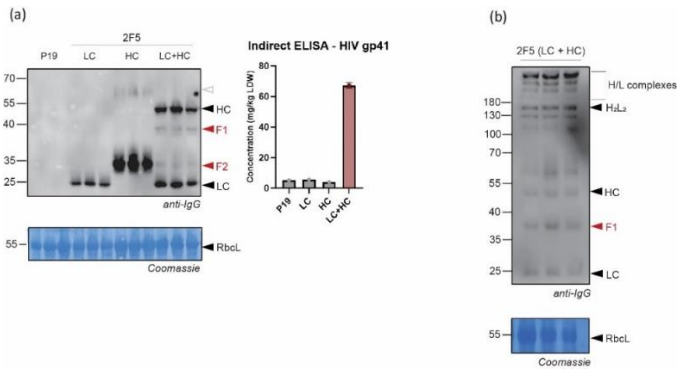

Figure 5.1 2F5 F2 fragment originates from HC overexpression (caption on next page).

(a) The light chain, the heavy chain or both light and heavy chains of 2F5 were transiently expressed by agroinfiltration in *N. benthamiana* and total extracts were generated five days later in triplicate and separated by reducing 12% SDS-PAGE and analysed by western blot using whole anti-IgG antibody. Coomassie staining of the large subunit of Rubisco was used to show loading. Total extract samples were also used for indirect ELISA assay, using a CHO-2F5 as a control for concentration calculations with n=3 for both control and test samples. **(b)** Transient overexpression of 2F5 LC + HC, where total extracts were analysed in triplicates under non-reducing conditions.

5.3 Light and heavy chains of 2F5 in the same T-DNA leads to increased accumulation

To examine whether the multiplicity of T-DNA vectors impacts IgG overexpression, the light and heavy chains were cloned into the same vector (L2::LC/HC) to be used for transient expression. As a comparison, two vectors carrying the light or the heavy chain (L1::LC + L1::HC) were mixed in 1:1 ratio before infiltration (**Figure 5.2a**). To account for same final optical density of agrobacteria cultures and for equal T-DNA insertion competition, L2 vector was mixed 1:1 with an empty vector control. Total extracts were collected five days post infiltration and samples were run on a gel under reducing or non-reducing conditions to ensure assembly of the full IgG complex (**Figure 5.2b**). In both cases, the full IgG complex was observed (non-reducing), as well as both light and heavy chains (reducing). Under reducing conditions the relative 2F5 (LC + HC) accumulation was calculated, with L2 vector resulting in a 8-fold increase compared to the 1:1 mix of L1 vectors. While both F1 and F2 fragments are visible in both samples, F1 and F2 proportionally accumulated in L2 samples, as the full HC accumulation is higher to begin with.

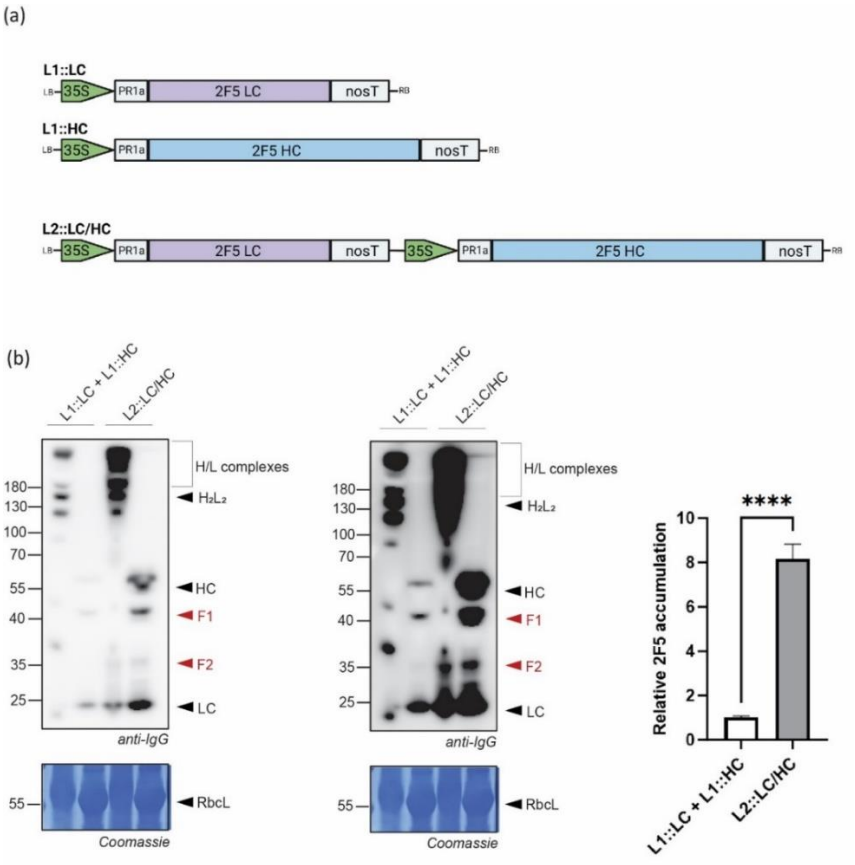

Figure 5.2 Light and heavy chains of 2F5 in the same T-DNA leads to increased accumulation.

(a) T-DNA of LC, HC, or LC/HC used for transient expression by agroinfiltration in *N. benthamiana.* In both cases both LC and HC coding sequences were under the Cauliflower mosaic virus 35S (35S) promoter and the nopaline synthase (Tnos) terminator. **(b)** Total extracts were generated and separated by reducing 12% SDS-PAGE and analysed by western blot using whole anti-IgG antibody. Left and right blot were generated following 10 and 20 seconds of exposure, respectively to allow for the higher molecular weight bands to be distinct. F1 and F2 fragments indicate processing products. One representative replicate of the triplicate is shown. Coomassie staining of the large subunit of Rubisco was used to show loading. Quantification of IgG accumulation (LC+HC) is depicted in respective graphs. Data were tested for normal distribution, while significance was determined with one-way ANOVA, following multiple comparisons and Tukey's post-hoc test. Error bars represent SE of n=3 experimental replicates.

5.4 2F5 is not efficiently secreted into the apoplast

5.4.1 Estimating 2F5 secretion by western blot analysis

To test whether 2F5 is secreted to the apoplast when expressed by agroinfiltration, we co-expressed the HC and LC of 2F5 with cytonuclear Green Fluorescent Protein (cGFP, (Jutras et al., 2021) as a cytonuclear control and secreted Red Fluorescent Protein (sRFP, Samalova et al., 2006) harbouring a signal peptide as a secretion control (**Figure 5.3a**). Apoplastic fluids and total extracts were generated from the same agroinfiltrated leaves co-expressing 2F5, sRFP, and cGFP and analysed by western blotting. Consistent with their predicted subcellular localisation, most cGFP was detected in total extracts (**Figure 5.3b** and **5.3c**), whereas sRFP was mostly detected in apoplastic fluids (**Figure 5.3b** and **5.3d**). 2F5, however, is hardly detected in the apoplast and both the HC and LC accumulated to high levels in total extracts, similar to cGFP (**Figure 5.3b** and **5.3e**). Calculated back to the same leaf area, these data indicate that 3.4%, 43%, and 3.6% of the cGFP, sRFP, and 2F5 detected in total extracts of wild-type plants were present in apoplastic fluids, respectively.

A similar low apoplastic accumulation was detected for cGFP, sRFP and 2F5 in the *sbt5.2* triple mutants, except that 3-fold more 2F5 accumulated in the triple *sbt5.2* mutant, both in apoplastic fluids as in total extracts (**Figure 5.3b-e**), consistent with previous data from Chapter 3 (**Figure 3.5b**). Calculated back to the same leaf area, these data indicate that 3.9%, 41.3%, and 2.8% of the GFP, RFP, and 2F5 detected in total extracts of the s*bt5.2#4-4* mutant were present in apoplastic fluids, respectively. Similar numbers were found for the *sbt5.2#8-11* mutant (5.1%, 47.1% and 3.6% for cGFP, sRFP and 2F5, respectively).

When analysing the separate signals originating from 2F5, we noticed that the F1 fragment distributes over the samples in a similar way as the HC, both being detected only in trace amounts in apoplastic fluids (**Figure 5.3f**,**g**), representing only 2.4% and 2.3% of the HC and F1 signals detected in total extracts. By contrast, the LC was more readily detected in apoplastic fluids (**Figure 5.3i**), representing 5.5% of the signal detected in total extracts. In addition, although weak, the F2 fragment is even more readily detected in apoplastic fluids (**Figure 5.3h**), representing 18.7% of the signal detected in total extracts. These data indicate that HC and fragment F1 accumulate at much lower relative levels in the apoplast when compared to the LC and fragment F2.

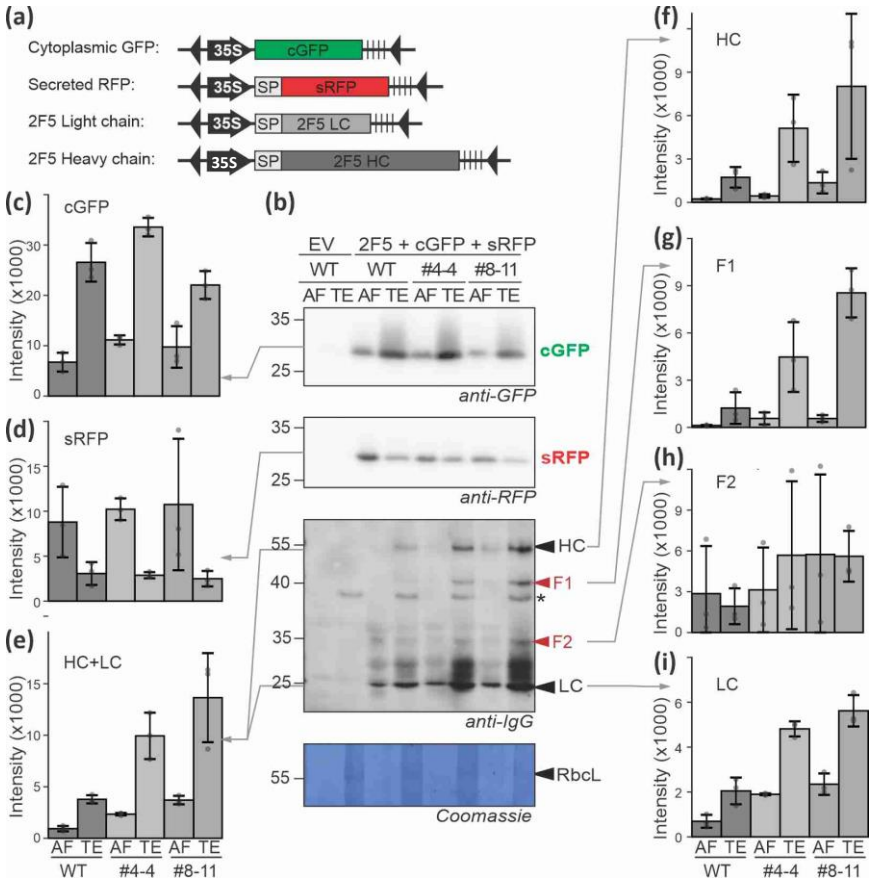

Figure 5.3 Transiently expressed 2F5 is not in the apoplast of agroinfiltrated leaves (caption on next page).

(a) T-DNAs for the expression of cytonuclear GFP (cGFP), secreted RFP (sRFP) and the HC and LC of 2F5. **(b)** Both HC and LC of 2F5 were co-expressed with a positive control (secreted sRFP), and a negative control (cytonuclear cGFP) for secretion. Total extracts and apoplastic fluids were isolated after 5 days from the same leaves in triplicate, separated on reducing 12% SDS-PAGE gels and analysed by western blotting using antibodies against GFP, RFP and IgG. One representative replicate of the triplicate is shown. *, background signal. Coomassie staining was used to show the large subunit of Rubisco in total extracts. **(c-i)** Chemilluminescence signals quantified from western blots quantified over the three replicates.

5.4.2 Assessing 2F5 secretion by confocal microscopy

To test whether 2F5 is secreted to the apoplast we used a different approach by estimating the co-localisation of previously tested markers with fluorescently-labelled 2F5 using confocal microscopy. The markers were the same used for western blotting (**Figure 5.3**), with cytonuclear Green Fluorescent Protein (cGFP, Jutras et al., 2021) as a cytonuclear control and secreted Red Fluorescent Protein (sRFP, Samalova et al., 2006) harbouring a signal peptide as a secretion control. Light chain and heavy chain of 2F5 were re-cloned in separate vectors as previously (L1, **Figure 5.2a**), with enhanced GFP (eGFP) or monomeric Scarlet (mScarlet, RFP derivative) in the C-terminus of the LC or HC coding sequences, respectively. The LC and HC were linked to the respective fluorophores using the GGGSGGG heptapeptide linker. To ensure that the fully assembled IgG would exhibit as close to native behaviour as possible, the corresponding chain that was co-expressed in untagged form.

To conduct co-localisation analysis, the following fluorescent construct pairs sGFP+sRFP or cGFP+cRFP were co-expressed as positive co-localisation controls in the apoplast and the cytosol, respectively. Similarly, cGFP+sRFP were co-expressed and was used as a negative co-localisation control. LC::eGFP was co-expressed with either cRFP or

sRFP, and untagged HC, while HC::mScarlet was co-expressed with either cGFP or sGFP, and the untagged LC. All samples were harvested 5 days following infiltration and imaged on a confocal microscope. Three representative images from each combination were used to conduct post-acquisition co-localisation analysis (**Figure 5.4; Table 5.1**).

The HC::mScarlet construct displayed a primarily cytosolic distribution (**Figure 5.4**; panels sGFP+HC::mScarlet and cGFP+HC::mScarlet), with the majority of mScarlet fluorescence co-localising with the cytosolic GFP marker. However, there are some notable regions (see white arrowheads) at the cell periphery where only mScarlet signal was detected, consistent with apoplastic localisation. This observation is not clearly supported by the correlation co-efficients (**Table 5.1**). The Pearson's correlation co-efficient for both sGFP+HC::mScarlet and cGFP+HC::mScarlet are approximately zero, suggesting no correlation. For cGFP+HC::mScarlet, Manders M1 and M2 values were close to 0.5, indicating moderate correlation, while, interestingly, for the sGFP+HC::mScarlet combination, the M2 value was much higher than the M1 value, indicating that a greater proportion of HC::mScarlet is co-localised with sGFP than the opposite. Another interesting observation is the apparent absence of HC::mScarlet in putative trans-vacuolar strands (**Figure 5.4**, see blue arrowheads). Overall, the HC::mScarlet distribution exhibits a similar behaviour as the negative control cGFP+sRFP, suggesting that only a small proportion of the HC localises to the apoplast with the majority remains in the cytosol.

The LC::eGFP construct displayed strong co-localisation with both the cytosolic and the apoplastic markers, as can be seen both in the representative images and all co-localisation co-efficients, which are highly similar to both positive control combinations. More specifically, the Pearson's correlation coefficient of 0.47 was observed between

sRFP+LC::eGFP and 0.31 between cRFP+LC::eGFP, suggesting stronger correlation with sRFP. Additionally, Manders's M1 coefficient was 0.84 and 0.6 for both the previous combinations, respectively, while the M2 coefficients were correspondingly 0.93 and 0.97. The Manders's coefficients indicate that a greater proportion of LC::eGFP correlates with sRFP than with cRFP, while the majority of both sRFP and cRFP correlate with LC::eGFP equally. These results together suggest that there is greater correlation of LC::eGFP with sRFP, and in the case of cRFP+LC::eGFP, a large amount of both fluorophores correlate however there remain regions of the images (and presumably the cells or apoplast) where LC::eGFP is present alone. Moreover, the LC::eGFP construct localises to putative nuclear structures (**Figure 5.4**, see pink arrowheads), similar to the cytosolic RFP marker, suggesting that a large portion of this construct remains in the cytosol. It is also noteworthy, that LC::eGFP displayed localisation in small punctate structures (**Figure 5.4**, see orange arrowheads).

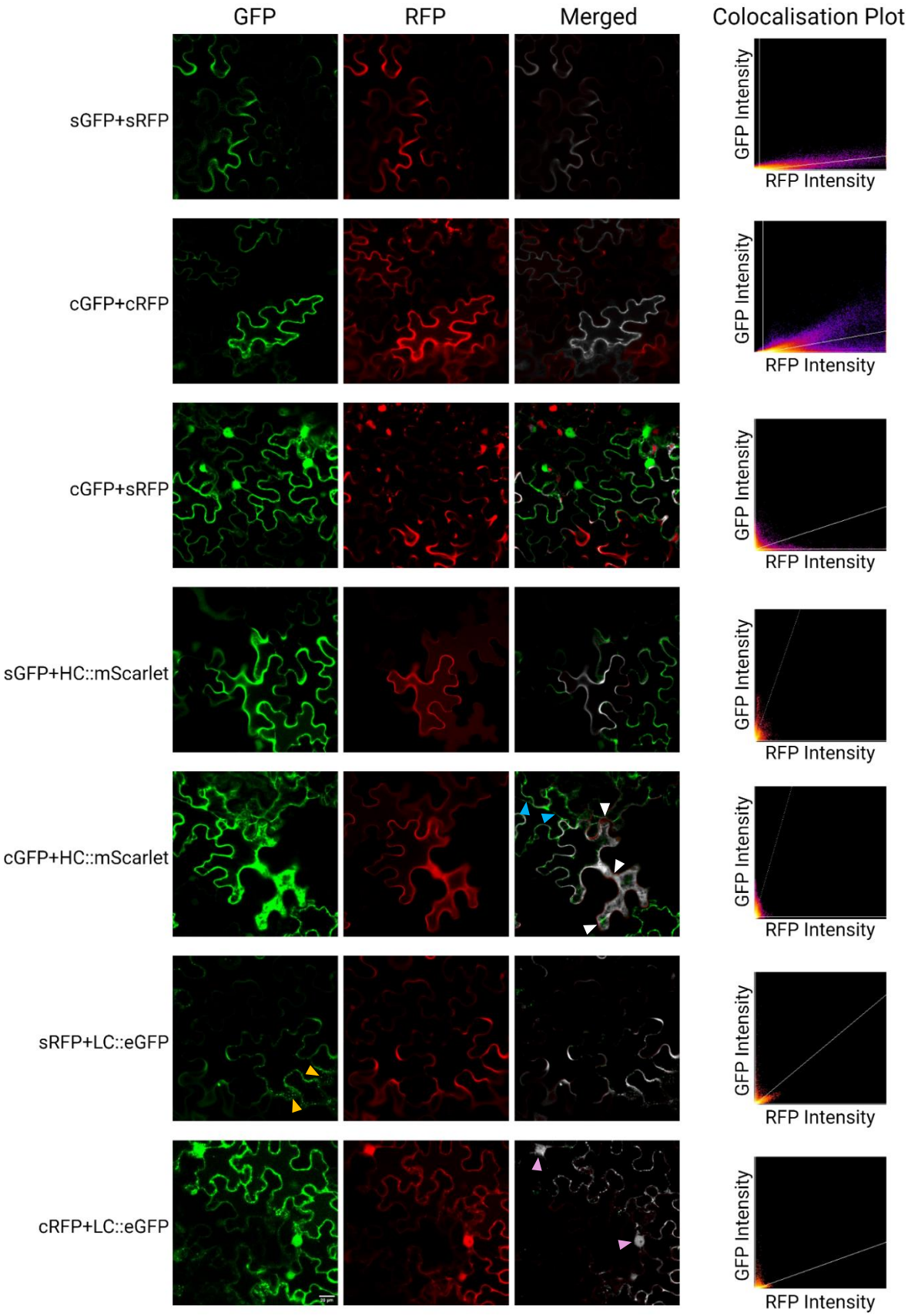

Figure 5.4 Co-localisation analysis of fluorescently-labelled 2F5 with cGFP, sGFP, cRFP, sRFP markers (caption on next page)

GFP and RFP channels of co-expressed HC::mScarlet or LC::eGFP with markers, along with their merged images. Co-localised areas of GFP/RFP in the merged images are shown in grey. Scatter plots of pixel intensities in the RFP channel (x axis) and GFP channel (y axis) for their respective images. One representative replicate of the triplicate is shown. Analysis was conducted according to (Bolte & Cordelières, 2006)

Table 5.1 Co-localisation co-efficient values of 2F5 upon transient expression with cytosolic and apoplastic markers.

Mander's M1 represents the proportion of GFP-containing pixels which also contain RFP signal. Mander's M2 represents the proportion of RFP-containing pixels which also contain GFP signal. Values represent the average of n=3.

	Pearson's correlation	Manders's M1	Manders's M2
sGFP+sRFP	0.27	0.4	0.39
cGFP+cRFP	0.14	0.33	0.43
cGFP+sRFP	-0.08	0.64	0.41
sGFP+HC::mScarlet	-0.02	0.16	0.51
cGFP+HC::mScarlet	0.06	0.43	0.57
sRFP+LC::eGFP	0.47	0.84	0.93
cRFP+LC::eGFP	0.31	0.6	0.97

5.5 Macroscopic fluorescence intensity of fluorescently-tagged 2F5

In an independent experiment, to macroscopically assess the fluorescence intensity, the constructs of LC::eGFP and HC::mScarlet were co-expressed with the respective constructs of the untagged chain. EV (empty vector), LCeGFP+HC, LC+HCmScarlet or LCeGFP+HCmScarlet were transiently expressed in *N. benthamiana* leaves and scanned for fluorescence 5 days later (**Figure 5.5a**). Although fluorescence intensities are low, the merged image shows the successful co-expression of both chains. Recording macroscopic fluorescence enables the non-invasive and fast

visualisation of fluorescence signals across larger sample areas of leaves. Its main advantages include capturing spatial distribution patterns, detecting heterogeneity across samples, and allowing for faster analysis before sampling for total extracts and western blotting.

Moreover, to examine the shift of the tagged HC compared to the untagged HC, LC+HC::mScarlet or LC+HC samples were run on protein gels and analysed by western blotting (**Figure 5.5b**). The tagged HC sample resulted in multiple different fragments (grey arrowheads), with possibly the band of HC-mScarlet protein appearing at approximately 80 kDa and potential proteolytic fragments in lower molecular weight. However, the F2 fragment was still visible, indicating that the truncated form of 2F5 HC that was previously reported (**Figure 5.1**) is present and/or some of the C-terminal mScarlet of HC might be cleaved off.

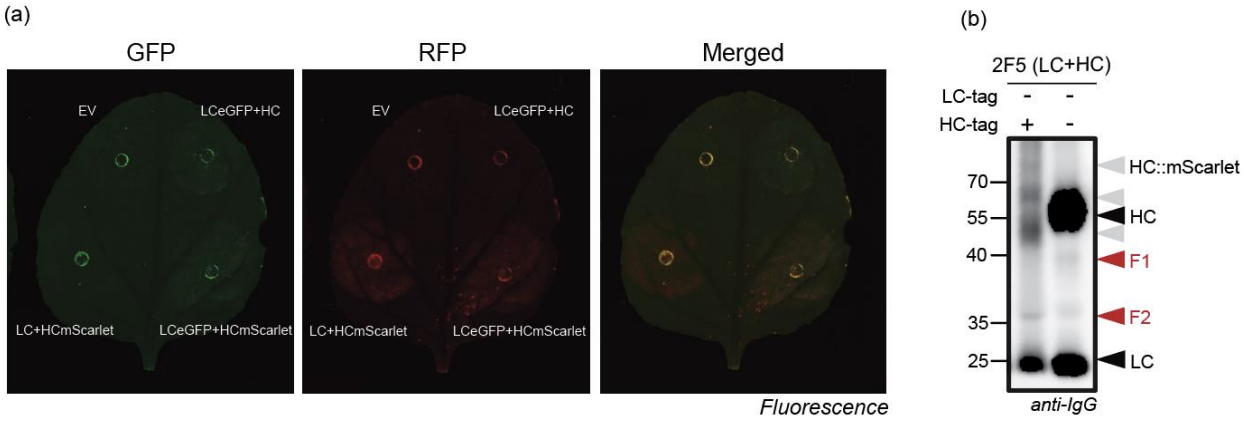

Figure 5.5 Macroscopic fluorescence intensity of fluorescently-tagged 2F5.

Fluorescence intensity was measured at 488 or 561 nm for GFP or mScarlet (RFP), respectively western blot analysis of the 2F5 LC+HC::mScarlet compared to untagged 2F5 LC+HC. Grey arrowheads indicate putative HC::mScarlet and respective cleavage products. Total extracts were generated and separated by reducing 12% SDS-PAGE and analysed by western blot using whole anti-IgG antibody.

5.6 *Arabidopsis thaliana* basic chitinase signal peptide results in increased 2F5 accumulation

To test various signal peptides (SPs) for secretion, 2F5 LC and HC were cloned with distinct SPs in the N-terminal (**Figure 5.6a**). The promoter CaMV 35S and the nos terminator were used for every construct as well as an identical backbone vector. *Nt*PR1a from *N. tabacum* is a common SP used to ensure travelling of recombinant proteins into the secretory pathway (Grosse-Holz, Madeira, et al., 2018; Zheng et al., 2024). *Nb*SBT5.2 SP was selected since SBT5.2 protease accumulates in the apoplast (Jutras et al., 2019; Puchol Tarazona et al., 2021). Another common SP for secretion that was tested is basic chitinase signal peptide from *Arabidopsis thaliana*, particularly tested in virus-like particles expression (Peyret et al., 2020; Ponndorf et al., 2021). Human gastric lipase signal peptide has been reportedly used for secretion in various species including tobacco (Gruber et al., 2001a; Najjar et al., 2011; Sams et al., 2017). Finally, attempts to increase IgG secretion efficiency in Chinese hamster ovaries (CHO) cells has given rise to multiple engineered SPs, including CHOH7 for the heavy and CHOL1 for the light chain, respectively (Haryadi et al., 2015). In all cases except for CHO SP, same SPs were used for both light and heavy chains. LC and HC of 2F5 were co-expressed in *N. benthamiana* leaves. Apoplastic fluids and total extracts were generated from the same agroinfiltrated leaves and analysed by western blotting. Basic chitinase SP led to about 7-fold increase in accumulation, followed by CHO SP with 3-fold increase compared to PR1a SP. However, SBT5.2 SP HC was not present in either total extracts or apoplastic fluids, while GL SP demonstrated lower levels in total extracts. Proteolytic processing of 2F5 to F1 fragment was present in all SPs tested (**Figure 5.6b**). Although F2 fragment was also present in all total extracts of SPs used, human gastric lipase SP exhibited higher F2 accumulation

compared to the control, regardless of the low HC accumulation. When it comes to secretion and accumulation in apoplastic fluids, basic chitinase demonstrated an almost 5-fold increase in 2F5 accumulation followed by CHO SP with almost 3-fold accumulation. However, this could be representative of the overall higher accumulation also observed in total extracts. Interestingly, LC was present in apoplastic fluids of all combinations and was comparable to the respective LC accumulation in total extracts. F2 fragment, a truncated form of 2F5 HC, was also present in apoplastic fluids of all SPs used.

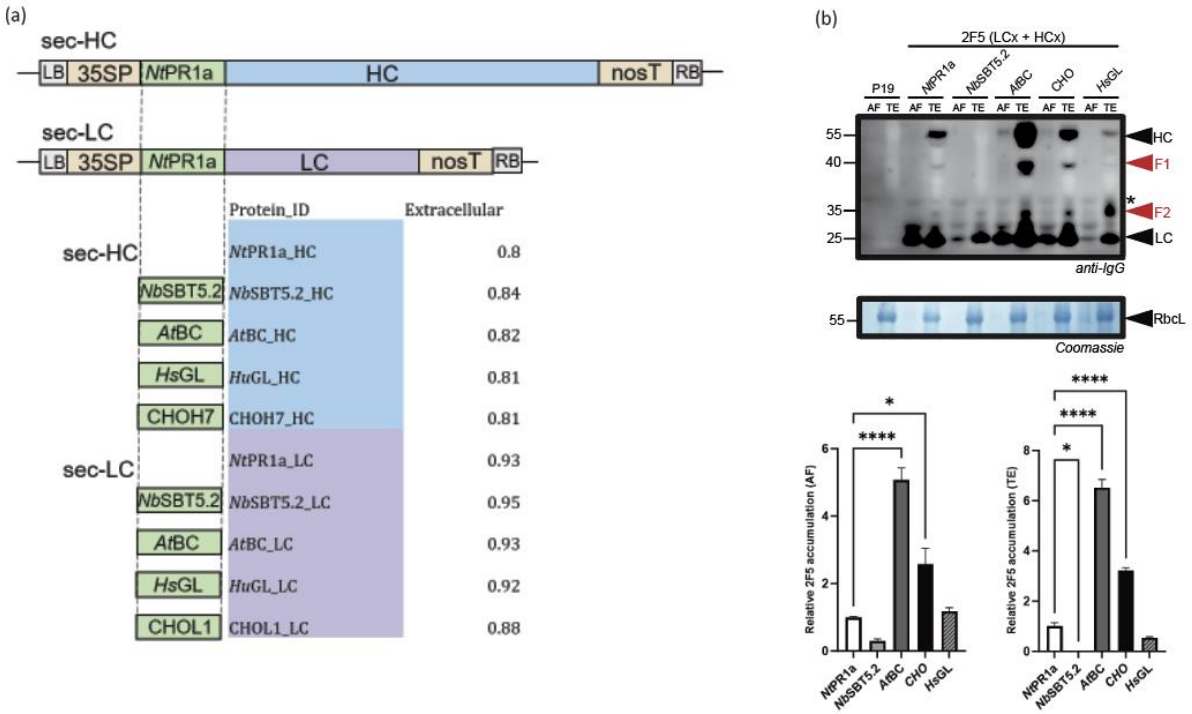

Figure 5.6 Different signal peptides lead to differences in expression levels rather than altered secretion of 2F5.

(a) T-DNAs used for 2F5 expression depicting the different signal peptides. The open reading frame of all constructs was tested for localisation prediction on DeepLoc/SignalP, with the respective confidence scores for extracellular localisation shown. **(b)** Total extracts and apoplastic fluids were isolated after 5 days from the same leaves in triplicate, separated on reducing 12% SDS-PAGE gels and analysed by western blotting using antibodies against IgG. One representative replicate of the triplicate is shown. *, background signal. Coomassie staining was used to show the large subunit of Rubisco in total extracts. Quantification of IgG

accumulation (LC+HC) is depicted in respective graphs. Data were tested for normal distribution, while significance was determined with one-way ANOVA, following multiple comparisons and Tukey's post-hoc test. Error bars represent SE of n=3 experimental replicates.

5.7 Expression of 2F5 in intracellular membranous protease-depleted plants does not impact HC processing

As observed in Chapter 3, 2F5 CDR H3 is still cleaved in *sbt5.2* mutants (**Figure 3.5b**) even though SBT5.2 has been proven to be the only protease to cleave 2F5 in apoplastic fluids (**Figure 2.11d**). For this reason, we screened candidate intracellular proteases along the secretory pathway by depleting various proteases. For the initial selection, we downloaded the available peptidase library of *N. benthamiana* from MEROPS (Rawlings et al., 2012) and selected for ER/Golgi localisation (DeepLoc), and high abundance (RPKM value, Grosse-Holz et al., 2018). The shortlisted proteases were either membranous or soluble proteases along the secretory pathway where the IgGs supposedly travel in before reaching the apoplast. The membranous protease shortlist was then analysed via phylogenetic analysis of the membranous intracellular proteases (data not shown), and 15 membranous proteases that were selected were successfully cloned into a TRV2 vector (**Table 5.2**). Plants were inoculated with tobacco rattle virus (TRV) carrying 300 bp fragments targeting these proteases or a fragment of GFP as a negative control. Three weeks following inoculation with TRV, plants were co-infiltrated with the LC and HC of 2F5. Due to time constraints, only one independent experiment was carried out. Most protease-depleted plants exhibited moderate to severe dwarfism (**S5.1 Figure**). Total extracts and apoplastic fluids were isolated 5 days post infiltration with 2F5 and run under reducing conditions. In all samples, HC expression was

particularly low while no protease-depletion resulted in preventing 2F5 CDR H3 cleavage (**Figure 5.7**). Overall accumulation of 2F5 in protease-depleted plants for presenilins 1 and 2, rhomboids 2, 4 and 6 was comparable to the *TRV::GFP* control. However, accumulation in all remaining protease-depleted plants demonstrated a descending trend compared to the control.

Table 5.2 Membranous intracellular proteases screened for 2F5 processing and overall accumulation.

Intracellular proteases were selected for their putative localisation along the secretory pathway (DeepLoc) and their abundance upon infiltration (Grosse-Holz et al., 2018).

Intracellular protease	Protease	Localisation	Target Gene(s)
Site-1 protease (S1P)	Ser	ER, Golgi	NbD028212/NbD030510
Presenilin 1 (Pres1)	Asp	ER, Golgi	NbD002262/NbD016859
Presenilin 2 (Pres2)	Asp	ER, Golgi	NbD009258/NbD050610
Rhomboid 1 (R1)	Ser	ER	NbD004525/NbD023046
Rhomboid 2(R2)	Ser	ER	NbD025824/NbD051472
Rhomboid 3 (R3)	Ser	ER, vacuole	NbD027617/NbD052150
Rhomboid 4 (R4)	Ser	ER	NbD031761/NbD039509
Rhomboid 5 (R5)	Ser	ER, vacuole	NbD036820
Rhomboid 6 (R6)	Ser	ER	NbD046698/NbD048580
Rhomboid 7 (R7)	Ser	ER	NbD048625
Signal peptide peptidase 1 (SPP1)	Asp	ER, vacuole, Golgi	NbD003119/NbD048409
Signal peptide peptidase 2 (SPP2)	Asp	ER	NbD005385/NbD048687
Signal peptide peptidase 3 (SPP3)	Asp	ER	NbD029194/NbD043687
Signal peptide peptidase 4 (SPP4)	Asp	ER, vacuole, Golgi	NbD013337/NbD017110
Signal peptide peptidase 5 (SPP5)	Asp	ER	NbD032031/NbD043189

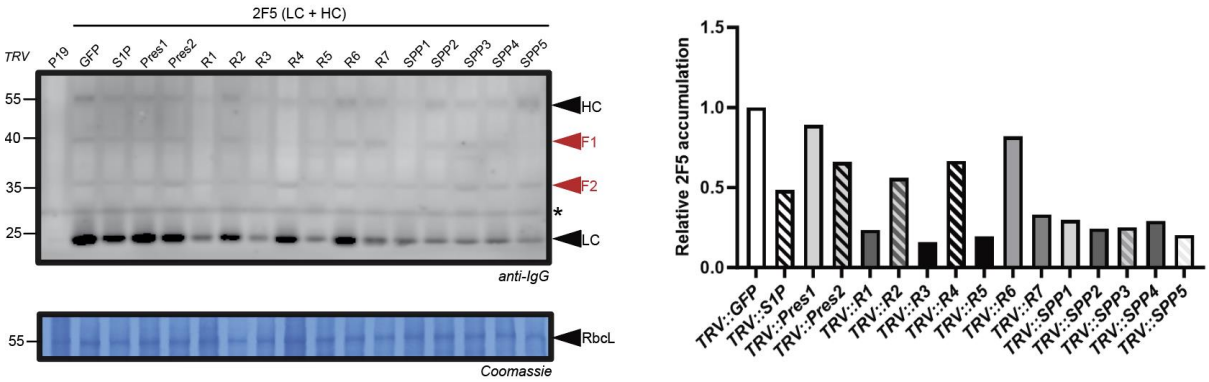

Figure 5.7 Expression of 2F5 in intracellular membranous protease-depleted plants does not impact HC processing.

15 different intracellular proteases were depleted in N. benthamiana by VIGS, using TRV vectors. Total extracts and apoplastic fluids were isolated after 5 days from the same leaves, separated on reducing 12% SDS-PAGE gels and analysed by western blotting using antibodies against IgG. Coomassie staining was used to show the large subunit of Rubisco in total extracts. Quantification of IgG accumulation (LC+HC) is depicted in respective graphs. *, background signal.

5.8 Mistargeting of 2F5 or VRC01 leads to hampered antigenicity and/or accumulation

To explore the impact of subcellular mistargeting on IgG proteolysis and overall accumulation, ER- and vacuolar-targeting constructs were used. $2F5_{ER}$ and $VRC01_{ER}$ carried a KDEL C-terminal for targeting to the ER, or a KISIA C-terminal for targeting to the vacuole immediately following the last amino acid of the heavy chain. However, in both cases only the HC carried these C-terminal sequences, as it has been previously validated that targeting signal to the HC alone can be enough to target the fully assembled IgG (Ocampo et al., 2016). All constructs, LC and HC of both antibodies also had the PR1a N-terminal signal peptide to enter the secretory pathway. LC and HC of 2F5 or VRC01 targeting the apoplast (sec), the ER or the vacuole (vac) were co-expressed in *N.*

benthamiana leaves. Total extracts were isolated from the same agroinfiltrated leaves for each biological replicate at 5 d.p.i. and analysed by western blotting (**Figure 5.8**). When 2F5 HC is designed to be retained to the ER, the same F1 fragment as seen in apoplastic 2F5 HC is present (**Figure 5.8a**). However, both ER HC and ER F1 demonstrate a slight shift in molecular weight, possibly due to the attached C-terminal KDEL peptide. Although no significant increase in accumulation is observed in the ER construct (protein blot), the concentration of binding to antigen is reduced. In the case of the 2F5 vacuolar construct, the HC was in significantly lower levels, while the LC remained to the same levels as the ER and apoplastic combinations. Similarly, the ER- or vacuolar-targeted VRC01 HC was severely degraded compared to the apoplastic HC (**Figure 5.8b**). Although VRC01 LC for both targets was significantly less that the secreted one, it was still much higher in accumulation than the respective HC they were co-expressed with. Interestingly, the ER-targeted HC + secreted LC co-expression sample demonstrated a shift of approximately 5 kDa of the LC.

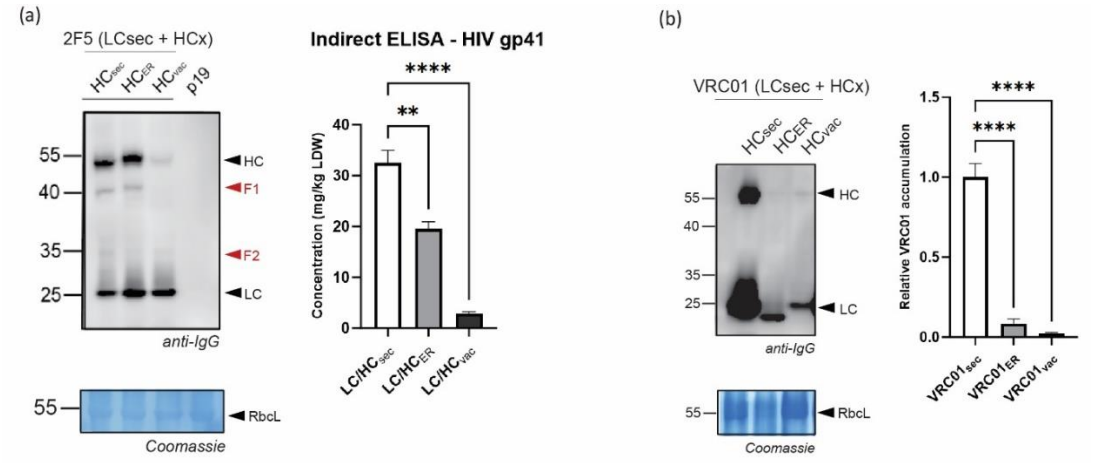

Figure 5.8 Mistargeting of 2F5 or VRC01 leads to hampered antigenicity and/or accumulation.

Total extracts of **(a)** 2F5 secreted, ER- or vacuolar targeting combinations **(b)** or of the respective VRC01 were isolated after 5 days from the same leaves in triplicate, separated on reducing 12% SDS-PAGE gels and

analysed by western blotting using antibodies against IgG. One representative replicate of the triplicate is shown. Coomassie staining was used to show the large subunit of Rubisco in total extracts. Indirect ELISA for 2F5 binding to gp41, or blot densitometry of VRC01 IgG accumulation (LC+HC) is depicted in respective graphs. Data were tested for normal distribution, while significance was determined with one-way ANOVA, following multiple comparisons and Tukey's post-hoc test. Error bars represent SE of n=3 experimental replicates.

5.9 Vacuolar 2F5 and VRC01 HC does not accumulate more in *vpe* mutants

Vacuolar processing enzyme mutants consist of Cys protease mutants, where *vpeabc* is a triple knockout for VPEa, VPEb, and VPEc, while *vpe1d* is a single mutant of VPEd as shown on **Table 3.2**. As seen previously (**Figure 5.8**), vacuolar targeting of the heavy chain of 2F5 or VRC01 led to decreased levels of HC, possibly due to the large number of proteases and low pH of the vacuole leading to degradation of free or in-complex HC. Hence, to examine if this effect is reversible, the vacuolar HC of 2F5 or VRC01 was co-expressed with the respective apoplastic version of LC, as previously described. Total extracts were isolated from the same agroinfiltrated leaves for each biological replicate at 5 d.p.i. and analysed by western blotting (**Figure 5.9**). 2F5 LC and HC accumulation levels in the *vpeabc* mutant remained the same to wild type, while accumulation is halved in *vpe1d* mutants for both chains (**Figure 5.9a**). F1 fragment that derives from the HC CDR H3 loop cleavage was present in in both WT and *vpe* mutants, while no F2 fragment is observed. Vacuole-targeting VRC01 levels in **Figure 5.9b** resembled the independent experiments demonstrated in **Figure 5.8b**, with LC accumulating much more than HC. Although VRC01 HC exhibited an upward trend in accumulation in all three replicates, this increase was not statistically significant.

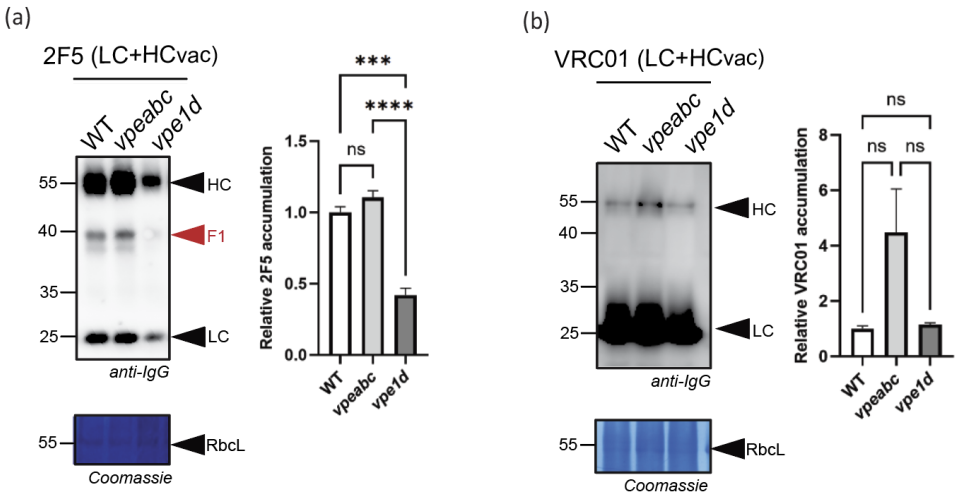

Figure 5.9 Vacuolar 2F5 and VRC01 HC does not accumulate more in *vpe* mutants.

Total extracts of vacuole-targeting **(a)** 2F5, **(b)** or VRC01 were isolated after 5 days from the same leaves in triplicate, separated on reducing 12% SDS-PAGE gels and analysed by western blotting using antibodies against IgG. One representative replicate of the triplicate is shown. Coomassie staining was used to show the large subunit of Rubisco in total extracts. Quantification of 2F5 or VRC01 IgG accumulation (LC+HC) is depicted in respective graphs. Data were tested for normal distribution, while significance was determined with one-way ANOVA, following multiple comparisons and Tukey's post-hoc test. Error bars represent SE of n=3 experimental replicates.

5.10 N-terminal BiP signal peptide leads to a 9-fold increase in 2F5 accumulation

Targeting recombinant proteins to a compartment that is low in protease abundance, such as the ER, can be a promising strategy for preventing unintended proteolysis. However, we previously showed that there was no significant effect in 2F5 processing or overall accumulation when using a C-terminal KDEL peptide in the HC. Although this approach may be promising for some IgGs, more optimisation in targeting signals could offer alternatives when designing mistargeting constructs. Therefore, we tested new constructs for 2F5 ER-retention, harbouring an N-terminal binding

immunoglobulin protein (BiP) signal peptide as well as the C-terminal KDEL simultaneously (**Figure 5.11a**). Moreover, we incorpoted these changes in both the LC and HC, and not solely in the HC as previously tested. The *Nt*PR1a::LC+*Nt*PR1a::HC-KDEL or BiP::LC-KDEL+BiP::HC-KDEL combinations were co-expressed in the same leaves, total extracts were isolated at 5 d.p.i. and analysed by western blotting (**Figure 5.10**). F1 fragment was still present in both cases, while 2F5 LC+HC accumulation with N-terminal BiP was consistently 9-fold higher than with the N-terminal *Nt*PR1a signal peptide.

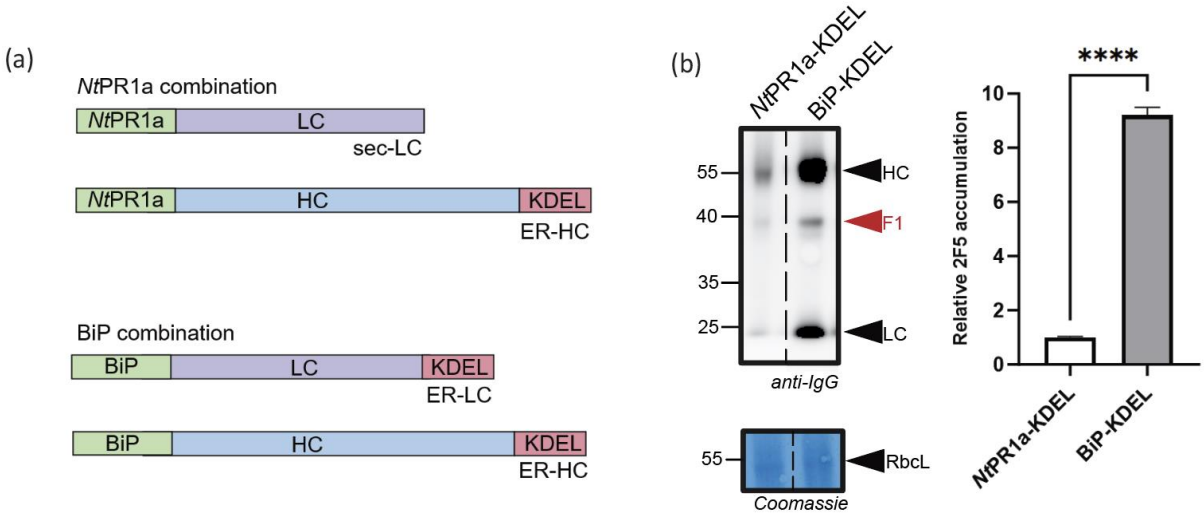

Figure 5.10 N-terminal BiP signal peptide leads to a 9-fold increase in 2F5 accumulation.

(a) T-DNAs used for 2F5 expression depicting the N- and C-terminal signal used for ER-retention. **(b)** Total extracts and apoplastic fluids were isolated after 5 days from the same leaves in triplicate, separated on reducing 12% SDS-PAGE gels and analysed by western blotting using antibodies against IgG. One representative replicate of the triplicate is shown. Coomassie staining was used to show the large subunit of Rubisco in total extracts. Quantification of IgG accumulation (LC+HC) is depicted in respective graphs. Significance was determined with t-test. Error bars represent SE of n=3 experimental replicates.

5.11 ER expansion and IgG accumulation: *constitutive activation of phosphocholine cytidylyltransferase*

The endoplasmic reticulum is characterised by an interconnected network with a continuous membrane structured by the major membrane lipid constituent, phosphatidylcholine (Caldo et al., 2019). The *cct1* mutant used in these experiments carries a mutation in the C-terminal lipid-binding domain of the *cct2* gene, which encodes phosphocholine cytidylyltransferase (CCT), a key enzyme in the *de novo* phosphatidylcholine (PC) biosynthesis. CCT catalyses the conversion of phosphocholine and CTP into CDP-choline, a rate-limiting step in PC production. In wild-type plants, CCT activity is tightly regulated by a C-terminal lipid-binding domain, which interacts with membrane phospholipids to control its function in response to cellular lipid composition. However, in the *cct1* mutant, this domain is mutated by site-directed mutagenesis introducing frame-shifting indels to remove the auto-inhibitory C-terminal domain, leading to a constitutively active enzyme that is no longer subject to normal feedback regulation (Göritzer et al., 2025). The constitutive activation of CCT in *cct1* leads to a sustained increase in phosphatidylcholine biosynthesis, which in turn promotes excessive ER membrane proliferation. This phenotype has been well-characterized in *Arabidopsis thaliana* (Craddock et al., 2015), where overactive CCT drives ER expansion, affecting overall lipid homeostasis and cellular architecture. Because phosphatidylcholine is the most abundant phospholipid in the ER, changes in its synthesis can influence membrane dynamics, protein trafficking, and organelle interactions.

5.11.1 Expression of 2F5 and 2G4 IgGs in cct1 mutants results in decreased accumulation

To assess overall performance of *cct1* mutants upon transient expression of IgGs, 2F5 or 2G4 LC+HC were co-expressed. In this case, the antibody chains contained the signal *Nt*PR1a for entering the secretory pathway but no other targeting signal. Total extracts from infiltrated leaves were isolated at 5 d.p.i. and analysed by western blotting (**Figure 5.11**). Both 2F5 and 2G4 IgGs accumulated approximately 30% less in *cct1* mutants compared to wild type control. Additionally, for both IgGs the difference in accumulation derived from the different HC levels, rather than LC levels, indicating an effect of ER proliferation only on HC accumulation.

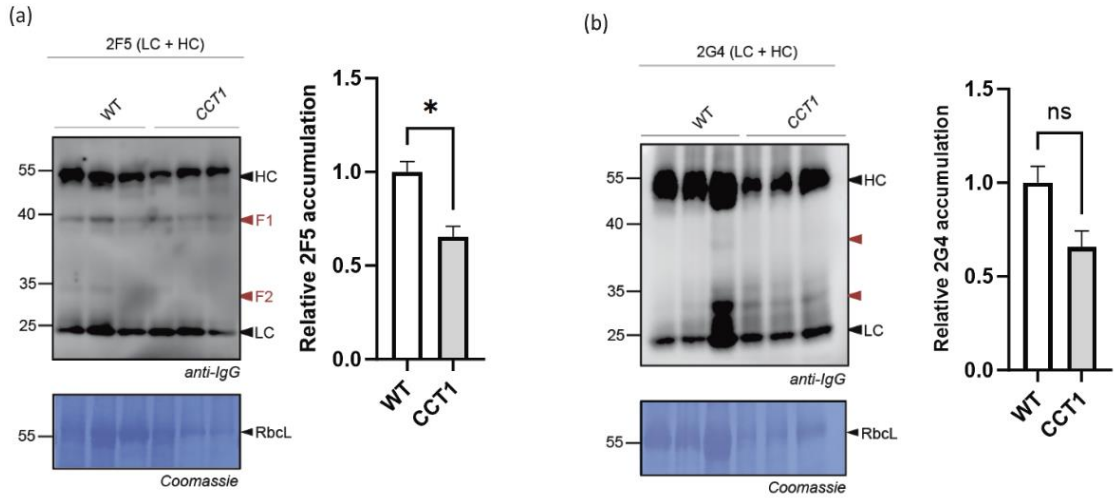

Figure 5.11 2F5 and 2G4 IgGs accumulate less in the *cct1* mutants.

Total extracts of apoplast-targeting **(a)** 2F5, **(b)** or 2G4 were isolated after 5 days of infiltration in WT or *cct1* plants in triplicate, separated on reducing 12% SDS-PAGE gels and analysed by western blotting using antibodies against IgG. Coomassie staining was used to show the large subunit of Rubisco in total extracts. Quantification of 2F5 or 2G4 IgG accumulation (LC+HC) is depicted in respective graphs. Data were tested for normal distribution, while significance was determined with one-way ANOVA, following multiple comparisons and Tukey's post-hoc test. Error bars represent SE of n=3 experimental replicates.

5.11.2 cct1 mutants tend to exhibit increased ER-stress

To better understand the response of *cct1* mutants to ER-stress, e.g., due to recombinant protein overexpression or enhanced ER proliferation, we estimated the levels of ER-stress response by using pBiP3a promoter driving GFP expression upon activation. *N. benthamiana* leaves of WT or *cct1* mutants were co-infiltrated with the *agrobacteria* harbouring the marker and either apoplast-targeted 2F5 (LC_{sec}+HC_{sec}), ER-targeted 2F5 *Nt*PR1a-KDEL HC with LC (LC_{sec}+HC-KDEL), ER-targeted 2F5 BiP-KDEL HC with LC (LC_{sec}+BiP::HC-KDEL), or empty vector as a non-encoding control. Four leaves of three independent experiments were scanned at 488 nm for GFP fluorescence (**Figure 5.12**). When comparing within the same construct combination but in different plants, e.g., EV in WT versus EV in *cct1*, a trend of increased fluorescence was observed in *cct1* mutants compared to WT across all combinations. However, this difference was not significant. When comparing the different construct combinations, e.g., EV versus $2F5_{sec}$, the lowest fluorescence intensity was emitted by leaf tissue cells expressing $2F5_{sec}$ or EV, followed by *Nt*PR1a-KDEL and finally by BiP-KDEL which emitted the highest fluorescence intensity.

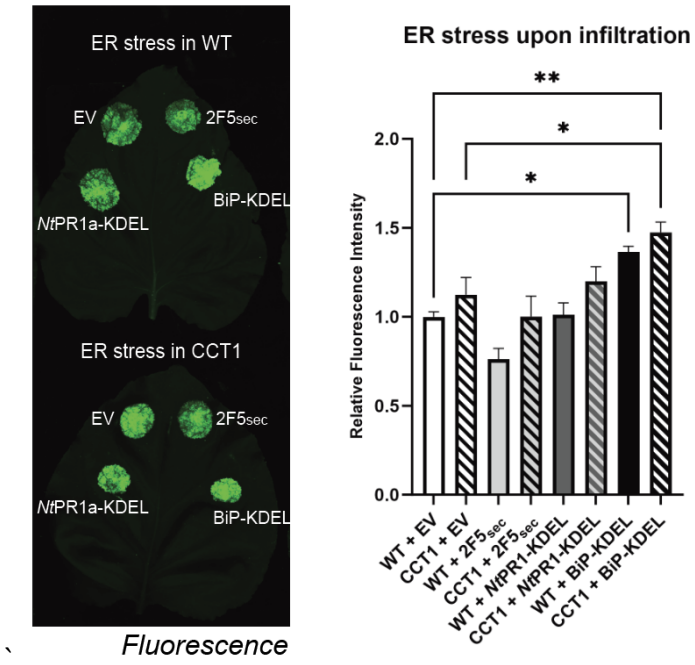

Figure 5.12 BiP-KDEL 2F5 results in significantly higher GFP fluorescence that indicates increase ER-stress response.

Quantification of GFP fluorescence is depicted in respective graph. Data were tested for normal distribution, while significance was determined with one-way ANOVA, following multiple comparisons and Tukey's post-hoc test. Error bars represent SE of four leaves and n=3 independent experimental replicates.

5.11.3 2F5 accumulates more using the BiP-KDEL design in both WT and cct1

To assess IgG accumulation levels in the different combinations of 2F5 constructs, the same samples generated from the previous experiment examining ER-stress response were harvested as total leaf extracts and analysed by western blotting (**Figure 5.13**). The three infiltration combinations involved ''sec'': *Nt*PR1a::2F5::LC or HC with no C-terminal target sequence, ''PR1a'': *Nt*PR1a::2F5::HC::KDEL with C-terminal KDEL plus *Nt*PR1a::2F5::LC with no C-terminal target sequence, and ''BiP'': BiP::2F5::LC::KDEL plus *Nt*PR1a::2F5::HC:: where both chains were carrying a C-terminal KDEL. When comparing within the same construct combination but in different plants, e.g., $2F5_{sec}$ in WT versus

$2F5_{sec}$ in *cct1*, a decrease in accumulation is observed across all constructs as previously shown in **Figure 5.11**. When comparing the different construct combination, e.g., $2F5_{sec}$ versus *Nt*PR1a-KDEL 2F5, BiP-KDEL 2F5 constructs resulted in an approximately 9-fold increase as previously described (**Figure 5.10**). Moreover, the *Nt*PR1a-KDEL 2F5 demonstrated comparable accumulation levels to $2F5_{sec}$ as noted in **Figure 5.8a**.

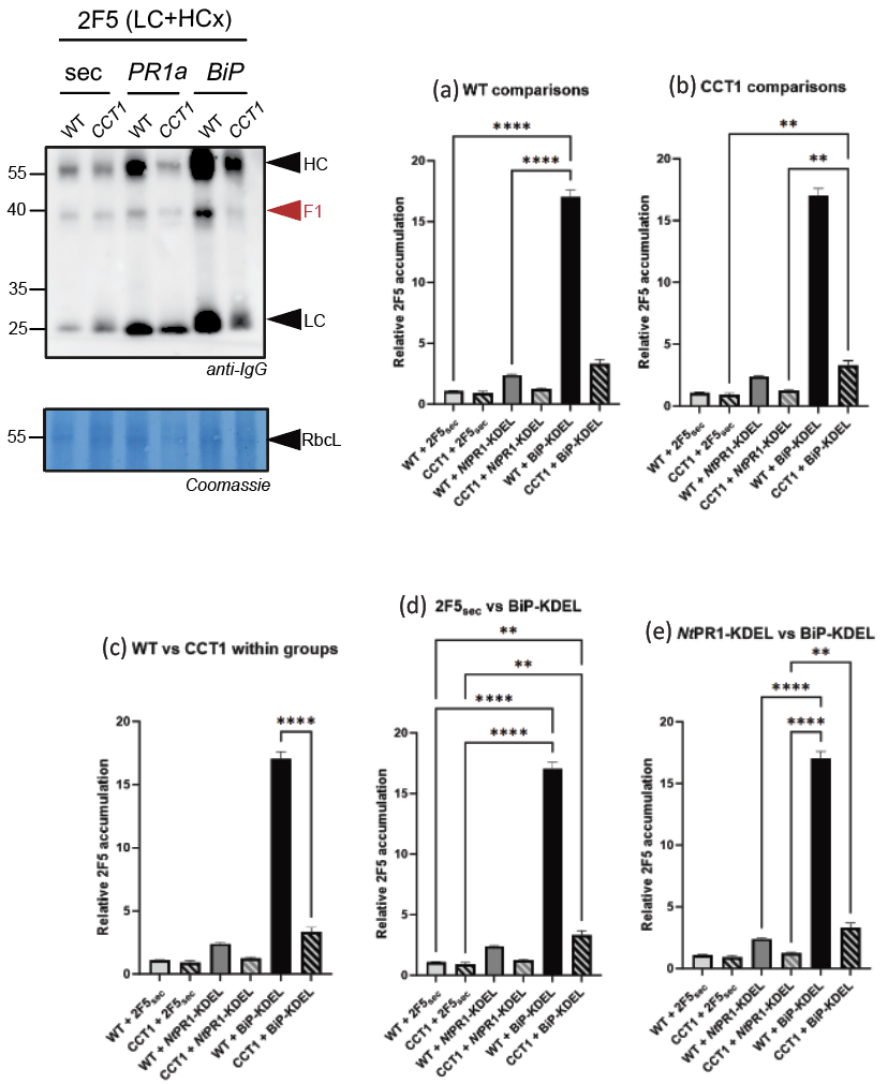

Figure 5.13 2F5 accumulates more using the BiP-KDEL design in both WT and *cct1*.

Total extracts of apoplast-targeted 2F5 (LC_{sec}+HC_{sec}; ''sec''), ER-targeted 2F5 *Nt*PR1a-KDEL HC with LC (LC_{sec}+HC-KDEL; ''PR1a''), ER-targeted 2F5 BiP-KDEL HC with LC (LC_{sec}+BiP-HC-KDEL; BiP), were isolated after 5 days of infiltration in WT or *cct1* plants in triplicate, separated on reducing 12% SDS-PAGE gels and analysed by western blotting using antibodies against IgG. Coomassie staining was used to show the large

subunit of Rubisco in total extracts. Quantification of 2F5 IgG accumulation (LC+HC) is depicted in respective graphs. Data were tested for normal distribution, while significance was determined with one-way ANOVA, following multiple comparisons and Tukey's post-hoc test. Error bars represent SE of n=3 experimental replicates.

Interestingly, in a similar experiment expressing VRC01$_{ER}$, accumulation of HC is observed a 5-fold higher in cct1 mutants (**Figure S5.2**). Moreover, VRC01$_{ER}$ LC shifts to a lower molecular weight in WT as seen in an independent experiment described previously in WT (**Figure 5.8b**). However, in *cct1* VRC01$_{ER}$ LC molecular weight is the same as seen in VRC01$_{sec}$ LC.

5.12 ER expansion and IgG accumulation: *dimerisation of an ER membrane-anchored polyprotein*

Recently, a polyprotein containing the BP80 vacuolar sorting receptor from *Pisum sativum* for ER anchoring (Brandizzi et al., 2002), flanked by two dimerising fluorescent proteins, was characterised for its ability to form a large self-organising de novo compartment in transformed cells of tobacco (Sandor et al., 2024). This polyprotein contains an N-terminal GFP facing the ER lumen, a Yellow Fluorescent protein (YFP) facing the cytosol, and a 22-amino acid transmembrane domain connecting the two proteins, thus named G22Y (**Figure 5.14a**). The structure of an expanded-like ER is hypothesised to form as a result of each fluorescent protein of the G22Y interacting with a fluorescent protein different G22Y on either side of the ER membrane, forming an oligomer and ultimately a helical pattern. During a time-course experiment of G22Y expression, the G22Y structures appear as small compartments at around 36 h following

transformation, aggregating into a large single compartment by 60 h (**Figure 5.14b**) Compartment stability was stable for up to six weeks.

5.12.1 G22Y is expressed successfully and forms compartment aggregates

To first test that the construct is working in our hands, we transiently expressed the G22Y polyprotein construct in leaves and used confocal microscopy to validate fluorescence. The GFP fluorescence co-localises with YFP fluorescence, indicating the functionality of both dimerising fluorescent proteins (**Figure 5.14c**).

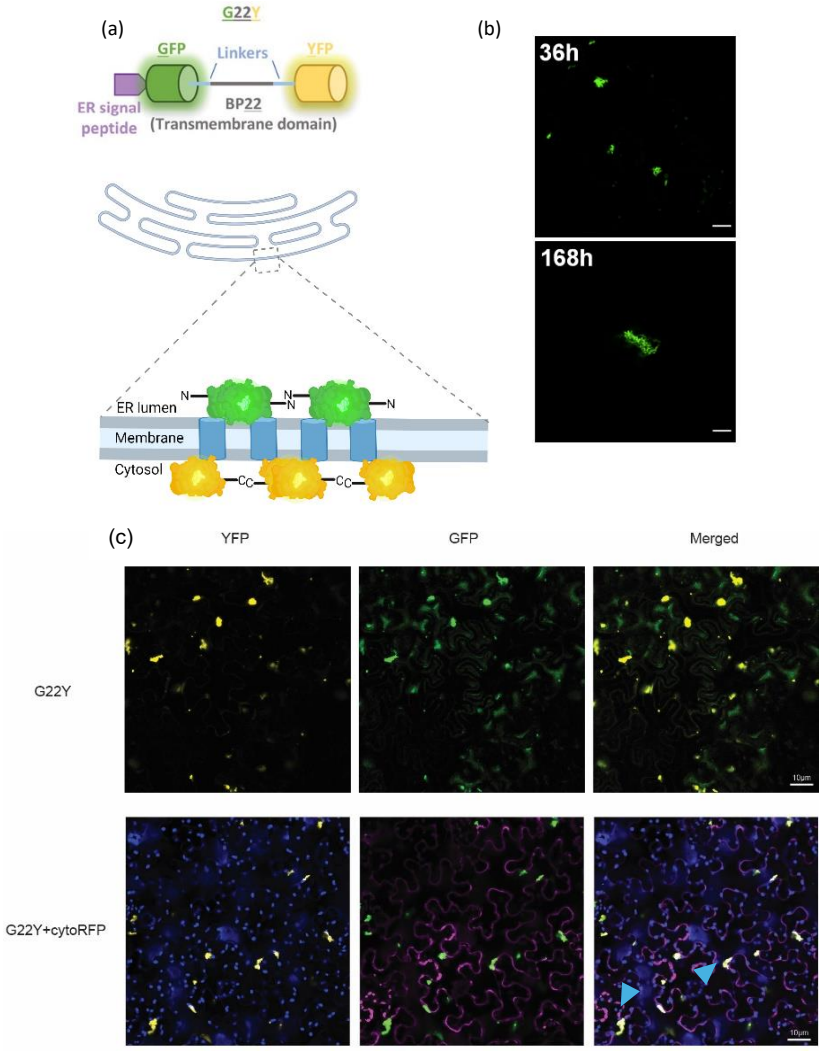

Figure 5.14 G22Y polyprotein forms an aggregated, expanded ER due to dimerisation (see caption on next page).

(a) The open reading frame of the G22Y polyprotein, and the respective representation once it anchors on the ER membrane. **(b)** Time-course of G22Y expression showing smaller compartments forming at 36 h, while being present up to 6 weeks later (Sandor et al., 2024). **(c)** Expression of G22Y or G22Y with a cytoplasmic RFP to allow for validation in our experiments. Open reading frame cartoon and time-course experiment were adapted by Sandor et al., 2024. Scale bar 10 μm.

5.12.2 Expression of ER-targeted 2F5 affects fluorescence levels of G22Y

To account for impact of overexpressing an ER-targeted 2F5 on G22Y fluorescence, the G22Y polyprotein with previously characterised 2F5 BiP-KDEL LC and HC, were co-expressed in leaves and fluorescence coming from GFP protein was measured at 5 d.p.i. As shown in **Figure 5.15a** fluorescence was almost halved when ER-targeted 2F5 is co-expressed compared to co-expression with an empty vector control. In parallel, to assess 2F5 BiP-KDEL accumulation with or without G22Y expression, total extracts from an identical independent experiment were isolated and analysed by western blotting (**Figure 5.15b**). The 2F5 BiP-KDEL accumulation was the same with or without G22Y expression, but interestingly only the F2 fragment and not F1 was present.

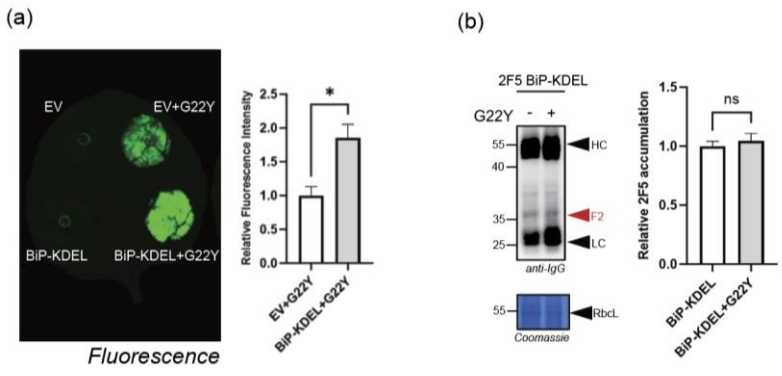

Figure 5.15 BiP-KDEL 2F5 expression results in significantly lower GFP fluorescence of the G22Y polyprotein (see caption on next page).

(a) Quantification of GFP fluorescence is depicted in respective graph. Error bars represent SE of three leaves (n=3 biological replicates) from one independent experiment. **(b)** Quantification of 2F5 BiP-KDEL (LC+HC) from western blot densitometry analysis. The experimental design was identical to (a) with 6 biological replicates pooled together from 3 independent experiments. In both cases, significance was calculated by t-test.

5.12.3 2F5 accumulates more using the BiP-KDEL design in both WT and cct1

As an alternative approach to keep an IgG inside the ER lumen, an anti-GFP IgG construct was created to bind to the ER lumen-facing GFP. LC and HC of a synthetic aGFP IgG were cloned in the same vector as the previously tested ER-targeted 2F5, under the same 35S promoter and nos terminator. However, the aGFP IgG is designed to have the initial *Nt*PR1a N-terminal sequence for secretion but no ER-targeting signal. The putative aGFP IgG structure and interaction with either pure GFP or with the G22Y complex were predicted by AlphaFold (**Figure S5.3**). The aGFP IgG was first tested for GFP binding by ELISA, using total extracts from leaves expressing aGFP IgG. However, due to several commercially available aGFP IgGs not being functional under ELISA conditions, the raw absorbance (450 nm) of total extracts containing aGFP is shown. aGFP IgG depicted successful binding to pure GFP, compared to an empty vector control (**Figure 5.16a**).

Next, we assessed aGFP IgG accumulation upon G22Y expression. Also, a secreted RFP (sRFP) was co-expressed as a control of a tested secreted protein not being trapped in ER interacting with G22Y in any way. We designed the co-expression experiment in two ways. First, the LC and HC from aGFP were co-expressed with sRFP and either G22Y or EV. Second, we followed sequential agroinfiltration, infiltrating the G22Y or EV first and then 4 days later co-expressing aGFP LC+HC and sRFP to allow for ER expansion aggregates to form before recombinant protein expression. Total extracts were isolated 5

d.p.i. of the aGFP IgG, accounting for 5 days in first case and 9 days in second case from initial infiltration. Total extracts were isolated and kept in -80 ^{o}C to be analysed together by western blotting (**Figure 5.16b**). aGFP IgG almost halved in accumulation in plants co-expressing G22Y, while RFP was in relatively similar accumulation levels. However, in the case of sequential infiltration, aGFP IgG and RFP expression was very low, due to post-translational gene-silencing.

To further test the potential of a recombinant IgG being expressed after ER expansion has been established, we re-designed the construct. In this case we used a heat-inducible promoter, ara2, that has been recently tested in *N. benthamiana* leaves (Forestier et al., 2023). 35S-driven aGFP or ara2-driven aGFP was expressed in leaves, and plant infiltrated with the ara2 construct were placed under heat treatment at 40 °C for 2 hours at 3 d.p.i. In both cases, total extracts were isolated at 5 d.p.i. of the aGFP IgG, accounting for 5 days in the case of 35S and 8 days in the case of ara2 from initial infiltration. Total extracts were isolated and kept in -80 ^{o}C to be analysed together by western blotting (**Figure 5.16c**). Plants that endured heat treatment showed no phenotypic differences (**Figure S5.4**). 35S::aGFP accumulation was approximately halved when co-expressed with G22Y as observed in **Figure 5.16b.** In the case of ara2::aGFP expression was significantly lower that 35S-driven aGFP, with a trend of G22Y co-expression leading to even less accumulation.

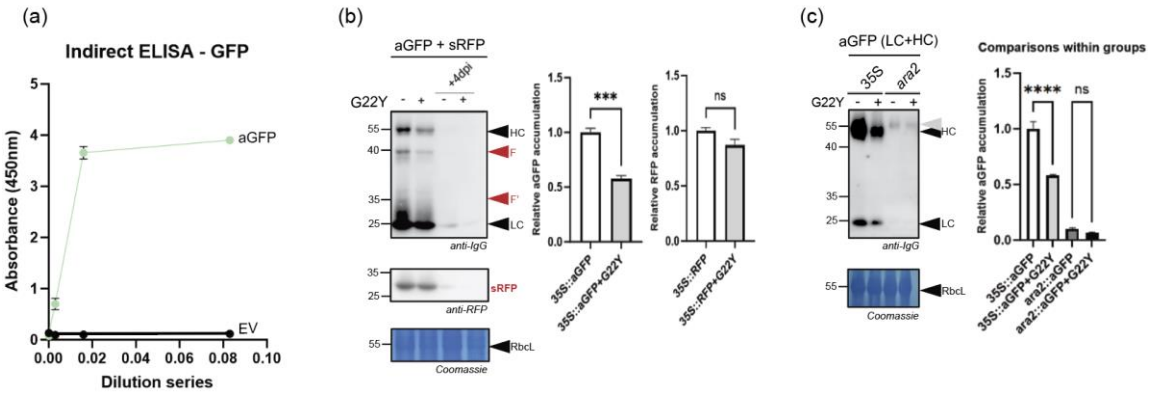

Figure 5.16 aGFP IgG successfully bind to GFP *in vitro* but accumulates in lower levels when co-expressed with G22Y.

(a) Indirect ELISA of aGFP IgG expressed *in planta* compared to an EV control. **(b)** Quantification of aGFP (LC+HC) or RFP from western blot densitometry analysis. Samples derived from 3 independent experiments. Significance was calculated by ANOVA and Tukey's post-hoc. **(c)** Quantification of aGFP (LC+HC) from western blot densitometry analysis for 35S- or ara2-driven aGFP expression, with or without G22Y. The experimental design contained 6 biological replicates pooled together from 3 independent experiments. Significance was calculated by ANOVA following Tukey's post-hoc.

Conclusions and Discussion

This Chapter focused on IgG localisation, IgG secretion and mistargeting to the ER or vacuole. Moreover, we tested the potential of an expanded ER phenotype combined with ER-targeted IgGs to assess its impact on processing and accumulation.

We first examined how the single chains, LC or HC, would be processed and accumulated compared to the heterodimer. HC overexpression leads to the dominant presence of the F2 fragment, while full HC is completely degraded (**Figure 5.1**). This 2F5 F2 fragment at around 30 kDa was observed previously *in planta*. In this study, even though chains were co-expressed, this F2 fragment would appear in different accumulations, an observation that is consistent with our data. However, we observed that co-expression of both chains drastically reduces the F2 signal. Previous studies in mammalian cells validated that free immunoglobulin heavy chains are generally considered toxic for cells (Kohler, 1980). When heavy chains are expressed without light chains, they tend to associate with the immunoglobulin heavy chain binding protein (BiP) in the endoplasmic reticulum, which blocks their transport and secretion (Hendershot, 1990; Ma et al., 1990), but instead tries to retain them back to the ER. This association with BiP is typically reversible, allowing for the potential assembly and secretion of complete antibodies when light chains become available. In another case, Chinese hamster ovary (CHO) cells containing surplus heavy chains formed aggregates of HC or degraded products. However, when they co-expressed BiP, a crucial immunoglobulin G (IgG) chaperone protein, a modest decrease in undesirable aggregates and fragments was observed (Ho et al., 2015). This reduction may be attributed to BiP's role in retaining more incomplete products within the cell, allowing for either proper assembly or degradation through the ER quality control system and ER-associated degradation (ERAD).

Moreover, we tested the effect on accumulation of a multi-gene vector harbouring both light and heavy chains compared to mixing the two vectors. Combining light and heavy chains in a single vector (L2::LC/HC) significantly increases 2F5 accumulation compared to separate vector expression (**Figure 5.2**). This setup also balances the proportion of F1 and F2 fragments relative to the full HC accumulation. This observation can be supported by the fact that not all cells will take up both T-DNAs of LC and HC in ideal ratios for the fully assembled complex. As described previously, LC/HC ratio can have a substantial impact on how quickly the complex is formed, for how long free LC or HC stays in the ER before the activation of the ERAD response, or how much aggregates are formed.

Western blotting and confocal experiments showed that only a small fraction of 2F5 is detected in apoplastic fluids of agroinfiltrated plants and that most 2F5 is detected in total extracts. The low level of 2F5 in apoplastic fluids of 2F5-expression leaves is remarkable and unexpected because it is widely assumed that IgGs accumulate in the plant apoplast (Diego-Martin et al., 2020; Hehle et al., 2011; Ocampo et al., 2016; Puchol Tarazona et al., 2021). Pulse-chase analysis with protoplasts of transgenic tobacco expressing IgG Guy13 demonstrated an efficient secretion (Frigerio et al., 2000). Similar experiments with tobacco expressing IgG 2G12 revealed that fully assembled antibody accumulates in the medium, whilst 2G12 assembly intermediates are not secreted (Hehle et al., 2011). In our study, 2F5 was targeted to the secretory pathway using a canonical signal peptide of tobacco PR1a, which has been frequently used to efficiently secrete other recombinant proteins such as fungal Avr9 (Hammond-Kosack et al., 1994), oomycete SgJRL (Kobayashi et al., 2022), and tomato Pip1 (Schuster Marianaand Paulus, 2022). In addition, PSORT predictions indicate that 2F5 does not contain any obvious subcellular targeting sequence that would redirect 2F5 to subcellular compartments. Our results are

nevertheless consistent with a previous study of transiently expressed 2F5 in *Nicotiana benthamiana* (Niemer et al., 2014). In this study, the HC accumulated in apoplastic fluids, but this signal is estimated to be <5% of the HC detected in total extracts (Niemer et al., 2014), consistent with our observation that only low levels of the HC accumulated in the apoplast (**Figure 5.3f**). However, Niemer et al. also detected a large amount of fragment F2 in apoplastic fluids, corresponding to an estimated 10-25% of the signal in the total extract (Niemer et al., 2014). This is consistent with our observation that fragment F2 accumulates in the apoplast at a relatively high intensity when compared to the signal in the total extract (**Figure 5.3h**). Our F2 signal, however, is relatively weak. Fragment F2 is thought to result from the degradation of excess HC in the hinge region by cysteine proteases and the observed variation in F2 accumulation seems to differ between experiments, indicating that this signal can occasionally dominate the IgG signals detected in apoplastic fluids (Niemer et al., 2014).

A previous subcellular localisation study using C-terminally RFP-tagged light and heavy chains of the IgG antibody 14D9 showed that, instead of accumulating in the vacuole or endoplasmic reticulum, 14D9 primarily localizes to the space between the ER of adjacent cells in agroinfiltrated Nicotiana benthamiana leaves (Ocampo et al., 2016). This study, however, focussed on vacuolar targeting and did not include markers for the apoplast or plasma membrane. Interestingly, however, this study showed that that HC-RFP of 14D9 accumulates in the ER when it is not co-expressed with the LC, consistent with the notion that the CH1 domain of the HC is unable to fold when the LC is absent and therefore remains in the ER (Feige et al., 2010). In contrast to ER-resident HC-RFP, LC-RFP of 14D9 accumulated in-between cells in the absence of the HC (Ocampo et al., 2016), which is consistent with our observed higher relative LC accumulation in the apoplast (**Figure 5.3i**).

Confocal imaging suggested that HC::RFP colocalisation with cytosolic cGFP was not significantly different to the negative control cGFP+sRFP when comparing Pearson's and Manders's coefficients. However, HC::RFP also localised exclusively within certain regions at the periphery of the cells, consistent with partial apoplastic localisation. This is in agreement with western blot results in this work, which suggest that only a small proportion of HC is targeted to the apoplast. Interestingly, LC::GFP showed better colocalization with sRFP, although it also colocalized with cRFP as well. This suggests, that similar to the HC, the LC is also only partially secreted to the apoplast, with a significant portion of the expressed LC remaining in the cytosol. This is, further supported by the presence of GFP fluorescence in structure reminiscent of transvacuolar strands, which would be expected from a protein localising to the cytosol.

A caveat of the confocal imaging approach to subcellular IgG localisation is the possibility of the fluorescent protein being cleaved from the HC or LC post-translation. This would result in a mixed population of LC::GFP and free GFP molecules being present in a single cell, which can confound protein localisation via fluorescence microscopy. Indeed, this has been demonstrated to occur with RFP-tagged aldolase expressed in *Arabidopsis* (Garagounis et al., 2017). Hence, the localisation of the light chain in the cytosol could be an artifact resulting from the degradation of the fluorescent marker, which would lead to a misleading subcellular distribution pattern. Proteolytic cleavage could separate the fluorescent tag from the LC, causing the marker to diffuse freely in the cytosol while the actual LC follows its intended secretory pathway. This possibility is particularly relevant given that proteolysis is a common issue in transient expression systems, especially in *N. benthamiana*, where endogenous proteases may target exposed linker regions between the protein of interest and the fluorescent tag. Additionally, degradation of the marker may occur after cellular stress or during sample processing,

further complicating accurate localisation studies. Another potential explanation for cytosolic LC localization is the presence of internal translation start sites within the LC sequence. If alternative start codons downstream of the signal peptide are recognised by the ribosome, truncated versions of LC lacking the ER-targeting signal could be synthesised. These truncated variants would remain in the cytosol instead of being directed to the secretory pathway. The likelihood of this occurring depends on factors such as mRNA secondary structure, ribosome efficiency, and the presence of Kozak consensus sequences near alternative start codons (Asano, 2014). Experimental validation, such as western blot analysis using an antibody specific to the LC, could help determine whether smaller, cytosolic LC fragments are present, supporting the hypothesis of alternative translation initiation. Additionally, it is important to recall that although the images shown are two-dimensional, they contain fluorescence from molecules in a 3D section of a leaf of approximately 10-20 µM. This means that fluorescence in different regions of an image may be derived from fluorophores that are distinctly located to the cytosol and apoplast, but which appear colocalised in a two-dimensional projection. Thus, observations of exclusively peripheral localisation is key in supporting apoplastic localisation of HC::RFP. Finally, it must be noted that, due to time-constraints, colocalisation analysis was carried on entire images, not specific regions of interest with the visualised cells, which can result in far mor accurate estimates of colocalisation. Because both Pearson's and Manders's coefficients are susceptible to the presence of a large number of empty (black) pixels and to differences in fluorescence intensities of the imaged fluorophores, this analysis can only be considered preliminary. Regardless of these limitations, the confocal imaging approach results are in agreement with western blot data, and support the notion that while a large proportion of LC and HC remain in the cytosol, a fraction of these proteins does indeed localise in the apoplast.

Different signal peptides lead to varying levels of 2F5 accumulation, with basic chitinase SP showing the highest increase, followed by CHO. Despite differences in HC accumulation, LC and the F2 fragment are consistently present in apoplastic fluids across all SPs tested. Studies on plant secretomes have revealed that more than half of naturally secreted proteins do not possess a signal peptide (Agrawal et al., 2010), which is generally considered necessary for guiding recombinant proteins to extracellular sites. An investigation found that merging the signal sequence and initial two amino acids from tobacco PR1b protein with bacterial ChiA protein improved its secretion efficacy in plant cells compared to ChiA with its original signal sequence (Lurid & Dunsmuir, 1992). Additionally, HRP C1a generated using GE from N. tabacum β-D-glucan exohydrolase demonstrated a higher rate of secretion in the BY2-cell system than its native SP and another SP derived from peroxidase (Matsui et al., 2006).

Depletion of selected intracellular proteases fails to inhibit 2F5 CDR H3 cleavage, suggesting that these proteases might not significantly impact HC processing or overall 2F5 accumulation (**Figure 8.8**). This might be due to two reasons. First, TRV infection itself might affect protein synthesis machinery dynamics due to stress. Several papers mention that TRV-based VIGS systems typically result in mild virus infection symptoms (Tian et al., 2015; Zhang et al., 2017). For instance, Zhang et al. (2017) notes that the TRV-mediated VIGS system has mild virus infection symptoms as one of its advantages. This suggests that while some stress may occur due to viral infection, it is usually not severe enough to significantly impact the experimental results. However, it's important to note that the stress response can vary depending on the plant species and the specific experimental conditions. For example, Shen et al. (2020) mentions that treated *Forsythia* plants were pruned below the injection site after 7-15 days of infection, which could be a measure to mitigate potential stress effects. Deng et al. (2020), focusing on *Centaurea*

cyanus, tested different infiltration methods and found that only apical meristem-infiltration was effective, suggesting that the plant's response to TRV infiltration can depend on the inoculation technique. Moreover, size of the vector has also been associated with stress, with larger RNAi fragments causing less severe phenotype (J. Zhang et al., 2017). Second, gene silencing of some of these proteases could affect protein synthesis dynamics and secretion indirectly by affecting other gen transcripts, or directly. For example, SPPs or S1P are involved in the signal peptide cleavage, once the protein is retrieved in the ER following translation (Bolhuis et al., 1999; Ng et al., 2007; Sun et al., 2015).

Targeting 2F5 to the ER or vacuole alters HC stability and antigen binding, with vacuolar targeting significantly reducing HC levels. VRC01 experiences similar degradation, indicating subcellular localization critically influences IgG stability. The vacuole is abundant in vacuolar processing enzymes (Vorster et al., 2019), although cases of vacuolar targeting reported high accumulation (Ocampo et al., 2016; Shaaltiel et al., 2007). In *vpeabc* mutants (**Figure 5.9b**), vacuole-targeting VRC01 demonstrated an upward trend in accumulation, although not significant. It has been reported that depleting VPE enzymes leads to less recombinant protein degradation and/or accumulation (Pillay et al., 2014; Singh et al., 2022).

In contrast, ER targeting using a N-terminal KDEL in the HC did not result in increased levels of 2F5 or in preventing cleavage (F1 fragment; **Figure 5.9a**). Previous studies reported increase of recombinant protein following ER retention, supposedly due to better folding and/or low abundance of proteases (Gruber et al., 2001b; Ocampo et al., 2016; Sainsbury & Lomonossoff, 2008). However, in our case it was not until we changed the N-terminal signal peptide from *Nt*PR1a to BiP, to obtain an almost 9-fold increase.

Other studies have successfully used N-terminal BiP or elastin-like polypeptide fusion to optimise ER retention (Floss et al., 2009; Gutiérrez et al., 2013; Islam et al., 2020; Marques et al., 2020; Soni et al., 2022).

Regarding the ER-expansion attempts, we followed two strategies: a naturally expanded ER based on endogenous phosphocholine cytidylyltransferase increased levels, or a synthetically expanded ER based on the dimerisation of polyprotein complexes anchoring on the ER membrane. In the first case, *cct1* producing BiP::2F5-KDEL demonstrated the highest ER stress response, followed by wild type expressing the same constructs (**Figure 5.12**), and wild type have also exhibited the highest 2F5 accumulation (**Figure 5.13**). This can further strengthen our speculation that BiP-KDEL combination retains 2F5 in the ER more successfully than KDEL alone. However, this hypothesis should be tested by confocal microscopy and immunolocalization with an ER localisation marker.

Similarly, in G22Y formation, 2F5 accumulation is not altered when expressing the BiP::2F5-KDEL that was proven promising for more efficient secretion (**Figure 5.14**).

Despite compartmentation, and especially expanded compartments having great potential, more optimisation is needed to obtain increased levels of recombinant proteins. In neither strategy was increased accumulation observed. A logical explanation for this phenomenon is that compartments need time to develop. During this formation period, proteins involved in the ER protein quality system might be unable to attach to the compartment and may be degraded or moved out of the cytosol. While the plant cell encounters forced ER expansion, it simultaneously and constitutively expresses a large heterologous protein that requires intricate post-translational modifications. This phenomenon might maximise ER stress response. Lastly, the aGFP IgG designed to bind to the lumen side of G22Y (GFP) did not accumulated more than the control, as it is

difficult to determine by AlphaFold interactions how they might be interacting inside the cell (**Figure S5.3**). Co-immunoprecipitation could shed more light in their interaction.

Supplementary Data

Figure S5.1 – Phenotypic differences between *N. benthamiana* plants depleted for membranous intracellular proteases following 3 weeks after virus-induced gene silencing (VIGS). *TRV::R6* grew indistinguishably from *TRV::GFP*. *TRV::SPP1, SPP2, SPP4, R3, R4, R7* and *Pres2* demonstrated a dwarf phenotype, approximately 25% smaller than *TRV::GFP. TRV::SPP3, SPP5, S1P, R1, R2, R5* and *Pres1* demonstrated a more severe dwarf phenotype, approximately 50% or more smaller than *TRV::GFP.* Scale bar 10cm.

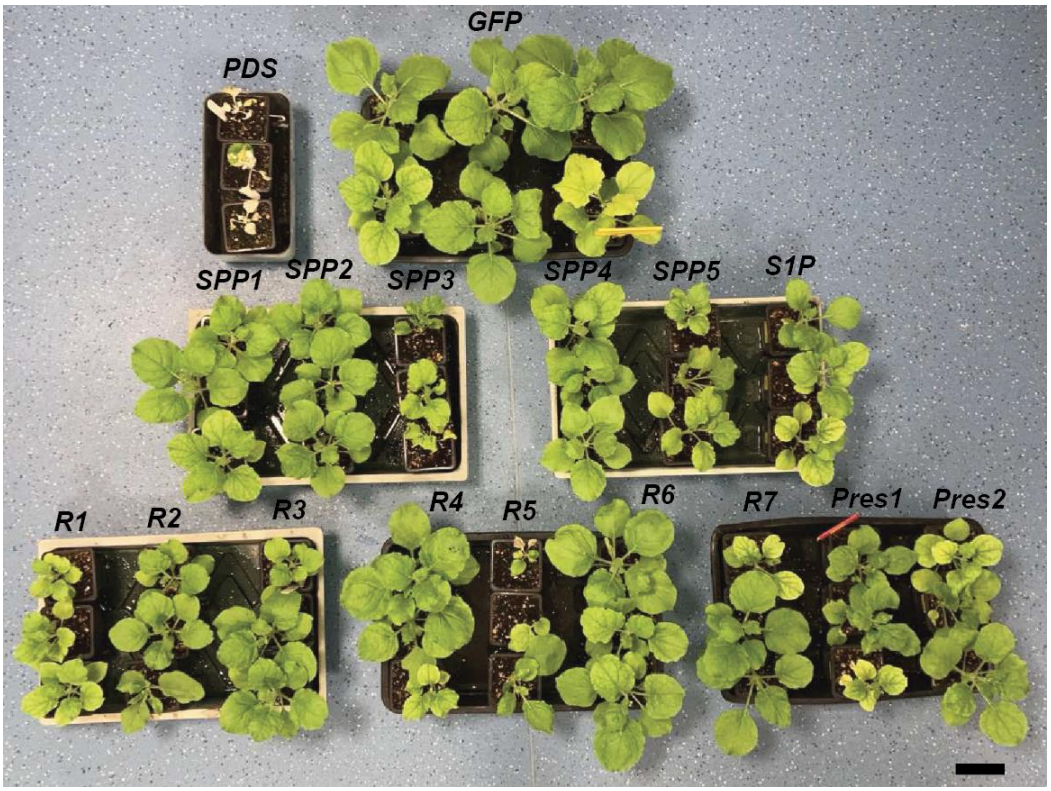

Figure S5.2 – ER-targeted VRC01 (VRC01$_{ER}$) expressed in WT or cct1 mutants. Total extracts were isolated at 5 d.p.i. and analysed by western blotting. In this case, VRC01$_{ER}$ (LC+HC) accumulated almost 5 times more in cct1 mutants. Interestingly, the shift of LC seen in WT and previously (**Figure 5.8b**) is restored in cct1 mutants, back to where apoplast-targeted VRC01 LC was observed. Quantification of VRC01$_{ER}$ (LC+HC) is depicted in graph and was calculated from n=3 independent experiment (t-test for significance).

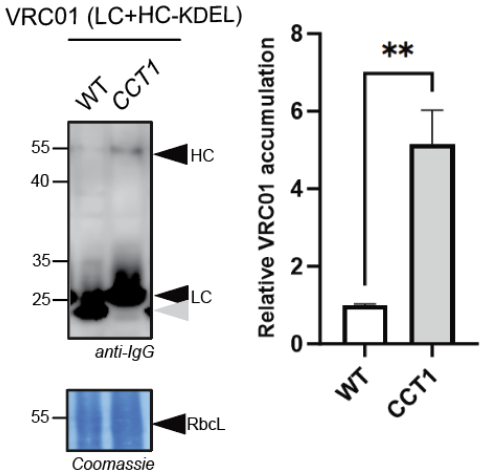

Figure S5.3 – Predicted aGFP IgG antibody interacting with GFP. (a),(b) model depicts AlphaFold-predicted interaction between aGFP IgG and free GFP. (c), (e) model depicts AlphaFold-predicted interaction between aGFP and GFP from the G22Y multimer. Grey: aGFP IgG; pink: aGFP CDR H3 loop; green: GFP; yellow: YFP; blue: BP22 transmembrane domain; orange: linkers.

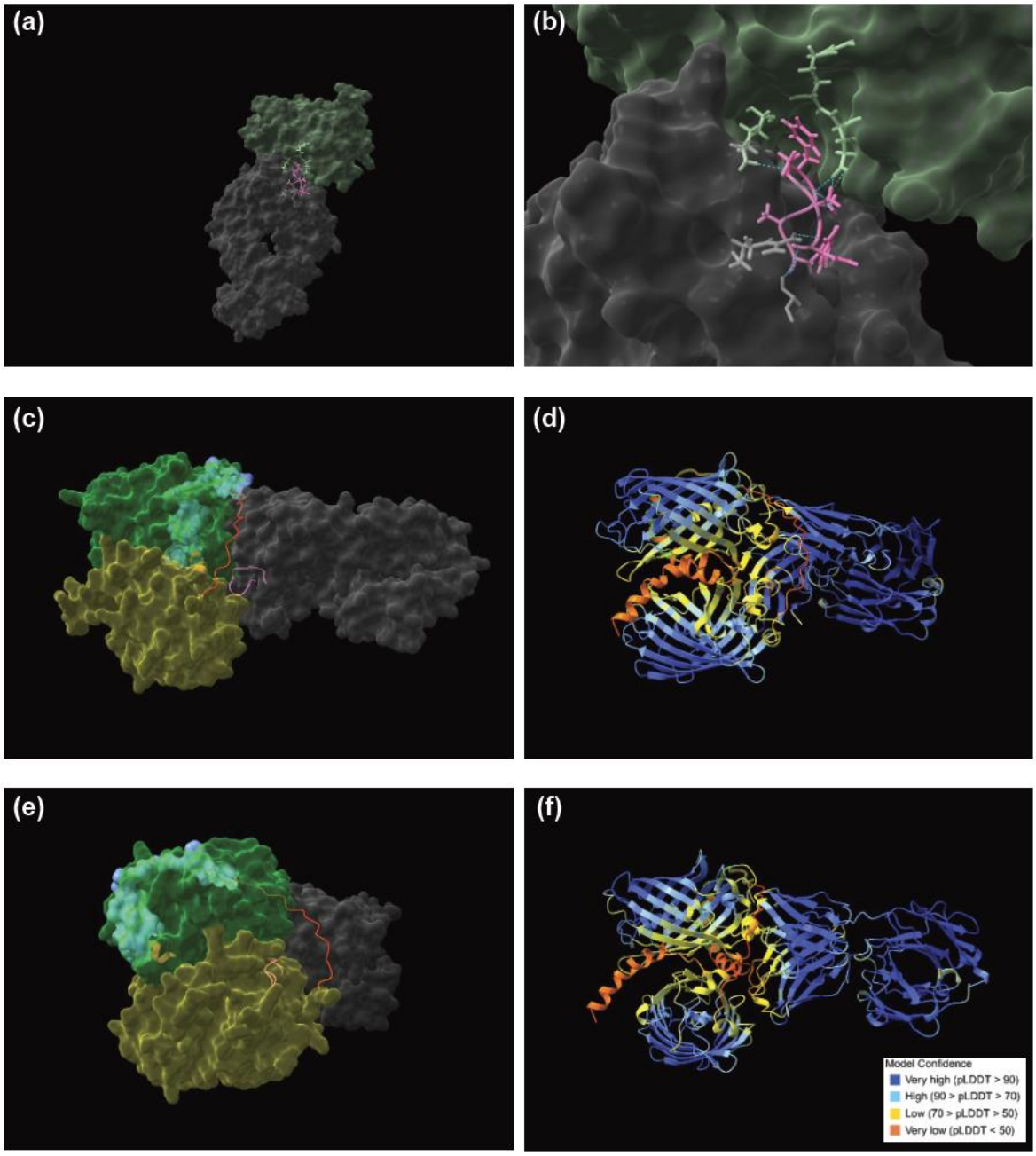

Figure S5.4 – No phenotypic differences in *N. benthamiana* plants following heat treatment for 2 hours. Scale bar 10cm.

References

Agrawal, G. K., Jwa, N. S., Lebrun, M. H., Job, D., & Rakwal, R. (2010). Plant secretome: Unlocking secrets of the secreted proteins. In *Proteomics* (Vol. 10, Issue 4, pp. 799–827). https://doi.org/10.1002/pmic.200900514

Alvarez, M. L., Topal, E., Martin, F., & Cardineau, G. A. (2010). Higher accumulation of F1-V fusion recombinant protein in plants after induction of protein body formation. *Plant Molecular Biology*, *72*(1–2), 75–89. https://doi.org/10.1007/s11103-009-9552-4

Arcalis, E., Stadlmann, J., Rademacher, T., Marcel, S., Sack, M., Altmann, F., & Stoger, E. (2013). Plant species and organ influence the structure and subcellular localization of recombinant glycoproteins. *Plant Molecular Biology*, *83*(1–2), 105–117. https://doi.org/10.1007/s11103-013-0049-9

Asano, K. (2014). Why is start codon selection so precise in eukaryotes? *Translation*, *2*(1), e28387. https://doi.org/10.4161/trla.28387

Bolhuis, A., Matzen, A., Hyyryläinen, H. L., Kontinen, V. P., Meima, R., Chapuis, J., Venema, G., Bron, S., Freudl, R., & Van Dijl, J. M. (1999). Signal peptide peptidase- and ClpP-like proteins of Bacillus subtilis required for efficient translocation and processing of secretory proteins. *Journal of Biological Chemistry*, *274*(35), 24585–24592. https://doi.org/10.1074/jbc.274.35.24585

Bolte, S., & Cordelières, F. P. (2006). A guided tour into subcellular colocalization analysis in light microscopy. In *Journal of Microscopy* (Vol. 224, Issue 3, pp. 213–232). Blackwell Publishing Ltd. https://doi.org/10.1111/j.1365-2818.2006.01706.x

Bosch, D., Castilho, A., Loos, A., & Steinkellner, A. S. and H. (2013). N-Glycosylation of Plant-produced Recombinant Proteins. In *Current Pharmaceutical Design* (Vol. 19, Issue 31, pp. 5503–5512). https://doi.org/http://dx.doi.org/10.2174/1381612811319310006

Brandizzi, F., Frangne, N., Marc-Martin, S., Hawes, C., Neuhaus, J. M., & Paris, N. (2002). The destination for single-pass membrane proteins is influenced markedly by the length of the hydrophobic domain. *Plant Cell*, *14*(5), 1077–1092. https://doi.org/10.1105/tpc.000620

Caldo, K. M. P., Xu, Y., Falarz, L., Jayawardhane, K., Acedo, J. Z., & Chen, G. (2019). Arabidopsis CTP:phosphocholine cytidylyltransferase 1 is phosphorylated and inhibited by sucrose nonfermenting 1-related protein kinase 1 (SnRK1). *Journal of Biological Chemistry*, *294*(43), 15862–15874. https://doi.org/10.1074/jbc.RA119.008047

Craddock, C. P., Adams, N., Bryant, F. M., Kurup, S., & Eastmond, P. J. (2015). PHOSPHATIDIC ACID PHOSPHOHYDROLASE regulates phosphatidylcholine biosynthesis in arabidopsis by phosphatidic acid-mediated activation of CTP: PHOSPHOCHOLINE CYTIDYLYLTRANSFERASE activityop. *Plant Cell*, *27*(4), 1251–1264. https://doi.org/10.1105/tpc.15.00037

Diego-Martin, B., González, B., Vazquez-Vilar, M., Selma, S., Mateos-Fernández, R., Gianoglio, S., Fernández-del-Carmen, A., & Orzáez, D. (2020). Pilot Production of SARS-CoV-2 Related Proteins in Plants: A Proof of Concept for Rapid Repurposing of Indoor Farms Into Biomanufacturing Facilities. *Frontiers in Plant Science*, *11*. https://doi.org/10.3389/fpls.2020.612781

Doran, P. M. (2006). Foreign protein degradation and instability in plants and plant tissue cultures. In *Trends in Biotechnology* (Vol. 24, Issue 9, pp. 426–432). https://doi.org/10.1016/j.tibtech.2006.06.012

Edkins, A., & Blatchheditors, G. (2023). *The Networking of Chaperones by Co-Chaperones Third Edition*.

Eisenach, C., Francisco, R., & Martinoia, E. (2015). Plant vacuoles. In *Current Biology* (Vol. 25, Issue 4, pp. R136–R137). Cell Press. https://doi.org/10.1016/j.cub.2014.11.056

Feige, M. J., Hendershot, L. M., & Buchner, J. (2010). How antibodies fold. In *Trends in Biochemical Sciences* (Vol. 35, Issue 4, pp. 189–198). https://doi.org/10.1016/j.tibs.2009.11.005

Floss, D. M., Sack, M., Arcalis, E., Stadlmann, J., Quendler, H., Rademacher, T., Stoger, E., Scheller, J., Fischer, R., & Conrad, U. (2009). Influence of elastin-like peptide fusions on the quantity and quality of a tobacco-derived human immunodeficiency virus-neutralizing antibody. *Plant Biotechnology Journal*, *7*(9), 899–913. https://doi.org/10.1111/j.1467-7652.2009.00452.x

Forestier, E. C. F., Cording, A. C., Loake, G. J., & Graham, I. A. (2023). An Engineered Heat-Inducible Expression System for the Production of Casbene in Nicotiana benthamiana. *International Journal of Molecular Sciences*, *24*(14). https://doi.org/10.3390/ijms241411425

Frigerio, L., Vine, N. D., Pedrazzini, E., Hein, M. B., Wang, F., K-C Ma, J., & Vitale, A. (2000). *Assembly, Secretion, and Vacuolar Delivery of a Hybrid Immunoglobulin in Plants*. www.plantphysiol.org

Garagounis, C., Kostaki, K. I., Hawkins, T. J., Cummins, I., Fricker, M. D., Hussey, P. J., Hetherington, A. M., & Sweetlove, L. J. (2017). Microcompartmentation of cytosolic aldolase by interaction with the actin cytoskeleton in Arabidopsis. *Journal of Experimental Botany*, *68*(5), 885–898. https://doi.org/10.1093/jxb/erx015

Göritzer, K., Melnik, S., Schwestka, J., Arcalis, E., Drapal, M., Fraser, P., Ma, J. K. C., & Stoger, E. (2025). Enhancing quality and yield of recombinant secretory IgA antibodies in Nicotiana benthamiana by endoplasmic reticulum engineering. *Plant Biotechnology Journal*. https://doi.org/10.1111/pbi.14576

Goulet, C., Khalf, M., Sainsbury, F., D'Aoust, M. A., & Michaud, D. (2012). A protease activity-depleted environment for heterologous proteins migrating towards the leaf cell apoplast. *Plant Biotechnology Journal*, *10*(1), 83–94. https://doi.org/10.1111/j.1467-7652.2011.00643.x

Grosse-Holz, F., Kelly, S., Blaskowski, S., Kaschani, F., Kaiser, M., & van der Hoorn, R. A. L. (2018). The transcriptome, extracellular proteome and active secretome of agroinfiltrated Nicotiana benthamiana uncover a large, diverse protease repertoire. *Plant Biotechnology Journal*, *16*(5), 1068–1084. https://doi.org/10.1111/pbi.12852

Grosse-Holz, F., Madeira, L., Zahid, M. A., Songer, M., Kourelis, J., Fesenko, M., Ninck, S., Kaschani, F., Kaiser, M., & van der Hoorn, R. A. L. (2018). Three unrelated protease inhibitors enhance accumulation of pharmaceutical recombinant proteins in Nicotiana benthamiana. *Plant Biotechnology Journal*, *16*(10), 1797–1810. https://doi.org/10.1111/pbi.12916

Gruber, V., Berna, P. P., Arnaud, T., Bournat, P., Clément, C., Mison, D., Olagnier, B., Philippe, L., Theisen, M., Baudino, S., Bénicourt, C., Cudrey, C., Bloës, C., Duchateau, N., Dufour, S., Gueguen, C., Jacquet, S., Ollivo, C., Poncetta, C., … Danzin, C. (2001a). Large-scale production

of a therapeutic protein in transgenic tobacco plants : effect of subcellular targeting on quality of a recombinant dog gastric lipase. In *Molecular Breeding* (Vol. 7).

Gruber, V., Berna, P. P., Arnaud, T., Bournat, P., Clément, C., Mison, D., Olagnier, B., Philippe, L., Theisen, M., Baudino, S., Bénicourt, C., Cudrey, C., Bloës, C., Duchateau, N., Dufour, S., Gueguen, C., Jacquet, S., Ollivo, C., Poncetta, C., … Danzin, C. (2001b). Large-scale production of a therapeutic protein in transgenic tobacco plants : effect of subcellular targeting on quality of a recombinant dog gastric lipase. In *Molecular Breeding* (Vol. 7).

Gupta, D., & Tuteja, N. (2011). Chaperones and foldases in endoplasmic reticulum stress signaling in plants. In *Plant Signaling and Behavior* (Vol. 6, Issue 2, pp. 232–236). https://doi.org/10.4161/psb.6.2.15490

Gutiérrez, S. P., Saberianfar, R., Kohalmi, S. E., & Menassa, R. (2013). Protein body formation in stable transgenic tobacco expressing elastin-like polypeptide and hydrophobin fusion proteins. *BMC Biotechnology*, *13*. https://doi.org/10.1186/1472-6750-13-40

Hammond-Kosack, K. E., Jones, D. A., & Jones', J. D. G. (1994). ldentification of Two Genes Required in Tomato for Full Cf-9-Dependent Resistance to Cladosporium fulvum. In *The Plant Cell* (Vol. 6).

Haryadi, R., Ho, S., Kok, Y. J., Pu, H. X., Zheng, L., Pereira, N. A., Li, B., Bi, X., Goh, L. T., Yang, Y., & Song, Z. (2015). Optimization of heavy chain and light chain signal peptides for high level expression of therapeutic antibodies in CHO cells. *PLoS ONE*, *10*(2). https://doi.org/10.1371/journal.pone.0116878

He, X., Haselhorst, T., von Itzstein, M., Kolarich, D., Packer, N. H., & Kermode, A. R. (2012). Influence of an ER-retention signal on the N-glycosylation of recombinant human α-l-iduronidase generated in seeds of Arabidopsis. *Plant Molecular Biology*, *79*(1–2), 157–169. https://doi.org/10.1007/s11103-012-9902-5

Hehle, V. K., Paul, M. J., Drake, P. M., Ma, J. K. C., & van Dolleweerd, C. J. (2011). Antibody degradation in tobacco plants: A predominantly apoplastic process. *BMC Biotechnology*, *11*. https://doi.org/10.1186/1472-6750-11-128

Hendershot. (1990). *Immunoglobulin Heavy Chain and Binding Protein Complexes Are Dissociated In Vivo by Light Chain Addition*.

Ho, S. C. L., Wang, T., Song, Z., & Yang, Y. (2015). IgG Aggregation Mechanism for CHO Cell Lines Expressing Excess Heavy Chains. *Molecular Biotechnology*, *57*(7), 625–634. https://doi.org/10.1007/s12033-015-9852-7

Irons, S. L., Nuttall, J., Floß, D. M., Frigerio, L., Kotzer, A. M., & Hawes, C. (2008). Fluorescent protein fusions to a human immunodeficiency virus monoclonal antibody reveal its intracellular transport through the plant endomembrane system. *Plant Biotechnology Journal*, *6*(7), 649–662. https://doi.org/10.1111/j.1467-7652.2008.00348.x

Islam, M. R., Choi, S., Muthamilselvan, T., Shin, K., & Hwang, I. (2020). In Vivo Removal of N-Terminal Fusion Domains From Recombinant Target Proteins Produced in Nicotiana benthamiana. *Frontiers in Plant Science*, *11*. https://doi.org/10.3389/fpls.2020.00440

Jan, C. H., Williams, C. C., & Weissman, J. S. (2014). Principles of ER cotranslational translocation revealed by proximity-specific ribosome profiling. *Science*, *346*(6210). https://doi.org/10.1126/science.1257521

Jutras, P. V., Grosse-Holz, F., Kaschani, F., Kaiser, M., Michaud, D., & van der Hoorn, R. A. L. (2019). Activity-based proteomics reveals nine target proteases for the recombinant protein-stabilizing inhibitor SlCYS8 in Nicotiana benthamiana. *Plant Biotechnology Journal*, *17*(8), 1670–1678. https://doi.org/10.1111/pbi.13092

Jutras, P. V., Soldan, R., Dodds, I., Schuster, M., Preston, G. M., & van der Hoorn, R. A. L. (2021). AgroLux: bioluminescent Agrobacterium to improve molecular pharming and study plant immunity. *Plant Journal*, *108*(2), 600–612. https://doi.org/10.1111/tpj.15454

Kobayashi, M., Utsushi, H., Fujisaki, K., Takeda, T., Yamashita, T., & Terauchi, R. (2022). A jacalin-like lectin domain-containing protein of Sclerospora graminicola acts as an apoplastic virulence effector in plant–oomycete interactions. *Molecular Plant Pathology*, *23*(6), 845–854. https://doi.org/10.1111/mpp.13197

Kohler, G. (1980). *Immunoglobulin chain loss in hybridoma lines (immunoglobulin variants/chromosome loss)* (Vol. 77, Issue 4). https://www.pnas.org

Lurid, P., & Dunsmuir, P. (1992). A plant signal sequence enhances the secretion of bacterial ChiA in transgenic tobacco. In *Plant Molecular Biology* (Vol. 18).

Ma, J., Kearney?, J. F., Hendershot~~, L. M., & Jude, S. (1990). ASSOCIATION OF TRANSPORT-DEFECTIVE LIGHT CHAINS WITH IMMUNOGLOBULIN HEAVY CHAIN BINDING PROTEIN. In *M&culur hnunolo~~* (Vol. 27, Issue 7).

Marques, L. É. C., Silva, B. B., Dutra, R. F., Florean, E. O. P. T., Menassa, R., & Guedes, M. I. F. (2020). Transient Expression of Dengue Virus NS1 Antigen in Nicotiana benthamiana for Use as a Diagnostic Antigen. *Frontiers in Plant Science*, *10*. https://doi.org/10.3389/fpls.2019.01674

Matsui, T., Hori, M., Shizawa, N., Nakayama, H., Shinmyo, A., & Yoshida, K. (2006). High-efficiency secretory production of peroxidase C1a using vesicular transport engineering in transgenic tobacco. *Journal of Bioscience and Bioengineering*, *102*(2), 102–109. https://doi.org/10.1263/jbb.102.102

Najjar, A., Robert, S., Guérin, C., Violet-Asther, M., & Carrière, F. (2011). Quantitative study of lipase secretion, extracellular lipolysis, and lipid storage in the yeast Yarrowia lipolytica grown in the presence of olive oil: Analogies with lipolysis in humans. *Applied Microbiology and Biotechnology*, *89*(6), 1947–1962. https://doi.org/10.1007/s00253-010-2993-5

Nausch, H., Mikschofsky, H., Koslowski, R., Meyer, U., Broer, I., & Huckauf, J. (2012). High-Level Transient Expression of ER-Targeted Human Interleukin 6 in Nicotiana benthamiana. *PLoS ONE*, *7*(11). https://doi.org/10.1371/journal.pone.0048938

Ng, S. Y. M., Chaban, B., VanDyke, D. J., & Jarrell, K. F. (2007). Archaeal signal peptidases. In *Microbiology* (Vol. 153, Issue 2, pp. 305–314). https://doi.org/10.1099/mic.0.2006/003087-0

Niemer, M., Mehofer, U., Torres Acosta, J. A., Verdianz, M., Henkel, T., Loos, A., Strasser, R., Maresch, D., Rademacher, T., Steinkellner, H., & Mach, L. (2014). The human anti-HIV antibodies 2F5, 2G12, and PG9 differ in their susceptibility to proteolytic degradation: Down-regulation of endogenous serine and cysteine proteinase activities could improve antibody production in plant-based expression platforms. *Biotechnology Journal*, *9*(4), 493–500. https://doi.org/10.1002/biot.201300207

Ocampo, C. G., Lareu, J. F., Marin Viegas, V. S., Mangano, S., Loos, A., Steinkellner, H., & Petruccelli, S. (2016). Vacuolar targeting of recombinant antibodies in Nicotiana benthamiana. *Plant Biotechnology Journal*, *14*(12), 2265–2275. https://doi.org/10.1111/pbi.12580

Peyret, H., Ponndorf, D., Meshcheriakova, Y., Richardson, J., & Lomonossoff, G. P. (2020). Covalent protein display on Hepatitis B core-like particles in plants through the in vivo use of the SpyTag/SpyCatcher system. *Scientific Reports*, *10*(1). https://doi.org/10.1038/s41598-020-74105-w

Pillay, P., Schlüter, U., van Wyk, S., Kunert, K. J., & Vorster, B. J. (2014). Proteolysis of recombinant proteins in bioengineered plant cells. *Bioengineered*, *5*(1), 15–20. https://doi.org/10.4161/bioe.25158

Ponndorf, D., Meshcheriakova, Y., Thuenemann, E. C., Dobon Alonso, A., Overman, R., Holton, N., Dowall, S., Kennedy, E., Stocks, M., Lomonossoff, G. P., & Peyret, H. (2021). Plant-made dengue virus-like particles produced by co-expression of structural and non-structural proteins induce a humoral immune response in mice. *Plant Biotechnology Journal*, *19*(4), 745–756. https://doi.org/10.1111/pbi.13501

Puchol Tarazona, A. A., Maresch, D., Grill, A., Bakalarz, J., Torres Acosta, J. A., Castilho, A., Steinkellner, H., & Mach, L. (2021). Identification of two subtilisin-like serine proteases engaged in the degradation of recombinant proteins in Nicotiana benthamiana. *FEBS Letters*, *595*(3), 379–388. https://doi.org/https://doi.org/10.1002/1873-3468.14014

Rawlings, N. D., Barrett, A. J., & Bateman, A. (2012). MEROPS: The database of proteolytic enzymes, their substrates and inhibitors. *Nucleic Acids Research*, *40*(D1). https://doi.org/10.1093/nar/gkr987

Sainsbury, F., & Lomonossoff, G. P. (2008). Extremely high-level and rapid transient protein production in plants without the use of viral replication. *Plant Physiology*, *148*(3), 1212–1218. https://doi.org/10.1104/pp.108.126284

Samalova, M., Fricker, M., & Moore, I. (2006). Ratiometric fluorescence-imaging assays of plant membrane traffic using polyproteins. *Traffic*, *7*(12), 1701–1723. https://doi.org/10.1111/j.1600-0854.2006.00502.x

Sams, L., Amara, S., Chakroun, A., Coudre, S., Paume, J., Giallo, J., & Carrière, F. (2017). Constitutive expression of human gastric lipase in Pichia pastoris and site-directed mutagenesis of key lid-stabilizing residues. *Biochimica et Biophysica Acta - Molecular and Cell Biology of Lipids*, *1862*(10), 1025–1034. https://doi.org/10.1016/j.bbalip.2017.07.002

Sandor, A., Samalova, M., Brandizzi, F., Kriechbaumer, V., Moore, I., Fricker, M. D., & Sweetlove, L. J. (2024). Characterization of intracellular membrane structures derived from a massive expansion of endoplasmic reticulum (ER) membrane due to synthetic ER-membrane-resident polyproteins. *Journal of Experimental Botany*, *75*(1), 45–59. https://doi.org/10.1093/jxb/erad364

Schuster Mariana and Paulus, J. K. and K. J. and van der H. R. A. L. (2022). Purification of His-Tagged Proteases from the ApoplastApoplast of Agroinfiltrated N. benthamianaNicotiana benthamiana (N. benthamiana). In S. and H. P. F. Klemenčič Marina and Stael (Ed.), *Plant Proteases and Plant Cell Death: Methods and Protocols* (pp. 53–66). Springer US. https://doi.org/10.1007/978-1-0716-2079-3_5

Shaaltiel, Y., Bartfeld, D., Hashmueli, S., Baum, G., Brill-Almon, E., Galili, G., Dym, O., Boldin-Adamsky, S. A., Silman, I., Sussman, J. L., Futerman, A. H., & Aviezer, D. (2007). Production of glucocerebrosidase with terminal mannose glycans for enzyme replacement therapy of Gaucher's disease using a plant cell system. *Plant Biotechnology Journal*, *5*(5), 579–590. https://doi.org/10.1111/j.1467-7652.2007.00263.x

Shin, C., Kim, K., Kang, Y. J., Kim, D. S., Seo, Y. J., Park, S. R., Kim, M. K., Lee, Y. K., Kim, D. S., & Ko, K. (2022). Effect of IgG Fc-fusion and KDEL-ER retention signal on prostate-specific antigen expression in plant and its immune in mice. *Plant Biotechnology Reports*, *16*(6), 729–740. https://doi.org/10.1007/s11816-022-00810-9

Singh, A. A., Pillay, P., Naicker, P., Alexandre, K., Malatji Kanyane, Mach, L., Steinkellner, H., Vorster, J., Chikwamba, R., & Tsekoa, T. L. (2022). *Transient proteolysis reduction of Nicotiana benthamiana-produced CAP256 broadly neutralizing antibodies using CRISPR/Cas9*. http://www.clcbio.com

Soni, A. P., Lee, J., Shin, K., Koiwa, H., & Hwang, I. (2022). Production of Recombinant Active Human TGFβ1 in Nicotiana benthamiana. *Frontiers in Plant Science*, *13*. https://doi.org/10.3389/fpls.2022.922694

Strasser, R. (2018). Protein Quality Control in the Endoplasmic Reticulum of Plants. In *Annual Review of Plant Biology* (Vol. 69, pp. 147–172). Annual Reviews Inc. https://doi.org/10.1146/annurev-arplant-042817-040331

Sun, L., Zhang, S. S., Lu, S. J., & Liu, J. X. (2015). Site-1 protease cleavage site is important for the ER stress-induced activation of membrane-associated transcription factor bZIP28 in Arabidopsis. *Science China Life Sciences*, *58*(3), 270–275. https://doi.org/10.1007/s11427-015-4807-6

Thomas, D. R., & Walmsley, A. M. (2014). Improved expression of recombinant plant-made hEGF. *Plant Cell Reports*, *33*(11), 1801–1814. https://doi.org/10.1007/s00299-014-1658-8

Tian, J., Cheng, L., Han, Z. yun, & Yao, Y. cong. (2015). Tobacco rattle virus mediated gene silencing in strawberry plants. *Plant Cell, Tissue and Organ Culture*, *120*(3), 1131–1138. https://doi.org/10.1007/s11240-014-0669-z

Vorster, B. J., Cullis, C. A., & Kunert, K. J. (2019). Plant vacuolar processing enzymes. In *Frontiers in Plant Science* (Vol. 10). Frontiers Media S.A. https://doi.org/10.3389/fpls.2019.00479

Xiang, L., Etxeberria, E., & Van Den Ende, W. (2013). Vacuolar protein sorting mechanisms in plants. In *FEBS Journal* (Vol. 280, Issue 4, pp. 979–993). https://doi.org/10.1111/febs.12092

Zhang, J., Yu, D., Zhang, Y., Liu, K., Xu, K., Zhang, F., Wang, J., Tan, G., Nie, X., Ji, Q., Zhao, L., & Li, C. (2017). Vacuum and co-cultivation agroinfiltration of (germinated) seeds results in tobacco rattle virus (TRV) mediated whole-plant virus-induced gene silencing (VIGS) in wheat and maize. *Frontiers in Plant Science*, *8*. https://doi.org/10.3389/fpls.2017.00393

Zhang, X., Li, H., Lu, H., & Hwang, I. (2021). The trafficking machinery of lytic and protein storage vacuoles: How much is shared and how much is distinct? In *Journal of Experimental Botany* (Vol. 72, Issue 10, pp. 3504–3512). Oxford University Press. https://doi.org/10.1093/jxb/erab067

Zheng, K., Lyu, J. C., Thomas, E. L., Schuster, M., Sanguankiattichai, N., Ninck, S., Kaschani, F., Kaiser, M., & van der Hoorn, R. A. L. (2024). The proteome of Nicotiana benthamiana is

shaped by extensive protein processing. *New Phytologist*, *243*(3), 1034–1049. https://doi.org/10.1111/nph.19891

Chapter 6

General Discussion & Future Research

This work investigated the *in vitro* and *in vivo* processing of various anti-viral IgGs, as well as their subcellular localisation and mistargeting in *N. benthamiana*, in pursuit of optimising IgG protein production *in planta*.

In **Chapter 2** we focused on screening proteases, with a particular focus on subtilases, in the degradation of different G immunoglugulins (IgG) within *Nicotiana benthamiana* apoplastic fluids *in vitro*. Experimental results revealed several key findings that significantly contribute to our understanding of recombinant antibody production in plant-based systems. Results underscore the substantial impact of subtilases, especially SBT5.2, on 2F5 degradation. Secondly, this Chapter demonstrates that different antibodies exhibit varying levels of susceptibility to cleavage by subtilases. This variability is seen by the three antibodies tested: The 2F5 antibody shows high susceptibility to degradation, indicating that it is particularly vulnerable in apoplastic fluids.

In contrast to 2F5, the COVA2-15 antibody demonstrates greater stability, suggesting that it is more resistant to subtilase-mediated degradation. The anti-Ebola 2G4 antibody exhibits intermediate stability, falling between the highly susceptible 2F5 and the more stable COVA2-15. These observations of processing patterns and stability among various antibodies lead to a crucial insight: a universal approach may not be effective for optimising recombinant antibody production in plant-based systems.

In **Chapter 3** we explored the processing and accumulation of different anti-viral IgG antibodies in protease-depleted *N. benthamiana* plants both by expressing protease

inhibitors and by targeted mutagenesis to abolish protease production. Before expressing IgGs in protease mutants, we conducted an expression timeline of each antibody, with 2F5 showing increased assembly and intermediate accumulation by days five to seven. COVA2-15 had stable assembly across all timepoints, while 2G4 peaked in full assembly on day five.

Interestingly, when testing protease inhibitor co-expression with antibodies, none of them resulted in higher 2F5 accumulation compared to controls, while some inhibitors (*Sl*CDI, *Nb*Pot1) led to decreased 2F5 accumulation. This rather unexpected result is contrary to expectations, as protease inhibitors are often used to protect recombinant proteins from degradation (Goulet et al., 2012a; Grosse-Holz et al., 2018; Jutras et al., 2019). The decreased accumulation observed specifically with SlCDI (Cys/Asp inhibitor) and *Nb*Pot1 (Ser inhibitor), suggests that these inhibitors may have unintended effects on protein production or plant cell processes. At the least it is possible that production of these two inhibitors in some way directly competes IgG production itself, potentially by competing for rare amino acids during protein translation.

These data indicate that the relationship between proteases, their inhibitors, and recombinant protein accumulation is more complex than initially thought. Inhibiting certain proteases may disrupt normal protein biosynthesis or turnover, potentially leading to negative effects on overall protein yields (Mangena, 2022). Adding complexity to this issue of reduced/unaltered IgG accumulation is the likely plant response to inhibition. Conceivably plants may respond to protease inhibition by increasing the transcription of protease-encoding genes to maintain homeostasis. For example, when the proteasome is inhibited by syringolin A, the expression of proteasome-related genes is upregulated (Michel et al., 2006).

The lack of positive effect from protease inhibitors could be due to the inhibitors not accumulating in the same cellular compartments as the recombinant proteins or being inactive under certain pH conditions. Alternatively, or in combination with the issue of distinct compartmentation, it is possible the chosen inhibitors may not target the specific proteases responsible for 2F5 degradation, or that multiple proteases are involved in the process. Perhaps an inactive version of every protease inhibitor as negative control of the respective inhibitors is needed to account for competition on translation machinery.

Unlike the co-expression of protease inhibitors, targeted depletion of the subtilase SBT5.2 led to a major increase in in 2F5 and 2G4 accumulation. Similarly, SBT1.4 depletion also boosted accumulation of both these antibodies. Moreover, *vpe* mutants showed increased accumulation of COVA2-15 and VRC01 antibodies. An interesting observation was that some other mutants (e.g., *sbt1.7*) resulted in lower IgG levels for certain antibodies. This variability in response across different protease depletions and antibody types underscores the nuanced nature of the plant proteolytic network and its influence on recombinant protein production.

Additionally, no significant differences between wild type and protease-depleted lines were observed when GFP was expressed. This ensured that any changes in IgG levels in these genetic backgrounds were not due to altered transformation efficiency, or other indirect general effects of protease deletion. These findings, in combination with the previously described mixed results with protease inhibitor co-expression, highlight the complexity of recombinant protein production *in planta* and the challenges in developing effective strategies to improve protein yields..

To fully harness the potential of this approach, it would be beneficial to conduct comprehensive analyses across a wider range of antibodies and protease mutants. Such extensive studies would provide a more complete picture of the protease-antibody interactions and help identify which specific proteases are most beneficial to deplete for each particular antibody. Furthermore, the findings suggest that combining multiple protease depletions or using a combination of protease depletion and protease inhibitor co-expression might yield better results for some antibodies. This multifaceted approach could potentially address the complex nature of the plant proteolytic network and provide a more robust solution for enhancing antibody yields across a broader range of antibody types. The different outcomes also highlight the potential for unexpected outcomes when manipulating the plant proteolytic network. The observation that some protease depletions led to decreased antibody accumulation support the idea that proteases may indirectly have other roles in cell homeostasis.

In **Chapter 4** the differential stability of different IgGs was examined. Interestingly, it was observed that COVA2-15 was more stable compared to 2F5 when incubated in apoplastic fluids. It was hypothesised that this enhanced stability was attributed to the presence of a disulphide bridge in the CDR H3 loop, which likely prevented steric accessibility of the loop by proteases. Cysteine mutation introducing potential disulphide bridges near the 2F5 cleavage site (*m1* and *m2*) resulted in a significant 2.5- and 3.5-fold increased accumulation compared to the wild-type antibody. However, the mechanism underlying this improvement may not be solely due to specific cleavage site protection but could involve overall stability enhancements of the antibody structure. Direct mutations at the P1 cleavage site of 2F5 (*m3, m4, m5*) produced varied effects on antibody stability and

accumulation. Some mutations led to decreased accumulation or, paradoxically, increased vulnerability to proteolytic processing. This highlights the complexity of antibody engineering and the need for careful consideration when modifying critical regions.

Additionally, eliminating the disulphide bridge in COVA2-15 CDR H3 loop had dramatic effects on the antibody stability and function. This modification led to increased susceptibility to proteolytic processing and dramatically reduced antigen binding capacity.

In combination, both the increased stability of 2F5 when potential disulphide bridge-forming cysteines were introduced, and the decreased stability of COVA2-15 when the native disulphide bridge was abolished, support the initial hypothesis, that disulfide bridge formation protects the CDR H3 loop from degradation. However, care should be taken when introducing such mutations as they may impact antigenicity. This balance between stability and function presents a significant challenge in antibody engineering.

In **Chapter 5** we focused on examining the impact of subcellular localisation on recombinant IgG yield and processing profiles. The 2F5 antibody demonstrates poor secretion efficiency into the apoplast when expressed in *N. benthamiana* leaves. Immunoblotting data revealed that only a small fraction, approximately 3-4% of the total 2F5 produced, was detected in apoplastic fluids. This low secretion rate suggests potential challenges in IgG processing and transport mechanisms within the plant cell.

Moreover, differences were observed in the accumulation patterns of the heavy chain (HC) and light chain (LC) of the 2F5 antibody, when assessed by western blot. The HC predominantly accumulates intracellularly, indicating possible retention within the

ER. In contrast, the LC exhibits a higher rate for secretion, suggesting differential transport of the two chains which can impact their processing differently. These results were also supported to an extent by confocal microscopy, which indicated higher co-localisation of an LC::GFP construct with a secreted sRFP marker, while an HC::RFP construct showed significantly lower correlation with a corresponding secreted sGFP marker. Although the caveats of the confocal approach to assessing subcellular localisation have already been discussed in the corresponding chapter, the results are in agreement with the previously described immunoblotting data. Conceivably, the lower molecular weight of LC facilitates export to the apoplast, while the much larger HC remains trapped within the cytosol or endomembrane system. The observed differential secretion patterns between the heavy chain and light chain components of the antibody suggest that the HC may be a limiting factor in the overall secretion process.

Additionally, it was found that the choice of signal peptides significantly influenced overall 2F5 accumulation levels. Among the tested options, the *A. thaliana* basic chitinase signal peptide proved most effective, resulting in a substantial increase of approximately 7-fold in 2F5 accumulation. This finding emphasises the importance of future research focus on optimised signal peptides.

Attempts to improve antibody accumulation through ER retention strategies yielded mixed results. The use of a KDEL tag on the HC alone did not lead to increased 2F5 accumulation or prevent cleavage. However, a more comprehensive strategy employing an N-terminal BiP signal peptide with C-terminal KDEL tags on both HC and LC chains proved highly effective, resulting in a remarkable 9-fold increase in accumulation.

Conversely, although not unexpectedly, vacuolar targeting of 2F5 or VRC01 antibodies had a detrimental effect on production. This approach resulted in decreased HC stability and overall lower accumulation levels. The observed reduction in stability is unsurprising, as the vacuolar environment may not be conducive to maintaining the integrity of recombinant proteins, likely due to increased exposure to proteolytic enzymes and low pH. The detrimental effects observed with vacuolar targeting, highlight the need for careful consideration when selecting subcellular targeting approaches.

Further efforts to enhance antibody accumulation through ER expansion strategies were also unsuccessful. Neither genetic manipulation using *cct1* mutants nor synthetic polyprotein expression (G22Y) led to increased antibody accumulation. This outcome indicates that factors beyond ER capacity may be limiting antibody production in this system. It is also important to consider that alterations of ER structure in both tested lines do result in ER stress and potentially generalised cell and whole plant stress, which might subsequently reduce recombinant protein yields.

The study demonstrates that optimizing signal peptides and implementing ER retention strategies can significantly enhance antibody accumulation in plant systems. These approaches likely improve protein folding efficiency and/or reduce degradation, thereby increasing overall yields. The remarkable 9-fold increase in accumulation achieved through the use of BiP signal peptides with KDEL tags on both antibody chains underscores the potential of targeted ER retention for maximizing recombinant protein production. However, these results demonstrate that not all subcellular targeting strategies are equally effective. Recently it has been reported that KDEL receptor ERD2, functions as a Golgi gatekeeper, instead of a recycling receptor, by capturing K/HDEL proteins and releasing them for retrograde transport to the ER (Alvim et al., 2023).

Instead, findings indicate that ERD2 predominantly resides at the cis-Golgi, functioning as a sorting checkpoint. This Golgi retention is essential for its activity, as demonstrated by mutations affecting its di-leucine motif, which disrupt its localisation and function. The conservation of ERD2 between plants and humans, along with its ability to sort KDEL proteins across species, suggests an ancient and regulated mechanism. The gatekeeper model proposes that ERD2 regulates ligand sorting within the Golgi, ensuring that specific proteins are retained for retrograde transport. This model addresses a limitation in the classical hypothesis: the high abundance of ER-resident proteins would render constant receptor recycling inefficient. Instead, ERD2 may remain stationary while directing ligand movement. Its retention at the Golgi depends on a distinct Golgi-localisation signal, preventing anterograde leakage, and its function is linked to ARF1 regulation and COPI vesicle formation. This paradigm shift raises questions about Golgi compartmentation, ligand release, and the evolution of ER-Golgi sorting mechanisms and retention dynamics.

In conclusion, the results of Chapter 5 emphasise the intricate nature of recombinant antibody production *in planta*. To maximise yields, careful optimisation of subcellular targeting and processing strategies is essential. The differential behaviour of antibody chains and the varied effects of different targeting approaches highlight the need for a much better understanding of heterologous protein production and trafficking in plant cells.

Moving forward, further research is needed to elucidate the specific mechanisms responsible for the poor secretion of some IgG antibodies. It is also necessary to develop a more comprehensive understanding of the factors influencing antibody stability and accumulation in different subcellular compartments. Ultimately, the potential of

combining multiple optimisation strategies to achieve synergistic improvements in antibody production must be investigated.

Towards unfolding the complexity of heterologous protein production

From designing gene expression vectors to selecting the ideal chassis, protein production yields are influenced by multiple factors, including host immune response, gene delivery efficiency, post-transcriptional gene silencing, mRNA stability, translation efficiency, protein folding and modifications, and successful translocation to the target compartment. In **Chapter 5**, we investigated the effect of having a single vector to simultaneously introduce both LC and HC coding sequences into the plant cell. Indeed, this approached lead to significant increase of 2F5 antibody. The multiplicity of T-DNA reported high rate of simultaneous transfer across for fluorescent recombinant protein (Carlson et al., 2023). However there is still a possibility that fluctuating T-DNA transfer or insertion levels can lead to chimeric expression across leaf cells (Pereman et al., 2019; Verhage, 2021). Moreover, in the case of antibodies this becomes more perplexed, as the ratio of LC and HC plays a pivotal role in IgG heterodimer assembly. This observation dictates that more accurate control of the LC/HC ratio could dramatically impact stabilisation.

Another strategy that has been extensively followed by the plant molecular pharming community is codon optimisation. Although careful design, especially of transcriptional regulatory domains is needed, when it comes to protein translation sometimes less is more. Several studies have shown that slowing translation, such as through mutant ribosomes, reduces translation speed, providing additional time for proper protein folding (Avolio et al., 2023; Knight et al., 2022; Sherman & Qian, 2013;

Siller et al., 2010). This approach could be of outstanding potential in plant-made antibodies.

Towards optimising secretion efficiency of IgGs in plant platforms

The subcellular localisation of recombinant proteins in plant cells, following their synthesis, is critical for their stability and quality as it involves folding, quality control, and post-translational modifications (Strasser, 2018). Studies on plant secretomes have revealed that more than half of naturally secreted proteins do not possess a signal peptide (Agrawal et al., 2010), which is generally considered necessary for guiding recombinant proteins to extracellular sites. We managed to acquire high accumulation of 2F5 with N-terminal *A. thaliana* basic chitinase (*At*BC) or an optimised combination of Chinese hamster ovaries cells' (CHO) signal peptides. This might be due to more efficient targeting to the endoplasmic reticulum and hence the secretory pathway route. However, this could be further validated by co-IP studies with BiP or other chaperones that might be involved in ER protein translocation.

In CHO cells, it has been reported that the native light and heavy chain signal peptides for secretion often do not lead to the most efficient secretion. In a study where they mixed and matched different signal peptides for different IgGs, it was obvious that different IgGs are secreted better with different N-terminal signal peptides (Haryadi et al., 2015). Interestingly, even the LC and HC secretion of the same IgG would be increased when using different signal peptides. Another approach that has been broadly successful is using fusion tags along with native or optimised signal peptides for more efficient secretion (Alvarez et al., 2010; Conley et al., 2011; Floss et al., 2009; Gutiérrez et al., 2013; Islam et al., 2020; Jiang et al., 2020; Joensuu et al., 2010; Pereira et al., 2014).

Since the apoplast has been consistently considered as the main compartment of recombinant protein degradation due to its abundance in proteases (Beritza et al., 2024; Goulet et al., 2012b; Hehle et al., 2011; Jutras et al., 2018, 2020; Niemer et al., 2014; Puchol Tarazona et al., 2021), it is essential to be aware of the secretion levels of IgGs and other recombinant proteins. This is important as it can make protease screening for IgG processing even more complex. For example, we confirmed by western blotting and confocal microscopy that most IgG is trapped intracellularly (**Chapter 5**). This indicates that 2F5 is not secreted into the apoplast and therefore not exposed to SBT5.2, that was previously shown to be the only protease cleaving 2F5 in vitro (**Chapter 2**; Puchol Tarazona et al., 2021). Although we cannot exclude that 2F5 accumulates in the apoplast in a non-extractable manner, e.g. immobilised to the cell wall or aggregates, we think this is unlikely because of the high solubility of 2F5 and because it would be cleaved by SBT5.2 in the apoplast.

References

Agrawal, G. K., Jwa, N. S., Lebrun, M. H., Job, D., & Rakwal, R. (2010). Plant secretome: Unlocking secrets of the secreted proteins. In *Proteomics* (Vol. 10, Issue 4, pp. 799–827). https://doi.org/10.1002/pmic.200900514

Alvarez, M. L., Topal, E., Martin, F., & Cardineau, G. A. (2010). Higher accumulation of F1-V fusion recombinant protein in plants after induction of protein body formation. *Plant Molecular Biology*, *72*(1–2), 75–89. https://doi.org/10.1007/s11103-009-9552-4

Alvim, J. C., Bolt, R. M., An, J., Kamisugi, Y., Cuming, A., Silva-Alvim, F. A. L., Concha, J. O., daSilva, L. L. P., Hu, M., Hirsz, D., & Denecke, J. (2023). The K/HDEL receptor does not recycle but instead acts as a Golgi-gatekeeper. *Nature Communications*, *14*(1). https://doi.org/10.1038/s41467-023-37056-0

Avolio, R., Agliarulo, I., Criscuolo, D., Sarnataro, D., Auriemma, M., De Lella, S., Pennacchio, S., Calice, G., Ng, M. Y., Giorgi, C., Esposito, F., & Matassa, D. S. (2023). Cytosolic and mitochondrial translation elongation are coordinated through the molecular chaperone TRAP1 for the synthesis and import of mitochondrial proteins. *Genome Research*, *33*(8), 1242–1257. https://doi.org/10.1101/gr.277755.123

Beritza, K., Buscaill, P., Song, S.-J., Jutras, P. V, Huang, J., Mach, L., Dong, S., & Van Der Hoorn, R. A. L. (2024). *SBT5.2s are the major active extracellular subtilases processing IgG antibody 2F5 in the Nicotiana benthamiana apoplast*.

Carlson, E. D., Rajniak, J., & Sattely, E. S. (2023). Multiplicity of the Agrobacterium Infection of Nicotiana benthamiana for Transient DNA Delivery. *ACS Synthetic Biology*, *12*(8), 2329–2338. https://doi.org/10.1021/acssynbio.3c00148

Conley, A. J., Joensuu, J. J., Richman, A., & Menassa, R. (2011). Protein body-inducing fusions for high-level production and purification of recombinant proteins in plants. In *Plant Biotechnology Journal* (Vol. 9, Issue 4, pp. 419–433). https://doi.org/10.1111/j.1467-7652.2011.00596.x

Floss, D. M., Sack, M., Arcalis, E., Stadlmann, J., Quendler, H., Rademacher, T., Stoger, E., Scheller, J., Fischer, R., & Conrad, U. (2009). Influence of elastin-like peptide fusions on the quantity and quality of a tobacco-derived human immunodeficiency virus-neutralizing antibody. *Plant Biotechnology Journal*, *7*(9), 899–913. https://doi.org/10.1111/j.1467-7652.2009.00452.x

Goulet, C., Khalf, M., Sainsbury, F., D'Aoust, M. A., & Michaud, D. (2012a). A protease activity-depleted environment for heterologous proteins migrating towards the leaf cell apoplast. *Plant Biotechnology Journal*, *10*(1), 83–94. https://doi.org/10.1111/j.1467-7652.2011.00643.x

Goulet, C., Khalf, M., Sainsbury, F., D'Aoust, M.-A., & Michaud, D. (2012b). A protease activity–depleted environment for heterologous proteins migrating towards the leaf cell apoplast. *Plant Biotechnology Journal*, *10*(1), 83–94. https://doi.org/https://doi.org/10.1111/j.1467-7652.2011.00643.x

Grosse-Holz, F., Madeira, L., Zahid, M. A., Songer, M., Kourelis, J., Fesenko, M., Ninck, S., Kaschani, F., Kaiser, M., & van der Hoorn, R. A. L. (2018). Three unrelated protease inhibitors enhance

accumulation of pharmaceutical recombinant proteins in Nicotiana benthamiana. *Plant Biotechnology Journal*, *16*(10), 1797–1810. https://doi.org/10.1111/pbi.12916

Gutiérrez, S. P., Saberianfar, R., Kohalmi, S. E., & Menassa, R. (2013). Protein body formation in stable transgenic tobacco expressing elastin-like polypeptide and hydrophobin fusion proteins. *BMC Biotechnology*, *13*. https://doi.org/10.1186/1472-6750-13-40

Haryadi, R., Ho, S., Kok, Y. J., Pu, H. X., Zheng, L., Pereira, N. A., Li, B., Bi, X., Goh, L. T., Yang, Y., & Song, Z. (2015). Optimization of heavy chain and light chain signal peptides for high level expression of therapeutic antibodies in CHO cells. *PLoS ONE*, *10*(2). https://doi.org/10.1371/journal.pone.0116878

Hehle, V. K., Paul, M. J., Drake, P. M., Ma, J. K. C., & van Dolleweerd, C. J. (2011). Antibody degradation in tobacco plants: A predominantly apoplastic process. *BMC Biotechnology*, *11*. https://doi.org/10.1186/1472-6750-11-128

Islam, M. R., Choi, S., Muthamilselvan, T., Shin, K., & Hwang, I. (2020). In Vivo Removal of N-Terminal Fusion Domains From Recombinant Target Proteins Produced in Nicotiana benthamiana. *Frontiers in Plant Science*, *11*. https://doi.org/10.3389/fpls.2020.00440

Jiang, M. C., Hu, C. C., Hsu, W. L., Hsu, T. L., Lin, N. S., & Hsu, Y. H. (2020). Fusion of a Novel Native Signal Peptide Enhanced the Secretion and Solubility of Bioactive Human Interferon Gamma Glycoproteins in Nicotiana benthamiana Using the Bamboo Mosaic Virus-Based Expression System. *Frontiers in Plant Science*, *11*. https://doi.org/10.3389/fpls.2020.594758

Joensuu, J. J., Conley, A. J., Lienemann, M., Brandle, J. E., Linder, M. B., & Menassa, R. (2010). Hydrophobin fusions for high-level transient protein expression and purification in Nicotiana benthamiana. *Plant Physiology*, *152*(2), 622–633. https://doi.org/10.1104/pp.109.149021

Jutras, P. V, Dodds, I., & van der Hoorn, R. A. L. (2020). Proteases of Nicotiana benthamiana: an emerging battle for molecular farming. *Current Opinion in Biotechnology*, *61*, 60–65. https://doi.org/https://doi.org/10.1016/j.copbio.2019.10.006

Jutras, P. V., Goulet, M. C., Lavoie, P. O., D'Aoust, M. A., Sainsbury, F., & Michaud, D. (2018). Recombinant protein susceptibility to proteolysis in the plant cell secretory pathway is pH-dependent. *Plant Biotechnology Journal*, *16*(11), 1928–1938. https://doi.org/10.1111/pbi.12928

Jutras, P. V., Grosse-Holz, F., Kaschani, F., Kaiser, M., Michaud, D., & van der Hoorn, R. A. L. (2019). Activity-based proteomics reveals nine target proteases for the recombinant protein-stabilizing inhibitor SlCYS8 in Nicotiana benthamiana. *Plant Biotechnology Journal*, *17*(8), 1670–1678. https://doi.org/10.1111/pbi.13092

Knight, T. J., Povey, J. F., Vito, D., Mohindra, A., Jaques, C. M., & Smales, C. M. (2022). Manipulation of mRNA translation elongation influences the fragmentation of a biotherapeutic Fc-fusion protein produced in CHO cells. *Biotechnology and Bioengineering*, *119*(12), 3408–3420. https://doi.org/10.1002/bit.28230

Mangena, P. (2022). Pleiotropic effects of recombinant protease inhibitors in plants. In *Frontiers in Plant Science* (Vol. 13). Frontiers Media S.A. https://doi.org/10.3389/fpls.2022.994710

Michel, K., Abderhalden, O., Bruggmann, R., & Dudler, R. (2006). Transcriptional changes in powdery mildew infected wheat and Arabidopsis leaves undergoing syringolin-triggered hypersensitive cell death at infection sites. *Plant Molecular Biology*, *62*(4–5), 561–578. https://doi.org/10.1007/s11103-006-9045-7

Niemer, M., Mehofer, U., Torres Acosta, J. A., Verdianz, M., Henkel, T., Loos, A., Strasser, R., Maresch, D., Rademacher, T., Steinkellner, H., & Mach, L. (2014). The human anti-HIV antibodies 2F5, 2G12, and PG9 differ in their susceptibility to proteolytic degradation: Down-regulation of endogenous serine and cysteine proteinase activities could improve antibody production in plant-based expression platforms. *Biotechnology Journal*, *9*(4), 493–500. https://doi.org/10.1002/biot.201300207

Pereira, E. O., Kolotilin, I., Conley, A. J., & Menassa, R. (2014). Production and characterization of in planta transiently produced polygalacturanase from Aspergillus niger and its fusions with hydrophobin or ELP tags. *BMC Biotechnology*, *14*. https://doi.org/10.1186/1472-6750-14-59

Pereman, I., Melamed-Bessudo, C., Dahan-Meir, T., Herz, E., Elbaum, M., & Levy, A. A. (2019). Single molecule imaging of T-DNA intermediates following Agrobacterium tumefaciens infection in Nicotiana benthamiana. *International Journal of Molecular Sciences*, *20*(24). https://doi.org/10.3390/ijms20246209

Puchol Tarazona, A. A., Maresch, D., Grill, A., Bakalarz, J., Torres Acosta, J. A., Castilho, A., Steinkellner, H., & Mach, L. (2021). Identification of two subtilisin-like serine proteases engaged in the degradation of recombinant proteins in Nicotiana benthamiana. *FEBS Letters*, *595*(3), 379–388. https://doi.org/https://doi.org/10.1002/1873-3468.14014

Sherman, M. Y., & Qian, S. B. (2013). Less is more: Improving proteostasis by translation slow down. In *Trends in Biochemical Sciences* (Vol. 38, Issue 12, pp. 585–591). https://doi.org/10.1016/j.tibs.2013.09.003

Siller, E., DeZwaan, D. C., Anderson, J. F., Freeman, B. C., & Barral, J. M. (2010). Slowing Bacterial Translation Speed Enhances Eukaryotic Protein Folding Efficiency. *Journal of Molecular Biology*, *396*(5), 1310–1318. https://doi.org/10.1016/j.jmb.2009.12.042

Strasser, R. (2018). Protein Quality Control in the Endoplasmic Reticulum of Plants. In *Annual Review of Plant Biology* (Vol. 69, pp. 147–172). Annual Reviews Inc. https://doi.org/10.1146/annurev-arplant-042817-040331

Verhage, L. (2021). Twelve genes at one blow: multiplex genome editing with CRISPR/Cas. In *Plant Journal* (Vol. 106, Issue 1, pp. 6–7). Blackwell Publishing Ltd. https://doi.org/10.1111/tpj.15228

Chapter 7

Materials and Methods

7.1 Bacterial strains and growth conditions

The *Escherichia coli* strain used for plasmid propagation was DH10β on lysogeny broth (LB) or agar, supplemented with appropriate antibiotics. Following heat shock transformation, *E. coli* transformants were selected on LB agar medium plates containing 50 μM kanamycin or carbenicillin. The *Agrobacterium tumefaciens* strain GV3101-pMP90 was used for transient transformation of *Nicotiana benthamiana*. Following heat shock transformation, *A. tumefaciens* transformants were selected on LB agar medium plates containing 25 μM rifampicin, 10 μM gentamycin, and 50 μM kanamycin or carbenicillin for the binary vector.

7.2 *Nicotiana benthamiana* cultivation

Wild-type *N. benthamiana* (LAB strain; Ranawaka et al., 2023) seeds were sown into a 3:1 mix of soil (Sinclair Modular Seed Peat reduced propagation mix) with vermiculite (Sinclair Pro Medium) in 7 cm square pots and grown at high humidity under transparent plastic covers for 5 days. Seedlings were uncovered and grown first for one week in the greenhouse at 22-23°C, 16 hr light/8 hr dark, at high humidity, and 80-120μmol/m^2s light intensity and watered three times per week. For the experiments where the Ara2 heat-inducible promoter was used, the plants were grown in the same light/dark regime and humidity. However, the growth chamber temperature was set at 40°C for the two last hours of the light cycle, on day 3 following infiltration.

7.3 Molecular cloning

The HC and LC of 2F5, 2G4, COVA2-15, aGFP were codon optimised for *N. benthamiana* and obtained from Twist Bioscience, carrying BsaI sites for Golden Gate cloning (See Appendix A for coding sequences, Figure 8.1, Engler et al., 2014; Marillonnet & Werner, 2015; Werner et al., 2012). All overexpression constructs carry the N-terminal *Nt*PR1a signal peptide from *Nicotiana tabacum* unless stated otherwise (**Appendix B**). All constructs were cloned into a Golden Gate binary vector containing the T-DNA with a Cauliflower Mosaic Virus 35S (CaMV 35S) promoter and either a nopaline synthase (nos) or 35S terminator following the Golden Gate protocol in a ratio of insert:backbone 2:1. Similarly, for designing the VIGS plasmids, the *Nb*SBTs genes were selected by a BLAST search in the Sol genomics network database (https://solgenomics.net/). The gene fragments targeting the subtilisin-like proteases were obtained from Invitrogen and were inserted into pJK037 (Morimoto et al., 2022) using Golden Gate cloning (BsaI sites), to generate the *TRV::GFP* and *TRV::NbSBT* plasmids. The VIGS plasmids for intracellular proteases were also cloned into pJK037. The protease inhibitor constructs were previously cloned and described (Grosse-Holz et al., 2018). Regarding the N-terminal signal peptides AtBC, *Nb*SBT5.2, *Hs*GL, CHO, and BiP, all plasmids were obtained from Twist Bioscience and cloned using BsaI sites into Golden Gate vectors. For the C-terminal ER-KDEL and vac-KISIA, or for the 2F5 (*m1-m5*) or COVA2-15 (*m1*) IgG mutants sequences were amplified using VeriFi® Hot Start Mix (PCR Biosystems), following by Mut Express MultiS Fast Mutagenesis Kit V2 (Vazyme). For the C-terminal fluorescent markers in 2F5 LC or HC, eGFP (pL0M-S-eGFP) or mScarlet (Twist Bioscience) were amplified using VeriFi® Hot Start Mix (PCR Biosystems) carrying appropriate overhangs for Gibson assembly cloning (NEBuilder® Gibson assembly, New England Biolabs; NEB). Plasmids carrying both LC

and HC of 2F5 (L2::2F5LC/2F5HC) were cloned by cutting the respective L1::2F5_LC and L1::2F5_HC using BpiI restriction enzyme and Golden Gate cloning. BsaI, BpiI or other enzymes used for cloning or restriction digestion were provided by NEB (NEBridge®, NEB HF® Enzymes). PCR amplification for cloning or screening was carried out following Bounce PCR using the AutoDelta feature on ProFlex PCR system as follows (Sam Mugford, 2018):

94°C	2 min	1 cycle
94°C 60°C to 45°C (1°C decrease per cycle) 72°C	30 sec 40 sec 1min per kb	15 cycles
94°C 45.6°C to 60°C (0.6°C increase per cycle) 72°C	30 sec 40 sec 1min per kb	25 cycles
72°C	6 min	1 cycle

All plasmids and primers used are listed in **Table 7.1** and **Table 7.2**, respectively.

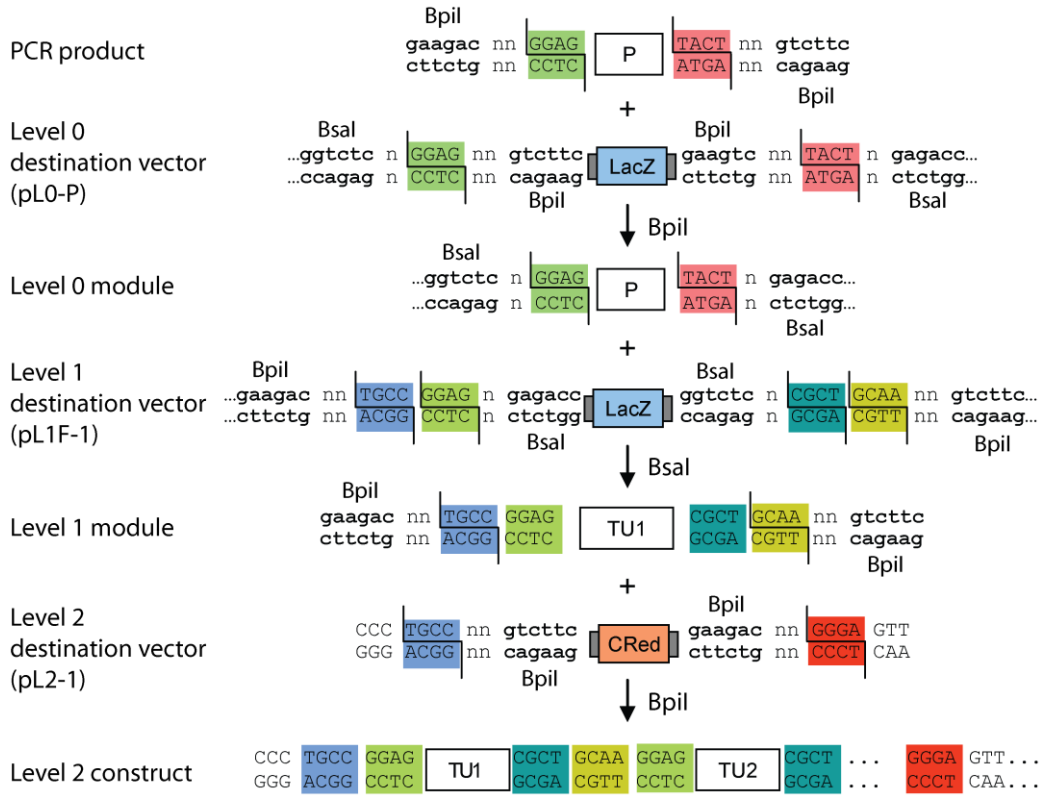

Figure 7.1 Overview of Golden Gate cloning vectors (adapted from Weber et al., 2011).

PCR product or synthesised fragment containing the fragment of interest (e.g. coding sequence) along with BpiI restriction sites to be used in Level 0 vector (single module vector; spectinomycin resistance). Multiple level 0 modules can then be combined and cloned using BsaI into level 1 vector (TU, transcription unit vector; e.g. promoter::signal peptide::coding_sequence::terminator; carbenicillin resistance) and be used for agroinfiltration. For multigene constructs, multiple level 1 vectors can be combined and cloned into level 2 vector using BpiI (multi-TU vector) and be used for agroinfiltration. Blue-white (lacZ) or red-white (CRed) screening was used in addition to antibiotic resistance for the correct clones.

Table 7.1 Plasmid list. pKB and plasmids from collaborators.

CDS, coding sequence; TU, transcription unit; TRV, Tobacco Rattle Virus.

Plasmid	Descriptive name	Reference
pKB001	L0_P19	This work
pKB002	L1_EV_control	
pKB007	L0_mScarlet	
pKB008	L0_nptII	
pKB009	L0_EPI1	
pKB010	L0_2G4_LC	
pKB011	L0_2G4_HC	
pKB012	L0_COVA_LC	
pKB013	L0_COVA_HC	
pKB014	L0_aGFP_LC	
pKB015	L0_aGFP_HC	
pKB016	L2_2F5_LC_2F5_HC	
pKB018	L0_NtPR1a2F5_LC	
pKB019	L0_NtPR1a2F5_HC	
pKB020	L1_35SP_2F5_LC_nosT	
pKB021	L1_35SP_2F5_HC_nosT	
pKB022	L1_2F5_HC_m1_T104C, I111C	
pKB023	L1_2F5_HC_m2_L106C, V109C	
pKB024	L1_2F5_HC_KDEL	
pKB025	L1_2F5_HC_KISIA	
pKB026	L1_35SP_2G4_LC_nosT	
pKB027	L1_35SP_2G4_HC_nosT	
pKB028	L1_35SP_COVA_LC_nosT	
pKB029	L1_35SP_COVA_HC_nosT	
pKB030	L1_aGFP_LC	
pKB031	L1_aGFP_HC	
pKB033	L1_2F5_m3_F107A	
pKB034	L1_2F5_m4_F107D	
pKB035	L1_2F5_m5_F107R	
pKB036	L1_COVA_m1_C103A, C107A	
pKB037	L1_35SP_2F5_HCmScarlet_nosT	

pKB038	L0_AtBC2F5_LC	
pKB039	L0_AtBC2F5_HC	
pKB040	L0_NbSBT5.22F5_LC	
pKB041	L0_NbSBT5.22F5_HC	
pKB042	L0_HsGL2F5_LC	
pKB043	L0_HsGL2F5_HC	
pKB044	L0_CHOL12F5_LC	
pKB045	L0_CHOH72F5_HC	
pKB046	L0_BiP2F5KDEL_LC	
pKB047	L0_BiP2F5KDEL_HC	
pKB048	L1_35SP_AtBC2F5_LC_nosT	
pKB049	L1_35SP_AtBC2F5_HC_nosT	
pKB050	L1_35SP_NbSBT5.22F5_LC_nosT	
pKB051	L1_35SP_NbSBT5.22F5_HC_nosT	
pKB052	L1_35SP_HsGL2F5_LC_nosT	
pKB053	L1_35SP_HsGL2F5_HC_nosT	
pKB054	L1_35SP_CHOL12F5_LC_nosT	
pKB055	L1_35SP_CHOH72F5_HC_nosT	
pKB056	L1_35SP_BiP2F5KDEL_LC_nosT	
pKB057	L1_35SP_BiP2F5KDEL_HC_nosT	
pKB058	L0_ara2P	
pKB059	L0_mCerulean_KDEL	
pKB060	L0_LCeGFP	
pKB061	L1_ara_BiP_LC	
pKB062	L1_ara_BiP_HC	
pKB063	L1_ara_GFP_LC	
Plasmid	**Alternative name**	**Reference**
pPB035	TRV2::GFP	Pierre Buscaill Beritza et al., 2024)
pPB058	TRV2::SBT1.7a	
pPB059	TRV2::SBT1.7c	
pPB065	TRV2::SBT1.9a	
pPB039	TRV2::SBT5.2	
pJK268c	35SP_P19_35ST	Kourelis et al., 2020
pICH41308	L0_CDS	Engler et al., 2014
pICH51277	L0_35SP_5UTR	

pICH41421	L0_nosT	
pICH47732	L1_P1_Fwd	
pICH47732	L1_P2_Fwd	
pFGH008	L1_35SP_NbPR4_35ST	Grosse-Holz et al., 2018
pFGH010	L1_35SP_SICDI_35ST	
pFGH047	L1_35SP_HsTIMP_35ST	
pFGH048	L1_35SP_EPI1_35ST	
pFGH049	L1_35SP_EPI12_35ST	
pFGH053	L1_35SP_NbPot1_35ST	
pFGH054	L1_35SP_SICYS8_35ST	
pFGH203	L1_35SP_Ala-HsTIMP_35ST	
pFGH214	L1_35SP_SICYS8-Q47P_35ST	
TRV1	TRV1	Liu et al., 2002
pJK037	TRV2gg (pL2M-TRV2)	Morimoro et al., 2022
TRV2::PDS	TRV2::PDS	Liu et al., 2002
pPJ048	35S_cytosolicGFP_35ST	Jutras et al., 2021
pPJ057	35S_secretedRFP_35ST	Beritza et al., 2024
pKZ153	pL1V2-F1-pBiP3a-GFP	Unpublished
pPJ040	VRC01 HC	Unpublished
pPJ041	VRC01 LC	Unpublished
pPJ042	VRC01 Hc - KISIA	Unpublished
pPJ043	VRC01 Hc - KDEL	Unpublished
pPJ056	Cytosolic RFP	Unpublished
-	Secreted GFP	Samalova et al., 2006
-	G22Y	Sandor et al., 2024
pKZ84	TRV::SSP1	Unpublished
pKZ85	TRV::SSP2	Unpublished
pKZ86	TRV::SSP3	Unpublished
pKZ87	TRV::SSP4	Unpublished
pKZ88	TRV::SSP5	Unpublished
pKZ89	TRV::S1P	Unpublished
pKZ90	TRV::Rhomboid1	Unpublished
pKZ91	TRV::Rhomboid2	Unpublished
pKZ92	TRV::Rhomboid3	Unpublished
pKZ93	TRV::Rhomboid4	Unpublished
pKZ94	TRV::Rhobmoid5	Unpublished

pKZ95	TRV::Rhobmoid6	Unpublished
pKZ96	TRV::Rhobmoid7	Unpublished
pKZ97	TRV::Presenelin1	Unpublished
pKZ98	TRV::Presenelin2	Unpublished

Table 7.2 Primer list.

Forward primer, FF; Reverse primer, RR.

Primer Name	Sequence
[KB001F]EPI1_CDS_L0_FF	gggaagacaaaatgCAGAGCCCTCAGGTTATCTCTCC
[KB001R]EPI1_CDS_L0_RR	gggaagacttaagcCTAACCCTCTTGAGGTGTAACCTT
[KB002F]NPTII_CDS_L0_FF	gggaagacaaaATGGTTGAACAAGATGGATTGCACGC
[KB002R]NPTII_CDS_L0_RR	gggaagacaaaagcTCAGAAGAACTCGTCAAGAAGGC
[KB003F]rt_SBT1.7A_FF	AATCCAACGGCCACCATTCT
[KB003R]rt_SBT1.7A_RR	TCTTGTATTGCTCCGCCGTT
[KB004F]rt_SBT1.7B_FF	AAGGTGGGGATCAAACCGTC
[KB004R]rt_SBT1.7B_RR	ATGACTTCTGCTCGTTCGCA
[KB005F]rt_SBT1.9a_FF	GACGCGATTCCACTACACGA
[KB005R]rt_SBT1.9a_RR	TTCAAGAACACAGCCGGGAA
[KB006F]rt_SBT5.2a_FF	GTTTCTGAGGCGGATGCAAG
[KB006R]rt_SBT5.2a_RR	CGGTTTGAGGAGGTTAGGGG
[KB007F]rt_SBT1.9b_FF	TCAAGCGAAAGCTCCATCGT
[KB007R]rt_SBT1.9b_RR	TATCCATCGTGTCGGCTGTG
[KB008F]seq_LBborder_FF	ggtggcaggatatattgtggtgtaaac
[KB008R]seq_RBborder_RR	gggtttacccgccaatatatcctgtca
[KB009F]gibson_35SP_FF	ttcgtgcagaagacaattgcGTCAACATGGTGGAGCAC
[KB009R]gibson_35SP_RR	tcatgtccatAATTGTAAATGTAATTGTAATGTTGTTTGTTG
[KB010F]gibson_SP_COVLC_his_FF	atttacaattATGGACATGAGAGTTCCAG
[KB010R]gibson_SP_COVLC_his_RR	tgctcaccatGTGATGGTGATGGTGATG
[KB011F]gibson_GFP_FF	tcaccatcacATGGTGAGCAAGGGCGAG
[KB011R]gibson_GFP_RR	tctgcttgacTTACTTGTACAGCTCGTCCATG
[KB012F]gibson_nost_FF	gtacaagtaaGTCAAGCAGATCGTTCAAAC
[KB012R]gibson_nost_RR	acaatgccgaattcggatccTCGATCTAGTAACATAGATGAC
[KB013F]gibson_35SP_FF	ttcgtgcagaagacaattgcGTCAACATGGTGGAGCACGACAC
[KB013R]gibson_35SP_RR	caagttccatAATTGTAAATGTAATTGTAATGTTGTTTGTTGTTTGTTGTTG
[KB014F]gibson_SP_COVHC_his_FF	atttacaattATGGAACTTGGACTTTCTTGGATTTTCC
[KB014R]gibson_SP_COVHC_his_RR	tgctcaccatGTGATGGTGATGGTGATGCCCATC
[KB015F]gibson_mCherry_FF	tcaccatcacATGGTGAGCAAGGGCGAGGAGG
[KB015R]gibson_mCherry_RR	tctgcttgacTTACTTGTACAGCTCGTCCATGCCG
[KB016F]gibson_nost_FF	gtacaagtaaGTCAAGCAGATCGTTCAAACATTTG
[KB016R]gibson_nost_RR	acaatgccgaattcggatccTCGATCTAGTAACATAGATGACAC
[KB017F]gib_35S2F5LCKDEL_FF	cgtgcagaagacaattgcGAATTCGGATCCGGAGGTCAAC
[KB017R]gib_35S2F5LCKDEL_RR	ttaaagttcatccttGCACTCGCCCCTATTG
[KB018F]gib_2F5LCTNOS_FF	GAGTGCAAGGATGAACTTTAAGCTTGTCAAGCAGATC
[KB018R]gib_2F5LCTNOS_RR	aatgccgaattcggatccTCGATCTAGTAACATAGATGACACCG
[KB019F]gib_35S2F5HCKDEL_FF	ttcgtgcagaagacaatagtTTGGAGGTCAACATGGTG
[KB019R]gib_35S2F5HCKDEL_RR	TTAAAGTTCATCCTTCTTGCCAGGGGACAAAGAAAG
[KB020F]gib_2F5HCTNOS_FF	CTGGCAAGAAGGATGAACTTTAAGCTTGTCAAGCAGA
[KB020R]gib_2F5HCTNOS_RR	acaagcaagaattcaagcttAGCGTCGATCTAGTAACATAG
[KB021F]gib_35S2F5LCNPIR_FF	ttcgtgcagaagacaattgcCCGGAGGTCAACATGGTG
[KB021R]gib_35S2F5LCNPIR_RR	AAGCTTATCTAATTGGATTGCACTCGCCCCTA
[KB022F]gib_2F5LCTNOS_FF	ATCCAATTAGATAAGCTTGTCAAGCAGATCGTTCAAAC
[KB022R]gib_2F5LCTNOS_RR	acaatgccgaattcggatccAGCGTCGATCTAGTAACATAG
[KB023F]gib_35S2F5HCNPIR_FF	cgtgcagaagacaatagtTTGGAGGTCAACATGGTG
[KB023R]gib_35S2F5HCNPIR_RR	TTATCTAATTGGATTCTTGCCAGGGGACAAAGA
[KB024F]gib_2F5HCTNOS_FF	TGGCAAGAATCCAATTAGATAAGCTTGTCAAGCAGAT

[KB024R]gib_2F5HCTNOS_RR	aagcaagaattcaagcttAGCGTCGATCTAGTAACATAG
[KB025F]gib_35S2F5LCKISIA_FF	ttcgtgcagaagacaattgcCCGGAGGTCAACATGGTG
[KB025R]gib_35S2F5LCKISIA_RR	TTAAGCAATAGAAATCTTGCACTCGCCCCTATTG
[KB026F]gib_2F5LCTNOS_FF	TGCAAGATTTCTATTGCTTAAGCTTGTCAAGCAGA
[KB026R]gib_2F5LCTNOS_RR	acaatgccgaattcggatccAGCGTCGATCTAGTAACATAG
[KB027F]gib_35S2F5HCKISIA_FF	ttcgtgcagaagacaatagtTTGGAGGTCAACATGGTG
[KB027R]gib_35S2F5HCKISIA_RR	TTAAGCAATAGAAATCTTCTTGCCAGGGGACAAAGAAAG
[KB028F]gib_2F5HCTNOS_FF	GGCAAGAAGATTTCTATTGCTTAAGCTTGTCAAGCAGA
[KB028R]gib_2F5HCTNOS_RR	acaagcaagaattcaagcttAGCGTCGATCTAGTAACATAG
[KB029F]seq_35S2F5LC_HC1_FF	CGTCGCAAAGGAGATCCTGATCTG
[KB030F]seq_35S2F5LC2_FF	CTATCCTTCGCAAGACCCTTCC
[KB031F]seq_2F5LC3_FF	GGAAGCTAAGGTGCAGTGGAAAG
[KB032F]seq_35S2F5HC2_FF	TGAAAGAATCTGGACCTCCTTTGG
[KB033F]seq_35S2F5HC3_F	CAAGAGAGGAACAGTACAACTC
[KB034F]SDM_no1_2F5_HC_FF	CCCTTTTCGGAGTTCCTTGCGCTAGGGGTCCTGTGAACG
[KB034R]SDM_no1_2F5_HC_RR	GAACTCCGAAAAGGGTGCAAGGACCCCTTCTATGAGCGC
[KB035F]SDM_no2_2F5_HC_FF	CCTGCTTCGGATGCCCTATTGCTAGGGGTCCTGTGAACG
[KB035R]SDM_no2_2F5_HC_RR	GGCATCCGAAGCAGGTGGTAGGACCCCTTCTATGAGCGC
[KB036F]SDM_2F5_HC_KDEL_FF	GAAGGATGAACTTTAAGCTTGTCAAGCAGATCGTTCAAAC
[KB036R]SDM_2F5_HC_KDEL_RR	TAAAGTTCATCCTTCTTGCCAGGGGACAAAGAAAGG
[KB037F]SDM_2F5_HC_NPIR_FF	GAATCCAATTAGATAAGCTTGTCAAGCAGATCGTTCAAAC
[KB037R]SDM_2F5_HC_NPIR_RR	TATCTAATTGGATTCTTGCCAGGGGACAAAGAAAGG
[KB038F]SDM_2F5_HC_KISIA_FF	AGATTTCTATTGCTTAAGCTTGTCAAGCAGATCGTTCAAAC
[KB038R]SDM_2F5_HC_KISIA_RR	AAGCAATAGAAATCTTCTTGCCAGGGGACAAAGAAAGG
[KB040F]35S_HC_hlinker_FF	ttcgtgcagaagacaatagtGTCAACATGGTGGAGCACGACACTCTGGTC
[KB040R]35S_HC_hlinker_RR	ctcctccagaTCCTCCTCCCTTGCCAGGGGACAAAGAAAG
[KB041F]hlinker_mScarlet_FF	gggaggaggaTCTGGAGGAGGAATGGTGAGCAAGGGCGAG
[KB041R]hlinker_mScarlet_RR	gacaagcttaCTTGTACAGCTCGTCCATGCCGCCGGTGGA
[KB042F]TAA_nost_FF	gctgtacaagTAAGCTTGTCAAGCAGATCGTTCAAACATTTG
[KB042R]TAA_nost_RR	acaagcaagaattcaagcttTCGATCTAGTAACATAGATGACACCGCGCG
[KB043F]BIP_2F5LC_FF	cggatgtttatttgcgttgtcctctgcaatagaagaggctacgaagttaGGTGCATTACAATTAACACAATCTCCC
[KB043R]BIP_2F5LC_RR	aagaagatgatcgccaacacaacggtactgttagctccaaacgagcgagccatTGTATCGATAATTGTAAATGT AAT
[KB044F]BIP_2F5HC_FF	tcttcggatgtttatttgcgttgtcctctgcaatagaagaggctacgaagttaAGGATCACCCTGAAAGAATCTG
[KB044R]BIP_2F5HC_RR	agatgatcgccaacacaacggtactgttagctccaaacgagcgagccatTGTATCGATAATTGTAAATGTAAT
[KB045F]RT_SBT5.2_FF	GGATTCGCGGCACGTTTATC
[KB045R]RT_SBT5.2_RR	GGTTAGGGGTGTTGTACGCA
[KB046F]hifi_2F5HC_link_FF	GCTTGTCAAGCAGATCGTTCAAACATTTGG
[KB046R]hifi_2F5HC_link_RR	TCCTCCTCCAGATCCTCCTCCCTTGCCAGGGGACAAAG
[KB047F]hifi_link_mScarlet_FF	gggaggaggatctggaggaggaATGGTGAGCAAGGGCGAGGCAGTGA
[KB047R]hifi_link_mScarlet_RR	ttgaacgatctgcttgacaagcAAGCTTACTTGTACAGCTCGTCCATGCC
[KB048F]hifi_2F5LC_link_FF	gctgtacaagtaaGCTTGTCAAGCAGATCGTTCAAACATTTGGC
[KB048R]hifi_2F5LC_eGFP_RR	TCCTCCTCCAGATCCTCCTCCGCACTCGCCCCTATTGAAAGACTTAGTC
[KB049F]hifi_link_mScarlet_FF	GGAGGAGGATCTGGAGGAGGAATGGTGAGCAAGGGCGAGGAGCTGTTC
[KB049R]hifi_link_eGFP_RR	TTATTGCCAAATGTTTGAACGATCTGCTTGACAAGCTTACTTGTACAGCTCGTCCATGCCGA GAGT
[KB050F]2F5_HC_SDM3(FG)_FF	CACCCTTGCTGGAGTTCCTATTGCTAGGGGTCCT
[KB050R]2F5_HC_SDM3(FG)_RR	ACTCCAGCAAGGGTGGTAGGACCCCT
[KB051F]colPCR_LB_RB_FF	GGCTGGTGGCAGGATATATT
[KB051R]colPCR_LB_RB_RR	TCTCTTAGGTTTACCCGCCA
[KB052F]2F5_HC_SDM3_FF	CACCCTTGCTGGAGTTCCTATTGCTAGGGGTCCT
[KB052R]2F5_HC_SDM3_RR	ACTCCAGCAAGGGTGGTAGGACCCCT
[KB053F]2F5_HC_SDM4_FF	CACCCTTGATGGAGTTCCTATTGCTAGGGGTCCT
[KB053R]2F5_HC_SDM4_RR	ACTCCATCAAGGGTGGTAGGACCCCT
[KB054F]2F5_HC_SDM5_FF	CACCCTTCGTGGAGTTCCTATTGCTAGGGGTCCT
[KB054R]2F5_HC_SDM5_RR	ACTCCACGAAGGGTGGTAGGACCCCT
[KB055F]COVA_HC_SDM1_FF	CGCTGGCGACGATGCTTACATCAAGCTTATCAGAGGTGGCC
[KB055R]COVA_HC_SDM1_RR	GCATCGTCGCCAGCGTAACCAGTATCCTTAGCGCAG
[KB056F]2F5_HC_ssDNA_link_FF	GAAGTCCCTTTCTTTGTCCCCTGGCAAGGGAGGAGGATCTGGAGGAGGAATGGTGAGCAAGG GCGAGGCAGTGATC
[KB056F]2F5_LC_ssDNA_link_FF	GACTAAGTCTTTCAATAGGGGCGAGTGCGGAGGAGGATCTGGAGGAGGAATGGTGAGCAAG GGCGAGGAGCTGTTC

7.4 Agroinfiltration of *Nicotiana benthamiana*

Agrobacterium cultures were resuspended in infiltration buffer (10 mM $MgCl_2$, 10 mM MES-K/ pH 5.7 with KOH, with filter-sterilized 100 µM acetosyringone added immediately before use) to reach a final OD_{600} of 0.3-0.5. In cases where multiple T-DNA vectors were used, *agrobacteria* cultures were mixed in ratio 1:1. Leaves of approximately 4-week-old *N. benthamiana* were used for infiltration, while the same leaf was infiltrated for each technical replicate to achieve the same developmental stage. After infiltration, the plants were grown for 5 days post-infiltration (dpi) in a growth chamber at 22-23 °C, 16 hr light/ 8hr dark, at high humidity and 80-120 µmol/m^2s light intensity, and 1 cm diameter leaf discs were harvested for analyses. For *in vivo* experiments six 1 cm diameter leaf discs were pooled per technical replicate, resulting in six biological replicates from three individual technical replicates (n=18).

7.5 Virus-induced gene silencing (VIGS)

The TRV1 and TRV2 plasmids were transformed into *Agrobacterium* strain GV3101 and mixed in a 1:1 ratio to a final OD_{600} of 0.5 for agroinfiltration. Two weeks old *N. benthamiana* were agroinfiltrated with *TRV::NbSBT*, *TRV::Intracellular_protesases* *TRV::GFP*, and 3 weeks after agroinfiltration successful silencing was assessed by checking for bleached leaves in *TRV::PDS* plants.

7.6 Generation of *sbt* mutants

N. benthamiana LAB was transformed by CRISPR-Cas9 editing to generate, *sbt* mutants by Biogle (Hangzhou, China). Primary transformants were selected for carrying mutations

in the target genes by sequencing PCR products generated from genomic DNA, and T2 plants were screened for homozygosity of the mutant alleles using the same sequencing primers. The screening was carried out by Dr Shi-Jian Song (Plant Chemetics Lab, Oxford).

7.7 Total and apoplastic fluid extraction

All samples were harvested 5 days post infiltration. For total extracts, six leaf discs (1 cm diameter) were harvested and ground to a fine powder using liquid nitrogen, and 150 µL phosphate-buffered saline (PBS) supplemented with Halt™ Protease Inhibitor Cocktail (Thermo, 78430) was added. Samples were then centrifuged for 25 minutes at 4°C and 13,000 x *g* and the supernatant was transferred into a new tube with loading dye for protein gel loading. For apoplastic fluids, the respective six leaves following leaf disc harvest were vacuum infiltrated with Milli-Q water. The leaf surfaces were then dried with tissue paper, and centrifuged in a 25 mL syringe hanging in a 50 mL tube at 1000 x *g* for 25 minutes at 4 °C. Aliquots of apoplastic fluids were collected from the 50 mL tube and were flash-frozen and stored at -20 °C until further use.

7.8 Antibody labelling

The 2F5 antibody was provided by Polynum Scientific (anti-gp41; AB001). IgGs were labelled using an amine-reactive dye (DyLight® 488 or 650 NHS Ester; Thermo, 46402) by diluting approximately 0.06 mg IgG in 100 µL PBS (pH 7.4) and adding 0.2 µg dye. The mix was incubated for 1 hour in the dark at room temperature. Excess dye was removed by loading the labelling mix into a column (Amicon® Ultra 0.5 centrifugal filter devices 3K; Merck, UFC500324) and centrifuged for 8 minutes at 10,000 x *g*. After loading another

100 µL PBS, the column was centrifuged for 8 minutes at 10,000 x *g*. The above step was repeated, the column was transferred upside-down into a new tube and centrifuged for 5 minutes. The labelled antibody was kept in aluminium foil at 2-8 °C and used within a month.

7.9 *In vitro* degradation assays

Fluorescently labelled 2F5 antibody was incubated in apoplastic fluid from *N. benthamiana* leaves. Samples were taken at zero and six-hour time points. The reaction was stopped by adding 4x loading dye with dithiothreitol (0.2 M Tris pH 6.8, 8% w/v SDS, 40% w/v glycerol, 0.4% w/v bromophenol blue, 0.6 M DTT; Thermo, R0862). The samples were then incubated at 95 °C for 5 minutes before sodium dodecyl-sulfate polyacrylamide gel electrophoresis (SDS-PAGE). The effect of protease inhibitors on the degradation of 2F5 in wild-type apoplastic fluid was investigated by pre-incubation for 30 minutes using chemical protease inhibitors 100 µM E-64 (Merck, E3132) or 1 mM phenylmethylsulfonyl fluoride (PMSF; Merck, 10837091001). For negative controls, the samples were treated with the same volume of dimethyl sulfoxide (DMSO; Merck, D8418).

7.10 SDS-PAGE and western blotting

The samples were incubated at 95 °C for 5 minutes before loading and separated at 170V in Invitrogen Novex vertical gel tanks. The Amersham® Typhoon (Cy2: 488 nm for labelled antibody, Cy5: 685 nm for ladder) was used to measure fluorescence. The proteins were also visualised by total protein staining with Instant Blue® Coomassie Protein Stain (Abcam, ab119211) or were transferred onto a polyvinylidene difluoride

(PVDF, BioRad) membrane for western blotting. For Western blot analysis, proteins were transferred to PVDF membranes using BioRad Trans-blot Turbo® according to the manufacturer's instructions (BioRad Kit, 1704275). Blots were blocked for 2 hours or overnight at 4°C with 5% (w/v) skim milk in PBS-T (PBS tablets; Merck, 524650, 0.1% Tween-20; Merck, P1379). The membrane was incubated with the secondary antibodies in 5% (w/v) skim milk for 2 hours at room temperature or overnight at 4°C (**Table 7.3**). Blots were washed twice with PBS-T for 5 minutes, developed using SuperSignal™ West Pico PLUS Chemiluminescent Substrate (Thermo 34580), and visualised using the ImageQuant® LAS-4000 imager. Image data were quantified using the open-source software ImageJ, and background values were subtracted based on control images.

Table 7.3 Antibody list.

All secondary antibodies were conjugated with HRP, horse radish peroxidase.

Antibody Name	Provider	Dilution
Goat anti-Human IgG (H+L) Secondary Antibody	Thermo Fisher	1:3000
Goat anti-Human Kappa Light Chain Secondary Antibody	Thermo Fisher	1:3000
Goat anti-Human IgG (Gamma chain) Cross-Adsorbed Secondary Antibody	Thermo Fisher	1:3000
Goat anti-GFP antibody	Abcam	1:3000
Rabbit anti-RFP antibody	Abcam	1:3000

7.11 Mild stripping of PVDF membrane for restaining

The membrane was incubated for 10 minutes in mild stripping buffer (for 200mL: 3g glycine, 0.2g SDS, 2ml Tween-20, pH 2.2), then the buffer was replaced with new buffer and incubated again for 10 minutes. The stripping buffer was then discarded and the membrane was incubated twice with PBS buffer for 10 minutes and twice with PBS-T buffer for 5 minutes. The membrane was checked for any signal using the ImageQuant® LAS-4000 imager. After the stripping being successful, the membrane blots were blocked

overnight with 5% (w/v) skim milk in PBS-T (PBS buffer supplemented with 0.1% (v/v) Tween-20) before incubating with an antibody for detection.

7.12 Activity-based protein profiling (ABPP)

ABPP was conducted for the *sbt5.2* knockout plants, using the fluorophosphonate (FP) TAMRA probe for targeting Serine hydrolases as described previously (Jutras et al., 2019). Briefly, 48 µL of apoplastic fluids, were adjusted to a solution containing 50 mM sodium acetate (NaAc) at pH 5 and 5 mM dithiothreitol (DTT). The mixture was then incubated for 1 hour with 0.5 µM FP-TAMRA (Thermo, 88318). To stop activity-based labelling, 1 mL of cold acetone was added. The samples were then centrifuged, the supernatant was removed, and the proteins were resuspended in a gel-loading buffer. These protein samples were heated and separated on a 12% SDS-PAGE at reducing conditions. SDS-PAGE gels were scanned for in-gel fluorescence using a Typhoon scanner with Cy3: 550 nm settings. Four biological replicates were used in each case for analysis (n=4).

7.13 Quenched IgG-hinge peptide assay

A quenched peptide that corresponds to a region upstream of the hinge region of IgGs (sequence TKVDKKVEP; GenScript) with DABCYL and Glu(EDANS) modifications was incubated at 10µM with 95µl apoplastic fluid in a black 96-well plate, and fluorescence was monitored for 15 minutes at 30-60 seconds intervals using Tecan plate reader C500 (excitation: 335nm, emission: 493nm; **Figure 7.2**).

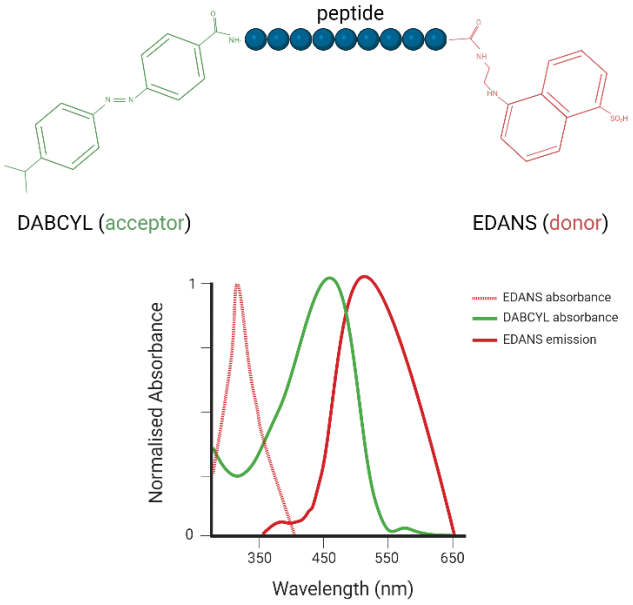

Figure 7.2 Quenched peptide design and absorbance profile.

7.14 Estimating secretion efficiency from western blots

Total leaf extracts (TE) samples derived from six individual leaf discs pooled together and mixed with 150 µL PBS buffer supplemented with protease inhibitor cocktail. Apoplastic fluids (AF) samples derived from pooling the same six leaves, following leaf disc removal used for TE, leading to 400 µl sample volume. The leaf areas were calculated using ImageJ (Polygon Tool and Analyze>Measure), converted to Total Leaf Area (cm^2) and normalised for the Loaded Fraction which represents the sample used for SDS-PAGE loading as follows:

$$Total\ Leaf\ Area\ (AF) = \frac{\sum whole\ leaf\ area - 6\ x\ leaf\ disc\ area}{area\ of\ 1cm^2}$$

$$Total\ Leaf\ Area\ (TE) = \frac{6\ x\ leaf\ disc\ area}{area\ of\ 1cm^2}$$

$$Loaded\ Fraction\ (AF\ or\ TE) = \frac{Total\ Leaf\ Area\ (AF\ or\ TE)}{percentage\ of\ loaded\ sample\ (\%;\ AF\ or\ TE)}$$

Western blot band intensities were calculated in ImageJ (Analyze>Gels>Plot Lanes) by calculating the area of the grey value distribution. The raw intensities were normalised to correspond to the respective normalised Loaded Fraction as follows:

$$\textit{Normalised intensities (AF or TE)} = \frac{Raw\ intensity\ (AF\ or\ TE)}{Loaded\ Fraction\ (AF\ or\ TE)}$$

Total leaf extracts contain the total protein content found in samples, so a secreted protein will appear in both the TE and the AF samples, with most of the protein being represented in AF samples as follows:

$$\textit{Percentage of secretion (\%)} = \frac{Normalised\ intensities\ (AF)}{Normalised\ intensities\ (TE)}\ x\ 100$$

7.15 RNA extraction

Isolation of total RNA was performed using the TRIzol® reagent (Thermo, 15596026).

Cell lysis and separation of phases – *N. benthamiana* leaves were ground to a fine powder and 50-100mg was added into microcentrifuge tubes along with 1ml of cold TRIzol reagent for each sample. After rigorous mixing the tubes were incubated at room temperature for 5 minutes. Next, 200µL of chloroform were added, tubes were stored at room temperature for 2-3 minutes and centrifuged for 15 minutes at 12,000g at 4°C. The aqueous phase containing the RNA was transferred to a new tube.

Isolation of RNA - Into the aqueous phase, 500µl of isopropanol were added and tubes were stored at room temperature for 10 minutes. Then they were centrifuged for 10 minutes at 12,000g at 4°C. The supernatant was discarded and the white gel-like pellet

was resuspended in 1mL of 75% ethanol. After mixing the tubes briefly, they were centrifuged for 5 minutes at 7,500g at 4°C. The supernatant was discarded and the RNA pellet was air dried for 10 minutes. The pellet was resuspended in 50µL sterile dH_2O and incubated in a water bath at 60°C for 15 minutes, before being stored at -70°C.

DNase treatment - Removal of genomic DNA from RNA was performed using DNase I and RiboLock RNase Inhibitor (Thermo) by adding the following components to an RNase-free tube:

Total RNA of each sample	1µg
10x reaction buffer with $MgCl_2$	1µL
DNase I	1µL
RiboLock RNase Inhibitor	0.5µL
Sterile dH_2O	to 10µL
Total volume	**10µL**

The above reaction was run according to the following program:

37°C	30 minutes*
65°C	10 minutes

*Note that the program was paused, tubes were immediately transferred on ice and 1µl of 50mM EDTA was added. The program continued to reach 65°C, then was paused again and tubes were placed back into the thermal cycler.

7.16 Semi-quantitative RT-PCR

Following RNA extraction and DNase treatment, reverse transcriptase PCR was conducted to estimate gene silencing in knock-down plants generated by VIGS. PCRBIO

1-Step Go RT-PCR Kit (PCR Biosystems, PB10.53-10) was used for one-step cDNA synthesis and PCR in a single tube:

Template RNA	1µg
2x 1-Step Go mix	12.5µL
20x RTase Go	1.25µL
Forward primer (10µM)	1µL
Reverse primer (10µM)	1µL
Sterile dH_2O	to 10µL
Total volume	**25µL**

The above reaction was run according to the following program following by running the samples in a 1% w/v agarose gel:

45°C	20 minutes	x1
95°C	2 minutes	x1
95°C 55-65°C 72°C	10 seconds 10 seconds 15 seconds per kb	x40

7.17 Protein purification

Small-scale protein purification from *N. benthamiana* leaves was done using either Protein A columns (Thermo, 20356), or Protein A magnetic beads (Thermo, 88846). For both purification methods 10-30g of infiltrated leaf tissue was used, depending on application. The leaves were ground and immediately mixed with 3:1 volume of cold extraction buffer (PBS 1X, 10mg/mL sodium ascorbate, 1mM EDTA, 2µM PMSF; pH 6.0)

and thoroughly mixed using a blender or vortex. The extracts were then filtered using Miracloth into 50mL tubes. The sample tubes were centrifuged at 10,000rpm at 4°C before finally being filtered using a 0.22µM filter.

7.17.1 Purification using Protein A columns

Column and buffers were equilibrated at room temperature. After opening the top cap of the column, the storage solution was discarded and the column was washed with 5mL of binding buffer (PBS 1X; pH 7.2-8.0). Next, each filtered sample was loaded into different columns and let drain. The column was washed with 15mL binding buffer and flowthroughs were collected if needed. Antibodies were eluted with 5mL elution buffer (0.1M glycine, 0.2M L-arginine; pH 3.0) in 500µL fractions, and 50µL neutralisation buffer (1M Tris pH 8.5-9.0) were immediately added to each fraction. The fractions with the highest absorbance (280nm) were pooled and used for downstream purposes. Used columns were regenerated by washing with 12mL elution buffer following by 5mL sodium azide 0.02% (w/v) and stored in sodium azide at 4°C until next use.

7.17.2 Purification using protein A magnetic beads

Dynabeads were resuspended and 50µL were transferred into clean tubes for each sample. The tubes were placed on the magnet rack to remove the storage solution. Next, each filtered sample was added into the tube, using approximately 1mL of crude extract. The tube containing the beads and the sample was incubated at room temperature for 30 minutes to an hour, or alternatively overnight at 4°C while rotating. The tube was then placed back to the magnet and the sample was removed. Then, the beads were washed thrice using 200µL 1x PBS pH 7.2, and once with 100µL 1x PBS, transferring the latter

into a clean tube. After removing the supernatant, the antibodies were eluted in 20µL elution buffer (50mM glycine pH 2.8), followed by addition of 20µL 1M Tris pH 7.5.

Where needed, buffer exchange from elution buffer to 1x PBS was done using centrifugal device (Amicon® Ultra 0.5 centrifugal filter devices 3K; Merck, UFC500324) or 10K dialysis cassettes (Thermo, 66385) according to the manufacturers' guidelines.

7.18 Protein concentration calculation

For estimating protein concentration, Bradford assay was used. In transparent 96-well plates, 100µL Bradford Reagent (Thermo, 23238) was incubated with the samples (5µL) or bovine serum albumin (BSA) for creating a standard curve (BSA concentrations in mg/ml: 1, 0.8, 0.7, 0.5, 0.4, 0.2, 0.1, 0). After incubation at RT for 5 minutes, the plates were read for absorbance at 595nm (Infinite M200, TECAN).

7.19 Quantitative enzyme-linked immunosorbent assay (ELISA)

For quantification of antigen-binding IgGs, ELISA was performed using total extracts as described previously with some modifications (Jiang et al., 2019, 2020). The 96-well microtiter plates (Nunc-Immuno, MaxiSorp, Thermo Fisher) were coated with 200µL 15ng/well antigen and incubated overnight at 4°C while shaking (coating buffer: 0.1 M carbonate/bicarbonate buffer; pH 9.6). Then, the coating buffer was discarded and wells were washed with 200µL PBST (1X PBS/0.05% Tween-20), following by 200µL sterile water. Blocking buffer (PBST, 3% skimmed milk; 200µL/well) was added and the plate was incubated for 2 hours at room temperature or overnight at 4°C while shaking. After

pouring the blocking buffer the wells were washed with PBST and sterile water once. Previously isolated total extracts were prepared by mixing with 1:3 (w/v) blocking buffer. Next, these samples were loaded in wells in triplicates following 3 serial dilutions (1:4, 1:20, 1:100), and left shaking for 2 hours. The wells were washed 3 times with PBST and sterile water. The secondary antibody (whole molecule anti-IgG-HRP; 1:5000) was added and incubated for 2 hours while shaking. The wells were washed 3 times with PBST and sterile water before adding 50µL of 3,3',5,5'-tetramethylbenzidine substrate (1-Step-TMB, Thermo). Within 5 minutes the colour of wells changed to blue and the reaction was stopped by adding another 50µL of 0.18M sulfuric acid with colour changed to yellow. Immediately after the absorbance at 450nm was measured. All measurements were performed in triplicates.

ELISA data analysis was carried out in GraphPad Prism v10.3.1, by interpolating the sample data according to the sigmoidal standard curve. Quantifications based on ELISA were performed using a four-parameter logistic interpolation (4PL), a standard curve-fitting method commonly used for sigmoidal dose-response data. A standard curve was generated by plotting known concentrations of pure IgGs against the corresponding absorbance values. Sample concentrations were then calculated by interpolating their absorbance values onto the fitted 4PL curve. The control IgG used for normalisation was either commercially available or purified from *N. benthamiana* leaves.

Table 7.4 Antigen list.

Antigen Name	**Provider**
Recombinant HIV1 gp41 protein	Abcam
SARS-CoV-2 Spike Protein (RBD) (aa319-541) His-tag	Thermo Fisher
Aequorea victoria GFP His-tag	Thermo Fisher

7.20 Fluorescent protein leaf imaging

To scan for leaf fluorescence the Amersham® Typhoon (Cy2: 488 nm for GFP, Cy3: 561 nm) was used. Measurements of fluorescent intensity were conducted in ImageJ. Each .tiff file was converted to 8-bit from Image>Type, Process>Find Edges, and 0-50 was adjusted for better overall contrast (maximum cursor to 0-50). The infiltrated areas were selected using the Polygon tool and measurements were taken as mean grey values normalised for surface area (Mean grey values = Intensity Density/Area). Images were overlayed by Image>Lookup Tables>Green and the Scale bar was added by Analyze>Tools>Scale Bar.

7.21 Confocal microscopy and co-localisation intensity analysis

Confocal microscopy imaging was conducted using a Zeiss LSM 880 Airyscan microscope on ZEN 2.3 SP1 software using a 40x 1.2NA water immersion lense. Three separate channels were set up for acquisition, using the 488, 561 and 633 nm laser lines with different detectors for GFP, RFP/mScarlet and chlorophyl autofluorescence, respectively, using line scanning mode. The pinhole for each channel was set to 1 airy unit (AU). Images acquired were 512x512 pixels. Gain and laser intensity settings were kept consistent throughout the experiment.

Co-localisation analysis was carried out using Fiji/ImageJ with the bioformats plugins (Bolte & Cordelières, 2006; Schindelin et al., 2012). Pixel intensity scatter plot graphs were generated using the co-localisation threshold option under the ''Analyze'' menu. Pearson's and Manders M1 and M2 co-localisation co-efficients were calculated using the coloc2 plugin for the ''Analyze'' menu.

7.22 Data visualisation and statistical analyses

SnapGene, Benchling and NEBuilder® were used for designing DNA constructs, sequence alignments, and cloning strategies. Protein structure predictions were performed using AlphaFold on ColabFold (Jumper et al., 2021; Mirdita et al., 2022), and protein structures were customised on ChimeraX v1.8 (Meng et al., 2023). Known protein structures were downloaded from Protein Data Bank (Berman et al., 2000). Multiple sequence alignments were performed on EMBL-EBI website using Clustal Omega (Madeira et al., 2024), while reverse translation on Expasy. Protein localisation probabilities were analysed on SignalP/DeepLoc (Teufel et al., 2022; Thumuluri et al., 2022). Protease and protease inhibitor information were retrieved from MEROPS database (Rawlings et al., 2012). Western blot or fluorescence images were analysed using ImageJ/Fiji (Schindelin et al., 2012). Figures and graphical representations were created with Adobe Illustrator and BioRender. GraphPad Prism v10.3.1 and custom Python scripts on Jupyter notebook were used for statistical analyses and graph visualisation (Kluyver et al., 2016).

References

Beritza, K., Buscaill, P., Song, S.-J., Jutras, P. V, Huang, J., Mach, L., Dong, S., & Van Der Hoorn, R. A. L. (2024). *SBT5.2s are the major active extracellular subtilases processing IgG antibody 2F5 in the Nicotiana benthamiana apoplast*.

Berman, H. M., Westbrook, J., Feng, Z., Gilliland, G., Bhat, T. N., Weissig, H., Shindyalov, I. N., & Bourne, P. E. (2000). The Protein Data Bank. In *Nucleic Acids Research* (Vol. 28, Issue 1). http://www.rcsb.org/pdb/status.html

Bolte, S., & Cordelières, F. P. (2006). A guided tour into subcellular colocalization analysis in light microscopy. In *Journal of Microscopy* (Vol. 224, Issue 3, pp. 213–232). Blackwell Publishing Ltd. https://doi.org/10.1111/j.1365-2818.2006.01706.x

Engler, C., Youles, M., Gruetzner, R., Ehnert, T.-M., Werner, S., Jones, J. D. G., Patron, N. J., & Marillonnet, S. (2014). A Golden Gate Modular Cloning Toolbox for Plants. *ACS Synthetic Biology*, *3*(11), 839–843. https://doi.org/10.1021/sb4001504

Grosse-Holz, F., Madeira, L., Zahid, M. A., Songer, M., Kourelis, J., Fesenko, M., Ninck, S., Kaschani, F., Kaiser, M., & van der Hoorn, R. A. L. (2018). Three unrelated protease inhibitors enhance accumulation of pharmaceutical recombinant proteins in Nicotiana benthamiana. *Plant Biotechnology Journal*, *16*(10), 1797–1810. https://doi.org/10.1111/pbi.12916

Jiang, M. C., Hu, C. C., Hsu, W. L., Hsu, T. L., Lin, N. S., & Hsu, Y. H. (2020). Fusion of a Novel Native Signal Peptide Enhanced the Secretion and Solubility of Bioactive Human Interferon Gamma Glycoproteins in Nicotiana benthamiana Using the Bamboo Mosaic Virus-Based Expression System. *Frontiers in Plant Science*, *11*. https://doi.org/10.3389/fpls.2020.594758

Jiang, M. C., Hu, C. C., Lin, N. S., & Hsu, Y. H. (2019). Production of human IFNγ protein in nicotiana benthamiana plant through an enhanced expression system based on bamboo mosaic virus. *Viruses*, *11*(6). https://doi.org/10.3390/v11060509

Jumper, J., Evans, R., Pritzel, A., Green, T., Figurnov, M., Ronneberger, O., Tunyasuvunakool, K., Bates, R., Žídek, A., Potapenko, A., Bridgland, A., Meyer, C., Kohl, S. A. A., Ballard, A. J., Cowie, A., Romera-Paredes, B., Nikolov, S., Jain, R., Adler, J., … Hassabis, D. (2021). Highly accurate protein structure prediction with AlphaFold. *Nature*, *596*(7873), 583–589. https://doi.org/10.1038/s41586-021-03819-2

Jutras, P. V., Grosse-Holz, F., Kaschani, F., Kaiser, M., Michaud, D., & van der Hoorn, R. A. L. (2019). Activity-based proteomics reveals nine target proteases for the recombinant protein-stabilizing inhibitor SlCYS8 in Nicotiana benthamiana. *Plant Biotechnology Journal*, *17*(8), 1670–1678. https://doi.org/10.1111/pbi.13092

Jutras, P. V., Soldan, R., Dodds, I., Schuster, M., Preston, G. M., & van der Hoorn, R. A. L. (2021). AgroLux: bioluminescent Agrobacterium to improve molecular pharming and study plant immunity. *Plant Journal*, *108*(2), 600–612. https://doi.org/10.1111/tpj.15454

Kluyver, T., Ragan-Kelley, B., Pérez, F., Granger, B., Bussonnier, M., Frederic, J., Kelley, K., Hamrick, J., Grout, J., Corlay, S., Ivanov, P., Avila, D., Abdalla, S., & Willing, C. (2016). Jupyter Notebooks—a publishing format for reproducible computational workflows. *Positioning and Power in Academic Publishing: Players, Agents and Agendas - Proceedings of the 20th International*

Conference on Electronic Publishing, ELPUB 2016, 87–90. https://doi.org/10.3233/978-1-61499-649-1-87

Liu, Y., Schiff, M., & Dinesh-Kumar, S. P. (2002). Virus-induced gene silencing in tomato. *Plant Journal*, *31*(6), 777–786. https://doi.org/10.1046/j.1365-313X.2002.01394.x

Madeira, F., Madhusoodanan, N., Lee, J., Eusebi, A., Niewielska, A., Tivey, A. R. N., Lopez, R., & Butcher, S. (2024). The EMBL-EBI Job Dispatcher sequence analysis tools framework in 2024. *Nucleic Acids Research*, *52*(W1), W521–W525. https://doi.org/10.1093/nar/gkae241

Marillonnet, S., & Werner, S. (2015). *Assembly of Multigene Constructs Using Golden Gate Cloning BT - Glyco-Engineering: Methods and Protocols* (A. Castilho, Ed.; pp. 269–284). Springer New York. https://doi.org/10.1007/978-1-4939-2760-9_19

Meng, E. C., Goddard, T. D., Pettersen, E. F., Couch, G. S., Pearson, Z. J., Morris, J. H., & Ferrin, T. E. (2023). UCSF ChimeraX: Tools for structure building and analysis. *Protein Science*, *32*(11). https://doi.org/10.1002/pro.4792

Mirdita, M., Schütze, K., Moriwaki, Y., Heo, L., Ovchinnikov, S., & Steinegger, M. (2022). ColabFold: making protein folding accessible to all. *Nature Methods*, *19*(6), 679–682. https://doi.org/10.1038/s41592-022-01488-1

Ranawaka, B., An, J., Lorenc, M. T., Jung, H., Sulli, M., Aprea, G., Roden, S., Llaca, V., Hayashi, S., Asadyar, L., LeBlanc, Z., Ahmed, Z., Naim, F., de Campos, S. B., Cooper, T., de Felippes, F. F., Dong, P., Zhong, S., Garcia-Carpintero, V., … Waterhouse, P. M. (2023). A multi-omic Nicotiana benthamiana resource for fundamental research and biotechnology. *Nature Plants*, *9*(9), 1558–1571. https://doi.org/10.1038/s41477-023-01489-8

Rawlings, N. D., Barrett, A. J., & Bateman, A. (2012). MEROPS: The database of proteolytic enzymes, their substrates and inhibitors. *Nucleic Acids Research*, *40*(D1). https://doi.org/10.1093/nar/gkr987

Sam Mugford, S. H. (2018). Bounce PCR. In *protocols.io dx.doi.org/10.17504/protocols.io.vhge*.

Samalova, M., Fricker, M., & Moore, I. (2006). Ratiometric fluorescence-imaging assays of plant membrane traffic using polyproteins. *Traffic*, *7*(12), 1701–1723. https://doi.org/10.1111/j.1600-0854.2006.00502.x

Sandor, A., Samalova, M., Brandizzi, F., Kriechbaumer, V., Moore, I., Fricker, M. D., & Sweetlove, L. J. (2024). Characterization of intracellular membrane structures derived from a massive expansion of endoplasmic reticulum (ER) membrane due to synthetic ER-membrane-resident polyproteins. *Journal of Experimental Botany*, *75*(1), 45–59. https://doi.org/10.1093/jxb/erad364

Schindelin, J., Arganda-Carreras, I., Frise, E., Kaynig, V., Longair, M., Pietzsch, T., Preibisch, S., Rueden, C., Saalfeld, S., Schmid, B., Tinevez, J. Y., White, D. J., Hartenstein, V., Eliceiri, K., Tomancak, P., & Cardona, A. (2012). Fiji: An open-source platform for biological-image analysis. In *Nature Methods* (Vol. 9, Issue 7, pp. 676–682). https://doi.org/10.1038/nmeth.2019

Teufel, F., Almagro Armenteros, J. J., Johansen, A. R., Gíslason, M. H., Pihl, S. I., Tsirigos, K. D., Winther, O., Brunak, S., von Heijne, G., & Nielsen, H. (2022). SignalP 6.0 predicts all five types of signal peptides using protein language models. *Nature Biotechnology*, *40*(7), 1023–1025. https://doi.org/10.1038/s41587-021-01156-3

Thumuluri, V., Almagro Armenteros, J. J., Johansen, A. R., Nielsen, H., & Winther, O. (2022). DeepLoc 2.0: multi-label subcellular localization prediction using protein language models. *Nucleic Acids Research*, *50*(W1), W228–W234. https://doi.org/10.1093/nar/gkac278

Weber, E., Engler, C., Gruetzner, R., Werner, S., & Marillonnet, S. (2011). A Modular Cloning System for Standardized Assembly of Multigene Constructs. *PLOS ONE*, *6*(2), 1–11. https://doi.org/10.1371/journal.pone.0016765

Werner, S., Engler, C., Weber, E., Gruetzner, R., & Marillonnet, S. (2012). Fast track assembly of multigene constructs using Golden Gate cloning and the MoClo system. *Bioengineered*, *3*(1), 38–43. https://doi.org/10.4161/bbug.3.1.18223

Appendices

Appendix A – Coding (CDS) and amino acid (aa) sequence of IgGs or fluorescent proteins used for transient expression

The N-terminal signal peptide of Nicotiana tabacum pathogenesis-related protein PR1a (green) was used, followed by a glycine linker (orange), the LC/HC of 2F5 and a stop codon (red). Underlined is the heptapeptide linker GGGSGGG while in bold are eGFP or mScarlet C-terminal sequences.

>PR1a_2F5_LC_CDS
ATGGGATTTGTTCTCTTTTCACAATTGCCTTCATTTCTTCTTGTCTCTACACTTCTCTTATTCCTAGTAATATCCCACTCTTGCCGTGCAGGTG
CATTACAATTAACACAATCTCCCTCCTCACTTAGTGCCTCCGTGGGGGATCGCATAACAATAACATGTAGAGCATCTCAGGGAGTGACCTCCGC
ACTTGCATGGTATCGACAAAAGCCAGGATCCCCCCCCTCAGTTGTTAATTTATGACGCATCAAGTTTGGAGTCAGGCGTGCCTTCCAGATTTTCG
GTTCCGGTTCAGGAACTGAATTTACACTGACAATAAGTACTCTAAGGCCAGAGGACTTTGCCACTTATTACTGTCAACAACTACATTTTTACCC
CCACACGTTCGGAGGTGGAACAAGGGTCGATGTACGTAGGACTGTTGCTGCTCCATCTGTTTTCATCTTCCCACCATCTGATGAGCAGCTCAAG
TCTGGAACTGCTTCTGTTGTTTGCCTCCTCAACAATTTCTACCCAAGGGAAGCTAAGGTGCAGTGGAAAGTTGATAATGCTCTCCAGTCCGGAA
ACTCCCAAGAATCTGTTACTGAGCAGGATTCCAAGGATTCTACTTACTCCCTCTCCTCAACTCTCACTCTCTCTAAGGCTGATTACGAGAAGCA
CAAGGTTTACGCTTGCGAAGTTACTCACCAGGGACTTTCTTCACCAGTGACTAAGTCTTTCAATAGGGGCGAGTGCTAA

>PR1a_2F5_LC_aa
MGFVLFSQLPSFLLVSTLLLFLVISHSCRAGALQLTQSPSSLSASVGDRITITCRASQGVTSALAWYRQKPGSPPQLLIYDASSLESGVPSRFS
GSGSGTEFTLTISTLRPEDFATYYCQQLHFYPHTFGGGTRVDVRRTVAAPSVFIFPPSDEQLKSGTASVVCLLNNFYPREAKVQWKVDNALQSG
NSQESVTEQDSKDSTYSLSSTLTLSKADYEKHKVYACEVTHQGLSSPVTKSFNRGEC

>PR1a_2F5_HC_CDS
ATGGGATTTGTTCTCTTTTCACAATTGCCTTCATTTCTTCTTGTCTCTACACTTCTCTTATTCCTAGTAATATCCCACTCTTGCCGTGCAGGTA
GGATCACCCTGAAAGAATCTGGACCTCCTTTGGTGAAGCCTACCCAGACTCTTACTCTGACCTGCTCCTTCTCTGGTTTCTCCCTGTCTGATTT
CGGTGTTGGTGTGGGTTGGATTAGACAGCCTCCTGGTAAGGCTCTTGAGTGGCTTGCTATCATCTACTCCGATGATGATAAGAGGTACAGCCCA
AGCCTTAACACCAGGCTTACCATCACCAAGGATACCAGCAAGAACCAGGTGGTGCTTGTGATGACTAGGGTTTCACCTGTCGACACCGCTACCT
ACTTTTGCGCTCATAGAAGGGGTCCTACCACCCTTTTCGGAGTTCCTATTGCTAGGGGTCCTGTGAACGCTATGGATGTTTGGGGTCAGGGTAT
TACCGTGACCATCAGCTCTACTTCAACTAAGGGACCATCTGTTTTTCCACTCGCTCCATCCTCTAAGTCTACTTCAGGTGGAACTGCTGCTCTT
GGATGCCTTGTTAAGGATTACTTTCCAGAGCCAGTGACTGTGTCTTGGAATTCTGGTGCTCTTACTTCCGGTGTTCATACTTTCCCAGCTGTGC
TTCAATCTTCCGGACTTTACTCTCTTTCCTCTGTTGTGACTGTGCCATCTTCTTCACTTGGCACTCAAACTTACATCTGCAACGTGAACCACAA
GCCATCCAACACAAAAGTGGATAAGAAGGTTGAGCCAAAGTCCTGCGATAAGACTCATACTTGTCCACCATGTCCAGCTCCAGAACTTCTTGGT
GGTCCTTCTGTTTTTTTGTTCCCACCAAAGCCAAAGGATACTCTCATGATCTCTAGGACTCCAGAGGTTACATGCGTTGTGGTTGATGTGTCTC
ATGAAGATCCAGAGGTGAAGTTCAACTGGTATGTGGATGGTGTTGAGGTGCACAACGCTAAGACTAAGCCAAGAGAGGAACAGTACAACTCCAC
TTACAGGGTTGTGTCTGTGCTTACTGTTCTTCACCAGGATTGGCTTAACGGCAAAGAGTACAAGTGCAAGGTGTCCAACAAGGCTTTGCCAGCT
CCAATCGAAAAGACTATCTCTAAGGCTAAGGGACAGCCAAGGGAACCTCAAGTTTACACTCTTCCACCATCTAGGGATGAGCTTACTAAGAACC
AGGTGTCCCTTACTTGCCTTGTGAAGGGATTTTACCCATCCGATATTGCTGTTGAGTGGGAGTCTAATGGACAGCCTGAGAACAACTACAAGAC
TACTCCACCAGTGCTCGATTCCGATGGATCATTCTTCTTGTACTCCAAGCTCACTGTGGATAAGTCTAGGTGGCAACAGGGAAACGTTTTCTCT
TGCTCTGTTATGCATGAGGCTCTCCACAATCACTACACTCAGAAGTCCCTTTCTTTGTCCCCTGGCAAGTAA

>PR1a_2F5_HC_aa
MGFVLFSQLPSFLLVSTLLLFLVISHSCRAGRITLKESGPPLVKPTQTLTLTCSFSGFSLSDFGVGVGWIRQPPGKALEWLAIIYSDDDKRYSP
SLNTRLTITKDTSKNQVVLVMTRVSPVDTATYFCAHRRGPTTLFGVPIARGPVNAMDVWGQGITVTISSTSTKGPSVFPLAPSSKSTSGGTAAL
GCLVKDYFPEPVTVSWNSGALTSGVHTFPAVLQSSGLYSLSSVVTVPSSSLGTQTYICNVNHKPSNTKVDKKVEPKSCDKTHTCPPCPAPELLG
GPSVFLFPPKPKDTLMISRTPEVTCVVVDVSHEDPEVKFNWYVDGVEVHNAKTKPREEQYNSTYRVVSVLTVLHQDWLNGKEYKCKVSNKALPA
PIEKTISKAKGQPREPQVYTLPPSRDELTKNQVSLTCLVKGFYPSDIAVEWESNGQPENNYKTTPPVLDSDGSFFLYSKLTVDKSRWQQGNVFS
CSVMHEALHNHYTQKSLSLSPGK

>PR1a_2G4_LC_CDS
ATGGGATTTGTTCTCTTTTCACAATTGCCTTCATTTCTTCTTGTCTCTACACTTCTCTTATTCCTAGTAATATCCCACTCTTGCCGTGCAGGTG
ATATTCAAATGACTCAATCTCCAGCTTCTCTTTCTGTTTCTGTTGGAGAAACTGTTTCTATTACTTGTAGAGCTTCTGAAAATATTTATTCTTC
TCTTGCTTGGTATCAACAAAAGCAAGGAAAGTCTCCACAACTTCTTGTTTATTCTGCTACTATTCTTGCTGATGGAGTTCCATCTAGATTTTCT
GGATCTGGATCTGGAACTCAATATTCTCTTAAGATTAATTCTCTTCAATCTGAAGATTTTGGAACTTATTATTGTCAACATTTTTGGGGAACTC
CATATACTTTTGGAGGAGGAACTAAGCTTGAAATTAAGAGGACTGTTGCTGCTCCATCTGTTTTCATCTTCCCACCATCTGATGAGCAGCTCAA
GTCTGGAACTGCTTCTGTTGTTTGCCTCCTCAACAATTTCTACCCAAGGGAAGCTAAGGTGCAGTGGAAAGTTGATAATGCTCTCCAGTCCGGA
AACTCCCAAGAATCTGTTACTGAGCAGGATTCCAAGGATTCTACTTACTCCCTCTCCTCAACTCTCACTCTCTCTAAGGCTGATTACGAGAAGC
ACAAGGTTTACGCTTGCGAAGTTACTCACCAGGGACTTTCTTCACCAGTGACTAAGTCTTTCAATAGGGGCGAGTGCTAA

>PR1a_2G4_LC_aa
MGFVLFSQLPSFLLVSTLLLFLVISHSCRAGDIQMTQSPASLSVSVGETVSITCRASENIYSSLAWYQQKQGKSPQLLVYSATILADGVPSRFS
GSGSGTQYSLKINSLQSEDFGTYYCQHFWGTPYTFGGGTKLEIKRTVAAPSVFIFPPSDEQLKSGTASVVCLLNNFYPREAKVQWKVDNALQSG
NSQESVTEQDSKDSTYSLSSTLTLSKADYEKHKVYACEVTHQGLSSPVTKSFNRGEC

>PR1a_2G4_HC_CDS
ATGGGATTTGTTCTCTTTTCACAATTGCCTTCATTTCTTCTTGTCTCTACACTTCTCTTATTCCTAGTAATATCCCACTCTTGCCGTGCAGGTG
AAGTTCAACTTCAAGAATCTGGAGGAGGACTTATGCAACCAGGAGGATCTATGAAGCTTTCTTGTGTTGCTTCTGGATTTACTTTTTCTAATTA
TTGGATGAATTGGGTTAGACAATCTCCAGAAAAGGGACTTGAATGGGTTGCTGAAATTAGACTTAAGTCTAATAATTATGCTACTCATTATGCT
GAATCTGTTAAGGGAAGATTTACTATTTCTAGAGATGATTCTAAGAGATCTGTTTATCTTCAAATGAATACTCTTAGAGCTGAAGATACTGGAA
TTTATTATTGTACTAGAGGAAATGGAAATTATAGAGCTATGGATTATTGGGGACAAGGAACTTCTGTTACTGTTTCTTCTACTTCAACTAAGGG
ACCATCTGTTTTTCCACTCGCTCCATCCTCTAAGTCTACTTCAGGTGGAACTGCTGCTCTTGGATGCCTTGTTAAGGATTACTTTCCAGAGCCA
GTGACTGTGTCTTGGAATTCTGGTGCTCTTACTTCCGGTGTTCATACTTTCCCAGCTGTGCTTCAATCTTCCGGACTTTACTCTCTTTCCTCTG
TTGTGACTGTGCCATCTTCTTCACTTGGCACTCAAACTTACATCTGCAACGTGAACCACAAGCCATCCAACACAAAAGTGGATAAGAAGGTTGA
GCCAAAGTCCTGCGATAAGACTCATACTTGTCCACCATGTCCAGCTCCAGAACTTCTTGGTGGTCCTTCTGTTTTTTTGTTCCCACCAAAGCCA
AAGGATACTCTCATGATCTCTAGGACTCCAGAGGTTACATGCGTTGTGGTTGATGTGTCTCATGAAGATCCAGAGGTGAAGTTCAACTGGTATG
TGGATGGTGTTGAGGTGCACAACGCTAAGACTAAGCCAAGAGAGGAACAGTACAACTCCACTTACAGGGTTGTGTCTGTGCTTACTGTTCTTCA
CCAGGATTGGCTTAACGGCAAAGAGTACAAGTGCAAGGTGTCCAACAAGGCTTTGCCAGCTCCAATCGAAAAGACTATCTCTAAGGCTAAGGGA
CAGCCAAGGGAACCTCAAGTTTACACTCTTCCACCATCTAGGGATGAGCTTACTAAGAACCAGGTGTCCCTTACTTGCCTTGTGAAGGGATTTT
ACCCATCCGATATTGCTGTTGAGTGGGAGTCTAATGGACAGCCTGAGAACAACTACAAGACTACTCCACCAGTGCTCGATTCCGATGGATCATT
CTTCTTGTACTCCAAGCTCACTGTGGATAAGTCTAGGTGGCAACAGGGAAACGTTTTCTCTTGCTCTGTTATGCATGAGGCTCTCCACAATCAC
TACACTCAGAAGTCCCTTTCTTTGTCCCCTGGCAAGTAA

>PR1a_2G4_HC_aa
MGFVLFSQLPSFLLVSTLLLFLVISHSCRAGEVQLQESGGGLMQPGGSMKLSCVASGFTFSNYWMNWVRQSPEKGLEWVAEIRLKSNNYATHYA
ESVKGRFTISRDDSKRSVYLQMNTLRAEDTGIYYCTRGNGNYRAMDYWGQGTSVTVSSTSTKGPSVFPLAPSSKSTSGGTAALGCLVKDYFPEP
VTVSWNSGALTSGVHTFPAVLQSSGLYSLSSVVTVPSSSLGTQTYICNVNHKPSNTKVDKKVEPKSCDKTHTCPPCPAPELLGGPSVFLFPPKP
KDTLMISRTPEVTCVVVDVSHEDPEVKFNWYVDGVEVHNAKTKPREEQYNSTYRVVSVLTVLHQDWLNGKEYKCKVSNKALPAPIEKTISKAKG
QPREPQVYTLPPSRDELTKNQVSLTCLVKGFYPSDIAVEWESNGQPENNYKTTPPVLDSDGSFFLYSKLTVDKSRWQQGNVFSCSVMHEALHNH
YTQKSLSLSPGK

>PR1a_COVA2-15_LC_CDS
ATGGGATTTGTTCTCTTTTCACAATTGCCTTCATTTCTTCTTGTCTCTACACTTCTCTTATTCCTAGTAATATCCCACTCTTGCCGTGCAGGTG
ATATCGTGATGACCCAGTCTCCTCTTTCTCTGCCTGTTACTCTTGGTCAGCCTGCCTCTATTAGCTGCAGGTCATCTCAGTCTCTGGTGTACTC
TGATGGCAACACCTTCCTGAACTGGTTTCAACAAAGGCCTGGTCAGTCTCCACGTCGGCTTATCTACCAGGTGAGCAACAGAGATTCTGGTGTG
CCTGATAGGTTCAGCGGTTCTGGTTCTGGTACTGACTTCACCCTGAAGATCAGCAGAGTTGAGGCTGAGGATGTGGGAGTGTACTATTGCATGC
AGGGTACTCATTGGCCTAGGACTTTTGGTCAGGGCACCAAGCTTGAGATCAAGAGGACTGTTGCTGCTCCATCTGTTTTCATCTTCCCACCATC
TGATGAGCAGCTCAAGTCTGGAACTGCTTCTGTTGTTTGCCTCCTCAACAATTTCTACCCAAGGGAAGCTAAGGTGCAGTGGAAAGTTGATAAT
GCTCTCCAGTCCGGAAACTCCCAAGAATCTGTTACTGAGCAGGATTCCAAGGATTCTACTTACTCCCTCTCCTCAACTCTCACTCTCTCTAAGG
CTGATTACGAGAAGCACAAGGTTTACGCTTGCGAAGTTACTCACCAGGGACTTTCTTCACCAGTGACTAAGTCTTTCAATAGGGGCGAGTGCTA
A

>PR1a_COVA2-15_LC_aa
MGFVLFSQLPSFLLVSTLLLFLVISHSCRAGDIVMTQSPLSLPVTLGQPASISCRSSQSLVYSDGNTFLNWFQQRPGQSPRRLIYQVSNRDSGV
PDRFSGSGSGTDFTLKISRVEAEDVGVYYCMQGTHWPRTFGQGTKLEIKRTVAAPSVFIFPPSDEQLKSGTASVVCLLNNFYPREAKVQWKVDN
ALQSGNSQESVTEQDSKDSTYSLSSTLTLSKADYEKHKVYACEVTHQGLSSPVTKSFNRGEC

>PR1a_COVA2-15_HC_CDS
ATGGGATTTGTTCTCTTTTCACAATTGCCTTCATTTCTTCTTGTCTCTACACTTCTCTTATTCCTAGTAATATCCCACTCTTGCCGTGCAGGTC
AGGTGCAGCTTCTTGAATCTGGTGGTGGTCTTGTTCAGCCTGGTGGTTCTCTTAGACTTAGCTGTGCTGCTAGCGGCTTCACCTTCTCTTCATA
CGCTATGTCTTGGGTGAGACAGGCTCCTGGTAAGGGTCTTGAATGGGCTTCTGCTATCTCTGGTTCTGGTGGCTCTACCTACTACGCTGATTCT
GTTGAGGGCCGTTTCACCATCAGCAGGGACAATTCTAAGAACACCCTGTACCTGCAGATGAACAGCCTGAGAGCTGAAGATACCGCTGTGTACT
ACTGCGCTAAGGATACTGGTTACTGCGGCGACGATTGCTACATCAAGCTTATCAGAGGTGGCCCTGATTACTGGGGTCAGGGTACTCTTGTGAC
CGTGTCATCTGCTTCAACTAAGGGACCATCTGTTTTTCCACTCGCTCCATCCTCTAAGTCTACTTCAGGTGGAACTGCTGCTCTTGGATGCCTT
GTTAAGGATTACTTTCCAGAGCCAGTGACTGTGTCTTGGAATTCTGGTGCTCTTACTTCCGGTGTTCATACTTTCCCAGCTGTGCTTCAATCTT
CCGGACTTTACTCTCTTTCCTCTGTTGTGACTGTGCCATCTTCTTCACTTGGCACTCAAACTTACATCTGCAACGTGAACCACAAGCCATCCAA
CACAAAAGTGGATAAGAAGGTTGAGCCAAAGTCCTGCGATAAGACTCATACTTGTCCACCATGTCCAGCTCCAGAACTTCTTGGTGGTCCTTCT
GTTTTTTTGTTCCCACCAAAGCCAAAGGATACTCTCATGATCTCTAGGACTCCAGAGGTTACATGCGTTGTGGTTGATGTGTCTCATGAAGATC
CAGAGGTGAAGTTCAACTGGTATGTGGATGGTGTTGAGGTGCACAACGCTAAGACTAAGCCAAGAGAGGAACAGTACAACTCCACTTACAGGGT
TGTGTCTGTGCTTACTGTTCTTCACCAGGATTGGCTTAACGGCAAAGAGTACAAGTGCAAGGTGTCCAACAAGGCTTTGCCAGCTCCAATCGAA
AAGACTATCTCTAAGGCTAAGGGACAGCCAAGGGAACCTCAAGTTTACACTCTTCCACCATCTAGGGATGAGCTTACTAAGAACCAGGTGTCCC
TTACTTGCCTTGTGAAGGGATTTTACCCATCCGATATTGCTGTTGAGTGGGAGTCTAATGGACAGCCTGAGAACAACTACAAGACTACTCCACC
AGTGCTCGATTCCGATGGATCATTCTTCTTGTACTCCAAGCTCACTGTGGATAAGTCTAGGTGGCAACAGGGAAACGTTTTCTCTTGCTCTGTT
ATGCATGAGGCTCTCCACAATCACTACACTCAGAAGTCCCTTTCTTTGTCCCCTGGCAAGTAA

>PR1a_COVA2-15_HC_aa
MGFVLFSQLPSFLLVSTLLLFLVISHSCRAGQVQLLESGGGLVQPGGSLRLSCAASGFTFSSYAMSWVRQAPGKGLEWASAISGSGGSTYYADS
VEGRFTISRDNSKNTLYLQMNSLRAEDTAVYYCAKDTGYCGDDCYIKLIRGGPDYWGQGTLVTVSSASTKGPSVFPLAPSSKSTSGGTAALGCL
VKDYFPEPVTVSWNSGALTSGVHTFPAVLQSSGLYSLSSVVTVPSSSLGTQTYICNVNHKPSNTKVDKKVEPKSCDKTHTCPPCPAPELLGGPS
VFLFPPKPKDTLMISRTPEVTCVVVDVSHEDPEVKFNWYVDGVEVHNAKTKPREEQYNSTYRVVSVLTVLHQDWLNGKEYKCKVSNKALPAPIE
KTISKAKGQPREPQVYTLPPSRDELTKNQVSLTCLVKGFYPSDIAVEWESNGQPENNYKTTPPVLDSDGSFFLYSKLTVDKSRWQQGNVFSCSV
MHEALHNHYTQKSLSLSPGK

>PR1a_ aGFP_LC_CDS
ATGGGATTTGTTCTCTTTTCACAATTGCCTTCATTTCTTCTTGTCTCTACACTTCTCTTATTCCTAGTAATATCCCACTCTTGCCGTGCAGGTG
ATATTCAACTTACTCAATCTCCAGCTATTATGTCTCCATCTCTTGGAGAAAGAGTTACTATGACTTGTACTGCTTCTTCTTCTGTTGGATCTTC
TTATCTTCATTGGTTTCAACAAAAGCCAGGATCTTCTCCAAAGCTTTGGATTTATTCTACTTCTAATCTTGCTTCTGGAGTTCCAGCTAGATTT
TCTGGATCTGGATCTGGAACTTCTTATTCTCTTACTATTTCTAGAATGGAAGCTGAAGATGCTGCTACTTATTATTGTCATCAATATCATAGAA
CTCCATATACTTTTGGAGGAGGAACTAAGCTTGAAATTAAGAGGACTGTTGCTGCTCCATCTGTTTTCATCTTCCCACCATCTGATGAGCAGCT
CAAGTCTGGAACTGCTTCTGTTGTTTGCCTCCTCAACAATTTCTACCCAAGGGAAGCTAAGGTGCAGTGGAAAGTTGATAATGCTCTCCAGTCC
GGAAACTCCCAAGAATCTGTTACTGAGCAGGATTCCAAGGATTCTACTTACTCCCTCTCCTCAACTCTCACTCTCTCTAAGGCTGATTACGAGA
AGCACAAGGTTTACGCTTGCGAAGTTACTCACCAGGGACTTTCTTCACCAGTGACTAAGTCTTTCAATAGGGGCGAGTGCTAA

>PR1a_ aGFP_LC_aa
MGFVLFSQLPSFLLVSTLLLFLVISHSCRAGDIQLTQSPAIMSPSLGERVTMTCTASSSVGSSYLHWFQQKPGSSPKLWIYSTSNLASGVPARF
SGSGSGTSYSLTISRMEAEDAATYYCHQYHRTPYTFGGGTKLEIKRTVAAPSVFIFPPSDEQLKSGTASVVCLLNNFYPREAKVQWKVDNALQS
GNSQESVTEQDSKDSTYSLSSTLTLSKADYEKHKVYACEVTHQGLSSPVTKSFNRGEC

>PR1a_ aGFP_HC_CDS
ATGGGATTTGTTCTCTTTTCACAATTGCCTTCATTTCTTCTTGTCTCTACACTTCTCTTATTCCTAGTAATATCCCACTCTTGCCGTGCAGGTG
AAGTTCAACTTCAACAATCTGGACCAGAACTTGTTAAGCCAGGATCTTCTATGAAGATTTCTTGTAAGGCTTCTGGATATTCTTTTACTGGATA
TACTATGAATTGGGTTAAGCAATCTCATGGACAAAATCTTGAATGGATTGGACTTATTAATCCATATAATGGAGGAACTAATTATAATCAAAAG
TTTAAGGGAAAGGCTACTCTTACTGTTGATAAATCTTCTTCTACTGCTTATATGGAACTTCTTGGACTTACTTCTGAAGATTCTGCTGTTTATT
ATTGTACTAGAGGAAATTCTGATTTTTCTGCTTGGTTTGCTTATTGGGGACAAGGAACTTCTGTTACTGTTTCTTCTACTTCAACTAAGGGACC
ATCTGTTTTTCCACTCGCTCCATCCTCTAAGTCTACTTCAGGTGGAACTGCTGCTCTTGGATGCCTTGTTAAGGATTACTTTCCAGAGCCAGTG
ACTGTGTCTTGGAATTCTGGTGCTCTTACTTCCGGTGTTCATACTTTCCCAGCTGTGCTTCAATCTTCCGGACTTTACTCTCTTTCCTCTGTTG
TGACTGTGCCATCTTCTTCACTTGGCACTCAAACTTACATCTGCAACGTGAACCACAAGCCATCCAACACAAAAGTGGATAAGAAGGTTGAGCC
AAAGTCCTGCGATAAGACTCATACTTGTCCACCATGTCCAGCTCCAGAACTTCTTGGTGGTCCTTCTGTTTTTTTGTTCCCACCAAAGCCAAAG
GATACTCTCATGATCTCTAGGACTCCAGAGGTTACATGCGTTGTGGTTGATGTGTCTCATGAAGATCCAGAGGTGAAGTTCAACTGGTATGTGG
ATGGTGTTGAGGTGCACAACGCTAAGACTAAGCCAAGAGAGGAACAGTACAACTCCACTTACAGGGTTGTGTCTGTGCTTACTGTTCTTCACCA
GGATTGGCTTAACGGCAAAGAGTACAAGTGCAAGGTGTCCAACAAGGCTTTGCCAGCTCCAATCGAAAAGACTATCTCTAAGGCTAAGGGACAG
CCAAGGGAACCTCAAGTTTACACTCTTCCACCATCTAGGGATGAGCTTACTAAGAACCAGGTGTCCCTTACTTGCCTTGTGAAGGGATTTTACC
CATCCGATATTGCTGTTGAGTGGGAGTCTAATGGACAGCCTGAGAACAACTACAAGACTACTCCACCAGTGCTCGATTCCGATGGATCATTCTT
CTTGTACTCCAAGCTCACTGTGGATAAGTCTAGGTGGCAACAGGGAAACGTTTTCTCTTGCTCTGTTATGCATGAGGCTCTCCACAATCACTAC
ACTCAGAAGTCCCTTTCTTTGTCCCCTGGCAAGTAA

>PR1a_ aGFP_HC_aa
MGFVLFSQLPSFLLVSTLLLFLVISHSCRAGEVQLQQSGPELVKPGSSMKISCKASGYSFTGYTMNWVKQSHGQNLEWIGLINPYNGGTNYNQK
FKGKATLTVDKSSSTAYMELLGLTSEDSAVYYCTRGNSDFSAWFAYWGQGTSVTVSSTSTKGPSVFPLAPSSKSTSGGTAALGCLVKDYFPEPV
TVSWNSGALTSGVHTFPAVLQSSGLYSLSSVVTVPSSSLGTQTYICNVNHKPSNTKVDKKVEPKSCDKTHTCPPCPAPELLGGPSVFLFPPKPK
DTLMISRTPEVTCVVVDVSHEDPEVKFNWYVDGVEVHNAKTKPREEQYNSTYRVVSVLTVLHQDWLNGKEYKCKVSNKALPAPIEKTISKAKGQ
PREPQVYTLPPSRDELTKNQVSLTCLVKGFYPSDIAVEWESNGQPENNYKTTPPVLDSDGSFFLYSKLTVDKSRWQQGNVFSCSVMHEALHNHY
TQKSLSLSPGK

>PR1a_ 2F5_LC_eGFP_CDS
ATGGGATTTGTTCTCTTTTCACAATTGCCTTCATTTCTTCTTGTCTCTACACTTCTCTTATTCCTAGTAATATCCCACTCTTGCCGTGCAGGTG
CATTACAATTAACACAATCTCCCTCCTCACTTAGTGCCTCCGTGGGGGATCGCATAACAATAACATGTAGAGCATCTCAGGGAGTGACCTCCGC
ACTTGCATGGTATCGACAAAAGCCAGGATCCCCCCCTCAGTTGTTAATTTATGACGCATCAAGTTTGGAGTCAGGCGTGCCTTCCAGATTTTCT
GGTTCCGGTTCAGGAACTGAATTTACACTGACAATAAGTACTCTAAGGCCAGAGGACTTTGCCACTTATTACTGTCAACAACTACATTTTTACC
CCCACACGTTCGGAGGTGGAACAAGGGTCGATGTACGTAGGACTGTTGCTGCTCCATCTGTTTTCATCTTCCCACCATCTGATGAGCAGCTCAA
GTCTGGAACTGCTTCTGTTGTTTGCCTCCTCAACAATTTCTACCCAAGGGAAGCTAAGGTGCAGTGGAAAGTTGATAATGCTCTCCAGTCCGGA
AACTCCCAAGAATCTGTTACTGAGCAGGATTCCAAGGATTCTACTTACTCCCTCTCCTCAACTCTCACTCTCTCTAAGGCTGATTACGAGAAGC
ACAAGGTTTACGCTTGCGAAGTTACTCACCAGGGACTTTCTTCACCAGTGACTAAGTCTTTCAATAGGGGCGAGTGCGGAGGAGGATCTGGAGG
AGGA**ATGGTGAGCAAGGGCGAGGAGCTGTTCACCGGGGTGGTGCCCATCCTGGTCGAGCTGGACGGCGACGTAAACGGCCACAAGTTCAGCGTG**
TCCGGCGAGGGCGAGGGCGATGCCACCTACGGCAAGCTGACCCTGAAGTTCATCTGCACCACCGGCAAGCTGCCCGTGCCCTGGCCCACCCTCG
TGACCACCTTCAGCTACGGCGTGCAGTGCTTCAGCCGCTACCCCGACCACATGAAGCAGCACGACTTCTTCAAGTCCGCCATGCCCGAAGGCTA
CGTCCAGGAGCGCACCATCTTCTTCAAGGACGACGGCAACTACAAGACCCGCGCCGAGGTGAAGTTCGAGGGCGACACCCTGGTGAACCGCATC
GAGCTGAAGGGCATCGACTTCAAGGAGGACGGCAACATCCTGGGGCACAAGCTGGAGTACAACTACAACAGCCACAACGTCTATATCATGGCCG
ACAAGCAGAAGAACGGCATCAAGGTGAACTTCAAGATCCGCCACAACATCGAGGACGGCAGCGTGCAGCTCGCCGACCACTACCAGCAGAACAC
CCCCATCGGCGACGGCCCCGTGCTGCTGCCCGACAACCACTACCTGAGCACCCAGTCCGCCCTGAGCAAAGACCCCAACGAGAAGCGCGATCAC
ATGGTCCTGCTGGAGTTCGTGACCGCCGCCGGGATCACTCACGGCATGGACGAGCTGTACAAGTAA

>PR1a_ 2F5_LC_eGFP_aa
MGFVLFSQLPSFLLVSTLLLFLVISHSCRAGALQLTQSPSSLSASVGDRITITCRASQGVTSALAWYRQKPGSPPQLLIYDASSLESGVPSRFS
GSGSGTEFTLTISTLRPEDFATYYCQQLHFYPHTFGGGTRVDVRRTVAAPSVFIFPPSDEQLKSGTASVVCLLNNFYPREAKVQWKVDNALQSG
NSQESVTEQDSKDSTYSLSSTLTLSKADYEKHKVYACEVTHQGLSSPVTKSFNRGECGGGSGGG**MVSKGEELFTGVVPILVELDGDVNGHKFSV**
SGEGEGDATYGKLTLKFICTTGKLPVPWPTLVTTFSYGVQCFSRYPDHMKQHDFFKSAMPEGYVQERTIFFKDDGNYKTRAEVKFEGDTLVNRI
ELKGIDFKEDGNILGHKLEYNYNSHNVYIMADKQKNGIKVNFKIRHNIEDGSVQLADHYQQNTPIGDGPVLLPDNHYLSTQSALSKDPNEKRDH
MVLLEFVTAAGITHGMDELYK

>PR1a_ 2F5_HC_mScarlet_CDS
ATGGGATTTGTTCTCTTTTCACAATTGCCTTCATTTCTTCTTGTCTCTACACTTCTCTTATTCCTAGTAATATCCCACTCTTGCCGTGCAGGTA
GGATCACCCTGAAAGAATCTGGACCTCCTTTGGTGAAGCCTACCCAGACTCTTACTCTGACCTGCTCCTTCTCTGGTTTCTCCCTGTCTGATTT
CGGTGTTGGTGTGGGTTGGATTAGACAGCCTCCTGGTAAGGCTCTTGAGTGGCTTGCTATCATCTACTCCGATGATGATAAGAGGTACAGCCCA
AGCCTTAACACCAGGCTTACCATCACCAAGGATACCAGCAAGAACCAGGTGGTGCTTGTGATGACTAGGGTTTCACCTGTCGACACCGCTACCT
ACTTTTGCGCTCATAGAAGGGGTCCTACCACCCTTTTCGGAGTTCCTATTGCTAGGGGTCCTGTGAACGCTATGGATGTTTGGGGTCAGGGTAT
TACCGTGACCATCAGCTCTACTTCAACTAAGGGACCATCTGTTTTTCCACTCGCTCCATCCTCTAAGTCTACTTCAGGTGGAACTGCTGCTCTT
GGATGCCTTGTTAAGGATTACTTTCCAGAGCCAGTGACTGTGTCTTGGAATTCTGGTGCTCTTACTTCCGGTGTTCATACTTTCCCAGCTGTGC
TTCAATCTTCCGGACTTTACTCTCTTTCCTCTGTTGTGACTGTGCCATCTTCTTCACTTGGCACTCAAACTTACATCTGCAACGTGAACCACAA
GCCATCCAACACAAAAGTGGATAAGAAGGTTGAGCCAAAGTCCTGCGATAAGACTCATACTTGTCCACCATGTCCAGCTCCAGAACTTCTTGGT
GGTCCTTCTGTTTTTTTGTTCCCACCAAAGCCAAAGGATACTCTCATGATCTCTAGGACTCCAGAGGTTACATGCGTTGTGGTTGATGTGTCTC
ATGAAGATCCAGAGGTGAAGTTCAACTGGTATGTGGATGGTGTTGAGGTGCACAACGCTAAGACTAAGCCAAGAGAGGAACAGTACAACTCCAC
TTACAGGGTTGTGTCTGTGCTTACTGTTCTTCACCAGGATTGGCTTAACGGCAAAGAGTACAAGTGCAAGGTGTCCAACAAGGCTTTGCCAGCT
CCAATCGAAAAGACTATCTCTAAGGCTAAGGGACAGCCAAGGGAACCTCAAGTTTACACTCTTCCACCATCTAGGGATGAGCTTACTAAGAACC
AGGTGTCCCTTACTTGCCTTGTGAAGGGATTTTACCCATCCGATATTGCTGTTGAGTGGGAGTCTAATGGACAGCCTGAGAACAACTACAAGAC
TACTCCACCAGTGCTCGATTCCGATGGATCATTCTTCTTGTACTCCAAGCTCACTGTGGATAAGTCTAGGTGGCAACAGGGAAACGTTTTCTCT
TGCTCTGTTATGCATGAGGCTCTCCACAATCACTACACTCAGAAGTCCCTTTCTTTGTCCCCTGGCAAGGGAGGAGGATCTGGAGGAGGA**ATGG**
TGAGCAAGGGCGAGGCAGTGATCAAGGAGTTCATGCGGTTCAAGGTGCACATGGAGGGCTCCATGAACGGCCACGAGTTCGAGATCGAGGGCGA
GGGCGAGGGCCGCCCCTACGAGGGCACCCAGACCGCCAAGCTGAAGGTGACCAAGGGTGGCCCCCTGCCCTTCTCCTGGGACATCCTGTCCCCT
CAGTTCATGTACGGCTCCAGGGCCTTCACCAAGCACCCCGCCGACATCCCCGACTACTATAAGCAGTCCTTCCCCGAGGGCTTCAAGTGGGAGC
GCGTGATGAACTTCGAGGACGGCGGCGCCGTGACCGTGACCCAGGACACCTCCCTGGAGGACGGCACCCTGATCTACAAGGTGAAGCTCCGCGG
CACCAACTTCCCTCCTGACGGCCCCGTAATGCAGAAGAAAACAATGGGCTGGGAAGCGTCCACCGAGCGGTTGTACCCCGAGGACGGCGTGCTG
AAGGGCGACATTAAGATGGCCCTGCGCCTGAAGGACGGCGGCCGCTACCTGGCGGACTTCAAGACCACCTACAAGGCCAAGAAGCCCGTGCAGA

TGCCCGGCGCCTACAACGTCGACCGCAAGTTGGACATCACCTCCCACAACGAGGACTACACCGTGGTGGAACAGTACGAACGCTCCGAGGGCCG
CCACTCCACCGGCGGCATGGACGAGCTGTACAAGTAA

>PR1a_ 2F5_HC_mScarlet_aa
MGFVLFSQLPSFLLVSTLLLFLVISHSCRAGRITLKESGPPLVKPTQTLTLTCSFSGFSLSDFGVGVGWIRQPPGKALEWLAIIYSDDDKRYSP
SLNTRLTITKDTSKNQVVLVMTRVSPVDTATYFCAHRRGPTTLFGVPIARGPVNAMDVWGQGITVTISSTSTKGPSVFPLAPSSKSTSGGTAAL
GCLVKDYFPEPVTVSWNSGALTSGVHTFPAVLQSSGLYSLSSVVTVPSSSLGTQTYICNVNHKPSNTKVDKKVEPKSCDKTHTCPPCPAPELLG
GPSVFLFPPKPKDTLMISRTPEVTCVVVDVSHEDPEVKFNWYVDGVEVHNAKTKPREEQYNSTYRVVSVLTVLHQDWLNGKEYKCKVSNKALPA
PIEKTISKAKGQPREPQVYTLPPSRDELTKNQVSLTCLVKGFYPSDIAVEWESNGQPENNYKTTPPVLDSDGSFFLYSKLTVDKSRWQQGNVFS
CSVMHEALHNHYTQKSLSLSPGKGGGSGGG**MVSKGEAVIKEFMRFKVHMEGSMNGHEFEIEGEGEGRPYEGTQTAKLKVTKGGPLPFSWDILSP**
QFMYGSRAFTKHPADIPDYYKQSFPEGFKWERVMNFEDGGAVTVTQDTSLEDGTLIYKVKLRGTNFPPDGPVMQKKTMGWEASTERLYPEDGVL
KGDIKMALRLKDGGRYLADFKTTYKAKKPVQMPGAYNVDRKLDITSHNEDYTVVEQYERSEGRHSTGGMDELYK

Appendix B – Coding (CDS) and amino acid (aa) sequence of N-terminal signal peptides

>*Nt*PR1a_CDS
ATGGGATTTGTTCTCTTTTCACAATTGCCTTCATTTCTTCTTGTCTCTACACTTCTCTTATTCCTAGTAATATCCCACTCTTGCCGTGCA

>*Nt*PR1a_aa
MGFVLFSQLPSFLLVSTLLLFLVISHSCRA

>*At*BC_CDS
ATGAAAACTAACCTTTTCCTGTTCCTGATCTTCAGCCTGCTGCTGAGCCTTTCATCTGCTGAGTTC

>*At*BC_aa
MKTNLFLFLIFSLLLSLSSAEF

>*Nb*SBT5.2_CDS
ATGAAAGGAATTATATCTTTGTTTTTCTGCTTTTCTCTTTTCATTGTCTCTTTCATATTAAGAGAAGCCGACTCA

>*Nb*SBT5.2_aa
MKGIISLFFCFSLFIVSFILREADS

>*Hs*GL_CDS
ATGTGGCTGCTTTTAACAATGGCAAGTTTGATATCTGTACTGGGGACTACACATGGTTTG

>*Hs*GL_aa
MWLLLTMASLISVLGTTHGL

>CHOL1_LC_CDS
ATGGATATGAGAGTTCCAGCTCAACTTCTTGGACTTCTTCTTCTTTGGCTTTCTGGAGCTAGATGT

>CHOL1_LC_aa
MDMRVPAQLLGLLLLWLSGARC

>CHOH7_HC_CDS
ATGGAATTTGGACTTTCTTGGGTTTTTCTTGTTGCTCTTTTTAGAGGAGTTCAATGT

>CHOH7_HC_aa
MEFGLSWVFLVALFRGVQC

>BiP_CDS
ATGGCTCGCTCGTTTGGAGCTAACAGTACCGTTGTGTTGGCGATCATCTTCTTCGGATGTTTATTTGCGTTGTCCTCTGCAATAGAAGAGGC
TACGAAGTTA

>BiP_aa
MARSFGANSTVVLAIIFFGCLFALSSAIEEATKL

Appendix C – Authorship Statement

Several materials, including plant lines or constructs were provided by other lab members or collaborators for experimentation. Initial VIGS silencing design and phylogenetic analysis of SBTs was done by Dr Pierre Buscaill. Protease knockouts for different *sbt* was outsourced to Biogle Genome Editing Centre, and homogeneity validation was performed by Dr Shi-Jian Song. *rd21* mutants were generated by Dr Alice Godson, and *vpe* mutants by Dr Emma Thomas. Protease inhibitors constructs were provided by Dr Friederike Grosse-Holz. VRC01 constructs were provided by Dr Philippe Jutras. GFP- and RFP-expressing constructs were provided by Dr Philippe Jutras, Dr Isobel Dodds and Dr Marketa Samalova. VIGS fragment for intracellular proteases were provided by Dr Kaijie Zheng. ER-stress marker was provided by Dr Kaijie Zheng and Matéo Paul. G22Y construct was provided by Dr Andras Sandor/Prof Sweetlove/Prof Ian Moore, and *cct1* mutants were kindly given by Prof Eva Stöger.

Appendix D – Publications in press (see following pages)

Viewpoints

Improving transient protein expression in agroinfiltrated *Nicotiana benthamiana*

Summary

Agroinfiltration of *Nicotiana benthamiana* is routinely used in plant science and molecular pharming to transiently express proteins of interest. Here, we discuss four phenomena that should be avoided to improve transient expression. Immune responses can be avoided by depleting immune receptors and employing pathogen-derived effectors; transcript degradation by using silencing inhibitors or RNA interference machinery mutants; endoplasmic reticulum stress by co-expressing chaperones; and protein degradation can be avoided with subcellular targeting, protease mutants and co-expressing protease inhibitors. We summarise the reported increased yields for various recombinant proteins achieved with these approaches and highlight remaining challenges to further improve the efficiency of this versatile protein expression platform.

Transient expression by infiltrating *Nicotiana benthamiana* leaves with *Agrobacterium tumefaciens* carrying genes of interest (agroinfiltration) is routinely used in plant science and molecular pharming. By transiently expressing genes of interest, one can investigate their roles in various biological processes without the need for stable transformation. Therefore, agroinfiltration facilitates the rapid assessment of gene function in a high-throughput manner, enabling more efficient functional genomic studies. The ability of agroinfiltrated *N. benthamiana* to rapidly produce large amounts of foreign proteins also makes it an attractive platform for molecular pharming. This method offers several advantages over other expression systems, such as mammalian cell culture and microbial fermentation. The plant-based transient expression typically has lower production costs and reduced risk of human pathogen contamination, is scalable, and has the potential for complex protein modifications including glycosylation. However, transient expression in *N. benthamiana* by agroinfiltration is still a challenge for many proteins, including antibodies and transmembrane glycoproteins, and can be further optimised. Here, we highlight four main processes that one needs to avoid to improve transient protein expression (Fig. 1).

Avoiding immune responses

Agroinfiltrated zones of *N. benthamiana* leaves normally show only weak chlorosis. However, various studies on the transcriptome, proteome, and metabolome revealed that extensive cellular reprogramming is taking place as cell homeostasis is deprioritised whilst immune responses increase (Table 1). Nearly 25% of the transcripts show differential abundance after agroinfiltration (Grosse-Holz *et al.*, 2018a). Upregulated genes are those involved in pathogen perception, immune signalling, protein folding, oxidative stress, and lignification (Grosse-Holz *et al.*, 2018a; Hamel *et al.*, 2023b). Downregulated genes include genes for photosynthesis and housekeeping proteins, consistent with the chlorotic response. Also, SWEET family sugar efflux transporters are downregulated (Grosse-Holz *et al.*, 2018a; Hamel *et al.*, 2023b), perhaps to reduce the viability of microbes in the apoplast (Chen, 2014). Within the extracellular proteome, 70% of the proteins increase in abundance upon agroinfiltration, and several without significant change in transcript abundance, suggesting post-transcriptional regulation (Grosse-Holz *et al.*, 2018a,b). This includes genes encoding pathogenesis-related proteins, cell wall remodelling proteins, molecular chaperones, and several lipases and esterases (Grosse-Holz *et al.*, 2018a; Hamel *et al.*, 2023b). Metabolomic changes include increased concentrations of phytol and α-tocopherol, consistent with chlorophyll degradation, and high levels of chlorogenic acid derivates, consistent with lignification (Drapal *et al.*, 2021). Collectively, these transcriptome, proteome, and metabolome changes are outputs of a basal immune response, similar to pattern-triggered immunity induced by microbe-associated molecular patterns (Zhang & Zhou, 2010). Consequently, various strategies can be taken to avoid or suppress immune responses upon agroinfiltration of *N. benthamiana* to improve transformation efficiencies. Avoidance of immune responses can be achieved by depleting immune receptors that recognise Agrobacterium in *N. benthamiana*. *Nb*CORE, for instance, is an immune receptor that recognises cold shock proteins of Agrobacterium but is expressed only in older *N. benthamiana* plants (Wang *et al.*, 2016). Depletion of *Nb*CORE with virus-induced gene silencing caused an eightfold higher transient green fluorescent protein (GFP) expression in older plants (Dodds *et al.*, 2023). Meanwhile, suppression of immune responses has been achieved with bacterial type-III effector AvrPto, which inhibits immune-related kinases (Xing *et al.*, 2007). Agrobacterium expressing AvrPto and the type-III secretion system have increased transformation efficiencies in various plants, including *N. benthamiana* (Raman *et al.*, 2022). These, and other, approaches to avoid and suppress immune response can significantly increase transient expression efficiencies.

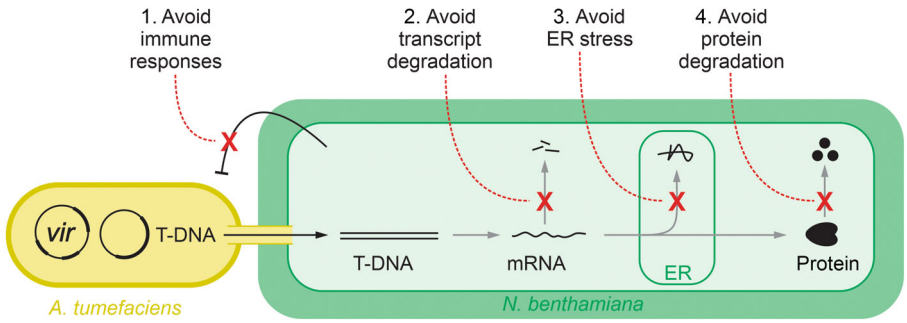

Fig. 1 Four phenomena to avoid to improve transient protein expression. Transient expression by infiltrating leaves of *Nicotiana benthamiana* with *Agrobacterium tumefaciens* is mediated by the transfer DNA (T-DNA) that is injected by the bacterium into the plant cell through the type-IV secretion system. Transient expression can be improved by avoiding immune responses; avoiding transcript degradation (silencing); avoiding endoplasmic reticulum (ER) stress caused by protein accumulation in the endoplasmic reticulum; and by avoiding protein degradation by plant proteases.

Table 1 Differential gene expression in *Nicotiana benthamiana* upon agroinfiltration.

Function	Transcriptomics	Proteomics	Metabolomics	References
Photosynthesis	↓	↓	↓	Grosse-Holz *et al*. (2018a); Drapal *et al*. (2021); Hamel *et al*. (2023b)
Cell wall remodelling (mainly lignification)	↑	↑	↑	Grosse-Holz *et al*. (2018a); Drapal *et al*. (2021); Hamel *et al*. (2023b)
Sugar depletion	↑	↑	–	Grosse-Holz *et al*. (2018a);Drapal *et al*. (2021); Hamel *et al*. (2023b)
ROS generation	↑	↑	↑	Grosse-Holz *et al*. (2018a); Hamel *et al*. (2023b)
Immune perception and signalling	↑	↑	n/a	Grosse-Holz *et al*. (2018a); Hamel *et al*. (2023b)
Proteases and inhibitors	↑	↑	n/a	Grosse-Holz *et al*. (2018a); Hamel *et al*. (2023b)
Lipases and esterases	↑	↑	n/a	Grosse-Holz *et al*. (2018a); Hamel *et al*. (2023b)
Salicylic acid signalling and SAR	↑	↑	n/a	Grosse-Holz *et al*. (2018a); Hamel *et al*. (2023b)
Chaperones and UPR-related	↑	↑	n/a	Grosse-Holz *et al*. (2018a); Hamel *et al*. (2023a,b)

↓, significant decrease in abundance; ↑, significant increase in abundance; –, no significant change; n/a, not assessed; UPR, unfolded protein response.

Avoiding transcript degradation

Transcripts encoded by transfer DNA (T-DNA) often become unstable through post-transcriptional gene silencing (PTGS), which usually starts on the third day after agroinfiltration. PTGS is triggered by low levels of antisense RNA generated by random T-DNA insertion and/or RNA-dependent RNA polymerase, which results in double-stranded RNA (dsRNA). dsRNA is a substrate for Dicer to generate small interfering RNAs (siRNAs) that target the degradation of homologous mRNAs. To overcome this, silencing inhibitor P19 of tomato bushy stunt virus is often co-expressed to suppress PTGS by sequestering siRNAs (Lombardi *et al*., 2009). But also, various knockout lines with reduced PTGS machinery have been generated. The removal of dicer-like proteins 2 and 4 in the *dcl2dcl4* double mutant of *N. benthamiana* resulted in higher transient expression levels (Matsuo & Matsumura, 2017; Matsuo, 2022). Likewise, the removal of RNA-dependent RNA polymerase 6 (*rdr6*) resulted in higher transient expression levels of GFP than the wild-type (WT) plants (Matsuo & Atsumi, 2019). However, in a combinatorial study, the *dcl2dcl4* plants support higher amounts of transiently expressed GFP and human fibroblast growth factor-1 than WT and *rdr6* plants (Matsuo, 2022). Likewise, other approaches to increase mRNA stability also improve transient expression. Different plant-derived untranslated regions (UTRs) can increase mRNA stability, even in the presence of P19 (Garabagi *et al*., 2012). Moreover, the hypertranslatable (HT) vector system incorporates virus-derived elements to boost transcription and translation, by increasing gene copy number and suppressing PTGS simultaneously (Sainsbury *et al*., 2009; Peyret & Lomonossoff, 2013).

Avoiding endoplasmic reticulum stress

Transient protein expression of proteins that are targeted to the secretory pathway can lead to endoplasmic reticulum (ER) stress due to the unfolded protein response. In plants, the ER quality control system promotes protein folding and processing of misfolded proteins (Strasser, 2018). Essential to quality control is the presence of folding factors and chaperones in the ER lumen to assist polypeptides in their correct folding. Chaperones include binding protein (BiP), HSP90 family proteins, calnexin, calreticulin, protein disulphide isomerases (PDIs), and peptidyl-prolyl isomerases (Gupta & Tuteja, 2011). Upregulation of chaperones is an important ER-stress response, and this often occurs in *N. benthamiana* upon agroinfiltration, especially when expressing large amounts of secreted proteins from other organisms (Ye *et al*., 2011; Margolin *et al*., 2020; Hamel *et al*., 2023a). ER stress also occurs upon the expression of high levels of membrane

New Phytologist

Table 2 Tackling proteolysis of recombinant proteins in agroinfiltrated *Nicotiana benthamiana*.

Approach	Description	Protein and accumulation[1]	Component	References
Protease inhibitor	Co-expression with protease inhibitors	C5-1 IgG antibody (LC; 70–80%)	*Sl*CDI; *Sl*CYS9	Goulet *et al*. (2012)
		C5-1 IgG antibody (HC; 85%)	*Sl*CDI	Goulet *et al*. (2012)
		C5-1 IgG antibody (40%)	*Sl*CYS8	Robert *et al*. (2013)
		H10 IgG antibody (HC; 7.5-fold)	*Sl*CYS8	Jutras *et al*. (2016)
		α-Galactosidase (4–14%)	*Nb*PR4, *Nb*Pot1 & *Hs*TIMP	Grosse-Holz *et al*. (2018b)
		Erythropoietin (16- to 27-fold)		
		VRC01 IgG antibody (2- to 10-fold)		
Protease knockdown/out	RNAi and gene editing	CAP256 IgG antibody (–)	*Nb*VPE-1a, *Nb*VPE-1b, and *Nb*CysP6	Singh *et al*. (2022)
Recombinant protein compartmentation	Retention to ER or storage in protein bodies; vacuolar targeting	Fungal xylanase xyn11A (10-fold)	HFBI	Saberianfar *et al*. (2015)
		Erythropoietin (twofold)	ELP	Saberianfar *et al*. (2015)
		Erythropoietin (twofold)	HFBI	Saberianfar *et al*. (2015)
		Interleucin-10 (threefold)	HFBI	Saberianfar *et al*. (2015)
		14D9 IgG antibody (10- to 15-fold)	ER; vacuole	Ocampo *et al*. (2016)
pH modulation of the plant secretory pathway	Co-expression with proton channels	α1-antichymotrypsin (fivefold)	Influenza M2 ion channel	Jutras *et al*. (2015, 2018)
		H3 influenza A (increase; ns)		
		HA influenza B (increase; ns)		

ELP, elastin-like polypeptide; H, hemagglutinin; HFBI, hydrophobin; VPE, vacuolar processing enzymes.
[1]Approximate accumulation according to authors' statements, – indicates no significant change, n/s indicates not specified.

proteins, such as viral glycoproteins. For instance, proteomic analysis has confirmed the increased abundance of PDIs, CRT, BiP, and ER-associated degradation components upon transient expression of a viral glycoprotein and an IgG antibody that trigger ER stress (Hamel *et al*., 2023a,b). Interestingly, different recombinant proteins may require specific chaperones for folding. Different IgG antibodies, for instance, either accumulate highly without triggering ER stress or accumulate poorly, associated with ER stress (Hamel *et al*., 2023a). To reduce ER stress upon agroinfiltration, molecular chaperones have been co-expressed alongside the target product. Human proteins are thought to be better folded by human chaperones than by plant chaperones given the divergence of the latter. Indeed, co-expression with human calreticulin caused a 13-fold increase in the transient expression of HIV glycoprotein gp140, whilst avoiding the induction of ER stress marker genes (Margolin *et al*., 2020). Likewise, co-expression with human calreticulin caused a threefold increase in the accumulation of the S protein ectodomain (Margolin *et al*., 2020; Song *et al*., 2022). The emerging message is that different recombinant proteins might require co-expression with specific chaperones to alleviate ER stress and increase protein folding and accumulation.

Avoiding proteolysis

Proteolysis is a huge obstacle in transient expression. Many recombinant proteins in agroinfiltrated leaves accumulate initially and then disappear at later timepoints, and sometimes accumulate as shorter fragments, which indicates their degradation by plant proteases. Degradation has been observed for various transmembrane glycoproteins and IgG antibodies and has been studied mostly for specific IgG antibodies. The *N. benthamiana* genome encodes for *c.* 1200 putative proteases but not all of these proteases degrade recombinant proteins, as they are organelle-specific, and many are not expressed or are inactive in agroinfiltrated leaves (Jutras *et al*., 2020). Most relevant for secreted recombinant proteins are probably papain-like Cys proteases (PLCPs), subtilisins, and pepsin-like Asp proteases that are abundant and active in the apoplast (Niemer *et al*., 2014; Deveuve *et al*., 2020; Puchol Tarazona *et al*., 2021). There are three main strategies taken to reduce proteolysis (Table 2). First, co-expression with protease inhibitors has increased yields of recombinant proteins. Co-expression with *Sl*CYS8, for instance, caused a threefold increase in the accumulation of full-length IgG antibody H10 (Jutras *et al*., 2016). Likewise, co-expression with *Nb*PR4, *Nb*Pot1, or *Hs*TIMP has increased the accumulation of IgG antibody VRC01, glycohormone erythropoietin, and α-galactosidase (Grosse-Holz *et al*., 2018b). Second, potentially harmful proteases can be depleted by silencing or genome editing. Transient depletion of vacuolar processing enzymes and PLCP *Nb*CysP6, for example reduced degradation of anti-HIV antibody CAP256 (Singh *et al*., 2022). Finally, proteolysis can be prevented by targeting the protein to different subcellular locations. For instance, targeting proteins to the vacuole or retaining them in the ER has increased yields of transiently expressed 14D9 antibody by 10- to 15-fold (Ocampo *et al*., 2016). Targeting recombinant proteins to protein bodies might be another way to avoid proteolysis (Schwestka *et al*., 2023). However, sensitivity to proteolysis very

much depends on the recombinant protein itself, and it seems unlikely that a single strategy will avoid proteolysis for all recombinant proteins.

Future prospects

Although agroinfiltration is already a great platform for protein expression, there are still numerous opportunities ahead of us to further improve this platform. Besides the four discussed areas, there is even more to gain from optimising co-expression, engineering post-translational modifications, targeting other subcellular locations, improving the protein extraction process, producing metabolites, and even optimising plant growth and agroinfiltration conditions. Much of these activities require ingenuity and the development and application of new scientific insights. There is an exciting time ahead of us.

Acknowledgements

The authors are financially supported by the BBSRC Interdisciplinary Bioscience DTP projects DDT00230 AP01.01 (KB) and AP01.15 (ECW), and ERC-2020-AdG project 101019324 'ExtraImmune' (RALH).

Competing interests

None declared.

Author contributions

KB, ECW and RALH conceived the topic and wrote the manuscript together. KB and ECW contributed equally to this work.

ORCID

Konstantina Beritza https://orcid.org/0009-0003-7343-4440
Renier A. L. van der Hoorn https://orcid.org/0000-0002-3692-7487
Emma C. Watts https://orcid.org/0000-0002-3974-6139

Konstantina Beritza†, Emma C. Watts† and Renier A. L. van der Hoorn*

The Plant Chemetics Laboratory, Department of Biology, University of Oxford, OX1 3RB, Oxford, UK
(*Author for correspondence: email: renier.vanderhoorn@biology.ox.ac.uk)
†These authors contributed equally to this work.

References

Chen LQ. 2014. SWEET sugar transporters for phloem transport and pathogen nutrition. *New Phytologist* **201**: 1150–1155.

Deveuve Q, Lajoie L, Barrault B, Thibault G. 2020. The proteolytic cleavage of therapeutic monoclonal antibody hinge region: more than a matter of subclass. *Frontiers in Immunology* **11**: 168.

Dodds I, Chen C, Buscaill P, van der Hoorn RAL. 2023. Depletion of the *Nb*CORE receptor drastically improves agroinfiltration productivity in older *Nicotiana benthamiana* plants. *Plant Biotechnology Journal* **21**: 1103–1105.

Drapal M, Enfissi EMA, Fraser PD. 2021. Metabolic effects of agro-infiltration on *N. benthamiana* accessions. *Transgenic Research* **30**: 303–315.

Garabagi F, Gilbert E, Loos A, Mclean MD, Hall JC. 2012. Utility of the P19 suppressor of gene-silencing protein for production of therapeutic antibodies in *Nicotiana* expression hosts. *Plant Biotechnology Journal* **10**: 1118–1128.

Goulet C, Khalf M, Sainsbury F, D'Aoust M-A, Michaud D. 2012. A protease activity-depleted environment for heterologous proteins migrating towards the leaf cell apoplast. *Plant Biotechnology Journal* **10**: 83–94.

Grosse-Holz F, Kelly S, Blaskowski S, Kaschani F, Kaiser M, van der Hoorn RAL. 2018a. The transcriptome, extracellular proteome and active secretome of agroinfiltrated *Nicotiana benthamiana* uncover a large, diverse protease repertoire. *Plant Biotechnology Journal* **16**: 1068–1084.

Grosse-Holz F, Madeira L, Zahid MA, Songer M, Kourelis J, Fesenko M, Ninck S, Kaschani F, Kaiser M, van der Hoorn RAL. 2018b. Three unrelated protease inhibitors enhance accumulation of pharmaceutical recombinant proteins in *Nicotiana benthamiana*. *Plant Biotechnology Journal* **16**: 1797–1810.

Gupta D, Tuteja N. 2011. Chaperones and foldases in endoplasmic reticulum stress signaling in plants. *Plant Signaling & Behavior* **6**: 232–236.

Hamel LP, Comeau MA, Tardif R, Poirier-Gravel F, Paré MÈ, Lavoie PO, Goulet MC, Michaud D, D'Aoust MA. 2023a. Heterologous expression of influenza haemagglutinin leads to early and transient activation of the unfolded protein response in *Nicotiana benthamiana*. *Plant Biotechnology Journal* **22**: 1146–1163.

Hamel LP, Tardif R, Poirier-Gravel F, Rasoolizadeh A, Brosseau C, Giroux G, Lucier JF, Goulet MC, Barrada A, Paré MÈ *et al.* 2023b. Molecular responses of agroinfiltrated *Nicotiana benthamiana* leaves expressing suppressor of silencing P19 and influenza virus-like particles. *Plant Biotechnology Journal* **22**: 1078–1100.

Jutras PV, D'Aoust MA, Couture MMJ, Vézina LP, Goulet MC, Michaud D, Sainsbury F. 2015. Modulating secretory pathway pH by proton channel co-expression can increase recombinant protein stability in plants. *Biotechnology Journal* **10**: 1478–1486.

Jutras PV, Dodds I, van der Hoorn RAL. 2020. Proteases of *Nicotiana benthamiana*: an emerging battle for molecular farming. *Current Opinion in Biotechnology* **61**: 60–65.

Jutras PV, Goulet MC, Lavoie PO, D'Aoust MA, Sainsbury F, Michaud D. 2018. Recombinant protein susceptibility to proteolysis in the plant cell secretory pathway is pH-dependent. *Plant Biotechnology Journal* **16**: 1928–1938.

Jutras PV, Marusic C, Lonoce C, Deflers C, Goulet M-C, Benvenuto E, Michaud D, Donini M. 2016. An accessory protease inhibitor to increase the yield and quality of a tumour-targeting mAb in *Nicotiana benthamiana* leaves. *PLoS ONE* **11**: e0167086.

Lombardi R, Circelli P, Villani ME, Buriani G, Nardi L, Coppola V, Bianco L, Benvenuto E, Donini M, Marusic C. 2009. High-level HIV-1 Nef transient expression in *Nicotiana benthamiana* using the P19 gene silencing suppressor protein of *Artichoke Mottled Crinckle Virus*. *BMC Biotechnology* **9**: 96.

Margolin EA, Strasser R, Chapman R, Williamson A-L, Rybicki EP, Meyers AE. 2020. Engineering the plant secretory pathway for the production of next-generation pharmaceuticals. *Trends in Biotechnology* **38**: 1034–1044.

Matsuo K. 2022. CRISPR/Cas9-mediated knockout of the *DCL2* and *DCL4* genes in *Nicotiana benthamiana* and its productivity of recombinant proteins. *Plant Cell Reports* **41**: 307–317.

Matsuo K, Atsumi G. 2019. CRISPR/Cas9-mediated knockout of the *RDR6* gene in *Nicotiana benthamiana* for efficient transient expression of recombinant proteins. *Planta* **250**: 463–473.

Matsuo K, Matsumura T. 2017. Repression of the *DCL2* and *DCL4* genes in *Nicotiana benthamiana* plants for the transient expression of recombinant proteins. *Journal of Bioscience and Bioengineering* **124**: 215–220.

Niemer M, Mehofer U, Torres Acosta JA, Verdianz M, Henkel T, Loos A, Strasser R, Maresch D, Rademacher T, Steinkellner H *et al.* 2014. The human anti-HIV antibodies 2F5, 2G12, and PG9 differ in their susceptibility to proteolytic degradation: down-regulation of endogenous serine and cysteine proteinase activities could improve antibody production in plant-based expression platforms. *Biotechnology Journal* **9**: 493–500.

Ocampo CG, Lareu JF, Marin Viegas VS, Mangano S, Loos A, Steinkellner H, Petruccelli S. 2016. Vacuolar targeting of recombinant antibodies in *Nicotiana benthamiana*. *Plant Biotechnology Journal* **14**: 2265–2275.

Peyret H, Lomonossoff GP. 2013. The pEAQ vector series: the easy and quick way to produce recombinant proteins in plants. *Plant Molecular Biology* **83**: 51–58.

Puchol Tarazona AA, Maresch D, Grill A, Bakalarz J, Torres Acosta JA, Castilho A, Steinkellner H, Mach L. 2021. Identification of two subtilisin-like serine proteases engaged in the degradation of recombinant proteins in *Nicotiana benthamiana*. *FEBS Letters* **595**: 379–388.

Raman V, Rojas CM, Vasudevan B, Dunning K, Kolape J, Oh S, Yun J, Yang L, Li G, Pant BD *et al.* 2022. *Agrobacterium* expressing a type III secretion system delivers *Pseudomonas* effectors into plant cells to enhance transformation. *Nature Communications* **13**: 2581.

Robert S, Khalf M, Goulet M-C, D'Aoust M-A, Sainsbury F, Michaud D. 2013. Protection of recombinant mammalian antibodies from development-dependent proteolysis in leaves of *Nicotiana benthamiana*. *PLoS ONE* **8**: e70203.

Saberianfar R, Joensuu JJ, Conley AJ, Menassa R. 2015. Protein body formation in leaves of *Nicotiana benthamiana*: a concentration-dependent mechanism influenced by the presence of fusion tags. *Plant Biotechnology Journal* **13**: 927–937.

Sainsbury F, Thuenemann EC, Lomonossoff GP. 2009. PEAQ: versatile expression vectors for easy and quick transient expression of heterologous proteins in plants. *Plant Biotechnology Journal* **7**: 682–693.

Schwestka J, Zeh L, Tschofen M, Schubert F, Arcalis E, Esteve-Gasent M, Pedrazzini E, Vitale A, Stoger E. 2023. Generation of multi-layered protein bodies in *N. benthamiana* for the encapsulation of vaccine antigens. *Frontiers in Plant Science* **14**: 1109270.

Singh AA, Pillay P, Naicker P, Alexandre K, Malatji K, Mach L, Steinkellner H, Vorster J, Chikwamba R, Tsekoa TL. 2022. Transient proteolysis reduction of *Nicotiana benthamiana*-produced CAP256 broadly neutralizing antibodies using CRISPR/Cas9. *Frontiers in Plant Science* **13**: 953654.

Song SJ, Kim H, Jang EY, Jeon H, Diao HP, Khan MRI, Lee MS, Lee YJ, Nam JH, Kim SR *et al.* 2022. SARS-CoV-2 spike trimer vaccine expressed in *Nicotiana benthamiana* adjuvanted with Alum elicits protective immune responses in mice. *Plant Biotechnology Journal* **20**: 2298–2312.

Strasser R. 2018. Protein quality control in the endoplasmic reticulum of plants. *Annual Review of Plant Biology* **69**: 147–172.

Wang L, Albert M, Einig E, Fürst U, Krust D, Felix G. 2016. The pattern-recognition receptor CORE of *Solanaceae* detects bacterial cold-shock protein. *Nature Plants* **2**: 16185.

Xing W, Zou Y, Liu Q, Liu J, Luo X, Huang Q, Chen S, Zhu L, Bi R, Hao Q *et al.* 2007. The structural basis for activation of plant immunity by bacterial effector protein AvrPto. *Nature* **449**: 243–247.

Ye C, Dickman MB, Whitham SA, Payton M, Verchot J. 2011. The unfolded protein response is triggered by a plant viral movement protein. *Plant Physiology* **156**: 741–755.

Zhang J, Zhou JM. 2010. Plant immunity triggered by microbial molecular signatures. *Molecular Plant* **3**: 783–793.

Key words: *Agrobacterium tumefaciens*, agroinfiltration, ER stress, gene silencing, immunity, *Nicotiana benthamiana*, proteolysis, transient expression.

Received, 22 March 2024; accepted, 2 May 2024.

Plant Biotechnology Journal
Open Access

Plant Biotechnology Journal (2024) **22**, pp. 2808–2810 doi: 10.1111/pbi.14406

Brief Communication

SBT5.2s are the major active extracellular subtilases processing IgG antibody 2F5 in the *Nicotiana benthamiana* apoplast

Konstantina Beritza[1], Pierre Buscaill[1], Shi-Jian Song[1], Philippe V. Jutras[1], Jie Huang[1], Lukas Mach[2], Suomeng Dong[3] and Renier A. L. van der Hoorn[1,*]

[1]*Plant Chemetics Laboratory, Department of Biology, University of Oxford, Oxford, UK*
[2]*Department of Applied Genetics and Cell Biology, University of Natural Resources and Life Sciences, Vienna, Austria*
[3]*Department of Plant Pathology, Nanjing Agricultural University, Nanjing, China*

Received 15 February 2024;
revised 8 April 2024;
accepted 26 May 2024.
**Correspondence* (Tel +44 1865 275077; fax +44 1865 275074: email renier.vanderhoorn@biology.ox.ac.uk)

Keywords: subtilase, apoplast, molecular pharming, *Nicotiana benthamiana*, IgG antibody.

Agroinfiltration of *Nicotiana benthamiana* has emerged as a main protein expression platform in plant science and molecular pharming but yields are often hampered by endogenous proteases degrading recombinant proteins. Many IgG antibodies, for instance, are degraded when expressed in *N. benthamiana* (Niemer *et al*., 2014). HIV-neutralizing IgG antibody 2F5 is cleaved in the H3 loop of the variable region of the heavy chain (HC) when incubated in apoplastic fluids (AF) of *N. benthamiana*, and this processing was blocked with Ser protease inhibitor PMSF (Niemer *et al*., 2014). Since the SBT5.2a subtilase (previously called SBT1) is the most abundant active Ser protease in the AF detected by activity-based proteomics (Jutras *et al*., 2019; Puchol Tarazona *et al*., 2021), this subtilase was heterologously expressed and shown to cleave 2F5 *in vitro* (Puchol Tarazona *et al*., 2021). Here, we investigated if SBT5.2 is also necessary to cleave 2F5 in AF.

We first found that fluorescently labelled 2F5 is similarly cleaved as unlabelled 2F5 in AF (Figure S1). Processing of fluorescent 2F5 is blocked by PMSF and in AF of plants transiently expressing subtilase inhibitor Epi1 but not expressing other protease inhibitors (Figure S2; Grosse-Holz *et al*., 2018). Virus-induced gene silencing (VIGS) using tobacco rattle virus (TRV) carrying fragments targeting the detected apoplastic subtilases revealed that AF of only *TRV::SBT5.2* plants was unable to cleave 2F5 (Figure S3), indicating that SBT5.2 is responsible for cleaving 2F5 in AF.

The *SBT5.2* fragment used for VIGS targets three *SBT5.2* homologues that are expressed in agroinfiltrated leaves (Figures S4 and S5). Genome editing using CRISPR/Cas9 was used to disrupt all three *SBT5.2* genes, resulting in two independent *sbt5.2* knockout lines that grow indistinguishable from wild-type plants (Figure S6). Activity-based profiling with FP-TAMRA demonstrated that these lines lack the most active subtilases in the AF, shown at 65–70 kDa in wild-type (WT) plants (Figure 1a). AF from *sbt5.2* mutants was unable to cleave 2F5 (Figure 1b), demonstrating that SBT5.2s are necessary for 2F5 cleavage.

Transient expression of the HC and light chain (LC) of 2F5 resulted in threefold more 2F5 accumulation in total extracts (TEs) of *sbt5.2* mutants compared with WT plants (Figure 1c). Also the Ebola-neutralizing IgG 2G4 accumulates more in *sbt5.2* mutants (Figure S7). Fluorescence of co-expressed GFP was similar between WT plants and *sbt5.2* mutants (Figure S8), indicating that SBT5.2 depletion promotes 2F5 accumulation post-transcriptionally. Remarkably, however, 2F5 processing is unaltered in *sbt5.2* mutants (Figure 1c). Similar results were obtained upon co-expression with Epi1 and in *TRV::SBT5.2* plants (Figure S9), indicating that 2F5 is not exposed to SBT5.2 in the apoplast.

To investigate whether 2F5 is secreted in agroinfiltrated plants, we transiently co-expressed 2F5 (HC + LC) with cytonuclear GFP and secreted RFP and isolated AF and TE from the same leaves. Western blot analysis revealed that only 3%–5% of the GFP detected in TE is detected in AF whereas 41%–47% of the total RFP is in the AF (Figure 1d). Neither GFP nor RFP distribute differently nor accumulate higher in the *sbt5.2* mutants. Importantly, only 2%–4% of both HC and LC of 2F5 were detected in AF (Figure 1d), indicating that 2F5 is not secreted and not exposed to SBT5.2 in the apoplast. Fragment F1 follows the same trend as HC and LC signals, while fragment F2 accumulates relatively abundantly in AF (Figure 1d). F2 is also easily detected in AF (Niemer *et al*., 2014) and originates from degradation of unassembled HC because it also accumulates when only HC is expressed (Figure S10). The distribution of 2F5 signals is similar between WT and *sbt5.2* plants but threefold more 2F5 accumulates in *sbt5.2* mutants (Figure 1d), consistent with Figure 1c.

The observation that most 2F5 is not secreted challenges the general assumption that IgGs are secreted and seems to contradict numerous reports on the detection of IgGs in the apoplast (e.g. Arcalis *et al*., 2013; Ocampo *et al*., 2016). Our data are nevertheless consistent with the literature. A previous study on transient 2F5 expression revealed that only an estimated 5% of the HC signal detected in TE was detected in AF (Niemer *et al*., 2014). Fluorescent fusion proteins of the HC of 2F5 were found to accumulate in pre-vacuolar compartments and the vacuole (Irons *et al*., 2008). Similar observations were made when studying 2G12, a different HIV-neutralizing IgG (Irons *et al*., 2008), and 2G4 (Figure S7). It has been speculated that

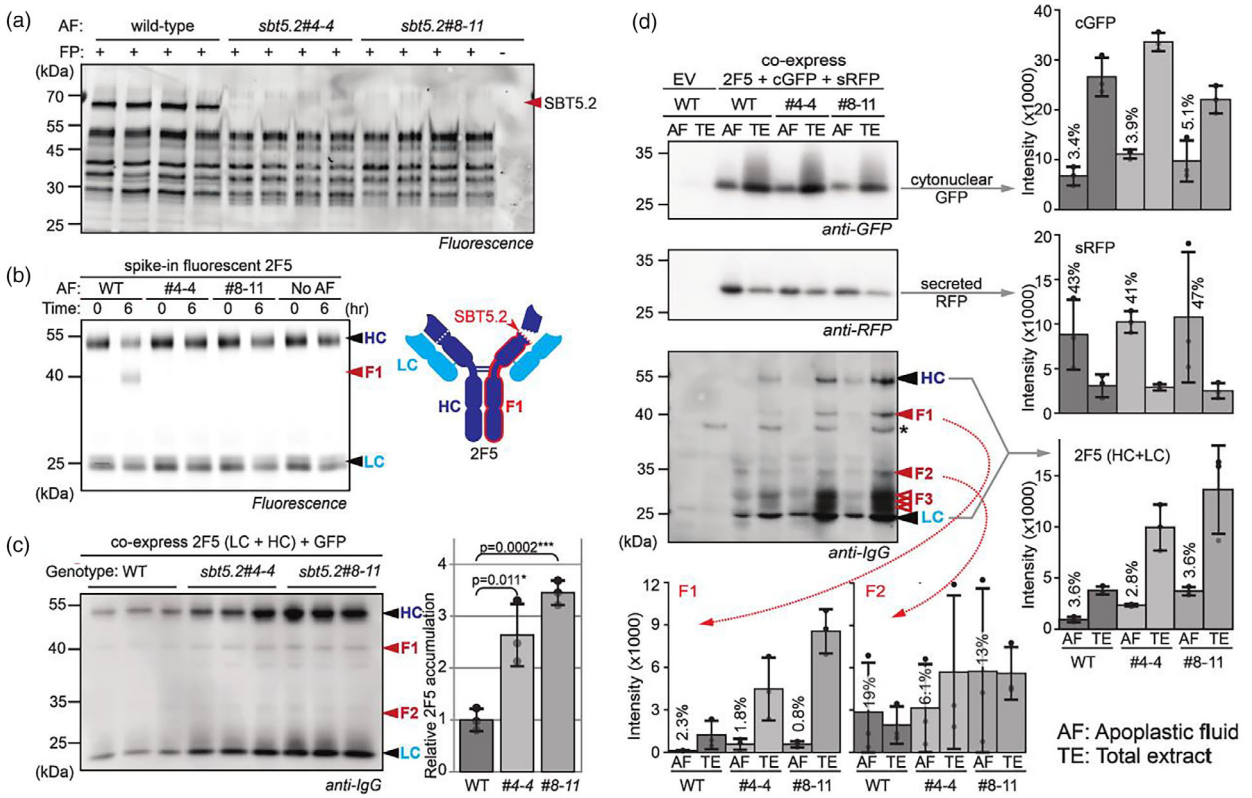

Figure 1 Deletion of three SBT5.2 proteases from *N. benthamiana* avoids 2F5 processing in the apoplast and increases 2F5 accumulation, even though 2F5 is not secreted. (a) SBT5.2 are major subtilases in the apoplast. AF was isolated from WT plants and two *sbt5.2* mutants (four replicates each) and active Ser hydrolases were detected with FP-TAMRA and fluorescence scanning. (b) 2F5 is no longer cleaved in AF of *sbt5.2* plants. Fluorescently labelled 2F5 was incubated with AFs from WT plants and *sbt5.2* mutants for 0–6 h, and samples were separated on reducing gels and scanned for fluorescence. (c) The *sbt5.2* mutants accumulate threefold more 2F5 upon transient expression. HC and LC of 2F5 were transiently co-expressed, and signals were quantified from the anti-IgG western blot from a reducing gel. Error bars represent SE of $n = 3$ replicates. (d) Transiently expressed 2F5 is not secreted into the apoplast. Both HC and LC of 2F5 were co-expressed with secreted sRFP and cytonuclear cGFP and TEs and AFs were isolated after 5 days from the same leaves in triplicate and analysed by western blotting from a reducing gel using antibodies against GFP, RFP and IgG. Chemiluminescence was quantified and plotted for each signal. F3 fragments are not detected in all experiments. The percentages indicate how much compared to the TE sample was detected in the AF. *, background signal. Error bars represent SE of $n = 3$ replicates.

secretion is prevented either by cryptic vacuolar targeting signals or by chaperone BiP, which remains bound to IgGs (Irons *et al.*, 2008). Thus, besides introducing a very useful protease mutant to the community to increase yields, this study also highlights an important controversy on the subcellular accumulation of IgGs in agroinfiltrated plants.

Acknowledgements

We thank Urszula Pyzio for plant care and Sarah Rodgers, Caroline O'Brian and Patricia Bowman for technical support. This project was financially supported by the Interdisciplinary DTC project DDT00230 (KB); BBSRC project BB/R017913/1 (PB); H2020 project 'Newcotiana' (PJ); UKRI project BB/W013932/1 (SS); and ERC projects 616449 and 101019324 (JH, RH).

Author contributions

RH conceived and managed the project. KB performed the majority of the experiments. PB produced VIGS constructs, initiated silencing experiments and conducted phylogenetic analysis. PJ produced pPJ057 (sRFP). SS selected *sbt5.2* lines with help from JH and SD. LM assisted with data interpretation. KB and RH wrote the article with input from all co-authors.

Conflicts of interest

None declared.

Data availability

All data are provided as figures and supplemental figures.

References

Arcalis, E., Stadlmann, J., Rademacher, T., Marcel, S., Sack, M., Altmann, F. and Stoger, E. (2013) Plant species and organ influence the structure and subcellular localization of recombinant glycoproteins. *Plant Mol. Biol.* **83**, 105–117.

Grosse-Holz, F., Madeira, L., Zahid, M.A., Songer, M., Kourelis, J., Fesenko, M., Ninck, S. *et al.* (2018) Three unrelated protease inhibitors enhance

accumulation of pharmaceutical recombinant proteins in *Nicotiana benthamiana*. *Plant Biotechnol. J.* **16**, 1797–1810.

Irons, S.L., Nuttall, J., Floss, D.M., Frigerio, L., Kotzer, A.M. and Hawes, C. (2008) Fluorescent protein fusions to a human immunodeficiency virus monoclonal antibody reveal its intracellular transport through the plant endomembrane system. *Plant Biotechnol. J.* **6**, 649–662.

Jutras, P.V., Grosse-Holz, F., Kaschani, F., Kaiser, M., Michaud, D. and van der Hoorn, R.A.L. (2019) Activity-based proteomics reveals nine target proteases for the recombinant protein-stabilizing inhibitor SlCYS8 in *Nicotiana benthamiana*. *Plant Biotechnol. J.* **17**, 1670–1678.

Niemer, M., Mehofer, U., Torres Acosta, J.A., Verdianz, M., Henkel, T., Loos, A., Strasser, R. *et al*. (2014) The human anti-HIV antibodies 2F5, 2G12, and PG9 differ in their susceptibility to proteolytic degradation: down-regulation of endogenous serine and cysteine proteinase activities could improve antibody production in plant-based expression platforms. *Biotechnol. J.* **9**, 493–500.

Ocampo, C.G., Lareu, J.F., Marin Viegas, V.S., Mangano, S., Loos, A., Steinkellner, H. and Petruccelli, S. (2016) Vacuolar targeting of recombinant antibodies in *Nicotiana benthamiana*. *Plant Biotechnol. J.* **14**, 2265–2275.

Puchol Tarazona, A.A., Maresch, D., Grill, A., Bakalarz, J., Torres Acosta, J.A., Castilho, A., Steinkellner, H. *et al*. (2021) Identification of two subtilisin-like serine proteases engaged in the degradation of recombinant proteins in *Nicotiana benthamiana*. *FEBS Lett.* **595**, 379–388.

Supporting information

Additional supporting information may be found online in the Supporting Information section at the end of the article.

Figure S1 Amine-reactive dye labelling does not affect 2F5 cleavage *in vitro*.
Figure S2 PMSF and Epi1 block 2F5 processing in apoplastic fluids.
Figure S3 *SBT5.2* silencing prevents 2F5 processing in apoplastic fluids.
Figure S4 VIGS targets three *SBT5.2* genes.
Figure S5 Phylogenetic analysis of subtilases and RPKM values for three *NbSBT5.2* genes.
Figure S6 Identification of *sbt5.2* triple KO mutants in *N. benthamiana*.
Figure S7 IgG 2G4 also accumulates more in *sbt5.2* mutant but not in the apoplast.
Figure S8 Transiently co-expressed GFP is not expressed more in the sbt5.2 mutants.
Figure S9 SBT5.2 depletion with Epi1 or VIGS does not affect 2F5 processing *in vivo*.
Figure S10 Fragment F2 originates from HC overexpression.
Table S1 Coding sequences for 2F5 and 2G4 expression.
Table S2 Plasmids used in this study.
Table S3 Virus-induced gene silencing (VIGS) fragments used in this study.
Table S4 Single-guide RNAs (sgRNAs) and primers used for sequencing of *sbt5.2* KO lines.

Acknowledgements

My gratitude and admiration go first to *Renier*. Thank you for your advice, your patience, and your continuous mentoring. When I first joined you for my Rotation project, I knew immediately that the lab would be the best fit. To *Mariana*, *Pierre*, and *Tee*, for being such talented postdocs and inspiring me to continue in academia. To *Brian* for his endless lab advice and our chats about cats. To *Jie* for being the best lab buddy on weekends. To *Chidam* for the philosophical conversations while pipetting. To the greatest coffee partner, *Joy* who always brought me joy. To *Issy* and *Alice* as they were always around when early DPhil blues hit. To *Emma*, *Kaijie*, *Song*, and *Nora* for being the most magnificent Molecular Pharming team one could ask for – thank you for all your help. To my students *Maria* and *Ieuan* for making me a better mentor. To *Felix* for getting me hooked on AlphaFold. To *Urszula*, *Patty*, *Sarah*, and *Caroline* as smooth lab work without them would be impossible. To the probably thousands of cute - and some not so cute – little *benthi* I massacred over the years.

To my mom and dad, *Vicky* and *Tasos*, for always celebrating my small victories. To my idols and sisters *Athena* and *Anastasia* for being so close even though they're so far away. To my beloved aunt *Hypatia* who left us too soon but motivated me to pursue research on therapeutics. To my one and only *Costy*, for keeping me sane and thriving. To my cat *Béchamel* for putting up with me when I squeezed her too often. To my most betterest friend *Hend*, for always knowing how to cheer me up. To *Katerina* for brightening my days during writing. To *Nick* and *Amalia* for their support and the never-ending memes exchange. To the *Oxford Dance Society*, *Tom* and *Hara* for keeping me sane – and fit - with dance classes. To *Oxford* for being the coolest place to live and study, with vintage libraries at every corner, endless artsy events or fancy formals, and wonderful people from around the globe – I cherish every moment.

Thank you *Oxford* for being my Ithaka.

Ithaka | C. P. Cavafy

As you set out for Ithaka
hope your road is a long one,
full of adventure, full of discovery.

Laistrygonians, Cyclops,
angry Poseidon—don't be afraid of them:
you'll never find things like that on your way
as long as you keep your thoughts raised high,
as long as a rare excitement
stirs your spirit and your body.

Laistrygonians, Cyclops,
wild Poseidon—you won't encounter them
unless you bring them along inside your soul,
unless your soul sets them up in front of you.

Hope your road is a long one.
May there be many summer mornings when,
with what pleasure, what joy,
you enter harbors you're seeing for the first time;

may you stop at Phoenician trading stations
to buy fine things,
mother of pearl and coral, amber and ebony,
sensual perfume of every kind—
as many sensual perfumes as you can;

and may you visit many Egyptian cities
to learn and go on learning from their scholars.
Keep Ithaka always in your mind.
Arriving there is what you're destined for.

But don't hurry the journey at all.
Better if it lasts for years,
so you're old by the time you reach the island,
wealthy with all you've gained on the way,
not expecting Ithaka to make you rich.

Ithaka gave you the marvelous journey.
Without her you wouldn't have set out.
She has nothing left to give you now.

And if you find her poor, Ithaka won't have fooled you.
Wise as you will have become, so full of experience,
you'll have understood by then what these Ithakas mean.

Ἰθάκη | Κ. Π. Καβάφης

Σὰ βγεῖς στὸν πηγαιμὸ γιὰ τὴν Ἰθάκη,
νὰ εὔχεσαι νᾶναι μακρὺς ὁ δρόμος,
γεμάτος περιπέτειες, γεμάτος γνώσεις.

Τοὺς Λαιστρυγόνας καὶ τοὺς Κύκλωπας,
τὸν θυμωμένο Ποσειδῶνα μὴ φοβᾶσαι,
τέτοια στὸν δρόμο σου ποτέ σου δὲν θὰ βρεῖς,
ἂν μέν᾽ ἡ σκέψις σου ὑψηλή, ἂν ἐκλεκτὴ
συγκίνησις τὸ πνεῦμα καὶ τὸ σῶμα σου ἀγγίζει.

Τοὺς Λαιστρυγόνας καὶ τοὺς Κύκλωπας,
τὸν ἄγριο Ποσειδώνα δὲν θὰ συναντήσεις,
ἂν δὲν τοὺς κουβανεῖς μὲς στὴν ψυχή σου,
ἂν ἡ ψυχή σου δὲν τοὺς στήνει ἐμπρός σου.

Νὰ εὔχεσαι νά ᾽ναι μακρὺς ὁ δρόμος.
Πολλὰ τὰ καλοκαιρινὰ πρωϊὰ νὰ εἶναι
ποὺ μὲ τί εὐχαρίστηση, μὲ τί χαρὰ
θὰ μπαίνεις σὲ λιμένας πρωτοειδωμένους·

νὰ σταματήσεις σ᾽ ἐμπορεῖα Φοινικικά,
καὶ τὲς καλὲς πραγμάτειες ν᾽ ἀποκτήσεις,
σεντέφια καὶ κοράλλια, κεχριμπάρια κ᾽ ἔβενους,
καὶ ἡδονικὰ μυρωδικὰ κάθε λογῆς,
ὅσο μπορεῖς πιὸ ἄφθονα ἡδονικὰ μυρωδικά.

Σὲ πόλεις Αἰγυπτιακὲς πολλὲς νὰ πᾷς,
νὰ μάθεις καὶ νὰ μάθεις ἀπ᾽ τοὺς σπουδασμένους.
Πάντα στὸ νοῦ σου νἄχῃς τὴν Ἰθάκη.
Τὸ φθάσιμον ἐκεῖ εἶν᾽ ὁ προορισμός σου.

Ἀλλὰ μὴ βιάζῃς τὸ ταξείδι διόλου.
Καλλίτερα χρόνια πολλὰ νὰ διαρκέσει.
Καὶ γέρος πιὰ ν᾽ ἀράξῃς στὸ νησί,
πλούσιος μὲ ὅσα κέρδισες στὸν δρόμο,
μὴ προσδοκώντας πλούτη νὰ σὲ δώσῃ ἡ Ἰθάκη.

Ἡ Ἰθάκη σ᾽ ἔδωσε τ᾽ ὡραῖο ταξίδι.
Χωρὶς αὐτὴν δὲν θἄβγαινες στὸν δρόμο.
Ἄλλα δὲν ἔχει νὰ σὲ δώσει πιά.

Κι ἂν πτωχικὴ τὴν βρῇς, ἡ Ἰθάκη δὲν σὲ γέλασε.
Ἔτσι σοφὸς ποὺ ἔγινες, μὲ τόση πείρα,
ἤδη θὰ τὸ κατάλαβες ᾗ Ἰθάκες τί σημαίνουν.